A Selection of published/presented papers

Volume I(1)
(1967-1979)

Papers 1-22

S Lee

A SELECTION OF PUBLISHED PAPERS

by S. LEE

UNIVERSITI MALAYA

A Selection of Published Papers by S. Lee

1. 1967 "Transition from Electromagnetic to Hot-Gas Driver in an Electric Shock Experiment", Int. J. Electronics vol. 22 p. 193 - 196. - H.H. Teh. S. Lee.

2. 1971 "High Current discharge in plasma focus experiment" proc. Symposium on Physics, Singapore- 182 - 195, S. Lee, Chen, Chow, Tan, Teh and Thong.

3. 1971 "Penyelidikan Fizik Plasma" Malayan Scientist 6, 42 - 44 B.C. Tan, S. Lee.

4. 1972 "Bow-shock effects on probe measurements" J. Applied Physics (U.S.A.) 43, 3980 - 3983, S. Lee and R.J. Sandeman.

5. 1972 "Current Sheath Studies in a Coaxial Plasma Focus Gun" J. of Plasma Physics (U.K.) 8, 21 - 31 - - S.P. Chow, S. Lee, B.C. Tan.

6. 1972 " High Speed Photography of a plasma focus" International J. of Electronics (U.K.) 33, 85 - 90- S. Lee, Chen, Chow, B.C. Tan, H.H. Teh, S.P. Thong.

7. 1973 "Coaxial plasma gun in mode I operation" - International J. of Electronics (U.K.) 35, 341-352 - Y.H. Chen and S. Lee.

8. 1973 "A simplified method of switching a 2 mega-ampere capacitor bank using a voltage division technique" Malaysian J. of Science 2(B), 157-169, S.P. Thong and S. Lee.

9. 1974 "Applying research techniques in a developing country" Australian National University News Vol. 9, 2 - 3, S. Lee.

10. 1975 "Dependence of focus intensity on mass and field distribution" - Proc. of Seventh European Conference on Controlled Fusion and Plasma Physics, Lausanne, Switzerland- I, Paper 65 - S. Lee and T.H. Tan.

11. 1975 "Measurement of neutrons from a focussed plasma" - Malaysian J. of Science 3(B) 159 - 163 - S. Lee and Y.H. Chen.

12. 1975 "The Plasma focus - A radial trajectory computation" - Proc. of Twelfth International Conference on Phenomena in Ionized Gases, Eindhoven, Netherland- I, Paper 353 - S. Lee and Y.H. Chen.

13. 1975 "Profiles of a transverse ionizing shock wave" Malaysian J. of Science 3(B), 165 - 176, S. Lee.

14. 1976 "Measurement of neutrons and x-rays from a vacuum spark" Physics letters 57A, 233 - 236, S. Lee and H. Conrads.

15. 1976 "The focus and CTR" Proc. Symposium on Plasma Focus Work in K.L., Malaysia, Paper 1 - S. Lee.

16. 1976 " Plasma Focus Work in K.L.," Proc. Symposium on Plasma Focus Work in K.L., Malaysia, Paper 2 - S. Lee.

17. 1976 "Effect of an axial bias field on the plasma focus" proc. of Symposium on Plasma Focus Work in K.L., Malaysia, Paper 4 - A.C. Chew, S. Lee, B.C. Tar

18. 1977 "Plasma Fusion Research at the University of Malaya" Simposium Fizik (U.M.) Mac 1977. Proceedings of Symposium pg. 67 - 74, S. Lee.

19. 1977 "Multiple Ionization in an Argon Plasma Focus" Simposium Fizik (U.M.) Mac 1977. Proceedings of Symposium pg. 149 - 154, Y.C. Yong, S. Lee.

20. 1977 "Neutron Detectors for Verification of Focus Energy Scaling" Simposium Fizik (U.M.) Mac 1977. Proceedings of Symposium pg. 103 - 108, C.S. Wong, S.P. Moo, S. Lee.

21. 1979 "Laser Safety Precautions" Proceedings of the Colloquium on Laser Developments and Applications Pg. 85-94, B.C. Tan, S.A. Husain, S. Lee, K.O. Lee, K.S. Low, A.C. Chew, Y.H. Chen, C. Grey Morgan.

22. 1979 "Laser Research Program at the University of Malaya" Proceedings of the Colloquium on Laser Developments and Applications Pg. 14-22, B.C. Tan, S.A. Husain, S. Lee, K.O. Lee, K.S. Low, A.C. Chew, Y.H. Chen, Raja Mustapha, C. Grey Morgan.

Int. J. Electronics, 1967, Vol. 22, No. 2, 193–196

RESEARCH NOTE

Transition from Electromagnetic to Hot-gas Driver in an Electric Shock Experiment†

By H. H. Teh and S. Lee

Department of Physics, University of Malaya, Kuala Lumpur, Malaya

[Received March 25, 1967]

§ Introduction

In the electric shock experiment described below it is shown that as the ambient pressure of the shock tube is increased there is a change in the nature of the piston which drives the shock front down the expansion chamber. At very low pressure the driver is electromagnetic, but at a slightly higher pressure the driver is the hot gas from the electric discharge.

§ 2. Experimental Arrangement

Two ring electrodes of 5 cm diameter were joined together by a quartz neck of the same diameter, serving as the discharge chamber. The ring electrodes were connected to two Pyrex glass tubes of the same diameter, placed along the axis of the discharge chamber and leading to two glass bulbs which served as sinks for the shock waves, as shown in fig. 1. A pinched discharge was initiated between the ring electrodes from a

Fig. 1

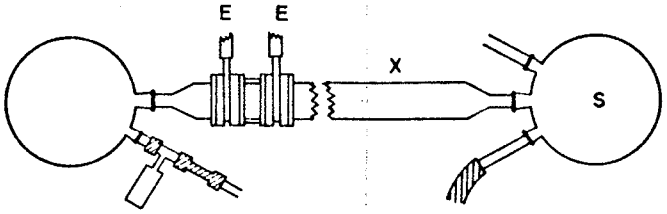

Electric shock tube with ring electrodes; EE, electrodes, X, expansion chamber, S, sink.

condenser bank consisting of 100 condensers of 0·6 microfarad each and charged at over 5 kv. The velocity of the luminous front travelling through one of the ring electrodes along the Pyrex tube which served as the expansion chamber was measured by photomultipliers. The times of arrival of the luminous front at stations placed 6 cm apart were recorded on a dual-trace oscilloscope and the average velocity was computed from the oscillograms.

---

† Communicated by Professor K. G. Emeleus.

§ 3. Observations

In the first series of experiments, the discharge voltage was kept constant at 10·4 kv while the ambient pressure was varied. The gas used was argon. The results are shown in fig. 2, where the logarithm of the peak velocity of the luminous front is plotted against the logarithm of the ambient pressure. The graph shows two straight lines, one with gradient $-0{\cdot}22$ and the other with gradient $-0{\cdot}67$.

In the second series of experiments the ambient pressure was kept constant while the discharge voltage was varied. The gas used was hydrogen. The results are shown in fig. 3, where the logarithm of the peak velocity of the luminous front is plotted against the logarithm of the discharge voltage. The gradient of the straight line graph is 0·495.

§ 4. Discussion

From figs. 2 and 3 it will be seen that at very low ambient pressure the peak velocity of the luminous front varies approximately as $P^{-1/4}$ and as $V^{1/2}$. This agrees with the snow-plough model of a pinch discharge, where the maximum velocity of the current sheath is given by:

$$U_{\max} = K\left(\frac{c^2 I^2}{100\pi\rho}\right)^{1/4},$$

where K is a constant, c the velocity of light, and ρ the gas density. This indicates that the driver of the shock is electromagnetic in nature like the driver of the current sheath in a pinch discharge. According to Cloupeau (1963), at below 1 mm Hg pressure the luminous shock front coincides with the contact surface. It is, therefore, immaterial whether the luminous front is the shock front or the contact surface. They both move with the same velocity.

However, at higher pressures, fig. 2 shows that $U_{\max}$ varies as $P^{-2/3}$, and there seems to be a clear transition from the region where $U_{\max}$ varies as $P^{-1/4}$ to the region where it varies as $P^{-2/3}$.

Now, according to Fowler and Lee (1955), the apparent resistance of the discharge, R, equal to the ratio of the voltage, V, across the electrodes and the discharge current, I, is given by:

$$R = R_0 \exp(-\theta I) + R_m + V_c/I,$$

where $V_c = 17 \pm 6$ for argon, $\theta = 5{\cdot}4 \times 10^5$,

$$R_0 \quad \text{varies as} \quad \frac{K_0 P^{2/3}}{V},$$

and

$$R_m \quad \text{varies as} \quad \frac{K_m P^{1/5}}{V}.$$

$K_0 = 200$ and $K_m = 220$ for argon (Fowler 1964). $I = 3 \times 10^4$ A in the present experiment.

Fig. 2

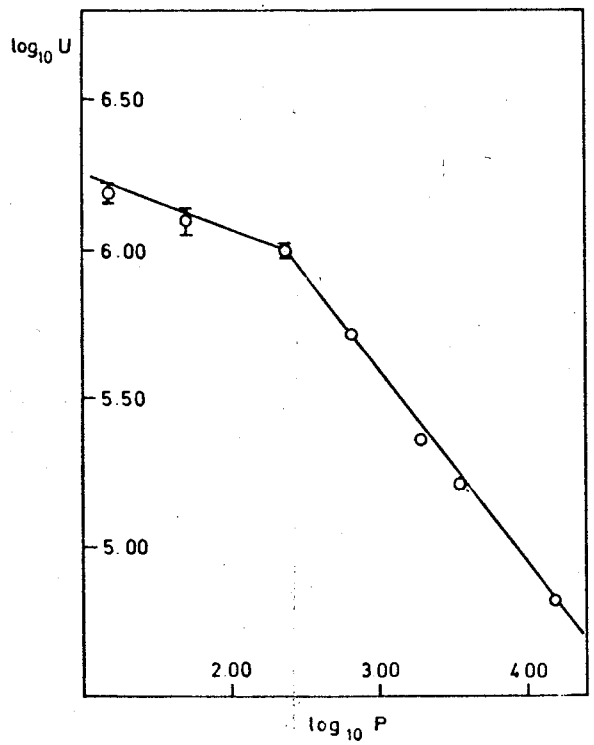

Graph of $\log_{10} U$ plotted against $\log_{10} P$ for argon at a constant voltage of 10·4 kv. U is in cm sec, P in 10^{-3} mm Hg.

Fig. 3

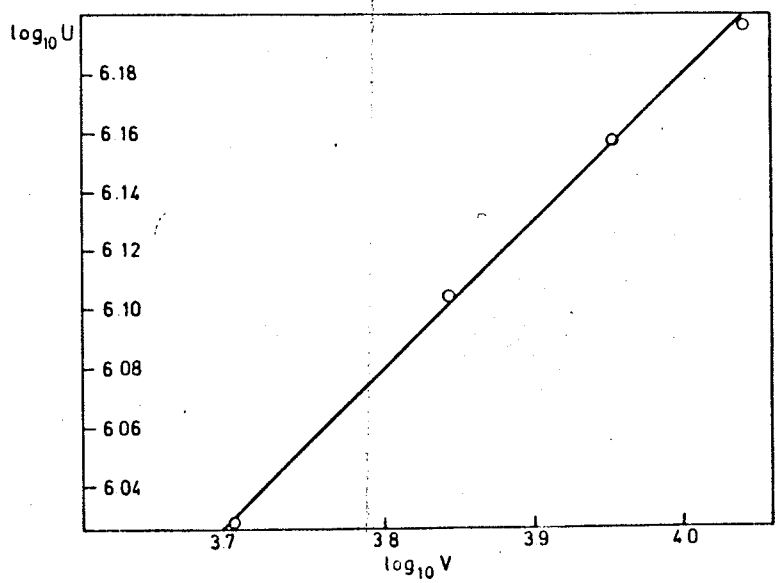

Graph of $\log_{10} U$ plotted against $\log_{10} V$ for hydrogen at a constant pressure of 1 mm Hg. Units as for fig. 2.

For very small values of t and large values of I, the second and third terms in the equation are small compared to the first term. R may, therefore, be taken as varying as R_0 or as $P^{2/3}$.

Thus, the second section of the graph in fig. 3 shows that the maximum velocity of the luminous front varies inversely as R_0. Since $I_0 = V/R_0$ where I_0 is the discharge current at very small t, this further shows that the maximum velocity of the luminous front varies as $I_0^2 R_0$ which is the rate of Coulomb heating of the gas in the discharge.

This interpretation agrees with Cloupeau's observation (1963) that "the luminous emission observed along the tube should often be interpreted as being due to direct ionization produced by the driver discharge and not to thermal ionization produced by the shock wave". It also shows that at pressures higher than 0·24 mm Hg, in this particular case, the driver is the hot gas from the discharge. A transition in shock wave velocity at nearly the same pressure has been recorded by Fowler (1966). It may be pointed out that most of Cloupeau's results were obtained at a relatively high pressure.

§ 5. Conclusion

In a shock driven by a pinched discharge, the driver is electromagnetic in nature when the pressure is very low. At higher pressures the driver is the hot gas from the discharge. The transition from one form of driver to the other seems to be quite distinct.

Acknowledgments

The authors wish to thank Dr. A. von Engel, Professor R. G. Fowler and Professor K. G. Emeleus for helpful discussion.

References

Cloupeau, M., 1963, *Physics Fluids*, **6**, 679.

Fowler, R. G., 1964, *Advances in Electronics and Electron Physics*, Vol. 20 (Academic Press), pp. 40, 41; 1966, *Rev. scient. Instrum.*, **37**, 545.

Fowler, R. G., and Lee, R. J., 1955, *Phys. Rev.*, **100**, 1234.

[*The Editors do not hold themselves responsible for the views expressed by their correspondents.*]

Procs. Symposium on Physics, Singapore 1971

HIGH CURRENT DISCHARGE IN PLASMA FOCUS EXPERIMENT

S. LEE, Y.H. CHEN, S.P. CHOW, B.C. TAN
H.H. TEH and S.P. THONG

Department of Physics, University of Malaya, Kuala Lumpur, Malaysia.

Abstract: The main features of the discharge experiment include the assembling of the 40 KV, 0.6 μF condensers in modules of 25, each switched by a 7703 ignitron. With two modules, the peak current obtainable at 26.8 KV is 505 KA. A method of ' current reinforcement' by delaying the discharge of one module relative to the other is also described.

This high current discharge is being applied to a plasma focus experiment; in which the ' snow-plowed' gas of a coaxial shock tube is focussed by inertial and magnetic forces to form a small region of extreme temperature, particle density and pressure. Streak and framing image converter pictures are presented of the steady shock region and the focus region.

Acknowledgement

We thank Mr. Lee Boon Kian and Mr. Ho Tet Soon for technical assistance in this project.

1. Introduction

The experimental facility centres upon the high current condenser discharge system currently undergoing development. One hundred condensers, each rated at 0.6μF, 40 KV, are being assembled, the total energy capacity being 48 KJ. The switching method for this system has previously been reported [1]. The method consists of a main spark gap switch (mechanically operated), in series with a parallel bank of auxiliary spark gaps, each in series with a condenser. The main advantage of this system is that, during charging, the voltage difference across the condensers is shared between the auxiliary spark gaps and the main switch, allowing the high voltage side of the main switch and the collector plate of the condensers to be at approximately half the bank voltage. Using ten condensers operating at 15 kilovolt, a peak current of 47 kiloamp was reported, with a discharge cycle time T of 10μs.

In the present extension to this work, the auxiliary spark gap system has been retined, and the main emphasis has been i) to increase the number of condensers to 50, ii) to operate at higher voltages and iii) to reduce the switch inductance. Tested at 26.8 KV , a peak current of 505 KA was meaured.

2. Reduction of inductance

A condenser and its transmission cable can be taken as an inductance L_o in series with a capacitance C_o . Discharging this system into a load of negligible impedance through a switch of inductance L_s gives a periodic time of $T = 2\pi [C_o (L_o + L_s)]^{1/2}$, assuming the damping is small. If we parallel n such condensers and cables, discharging into the same load and through the same switch, the periodic time is now $T = 2\pi [nC_o (L_o/n + L_s)]^{1/2}$. If we now have the condition $L_s \ll L_o/n$, the periodic time T remains unchanged with increase in the number of parallel branches. The current amplitude in such a case increases in direct proportion to n. This is the optimum in high current discharge design. However, as n is

increased, this condition is not fulfilled. For example, with a L_o of 500 nH (typical of this system), and n = 10, this condition cannot be fulfilled as, in the present state of the art, switch inductance, for such high currents and voltages, cannot be reduced much below 20 nH. For example, using wide, parallel-plate geometry for the lowest possible inductance, the free-air, mechanically operated switch of this system was found to have an inductance of 22 nH. Therefore, for highest performance, it is necessary to have modules, each with n condensers and each switched by a low inductance switch, iwth n being kept small.

3. The module system

As a compromise between minimizing inductance and maximizing technical economy, the present system uses modules of 25 condensers, each module being switched by a 7703 ignitron. This tube, rated at 100KA peak current, has been tested in this system to 300 KA each, without affecting performance. Tube inductance is 40 nH. The circuit for a module is shown in Fig. 1. The load is put across

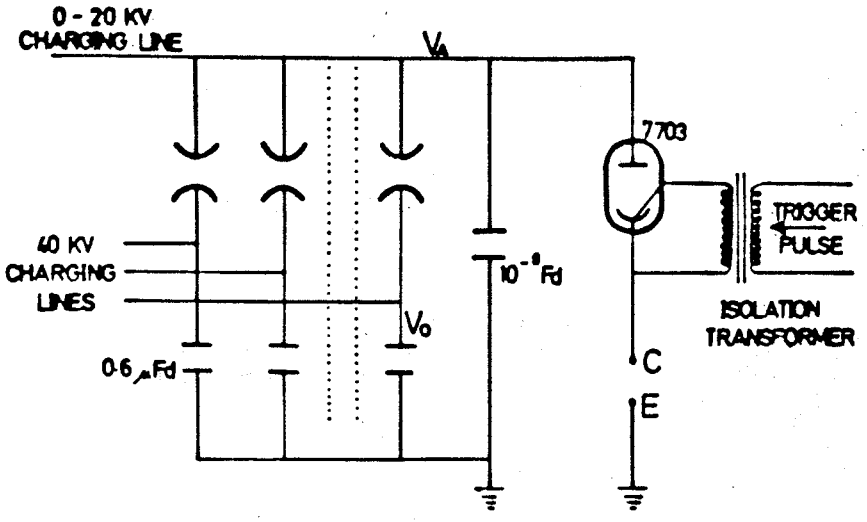

Fig. 1 25-CONDENSER MODULE

CE. For parallel operation of modules, the cathodes of the ignitrons are strapped together at C . Such a cathode-strapped system affords maximum isolation of modules. The testing has proceeded to the following stage:

one module	28 KV	$\hat{I}$ = 306 KA	T = 8.2 μs
two modules	26.8 KV	$\hat{I}$ = 505 KA	T = 8.4 μs.

The slight increase in T, for two-module operation, representing a slight loss in peak current, was due to non-negligible load inductance. These measurements were made with current coils, both in the current-transformer mode and in the Rogowski mode.

An added advantage of the module system is that the modules can be fired with predetermined phase difference ϕ between them, ϕ being variable from 0 to 360° and beyond. This is accomplished by setting a delay between the trigger pulses to the ignitrons (fig. 2).

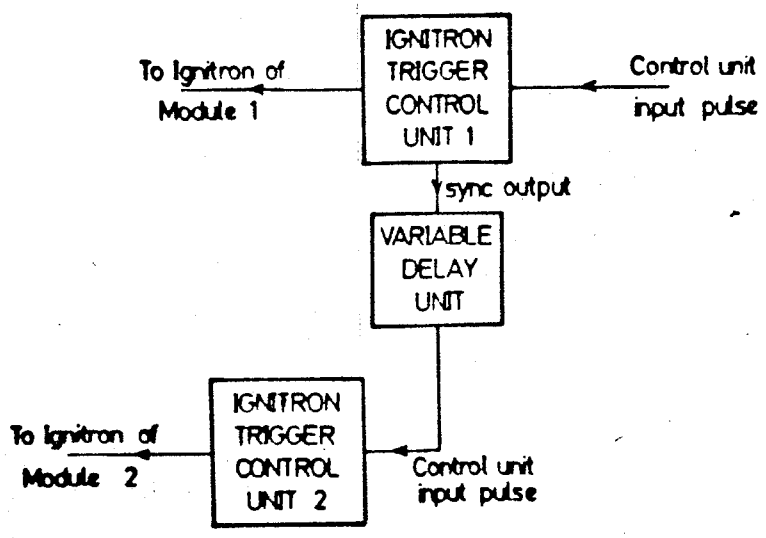

Fig. 2 SCHEMATIC OF INTER-MODULE PHASE ADJUSTMENT

With this mode of operation (current reinforcement), a small current discharge can be used to preheat a plasma, preparing it for the

subsequent larger current. Reproducible control of Φ (to better than 4^{o} , corresponding to 0.1 microsec) is achieved. An example is shown in Fig. 3, of current measurements with two modules

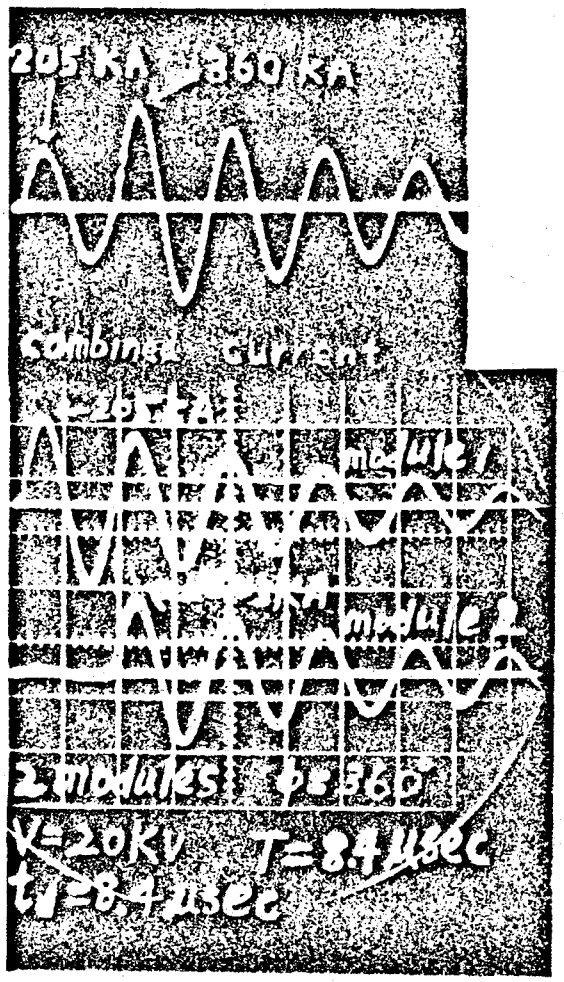

operated with a phase difference of 360^{o}.

Fig. 3 Oscillograms of discharge currents of two modules in ' delayed' mode of operation: measured with calibrated current transformers. Top trace : combined current, Middle: current of module 1, Bottom: current of module 2. Time scale: 5 μs/division.

4. Plasma Focus Experiment:

In parallel with the development of the condenser bank, a plasma focus experiment is in progress. This is a remarkably simple way to generate a plasma of the most extreme conditions of temperature, density and pressure [2]. A current sheet (fig. 4), propelled by its

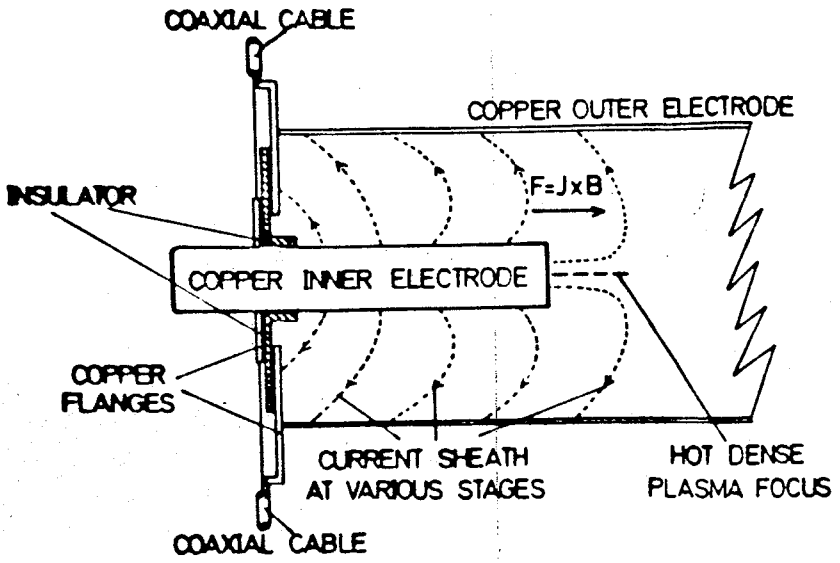

Fig.4. SCHEMATIC OF PLASMA FOCUS EXPERIMENT

own J x B force, is propagated down the annular region between two coaxial cylinders, preceded by a shock front. This is called the steady shock region. The inner, conducting, cylinder terminates in a flat face (the tongue). On arrival at the tongue, the shock wave implodes inwards towards the axis, followed by the current sheet. The original gas in the tube, heated by the shock wave, and ' show-plowed' into the region between the shock front and the current sheet, is now further compressed by the inertial forces of the fast moving plasma and by the magnetic forces of the current sheet, into a tiny filament along the axis.

In a similar device, Mather and Bottoms [2] have estimated the diameter of the filament as 0.1 mm, and the particle density as 10^{25} to 10^{26} particles/m^3. With a current of 500 KA, the pressure due to the azimuthal magnetic field pinching this column is seen to be:

$$\frac{B^2}{2\mu} = \frac{\mu_i^2}{8\pi^2 r^2} = 1.6 \times 10^{10}\ N/m^2 \simeq 10^5 \text{ atmospheres}$$

Assuming there is a moment of static equilibrium at minimum focus, the plasma temperature can be estimated as 2 kev $2 \times 10^{7\,o}K$. Such a plasma opens up a very wide field of soft x-ray spectorscopy , which in this region of temperature and density, particularly for hydrogen and its isotopes, takes over from optical and u.v. spectroscopy as the important diagnostic tool. Mather has also observed fluxes of 10^9 neutrons per discharge from the focus region.

In these experiments, we have used a copper centre electrode 5 cm in diameter, and an outer glass tube (9 cm in diameter) in place of the usual outer copper cylinder (Fig. 4a). This choice of an outer glass

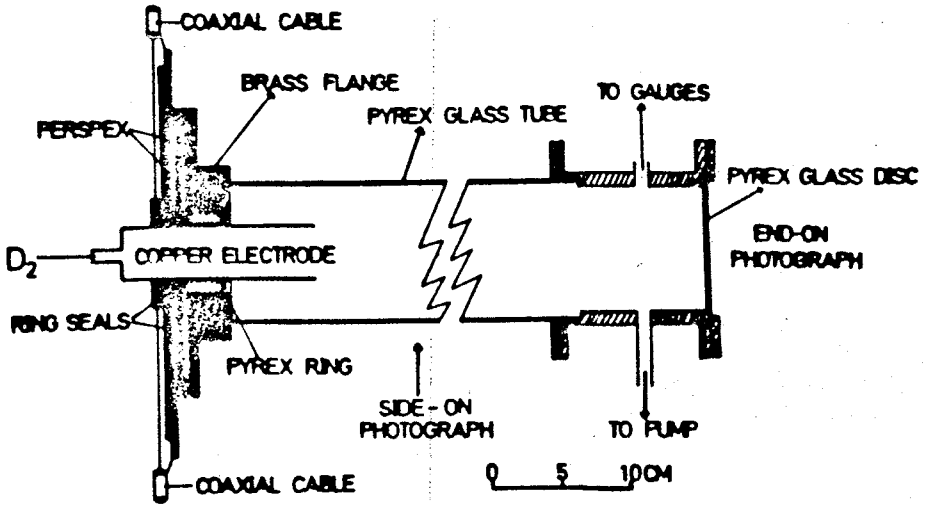

Fig 4a COAXIAL FOCUS DEVICE WITH GLASS RETURN

cylinder enables photographic observations of the steady shock region, and the transition to the plasma focus; and is based on the observation of Brennan [3] that the gross behaviour of a coaxial shock tube is independent of whether the outer electrode is of copper or glass. Fig. 5

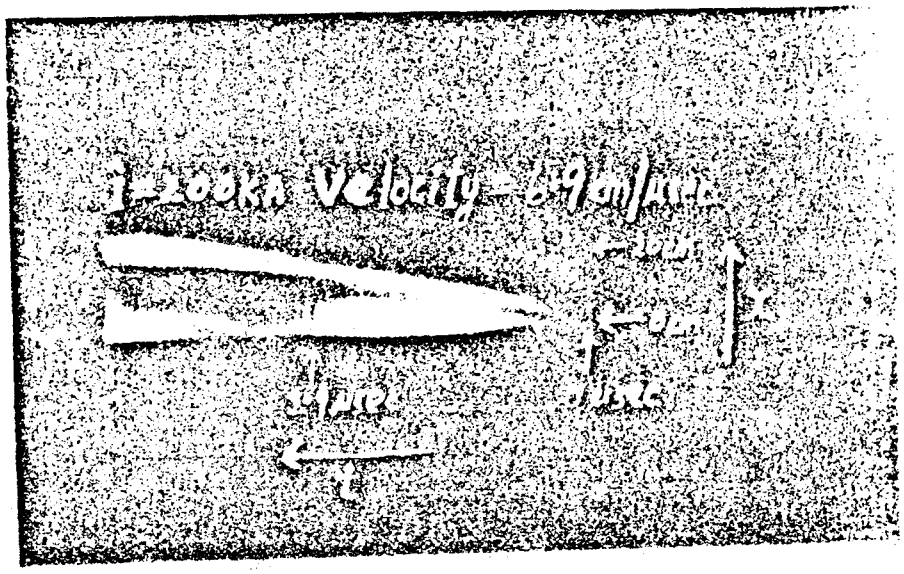

Fig. 5 Streak picture from side of pyrex return focus tube. The back-wall is indicated by ' 0 CM' , direction down the tube by x and time by t .

shows a streak picture giving the distance-time relationship of the luminous fronts. Besides giving the propagation velocities, this streak picture also shows the motion of the second current sheet moving out from the back wall at the start of the second half cycle. It also indicates ' current shedding' during the first half cycle; i.e. not all the current moves down the tube with the main current sheet; some of it moves with very slow velocity casuing the luminous patch that hardly leaves x = 0 (i.e. the back wall). There is also indication of shock front-

current sheet separation; which is shown more clearly in fig. 6. The less luminous shock front ahead of the more luminous current sheet arrives at the tongue first, as indicated by the onset of luminosity in the tongue region, before the arrival of the current sheet.

Framing photographs of the focus, both end-on and from the side, have also been taken. The framing rate of one per μ s (with 0.1 μ s exposure) is not really satisfactory, since the photographs indicate

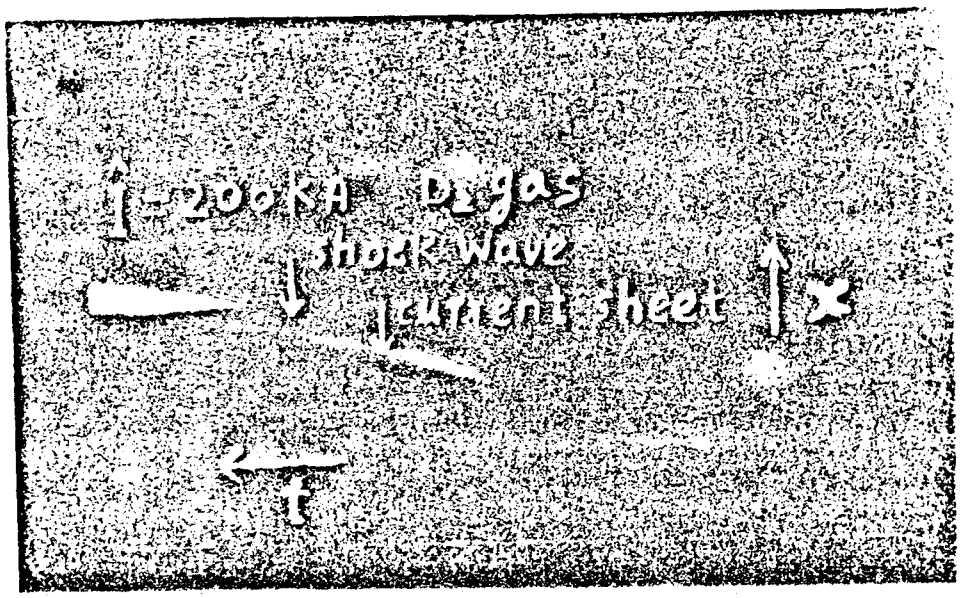

Fig. 6 Streak picture showing shokc front-current sheet separation. In the shock propagation region, the shock front, indicated here, is faintly visible in the polaroid original. At the focussing face, the sudden burst of luminosity indicates the arrival of the shock wave.

that considerable action is missed between frames. Fig. 7 shows the gross focussing action, followed by expansion, as seen from the side. The sequence is as indicated by the numbers, and in each frame, the

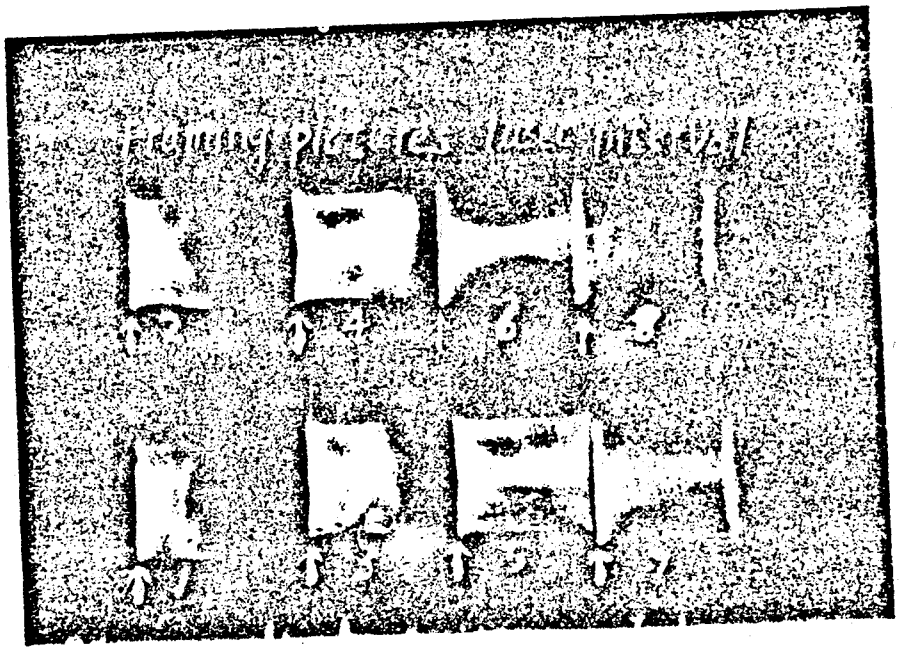

Fig. 7 Image Converter pictures of gross focussing action, taken from the side.

' tongue' is near the left edge and in line with it. Fig. 8 has one frame (No. 4) which shows quite clearly the focussing action of the current

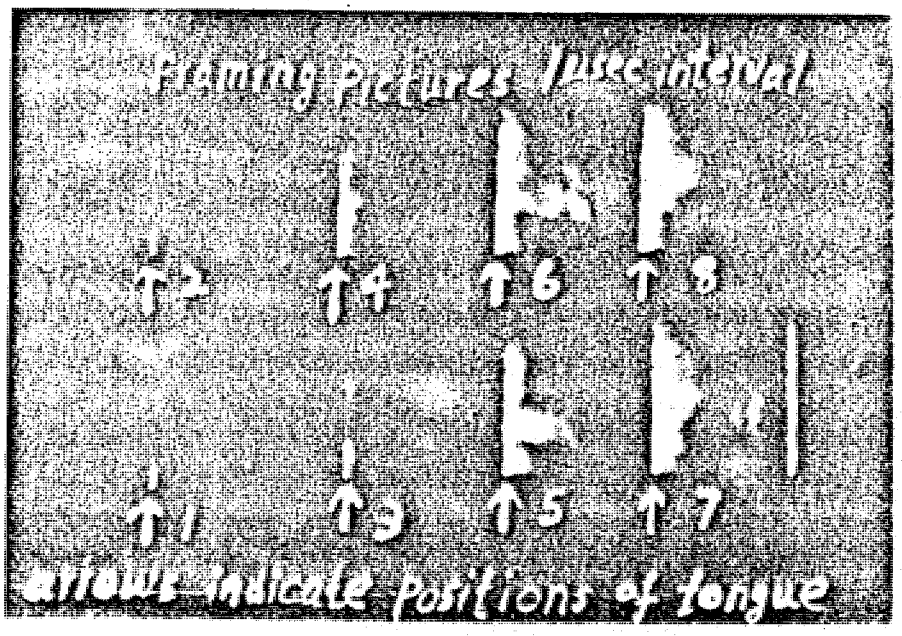

Fig. 8 Image Converter pictures showing focussing action of current sheet (frame 4), taken from the side.

sheet. Fig. 9 shows a sequence taken end-on. The minimum focus occurs at about the time of the second frame. Fig. 10 shows a current trace witha distinct dip occurring at the time of focus, indicating a sharp increase in inductance at this time.

One important observation is that in certain ranges of operation, the current sheet is regular and collapses symmetrically towards the

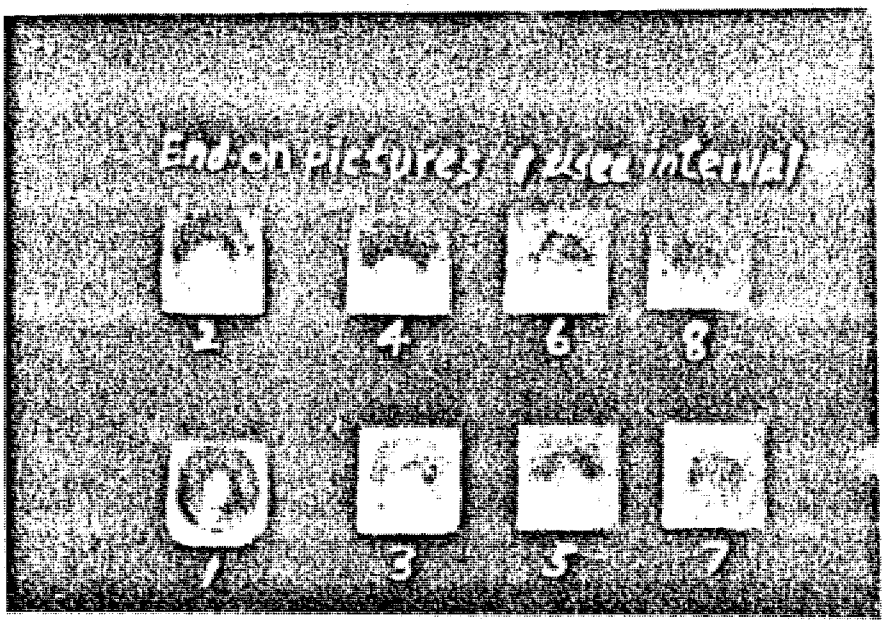

Fig. 9 Image Converter pictures taken end-on. Minimum focus occurs about the time of frame 2.

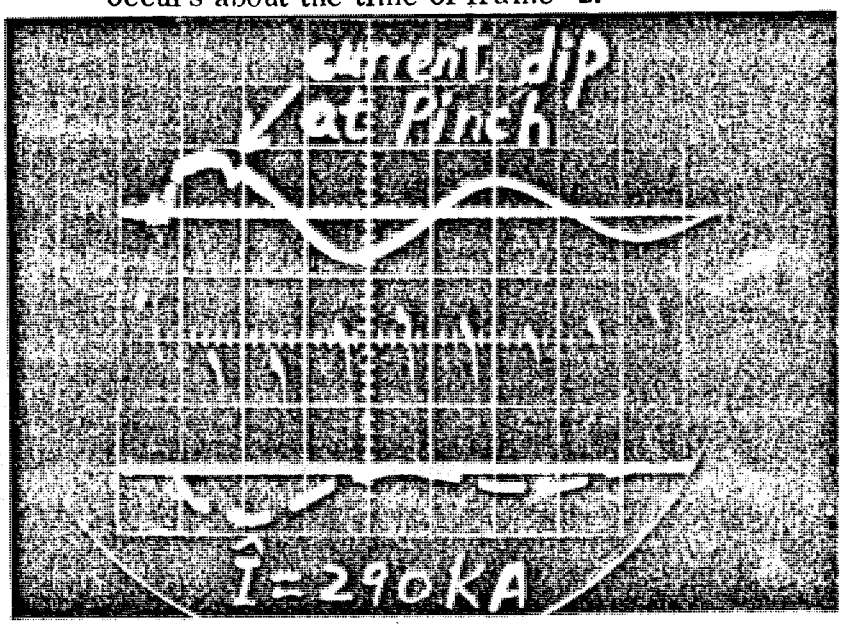

Fig. 10 Oscilogram of discharge current, showing current dip at time of focus (Top trace). Image Converter timing markers are displayed on bottom trace.

193

axis, whereas in other ranges, irregularity and asymmetry dominate. The important parameters affecting this situation appear to include a large number of parameters which we have varied, namely, operating pressure, peak current, electrode length and even back wall insulation shape and material. Another important observation is that the foci formed from subsequent half cycles appear to be more symmetrical than the focus fo the first half cycle. An important consideration is whether sufficient gas is left behind by the ' snow-plow' action of the first current sheet to allow dense foci to be formed by the subsequent half cycles. If such subsequent dense foci can be formed, the current reinforcement method, mentioned above, can prove of importance. For example, a higher frequency current, of 100 to 200 KA, from a sub-module of 5 condensers, can be discharged to form the first one or two foci, to be reinforced by a 500 KA peak current in the third half cycle. This work is in progress, together with the development of two other modules to bring the current capability to above 1000 KA. Plans for magnetic probing, neutron and soft x-ray detection and faster photography are also being made.

Fig. 11 shows a photograph of the plasma focus device at present in operation.

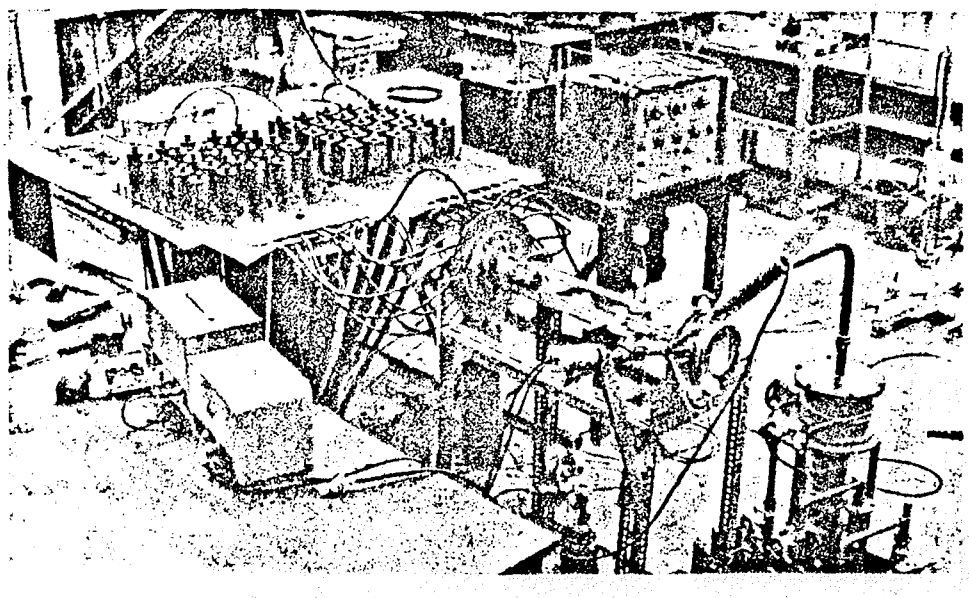

Fig. 11 Photograph of experimental set-up. In the centre is shown the pyrex return focus tube. The inner electrode can be seen through the glass tube. The high voltage collector plates of the two modules, each with 25 cable connections, are also shown with the coaxial transmission cables leading downwards to the condensers, which are on a lower platform, not shown.

References:

[1] C. P. Lim, S. P. Thong and B. C. Tan, Journal of SNAS 1 (1969) 63

[2] J. W. Mather and P. J. Bottoms, Physics of Fluids 11 (1968) 611

[3] M. H. Brennan, Seven AINSE Plasma Physics Conference, 1969; 'Discharge and Plasma Physics Research at Flinders University' (Unpublished).

MALAYAN SCIENTIST VOL. 6. 1971/72 UNIVERSITY OF MALAYA

PENYELIDIKAN FIZIK PELASMA

Oleh

B. C. TAN DAN S. LEE

Semua benda terdiri daripada atom2. Tiap2 atom mempunyai satu nukelias yang berchas positif, nukelias itu di-kelilingi oleh lektron2 yang berchas negatif. Nombor2 chas positif dan chas negatif ialah sama, akibat-nya atom itu nuteral. Tetapi, jika suhu suatu benda di-naikkan ka-titek yang chukup tinggi, apabila satu dua atau pun lebeh lektron2 mendapat tenaga haba mereka boleh mencheraikan dari atom itu menjadi lektron2 bebas. Keadaan atom tersebut di-katakan terion dan sa-kumpulan atom2 yang terion dan lektron2 bebas di-namakan pelasma. Walau pun di-bumi ini pelasma jati tidak di-adakan kechuali kejadian saketika, umpama-nya di-kawasan dimana kilat berlaku atau didalam pusat kebakaran hutan, adalah di-taksirkan bahawa lebeh 99.9 peratus benda di-alam yang di-ketahui ini ialah didalam keadaan pelasma. Kebanyakan pelasma ini terujud di-dalam dua bentok, iaitu sasuatu gas yang terlampau nipis yang bergerak di-luas antara chakrawala2, dan yang kedua-nya gas yang terlampau padat di-bintang2, chontoh-nya matahari.

Fizik Pelasma ialah sesuatu chawangan Sains yang mustahak oleh kerana pengetahuan keadaan pelasma tentu-lah dapat membantu kita memaham bahagian besar alam yang di-ketahui. Sechara yang baik untok mengetahui Fizik Pelasma ialah mempelajari tindakbalas2 pelasma di-matahari. Tindakbalas2 tersebut membakalkan tenaga yang terbesar sekali serta dengan tidak berkeputusan dan tenaga ini-lah menyokong semua jiwa2 di-bumi kita. Satu soalan yang kita mesti bertanya ialah, boleh-kah sesuatu puncha tenaga seperti ini di-benakan di-makmal supaya menambahkan puncha2 tenaga di-bumi ini yang berkurang dengan chepat-nya iaitu minyak tanah dan batu arang.

Satu masaalah yang sangat menarek ialah berkenaan dengan keluaran tenaga matahari iaitu sebanyak 4×10^{33} erga/saat. Bagaimana-kah tenaga yang sebesar demikian di-buat ? Suhu permukaan effektif matahari kira2 6000°C dan suhu dalam-nya kira2 setinggi 20,000,000°C. Pada suhu semacham ini tenaga boleh di-keluarkan didalam peroses paduan nukelias. Sebahagian besar dari matahari terdiri daripada pelasma hiderojan, iaitu sekumpulan nukelias2 hiderojan (H^1) dan letron2 bebas. Persamaan2 paduan nukelias itu ialah :—

$$_1H^1 + {}_1H^1 \longrightarrow {}_1H^2 + \beta^+ + \nu \qquad \text{(i)}$$

$$_1H^1 + {}_1H^2 \longrightarrow {}_2He^3 + \gamma \qquad \text{(ii)}$$

$$_2He^3 + {}_2He^3 \longrightarrow {}_2He^4 + 2\,{}_1H^1 \qquad \text{(iii)}$$

Untuk kejadian bersamaan yang ketiga, tindakbalas2 pertama dan kedua haruslah berlaku dua kali tiap2 satu Keputusaan persamaan2 ialah :—

$$4\,{}_1H^1 \longrightarrow {}_2He^4 + 2\,{}_1\beta^+ + 2\gamma + 2\nu$$

Positeron2 β^+ di-musnahkan apabila mereka menemui dengan lektron2 bebas untuk membentukkan chahaya2 γ. Tenaga kinetik nuterino ν sangat kechil. Akibat-nya, empat nukelias2 hiderojan menjadi satu nukelias helian

didalam tindakbalas paduan itu. Jisim empat nukelias2 hiderojan itu lebeh daripada jisim satu nukelias helian. Perbezaan jisim itu di-tukarkan menjadi tenaga menurut perhubongan Einstein yang terkenal, $E = mc^2$. Persamaan ini menentukan bahawa jisim m gram senilai dengan tenaga mc^2 erga, $c = 3 \times 10^{10}$ sm/saat ialah laju chahaya. Dengan mengunakan perhubongan Einstein itu, jumlah keluaran tenaga apabila empat nukelias2 hiderojan menukarkan menjadi satu nukelias helian (He^4) ialah kira2 4×10^{-5} erga atau 25 MeV (eV ialah yunit tenaga. $1 eV = 1.6 \times 10^{-12}$ erga dan 1 MeV = 1,000,000 eV). Bagitulah, pada tiap2 nukelias hiderojan yang di-musnahkan tenaga sebanyak 1×10^{-5} erga di-ujudkan dan oleh sebab satu gram unsur matahari mempunyai 2×10^{23} nukelias hiderojan, bekalan tenaga itu boleh mengeluarkan kira2 2×10^{18} erga/gram. Kita boleh mengitong bahawa 2×10^5 gram unsur matahari di-binasakan tiap2 saat supaya mengbekalkan tenaga sebanyak 4×10^{23} erga/saat. Dalam yunit biasa dan mudah difahami, 17,000 tan unsur matahari itu di-musnahkan ataupun di-bakarkan. Mujurlah, matahari berat-nya 2×10^{27} tan serta buleh-lah tahan lagi berjuta2 tahun.

Dengan jelas-nya kita dapat melihat bahawa peroses paduan nukelias ialah sesuatu bekalan tenaga yang besar sekali. Masaalah sekarang ialah bagaimana tenaga ini dapat di-kawalkan serta di-gunakan supaya membuat kerja yang bertaedah bagi manusia. Bom hiderojan ialah chontoh satu paduan nukelias yang tidak di-kawal dan kita mengetahui malapetaka yang boleh di-datangi oleh-nya. Walau pun beberapa pakar2 Fizik diseluroh dunia menumpukan fikiran2-nya terhadap masaalah tindakbalas habanukelias terkawal (controlled thermonuclear reaction or CTR) sampai pada masa sekarang, tidak sesiapa pun berjaya membena sebuah riaktor CTR yang selamat, ekonomi dan chekap. Akan tetapi, usaha mencharı-nya tetap berjalan terus. Keperchayaan sekarang ialah fizik asasi pelasma tidak difahami dengan betul. Oleh kerana itu, penubohan didalam tiap2 ranchangan mencharı riaktor CTR adalah suatu kursus bagi memahami fizik asasi pelasma.

Dalam penyesiatan makmal pelasma yang padat dan panas adalah dua mesaalah, yang pertama penghasilan pelasma itu dan kedua mengumpulkan-nya. Untuk penghasilan biasa-nya tenaga di-panchutkan masok ka-gas didalam satu bekas. Tenaga itu mesti di-panchutkan dengan chukup chepat dan chara yang hanya dapat dilakukan ialah dengan mengunakan litar letrik. Sambil pelasma itu menjadi panas, ia mengbangunkan tekanan yang sangat kuat dan mulai mengembang. Pengembangan itu menyebabkan penyejokan, lagi pula apabila pelasma itu melanggar dinding bekas-nya, ia menyejokkan diri-nya lagi. Jika peroses tersebut di-biarkan, dengan pantas-nya suhu menjadi terlamau rendah untuk menghidupkan keadaan pelasma itu. Dengan mengunakan magnet masaalah mengumpulkan pelasma didalam suatu isi padu terhad sudah di-uraikan dengan sedikit sebanyak. Zarah2 yang berchas di-pengarohi oleh medan2 magnet, akibat-nya medan2-nya boleh di-bentokkan dan zarah2 tersebut di-tahan supaya tidak keluar daripada sistem itu.

Suatu ranchangan untok menyelideki Fizik Pelasma telah di-jalankan di-Jabatan Fizik Universiti Malaya beberapa tahun yang kebelangan ini. Fasa pertama untok mendapatkan perkakas2 yang sesuai sudah selesai (sudah semestinya perkakas2 khas, mesti dibeli dari masa kesemasa). Makmal Pelasma sekarang mempunyai sebuah kamera Imacon yang boleh mengambil 10 juta foto sesaat dan beberapa buah rakamayun yang penting perlu untok ukoran asasi. Bekalan tenaga untok perchubaan2 datang-nya daripada suatu benk terdiri daripada 100 buah kondensar2 (muatan sebuatnya 0.6uf). Tenaga maksima di-simpan oleh benk itu sebanyak 48.000 Joules jika voltan tindakan

ialah 40kV. Sunggoh pun ini bukanlah nilai tenaga yang menaajubkan, tetapi jika kita ingat bahawa benk ini berkeupayaan melepaskan tenaga-nya dalam 10 mikerosaat, kuasa panchutan maksima yang di-dapati ialah kira2 4 x 10^8 wat (400 megawat). Jika hanya 480 Joules (1%) daripada tenaga ini ditaroh kesuatu fokas pelasma isipadu 1/100 sm^{-3}), ini masch suatu tenaga yang menaajubkan didalam ruang dan masa. Pengbenaan benk tersebut di-jalankan dalam empat peringkat. Sesuku benk itu telah selesai dan di-gunakan dengan senentiasa menyampai ke 350,000 ampiar arus maksima. Didalam masa menulis ini, lagi sesuku benk telah di-uji dan arus maksima sebanyak 505,000 ampiar di-dapati, voltan tindakan hanya 26.8 kV. Pada penengahan tahun 1971, seluroh benk itu akan di-bereskan. Arus maksima yang boleh di-harap lebeh sedikit dari satu juta ampiar.

Masaalah2 teknik yang terbabit dengan pengeluaran dan pengawalan arus yang teramat besar sangat kompleks tetapi menarek hati. Chontoh-nya, keperluan untok arohan terkechil memerlukan lorong2 kadaralir yang berhampiran. Tetapi, oleh sebab kedekatan-nya, masaalah penebatan terbit. Tambahan pula denyutan sawat sebanyak beberapa ratus tan menindakkan pada tiap2 inchi pengalir sewaktu arus maksima. Lagi satu masaalah mengenai pemetek untok arus yang terlampau tinggi ini. Beberapa buah ikniteron sedang di-gunakan tetapi ketetapan pemetekan ikniteron itu adalah terhad kira2 0.1 pejuta saat (or 1 x 10^{-7} sec.). Lama-kelamaan ketetapan ini pun tidak chukup baik.

Teknik2 asasi untok pengukoran arus, halaju kepala arus (kira2 200,000 b.s.j.), voltan dan penyegerakan masa bawah mikerosaat sekarang dikaji, bersama2 dengan membena dan menguji benk kondenser, sistem2 hampagas dan perkakas fokas pelasma. Kawasan2 fokas pelasma sudah ditetapkan. Perojek yang di-jalankan sedang berpindah ka-fasa kedua, pada masa ini pemetek yang lebeh baik, ukoran2 sepektera, dugaan magnet dan pengesanan nuteron akan di-buat

Tindakbalas paduan nukelias yang sedang di-kaji ia-lah :—

$$_1D^2 + {}_1D^2 \longrightarrow {}_2He^3 + {}_0n^1$$

iaitu dua deuteron (D^2) mengfius serta satu nukelias helian dan satu nuteron (n^1) dikeluarkan bersama2 dengan tenaga sebanyak 3.27 MeV.

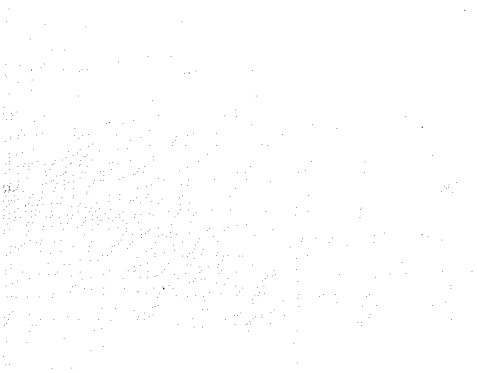

Bow-shock effects on probe measurements

S. Lee
Physics Department, University of Malaya, Kuala Lumpur, Malaysia

R. J. Sandeman
Physics Department, SGS, Australian National University, Canberra, Australia

(Received 29 November 1971; in final form 24 March 1972)

Probe measurements of pressure and magnetic field are of importance in electromagnetic-shock-tube diagnostics. The effect of the bow shock on such measurements, in transverse shock waves in the ionizing-hydromagnetic regimes, is considered. The bow-shock jump equations are first solved, then the total stagnation pressure is obtained assuming an isentropic compression towards the stagnation point. The pressure measured at the stagnation point of the probe is seen to be less than the free-stream total gas pressure. The magnetic field is considered in terms of a simple model taking into account the field and flow distributions outside of the stagnation streamline. This analysis shows that the magnetic field measured at a coil is also less than the free-stream magnetic field.

I. INTRODUCTION

The measurements of magnetic field and pressure are of basic importance in the diagnostics of the electromagnetic shock tube. In the presence of appreciable electron density from precursor ionization, shock ionization, or driver-current ionization, the only direct way of detecting the "viscous" shock front is by means of the pressure probe. Rudderlow's work[1] has shown that a properly designed probe will also yield quantitative information on pressure amplitudes. The presence of the probe in the flow causes perturbation. The distortion of the magnetic field due to the effect of the probe on the current flow has already been discussed.[2]

Another perturbation is the presence of a bow shock, since a bow shock will shield the probe from the free stream, so that the stagnation pressure measured at the probe face is not the free-stream stagnation pressure, but is rather the bow-shock stagnation pressure. Likewise, the magnetic field measured at a coil is not the free-stream magnetic field. All normal shock experiments[3–6] have a flow velocity exceeding the slow magnetoacoustic speed. This is also true for transverse shock experiments operated in the Ohmic dissipation regime. The only disturbance speed behind such a shock wave is the gas-dynamic sound speed, and not the vector sum of the gas-dynamic sound speed and the Alfvén speed.[7,8] A bow shock is therefore present on the probe inserted into the flow in all these experiments.

We consider only the transverse shock situation. The jump equations[9] are solved along the stagnation streamline and a subsequent isentropic compression to the stagnation point enables the stagnation pressure to be obtained as a function of the free-stream gas pressure. A simplified model is then used to consider the field and flow lines outside the stagnation streamline. The effect of the distribution of these lines on the probe measurements is discussed.

II. BOW-SHOCK JUMP

The following assumptions are made: (a) The bow shock is detached and stationary with respect to the laboratory coordinates. (b) The flow is one dimensional and normal to the bow shock. This is correct only along the stagnation streamline which lies along the probe axis.

Further, the flow is conducting on both sides of the bow shock so that the density ratio $\Gamma_3=\rho_3/\rho_2$ across the bow shock is equal to the ratio of the magnetic fields $\beta_3=B_3/B_2$. With this hydromagnetic model, the jump equations across the bow-shock form a closed system with which the post-bow-shock properties, denoted by the subscript 3, can be expressed in terms of the free-stream properties, denoted by the subscript 2. Over a wide range of electromagnetic-shock-tube operation, when the gas is either fully ionized or "freely" ionizing, the value of γ, the ratio of specific heats, can be considered as unchanged across the bow shock. The enthalpy equation then takes a very simple form and the bow-shock jump equations can be reduced to a cubic equation in Γ_3:

$$a\Gamma_3^3+b\Gamma_3^2+c\Gamma_3+d=0, \tag{1}$$

where

$$a=(2-\gamma)/\gamma, \quad b=r_p+\tfrac{1}{2}(\gamma-1)(4+r_N),$$
$$c=-(r_p+r_N+1), \quad d=[(1+\gamma)/2\gamma]r_N,$$
$$r_p=P_2/P_{B2}, \quad r_N=P_{N2}/P_{B2}.$$

The symbols P, $P_B=\frac{1}{2}B^2/\mu$ (where μ is the permeability), and $P_N=\rho q^2$ denote, respectively, the static pressure, the magnetic pressure, and the Newtonian impact pressure.

The bow-shock pressure ratio $Y_3=P_3/P_2$ is obtained as

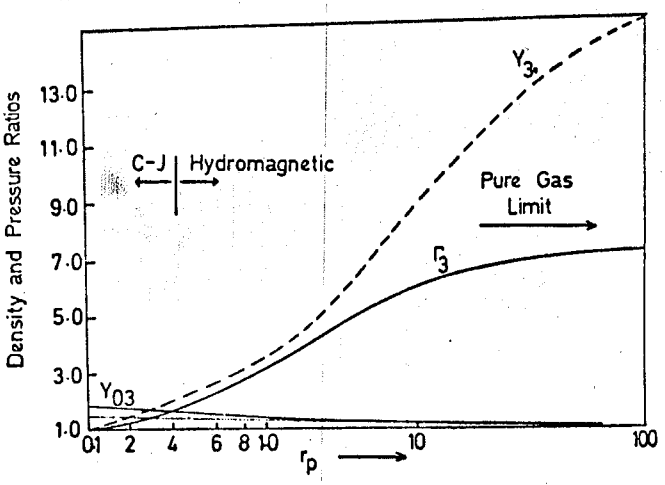

FIG. 1. Computed density and pressure ratios across the bow shock and at the stagnation point as a function of $r_p=P_2/P_{B2}$. The fourth trace (not labeled in the figure) is the graph of Γ_{03}. The point $r_p=0.3$ is the CJ ionizing-hydromagnetic transition point for the main shock wave.

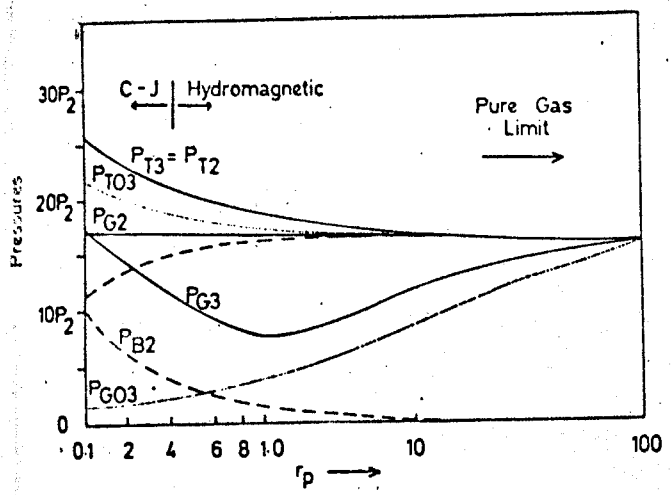

FIG. 2. Computed magnetic pressure, total gas pressure, and total pressure in the free stream, across the bow shock, and at the stagnation point in units of free-stream static pressure P_2 as a function of r_p.

$$Y_3 = 1 + \frac{r_N}{r_p}\frac{\Gamma_3 - 1}{\Gamma_3} + \frac{1}{r_p}(1 - \Gamma_3^2). \tag{2}$$

The ratios Γ_3 and Y_3 are given by Eqs. (1) and (2) as functions of two parameters r_p and r_N. In order to reduce the number of parameters to one, a relationship between r_p and r_N is sought. This relationship depends on the regime of operation of the primary shock. If the primary shock is hydromagnetic, then the jump equations for the primary shocks yield

$$r_N = r_p(\Gamma - 1) + (\Gamma^2 - 1)(\Gamma - 1)/\Gamma^2, \tag{3}$$

where the primary shock density ratio Γ is a function purely of the ambient magnetic field B_1 and main shock velocity q_1. If the primary shock is ionizing, then an empirical relationship, such as the Chapman-Jouguet (CJ) hypothesis,[7] is required to close the system of primary shock jump equations. Using this hypothesis, the relationship between r_N and r_p is obtained as

$$r_N = r_p\gamma(\Gamma - 1)^2. \tag{4}$$

A structural limit on the preshock electric field[9] requires that if the CJ hypothesis is applied to the transverse ionizing shock wave,[7] the shock wave must become hydromagnetic at a magnetic Mach number M_A which is γ dependent. For freely ionizing argon, $\gamma = 1.135$, and the shock is ionizing when $M_A < 4.5$ (corresponding to $r_p < 0.3$), and is hydromagnetic when $M_A > 4.5$ (corresponding to $r_p > 0.3$). The value of Γ rises from 4.9 at $r_p = 0.3$ to the pure-gas value of 15.8 at $r_p \to \infty$.

Using this ionizing-hydromagnetic model for the main shock, Eq. (4) is used when $r_p < 0.3$ and Eq. (3) is used when $r_p > 0.3$; so that Eqs. (1)–(4) give the bow-shock ratios Γ_3 and Y_3 as functions of a single parameter r_p which itself is a function of the main shock M_A.

Values of Γ_3 and Y_3 are computed from $r_p = 0.1$–100, and shown in Fig. 1. It is seen that Γ_3 goes from a value of 1 in the large-field limit ($r_p \to 0$) to a value of 7.3 in the small-magnetic-field limit (pure-gas limit $r_p \to \infty$).

III. STAGNATION POINT

The flow velocity after the bow shock is reduced to zero in the compression to the stagnation point. Assuming that this compression is isentropic enables us to obtain a solution of the stagnation point in the form

$$Y_{03} = (\Gamma_{03})^\gamma, \tag{5}$$

$$(\Gamma_{03})^{\gamma-1} + g\Gamma_{03} + h = 0, \tag{6}$$

where $g = 2(\gamma - 1)\Gamma_3^2/\gamma r_p Y_3$ and $h = -[a + 1 + (\gamma - 1)r_N/2r_p\Gamma_3 Y_3]$ and the subscript 03 indicates the bow-shock stagnation point. Using Eqs. (5) and (6), Γ_{03} and Y_{03} are evaluated as functions of r_p, and shown in Fig. 1. At the $r_p \to \infty$ (pure-gas) limit, Γ_{03} and Y_{03} tend towards 1.06 and 1.07, respectively.

It is useful to compare the relative values of the magnetic and static pressure, the total gas pressure $P_G = P + P_N$, and the total pressure $P_T = P_G + P_B$ during the bow-shock jump and the subsequent isentropic compression. The pressures, in units of P_2, are plotted as functions of r_p in Fig. 2.

The magnetic field has a marked effect on the total gas pressure. For example, for $r_p = 1$, in state 2, $P_{B2} = P_2$, while P_{G2} is $16.5P_2$. Across the bow shock, P_{G3} has dropped to $7.5P_2$, while P_{B3} has increased to $10P_2$. Compressing to the stagnation point, P_{G03} has dropped further to $3.7P_2$, while P_{B03} has increased to $13P_2$. In an experimental situation the output of a pressure probe is related to the net pressure exerted on the probe face at the stagnation point. The net pressure is P_{T03} minus the magnetic pressure behind the probe face, inside the probe. This magnetic pressure has now to be estimated.

IV. FIELD AND FLOW DISTRIBUTIONS

To do this we discuss the effect of the bow-shock curvature outside the stagnation streamline in terms of the distribution of field and flow lines. For simplicity, only the plane along which both the stagnation streamline and the transverse field lines lie will be considered. At a point Q (Fig. 3), where the flow enters the bow shock at an angle $\frac{1}{2}\pi - \theta$ to the shock normal, the normal velocity component is reduced from $q_p \sin\theta$ to $q_p \sin\theta/\Gamma_{Q3}$, while the tangential component of velocity remains unchanged across the shock. Similarly, the tangential component of the induction $B_2 \sin\theta$ is increased to $\Gamma_{Q3}B_2 \sin\theta$ across the bow shock, while the normal component is unaffected. The streamlines therefore bend away from the stagnation streamline, while the B lines bend upstream. However, because of the symmetry of the flow about the stagnation streamline, the field passing through Q must also pass through its image Q' on the other side of the bow shock. The precise path taken by the B lines between Q and Q' will be governed by its interaction with the flow.

Without going into the details of this interaction, we can estimate this path by using the stagnation condition, and the knowledge that the density and magnetic flux ratios (compared to the free-stream values) are greatest along the stagnation streamline, and decrease towards Q. In the ionizing shock regime, along the stagnation streamline, Γ_3 is 1.4, and the density ratio at the stagnation point compared to the free stream, i.e., the

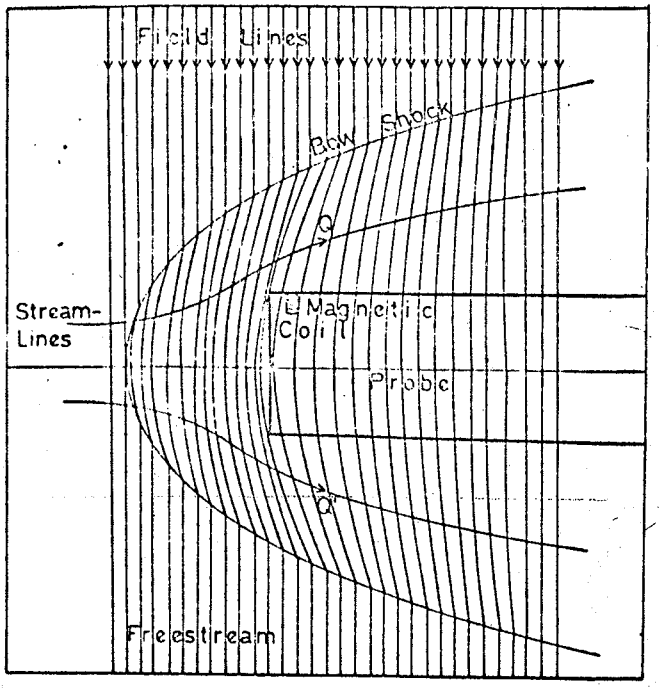

FIG. 3. Illustration of the deflection of the transverse field lines through the bow shock, their compression towards the stagnation point, and their rarefaction behind the stagnation point.

product of Γ_3 and Γ_{03}, is 1.9. If we assume that the detachment distance is of the order of the probe diameter, and that the bow-shock shape is as shown in Fig. 3, the problem can now be approximately solved by geometrically fitting the field lines into the spaces to give the correct relative densities of magnetic flux at the stagnation region and in the regions around Q and Q'. This gives a field-line distribution of the order illustrated in Fig. 3.

With such a distribution it can easily be seen that the density ratio at Q, just after the bow shock, is greater than unity. For example, for a Mach 3.5 flow in the free stream, a maximum estimate of B_{Q3} is $1.22B_2$. As the field lines approach the surface of the probe, they must spread apart in order to satisfy the condition of stagnation compression on the probe tip. A gas-dynamic analysis of the flow lines as they deflect around the probe shows that in the subsequent expansion the density ratio (compared to free stream) decreases to below unity. This agrees with our geometrically fitting of field lines. The magnetic field measured by a probe, positioned as shown just behind the head of the probe, will thus be less than the free-stream value, the difference being dependent on the curvature of the field lines due to the bow shock. In the ionizing shock regime ($r_p < 0.3$), the curvatures are small and the measured field can be approximated to the free-stream field. This becomes exactly true in the high-magnetic-field limit ($r_p \to 0$). For small fields however ($r_p \to \infty$), the combination of increased stagnation densities (Fig. 2) and decreased detachment distances[10] will result in large curvatures in field lines so that the field measured at the coil will be significantly smaller than the free-stream field.

The net pressure exerted on the stagnation point of the pressure-probe front face may now be written as

$$P_{TM} = P_{T03} - P_{B2} = P_2\left(Y_{03}Y_3 + \frac{\Gamma_{03}\Gamma_3^2}{r_p} - \frac{1}{r_p}\right), \tag{7}$$

where the error involved, in taking P_{B2} as the pressure behind the front surface of the probe, is small, particularly in the ionizing shock regime. For $r_p > 0.3$, the error involved in taking P_{B2} as the magnetic pressure behind the probe face may become large. However, for $r_p \to \infty$, Eq. (7) becomes exact since the magnetic pressure is everywhere negligible.

As expected, the pressure P_{TM} is a function not only of the free stream P_2, but is also a function of r_p and the bow shock Y_3 and Γ_3, and the isentropic compression Y_{03} and Γ_{03}. The ratio P_{TM}/P_{G2} is plotted in Fig. 4. The value of P_{TM} rises from $0.7P_{G2}$ at $r_p \simeq 0.1$ towards P_{G2} as $r_p \to \infty$.

Since pressure probes used in electromagnetic shock tubes usually have conducting walls, the distortion due to the shielding effect of the walls must also be borne in mind. For example, for field variations occurring in the free stream with a characteristic time greater than four times the characteristic diffusion time of the conducting wall, a 22% distortion of the field for a point inside the probe wall has to be accounted for.

V. CONCLUSION

The above approximate considerations indicate that, in the ionizing regime, the measured magnetic induction will be slightly less than the free-stream induction. The pressure at the probe stagnation point is P_{TM}, which is less than the free-stream total gas pressure. The measured pressure, however, will be less than P_{TM} since the pressure, averaged over the whole front face, can be expected to be less than that at the stagnation point. This approximate analysis is sufficient to show that the bow shock has to be considered in quantitative probe measurements of pressure and magnetic field. It is further noted that, for pressure and magnetic field measurements in other bias field geometries, bow-shock effects may have to be taken into account; particularly in view of its ability to deflect field lines. This field-line deflection can be of special importance in experiments designed to detect switch-on shocks.

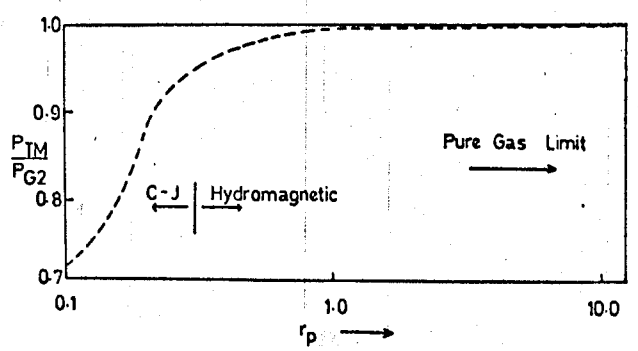

FIG. 4. Computed values of P_{TM}, the net total pressure exerted at the stagnation point of the probe, normalized to the free-stream total gas pressure.

ACKNOWLEDGMENT

One of us (S. L.) would like to thank the Australian National University for a Ph.D. research scholarship (1966–1969) which made this work possible.

[1]W. H. Rudderlow, J. Appl. Phys. 39, 1 (1968).
[2]R. H. Huddlestone and S. L. Leonard, *Plasma Diagnostics* (Academic, New York, 1965), p. 69.
[3]M. H. Brennan, I. G. Brown, D. D. Millar, and C. N. Watson-Munro, J. Nucl. Energy C 5, 229 (1963).
[4]J. B. Heywood, Phys. Fluids 9, 1150 (1966).
[5]B. Miller, Phys. Fluids 10, 9 (1967).
[6]L. S. Levine, Phys. Fluids 11, 1479 (1968).
[7]S. Lee, Ph.D. thesis (Australian National University, 1969) (unpublished).
[8]S. I. Pai, *Proceedings of the Fifth Midwestern Conference of Fluid Mechan* (University of Michigan Press, Ann Arbor, 1957), p. 251.
[9]C. K. Chu, Phys. Fluids 7, 1349 (1964).
[10]S. I. Pai and E. T. Kornowski, in *Engineering Aspects of Magnetohydrodynamics*, edited by C. Mannal and N. W. Mather (Columb U.P., New York, 1962), p. 97.

Transient behavior of a cavity

William R. Faust
Naval Research Laboratory, Washington, D. C. 20390
(Received 14 April 1972)

An expression for the transient electric field setup in a lossless cylindrical cavity by a short pulse of electrons has been derived by means of the Laplace transformation. It is found that longitudinal and radial fields are set up in the cavity. Expressions for the electric field have been evaluated as a function of time for several different points within a representative cavity.

INTRODUCTION

A cavity resonator when excited by a current pulse which makes the transit from one side to the other of the cavity in times comparable with a resonant period presents some interesting mathematical problems. The origin of such a pulse is in the "Compton current" which flows in an evacuated device (satellite) due to an incident pulse of γ rays. Generally, most analyses[1,2] deal with the steady-state response in a single mode when excited by an rf signal, rather than the over-all excitation produced by a pulse.

Specifically the problem considered here is to calculate the transient behavior of a lossless cylindrical cavity when excited by a short burst of electrons which are emitted from one side and travel at a velocity v to the opposite side. In order to simplify the mathematical complexity of the problem the electron velocity will be assumed to be independent of the induced field. This is the case when the initial electron energy is large compared with the energy extracted from the induced field the cavity.

FIELD EQUATIONS

Consider a cylinder of radius a and length l aligned so that the axis of the cylinder lies along the z axis of a Cartesian-coordinate system. N electrons per square meter of velocity v are released at time zero from the base of the cylinder lying in the xy plane, in a very short pulse which will be approximated by a δ function.

The field equations[3] give for the electric field

$$\nabla\times\nabla\times\mathbf{E}+\frac{1}{c^2}\frac{\partial^2 E}{\partial t^2}=-\mu_0\frac{\partial j}{\partial t}. \tag{1}$$

According to the assumptions made above the only nonvanishing component of the current is

$$j_z=-eN\delta(t-z/v). \tag{2}$$

By virtue of the equation of continuity, it follows that

$$\rho=-(eN/v)\delta(t-z/v)=\epsilon_0\nabla\cdot\mathbf{E}. \tag{3}$$

Because E_z is a Cartesian component of the field an equation containing only E_z may be obtained directly Eqs. (1) and (3), namely

$$\nabla^2 E_z-\nabla_z\left(\frac{\rho}{\epsilon_0}\right)-\left(\frac{1}{c^2}\right)\frac{\partial^2 E_z}{\partial t^2}=+\mu_0\frac{\partial j_z}{\partial t}.$$

If it is assumed that E_θ vanishes, as a result of symmetry, then a relation between E_z and E_r may be found, viz.,

$$-\frac{\partial^2 E_r}{\partial z^2}+\frac{1}{c^2}\frac{\partial^2 E_r}{\partial t^2}+\frac{\partial^2 E_z}{\partial r\partial z}=0.$$

Alternatively, the divergence equation (3) may be utilized instead of Eq. (5) to give

$$\frac{1}{r}\frac{\partial}{\partial r}(rE_r)+\frac{\partial}{\partial z}E_z=\frac{\rho}{\epsilon_0}.$$

By virtue of Eqs. (2) and (3) and application of the Laplace transform to Eqs. (4) and (6) there results

$$\frac{\partial^2\tilde{E}_z}{\partial r^2}+\frac{1}{r}\frac{\partial\tilde{E}_z}{\partial r}+\frac{\partial^2\tilde{E}_z}{\partial z^2}-\frac{s^2}{c^2}\tilde{E}_z=-\left(\frac{eNs}{\epsilon_0}\right)\left(\frac{1}{c^2}-\frac{1}{v^2}\right)\exp\left(-\frac{sz}{v}\right.$$

and

$$\frac{\partial^2\tilde{E}_r}{\partial z^2}-\left(\frac{s^2}{c^2}\right)\tilde{E}_r=+\frac{\partial^2\tilde{E}_z}{\partial r\partial z}.$$

Here

$$\tilde{E}(r,z,s)=\int_0^\infty E(r,z,s)\exp(-st)\,dt$$

is the Laplace transformation[4] of E and the initial conditions which arise from the assumption that the initial charges and currents are zero,

$$E_{z,r}=\frac{\partial}{\partial t}E_{z,r}=0$$

have been used. The boundary conditions are that $\tilde{E}_z$ and $\tilde{E}_r$ remain finite in the cylindrical volume, and vanish the surface, i.e.,

$$\tilde{E}_r(z=0,l)=0 \quad\text{and}\quad \tilde{E}_z(r=a)=0.$$

J. Plasma Physics (1972), *vol.* 8, *part* 1, *pp.* 21–31
Printed in Great Britain

Current sheath studies in a co-axial plasma focus gun

By S. P. CHOW, S. LEE AND B. C. TAN
Physics Department, University of Malaya, Kuala Lumpur, Malaysia

(Received 17 September 1971 and in revised form 8 December 1971)

A co-axial plasma focus device is operated in deuterium gas at ambient pressures from 0·2 to 0·7 mm Hg and condenser bank voltages from 10 to 22 kV. Magnetic probing reveals an axisymmetric parabolic current sheath which propagates down the co-axial tube (steady propagation region) and collapses off the end of the co-axial gun forming a dense plasma focus. The state of the plasma just before the focusing action is very much dependent on the velocity in the steady propagation region. This velocity is experimentally studied and compared with a snowplough theory. The collapsing phase of the current sheath is studied using high speed framing photography and current and voltage measurements. The results indicate a focus of length 1·5 cm and radius less than 1·7 mm.

1. Introduction

The dense plasma focus produced by a hydromagnetic co-axial gun system is a region of extreme high temperature and particle density (Mather 1965; Peacock *et al.* 1969). Basically, two distinct phases are involved in the focus formation. The first is the formation of an axisymmetric current sheath at the insulator end of the gun and the subsequent propagation of the current sheath by its own $\mathbf{J} \times \mathbf{B}$ force, towards the open end of the co-axial gun. The current sheath entrains within itself all the gas encountered in its motion along the co-axial electrodes. The second is the rapid collapse of the current sheath off the end of the co-axial gun resulting in the formation of a thin filament of extremely hot and dense plasma. The diameter of the filament has been estimated to be between 1 and 2 mm, and it lasts from between 100 and 200 ns (Mather 1965; Patou, Simonnet & Watteau 1969).

As the dynamics of the collapse of the current sheath during 'focusing' must depend on the state of the gas just before the collapse, it is important in any plasma focus device to determine the velocity and shape of the current sheath at this time. This paper presents some current sheath velocity measurements which are compared with the predictions of a snowplough model. Current distributions in both axial and radial directions during the acceleration phase of the discharge are studied using magnetic probes. The rapid collapse of the current sheath off the end of the co-axial gun is investigated by high speed photography using an image converter camera (Imacon), and also by voltage and current measurements.

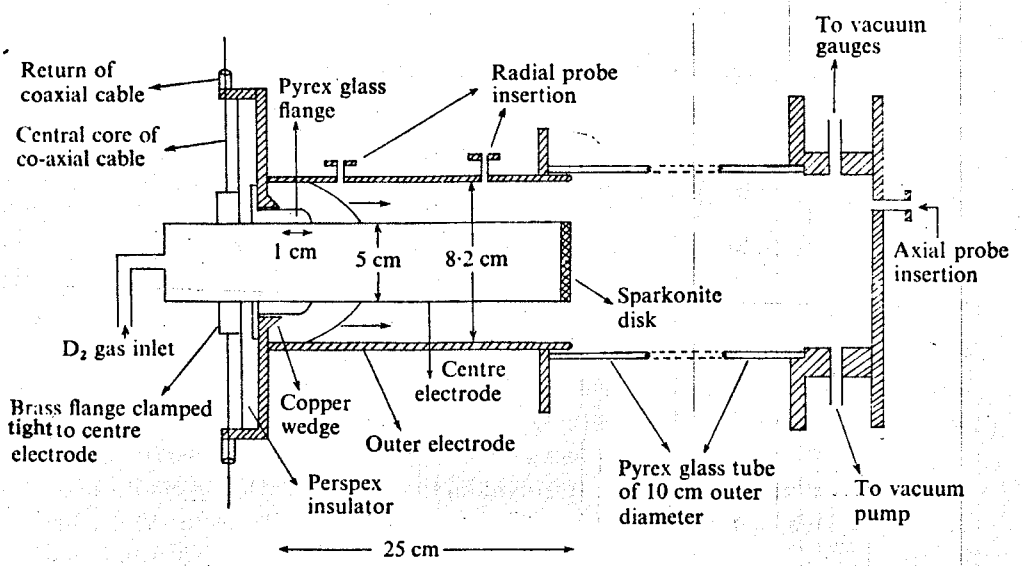

FIGURE 1. Schematic diagram of plasma focus device.

2. Experimental

A schematic diagram of the plasma focus device is shown in figure 1. The device itself consists of two co-axial copper electrodes of length 25 cm. The diameter of the outer electrode is 8·2 cm, and that of the inner electrode is 5·0 cm. The inner electrode is hollow with a Sparkonite† disk welded to the end of it. This helps to reduce erosion of the centre electrode. A cylindrical copper wedge of 45° is attached to the insulator end of the outer electrode to ensure a prompt and fast initial discharge. The slower mode of discharge initiation, mode II operation (Mather 1964) is used in this device by having a Pyrex glass flange which extends along the centre electrode for 1 cm from the sharp copper wedge of the outer electrode.

The capacitor bank consists of two modules, each with 25 pieces of 'Wego' 0·6 μF, 40 kV high frequency discharge condensers and each module switched by a 7703 ignitron (Lee, Thong & Tan 1971*a*). The plasma focus tube is connected to the bank via 20 co-axial cables. At 22 kV, the bank delivers to the focus tube a current of 400 kA, with a period of 9·6 μs. The centre electrode is positive.

The device is filled with deuterium gas with pressure varying from 0·2 to 0·7 mm Hg, and experiments are conducted with bank voltages ranging from 10 to 22 kV. However, most of the experiments are conducted with the bank voltage at 18 kV and an ambient gas pressure of 0·3 mm Hg. The vacuum system is pumped down to below 2×10^{-4} mm Hg in between shots, and a static filling procedure of deuterium gas into the discharge chamber is used.

The discharge current from the condenser bank is measured by a current transformer and the voltage across the electrode terminals at the breech end

† Trade name of a copper tungsten alloy manufactured by Mallory Metal Company.

of the gun is measured by a resistive voltage divider. A photo-diode (EG & G SGD-100 silicon diffused photodiode) with a rise-time of 10 ns is used to detect the arrival of current sheath just off the end of the electrode system.

Magnetic probes are used to measure the arrival of the current sheath, the magnitude of the azimuthal field and the field distribution following the current front. Probes are inserted both in the radial as well as axial positions. The radial probes each consists of 30 turns of SWG 46 copper wire (the axial probe has 10 turns) wound on a 1 mm diameter polythene former. Measurements are made as a function of radius at the axial positions $z = 21$ cm, 15 cm and 6 cm ($z = 0$ at the copper wedge), and also as a function of z at radius $r = 3{\cdot}3$ cm. From the data obtained, the velocity of the current sheath at different positions along the coaxial gun system is determined.

The region just off the end of the centre electrode can be viewed optically through the outer Pyrex glass tube. A high speed image converter camera (Imacon), with a framing speed of 10^7 frames s^{-1} and exposure time of 20 ns is used to record the rapid collapse of the current sheath and the formation of the focus. The triggering of the camera can be delayed to the desired value using a delay unit (Philips PP1122).

3. Results

3.1. *Snowplough theory and velocity of current sheath*

The snowplough model assumes that all the gas swept up by the current sheath propagates at the current sheath speed, and that wall friction may be neglected. Calculation of the velocity of the current sheath in the gun involves known values of ambient gas pressure, geometry of electrodes and the discharge current. Essentially, the model assumes that the force acclerating the total mass of gas swept up by the current sheath equals the electromagnetic driving force of the current sheath. Under these conditions, the momentum balance equation becomes, in mks units,

$$\frac{d}{dt}\left[(\rho Az)\frac{dz}{dt}\right] = \frac{B^2}{2\mu}A = \int_a^b \frac{\mu^2 I^2}{2\mu(2\pi r)^2}\,2\pi r\,dr, \tag{1}$$

where $B = \mu I/(2\pi r)$ is the magnetic field associated with the discharge current I, ρ is the gas density, a and b are the respective radii of the inner and outer electrodes, and A is the inter-electrode cross-sectional area.

Assuming $I = I_0 \sin \omega t$ (where I_0 is the peak current, ω the angular frequency), and putting in the boundary condition $z = 0$ at $t = 0$, (1) can be integrated to give

$$\frac{dz}{dt} = U_c\left(t - \frac{\sin 2\omega t}{2\omega}\right)\Big/\left[2\left(t^2 + \frac{\cos 2\omega t}{2\omega^2} - \frac{1}{2\omega^2}\right)\right]^{\frac{1}{2}}, \tag{2}$$

where

$$U_c^2 = \frac{\mu I_0^2 \ln(b/a)}{4\pi^2\rho(b^2 - a^2)}, \tag{3}$$

and U_c is referred to as the constant current velocity corresponding to current value I_0.

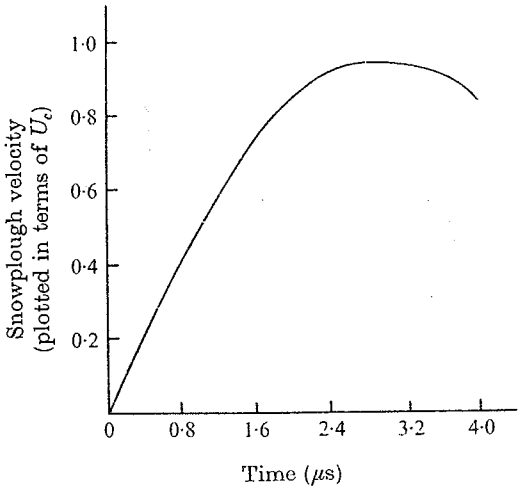

FIGURE 2. Snowplough velocity as a function of time, plotted in terms of U_c.

Using the theory mentioned above, a graph of dz/dt *vs* time t, with discharge period $T = 9{\cdot}6\,\mu$s and $\omega = 6{\cdot}55 \times 10^5$ radians s^{-1}, is drawn and shown in figure 2. Plotted in terms of U_c, the velocity increases with time reaching its peak value of $0{\cdot}95U_c$ at $t = 2{\cdot}9\,\mu$s.

3.2. *Average velocity measurement*

The average velocity of the current sheath in the co-axial gun is measured experimentally by a photodiode with a glass fibre optics as a collimator. The fibre optics is pointed at a position 2 mm off the end of the centre electrode. Figure 3 (plate 1) shows a typical photodiode signal, together with the discharge current wave-form. The noise at the beginning of the signal is a characteristic of the electromagnetic pick-up when a condenser bank discharges. The light front appears $2{\cdot}9\,\mu$s after the initial current discharge, having travelled a distance of 25·2 cm along the co-axial electrodes. This gives an average velocity of 8·7 cm μs^{-1}.

The average velocity of the light front as a function of current at different pressures is shown in figure 4. Fitted into the same graphs are the velocities predicted by the snowplough theory. As the snowplough velocity predicted by (2) and (3) is a function of time, an average value based on these equations is sought. The experimental average velocities are measured at different times ranging from $2{\cdot}0\,\mu$s to $4{\cdot}1\,\mu$s after the initial current discharge, their corresponding theoretical average velocities in terms of U_c are found from figure 2 with values varying from $0{\cdot}53U_c$ to $0{\cdot}71U_c$. Knowing U_c from (2), the theoretical snowplough velocities can thus be estimated.

At the low pressure, when $p = 0{\cdot}2$ mm Hg, the measured values agree well with those estimated from snowplough theory. However, at higher pressures of 0·4 and 0·7 mm Hg, the experimental values are higher than those predicted. This could be due to the inefficient snowplough action by the current sheath (which is assumed to be 100 % efficient in the snowplough theory), i.e. the current

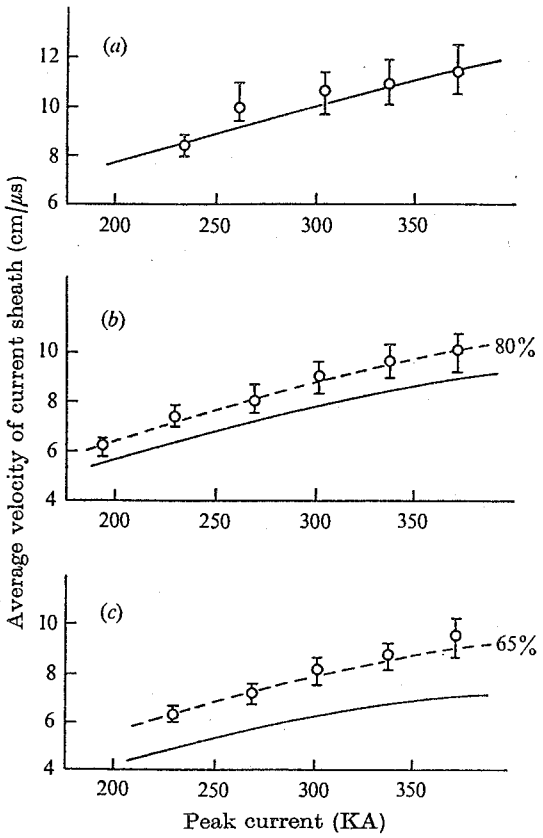

FIGURE 4. Average velocity of current sheath as a function of discharged current at pressures 0·2, 0·4 and 0·7 mm Hg. ——, theoretical results based on 100 % snowplough efficiency; – – – –, results using a modified snowplough efficiency; ○, experimental points. p: (*a*) 0·2 mm Hg, (*b*) 0·4, (*c*) 0·7.

sheath does not carry along with it all the gas particles encountered. The value of U_c in (3) is thus underestimated.

Assuming a 80 % snowplough action, the values of U_c and hence the predicted average velocities are both increased by a factor of 1·11. With this modification, the theoretical values fit in very well with the experimental results at $p = 0{\cdot}4$ mm Hg. Similar results are obtained for $p = 0{\cdot}7$ mm Hg but with a modified snowplough efficiency of 65 %. Thus, it appears that the snowplough action has a pressure dependence.

The magnetic field in the steady propagation region is proportional to $1/r$ and this gives rise to a $1/r^2$ fall-off in magnetic pressure. Plasma flow parallel to the current sheath and balanced by this $1/r^2$ fall-off in magnetic pressure is responsible for a characteristic parabolic current front at the run-down phase (see § 3.3). This in turn produces an outward component of mass flow and a build up of mass occurs at the outer electrode. A proper snowplough treatment must take this radial plasma loss into account and may explain the 65–80 % snowplough efficiency mentioned above.

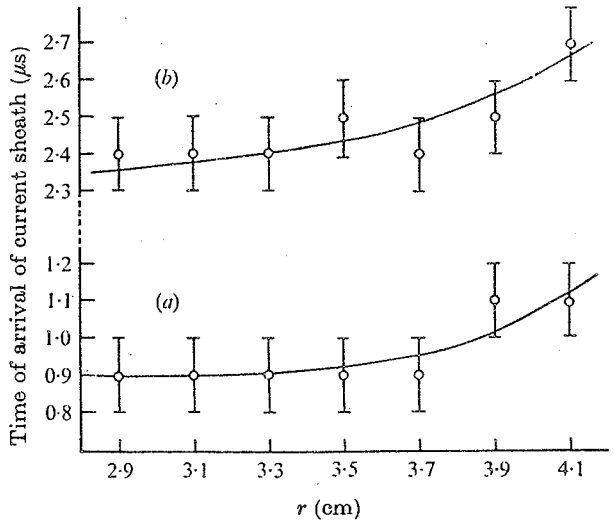

FIGURE 6. Time of arrival of current sheath plotted against the radial position of magnetic probe. z: (*a*) 6 cm, (*b*) 21.

3.3. *Magnetic field measurement*

Magnetic field measurements are made at axial positions $z = 6$ cm, 15 and 21 cm as a function of radius. A typical $B_\theta(t)$ signal is shown in figure 5(*a*) (plate 1), together with the current wave-form. The field signal rises sharply because of the large current at the current sheath, and decreases in its intensity as the latter moves down the tube. The fast rise time of the current sheath indicates a sheath thickness of 2–3 cm and the sheath carries along with it most of the discharge current as it travels towards the end of the tube. The shot-to-shot reproducibility of the discharge is good, as indicated by a typical superposition of 3 traces in figure 5(*b*) (plate 1). The current sheath is axisymmetric. This is revealed by measurements of 3 radial probes spaced 120° apart, and placed at positions $z = 18$ cm and $r = 3{\cdot}3$ cm. The times of arrival and the thickness of the current sheath according to the 3 probes are the same to within 5%.

The time of arrival of the current sheath plotted as a function of radius is shown in figure 6, which indicates that the portion of the current front nearer the outer electrode lags behind the portion near the centre electrode. From the results of figure 6, current profiles of r *vs.* z at fixed times $t = 1{\cdot}12\,\mu$s and $t = 2{\cdot}66$ are deduced and shown in figure 7. At $z = 6$ cm, the current sheath is almost planar. However, at $z = 15$ and 21 cm, it is canted at an angle of about 45°. The parabolic current sheath could be owing to the fact that the magnetic pressure $B^2/2\mu$ is greater near the centre electrode as compared with that near the outer electrode, and this is to be expected because of the radial dependence of magnetic pressure (Mather 1968).

The magnitude of the field as a function of radius is shown in figure 8, and it has a $1/r$ fall-off as expected from the relation $B = \mu I/2\pi r$. However, it must be borne in mind that a substantial axial current J_z is expected at the parabolic

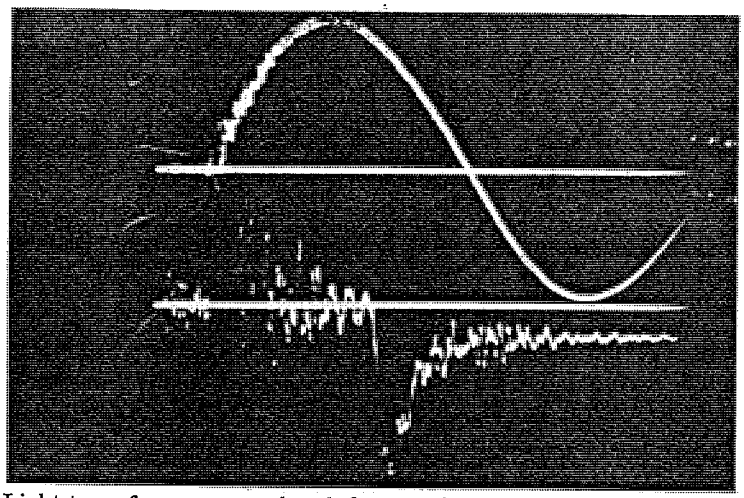

FIGURE 3. Light trace from current sheath for a typical discharge. The top trace shows the current wave-form, while the bottom trace shows the photodiode signal. Time sweep: 1 μs cm^{-1}; condenser bank voltage: 19·1 kV; deuterium pressure: 0·7 mm Hg; peak current 340 kA; average velocity of current sheath: 8·7 cm μs^{-1}.

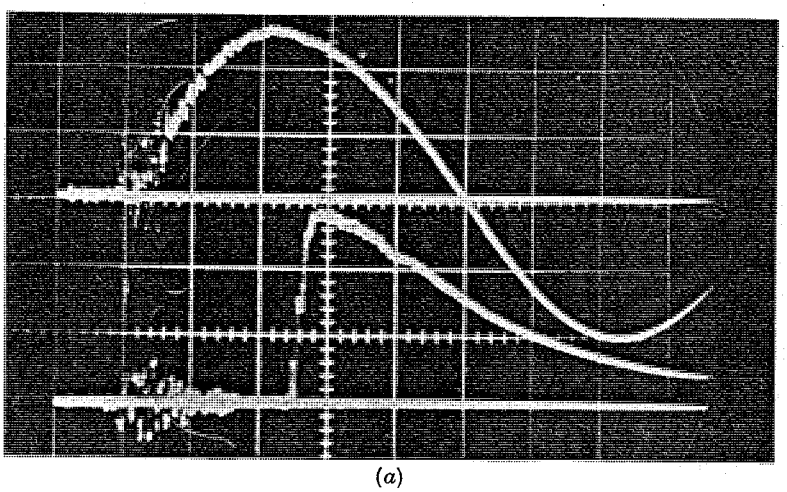

(*a*)

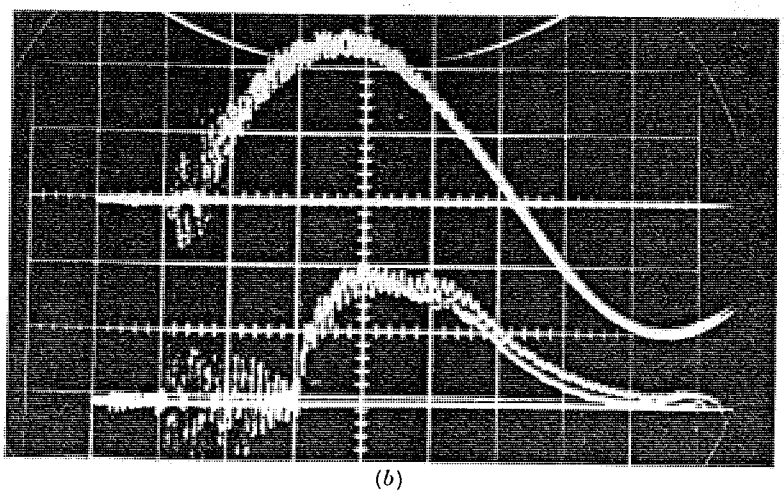

(*b*)

FIGURE 5. (*a*) Oscillograms of current (top trace) and magnetic field (bottom trace) signals for a typical shot. (*b*) Oscilloscope waveforms of good reproducibility of the discharges, with 3 shots superimposed.

(*Facing p.* 26)

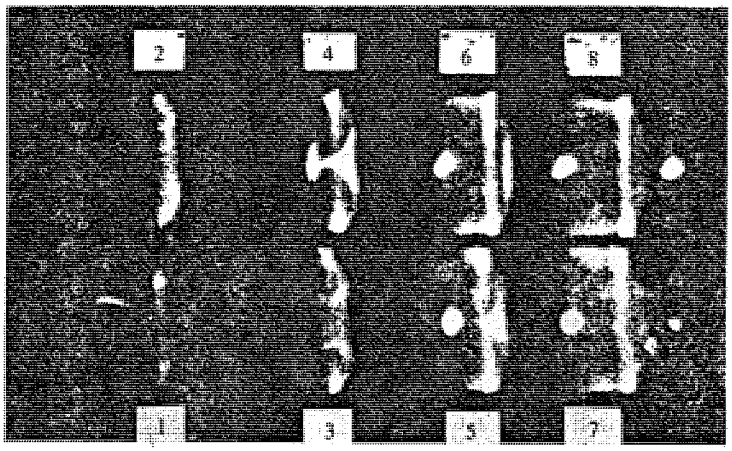

FIGURE 12. Image-converter photographs taken transverse to the discharge tube off the end of the electrodes, interval between frames is 0·1 μs; exposure time 20 ns. Frame 1 shows the arrival of the current sheath.

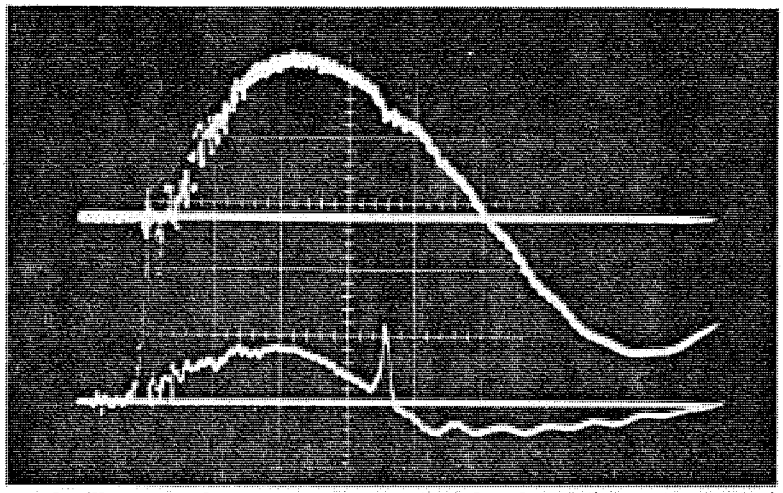

FIGURE 13. Oscillogram of current (top trace) and voltage (bottom trace) signals for a typical focusing shot with the operating parameters: bank voltage 18·2 kV, deuterium pressure 0·3 mm Hg, peak current 320 kV, voltage trace 5 kV/cm, and time sweep 1 μs cm^{-1}.

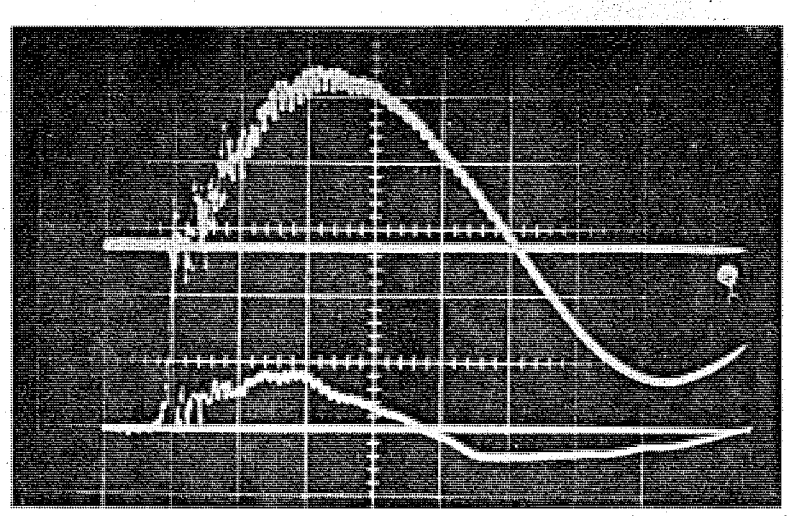

FIGURE 14. Oscillogram of current and voltage signal for a typical non-focusing shot. There is no current dip and voltage spike, as there is in figure 13.

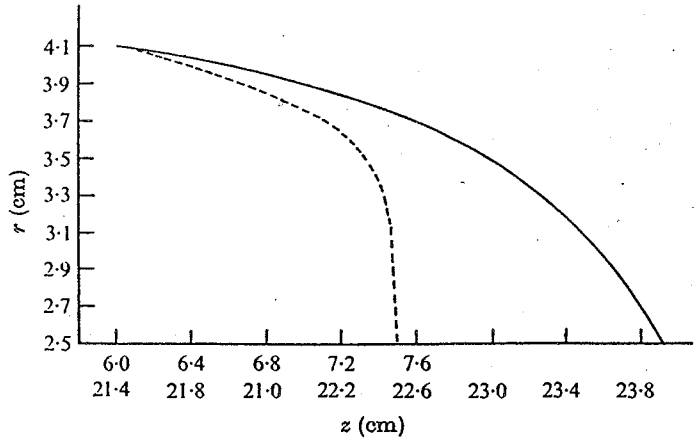

FIGURE 7. The current sheath profiles at (*a*) $t = 1{\cdot}12\ \mu$s (z varies from 21 cm to 23·8), (*b*) $t = 2{\cdot}66\ \mu$s (z varies from 6 cm to 7·5), deduced from figure 6.

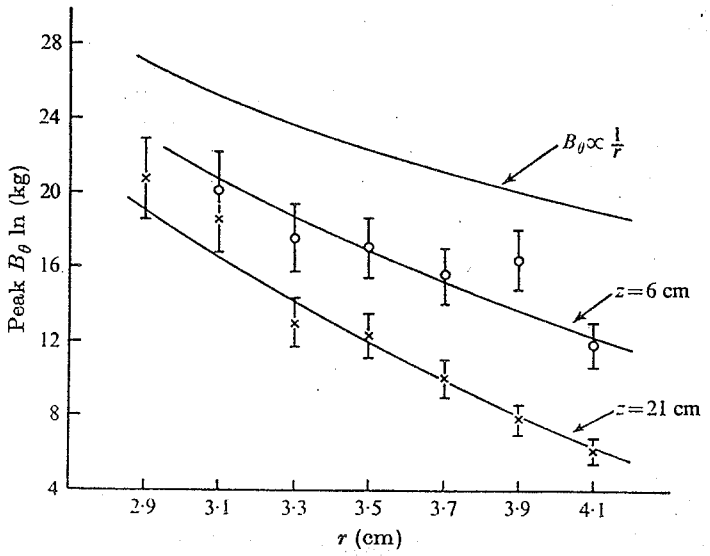

FIGURE 8. The peak magnetic field as a function of radial position of magnetic probe at $z = 6$ cm and 21 cm. A normalized $B_\theta \propto 1/r$ curve is included.

plasma current front (Mather 1965), in addition to the radial current J_r. This can be expected to affect the magnetic fields measured in this system.

A B_θ probe is introduced from the end of the tube and moved along in the axial direction to measure the maximum value of B_θ at different values of z. This is shown in figure 9. The results show that the peak field is almost constant for the first 13 cm along the tube and the constant value corresponds to that of the peak current. However, as the current sheath travels further down, the peak magnetic field decreases indicating a drop in current. At $z = 21$ cm, which corresponds to the time of peak current $t = 2{\cdot}4\ \mu$s, the field measurement shows that the current sheath carries only 75 % of the peak current. This confirms a

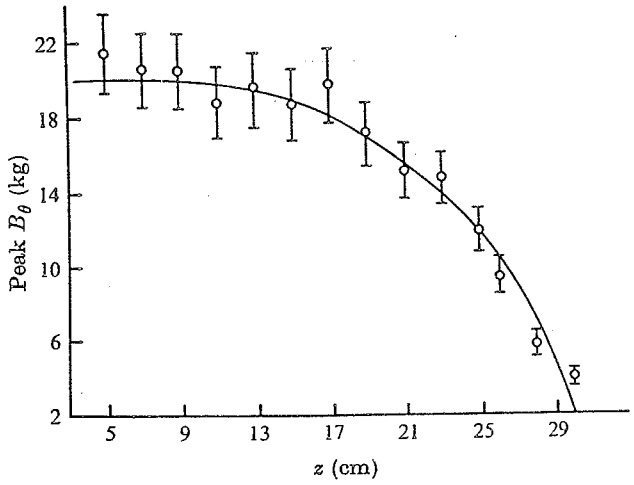

FIGURE 9. Variation of peak magnetic field at different axial positions z. All results are obtained with bank voltage 18 kV, deuterium pressure 0·3 mm Hg and magnetic probe placed at radial position r = 3·3 cm.

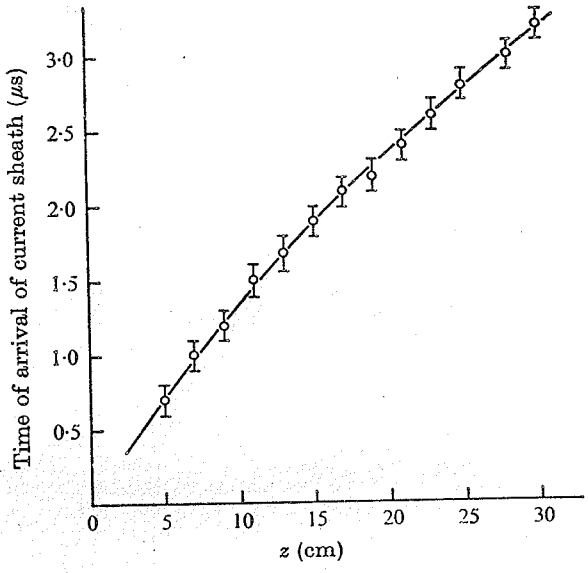

FIGURE 10. Time of arrival of current sheath at different z. Probe position r = 3·3 cm.

current shedding effect (Lee *et al.* 1971*b*), in which the current sheath does not carry along with it the full discharge current. A proportion of the total current is left behind, probably as a slow-moving diffuse current layer behind the main current sheath, or as a stationary layer at the insulator end of the co-axial gun (Dattner & Eninger 1964).

The times of arrival of the current sheath at different z positions are shown in figure 10 (from which figure 11 is obtained), showing velocity as a function of time. These curves indicate a slight acceleration of current sheath as it propagates

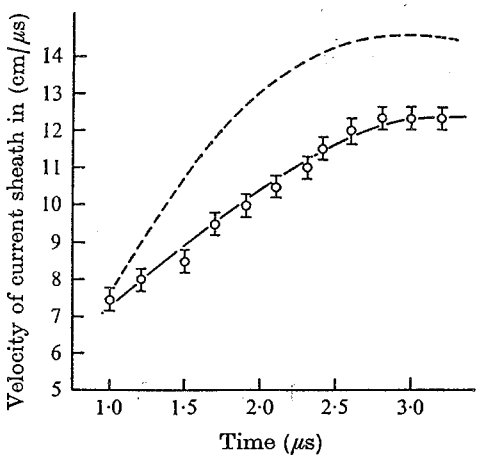

FIGURE 11. Velocity of current sheath as a function of time, deduced from figure 10. ----, a theoretical prediction based on snowplough model.

towards the end of the gun, reaching a terminal velocity of 12·3 cm μs^{-1} at time $t = 2{\cdot}9\,\mu s$. A theoretical curve based on snowplough model from (2) is fitted into figure 11. The results show that the theoretical velocities are higher than the experimental values. This may be attributed to the current-shedding effect mentioned earlier. In the experiment, the current sheath in effect carries a lower current value than that used in the theoretical predictions. This gives rise to a lower experimental velocity.

3.4. *The plasma focus formation*

A sequence of the radial collapse photographed with an image converter camera (Imacon) is shown in figure 12 (plate 2). The first frame shows the arrival of the current sheath just off the end of the centre electrode. The second frame taken 0·1 μs after the first frame begins to show the radial collapse. The collapse becomes very clear at the third frame, while the fourth frame shows the formation of a thin filament. At the fifth frame, a tiny filament about 2 cm off the centre electrode is observed. The actual plasma focus (minimum focus) forms somewhere between the fourth and fifth frames, and the bright spot off the centre electrode in the fifth frame is a result of intense anode glow which occurs after the focus formation.

The radius of the focus is estimated from the fourth frame to be about 1·7 mm. But the minimum focus lies somewhere between the fourth and fifth frames, and is less than 1·7 mm. The length of the focus is 1·5 cm to 2·0 cm, as indicated by the fourth frame. Similar results have been reported by Patou *et al.* (1969).

The initial collapse of the current sheath is slow. However, the speed increases subsequently to about 15 cm μs^{-1} just prior to the formation of the focus.

The formation of the plasma focus is accompanied by two observations. At the time of focusing, there is a sharp drop in current, the current discontinuity. Correspondingly, there is a sudden rise in voltage as a result of the sudden increase in inductance across the terminals of the electrodes. These effects are

clearly shown in the current and voltage oscillograms in figure 13 (plate 2), as a current dip and voltage spike at $t = 3{\cdot}3\,\mu$s. For non-focusing shots, the current and voltage wave-forms are smooth without any dip or spike, as shown in figure 14 (plate 2).

The extent to which the current drops and voltage rises at the time of focusing depends on the electromagnetic-mechanical energy transfer between the condenser bank and the focus device at this time at an initial bank voltage of 18 kV. Different voltage spikes have been obtained ranging from 0 kV (for non-focusing shots) to 15 kV for focusing shots.

3.5. *Estimation of the radius of the focus*

From the voltage signal, the radius of the focus can be estimated. Neglecting plasma resistance, the voltage and inductance at time t' across the terminals of the shock tube with discharge current I are given by

$$V = \frac{d}{dt}(LI), \tag{4}$$

$$L(t') = \frac{1}{I(t')}\int_0^{t'} V(t)\,dt. \tag{5}$$

Denoting by t_1 the time just before focus, and by t_c that at focus, with I_{t_1}, I_t and L_{t_1}, L_{t_c} as their corresponding current and inductance, L_{t_1} and L_{t_c} can be obtained from (5) by measuring the area of the $V(t)$ curve between times 0 and t_1, t_c, respectively. Putting r_f and x to be the radius and length of the plasma focus, a and b be the inner and outer radii of the co-axial system, the change in inductance during the pinch is given by

$$L_{t_c} - L_{t_1} = \frac{\mu x}{2\pi}\left[\ln\left(\frac{b}{r_f}\right) - \ln\left(\frac{b}{a}\right)\right]. \tag{6}$$

The radius of the plasma focus r_f can be calculated from (6) after getting L_{t_c}, L_{t_1} from the voltage trace. A typical set of values, $L_{t_c} = 40{\cdot}5$ nH, $L_{t_1} = 34{\cdot}6$ nH, $x = 1$ cm, $b = 4{\cdot}1$ cm and $a = 2{\cdot}5$ cm, gives a focus of radius 1·3 mm. This is consistent with the observation by high-speed photography.

4. Conclusion

Using a snowplough model adapted for sinusoidal current, reasonably good agreement between experimental and theoretical values of velocity is obtained at 0·2 mm Hg pressure. Above 0·4 mm Hg ambient pressure, the experimental values are higher than the theoretical values, and this can be accounted for by a model assuming only 65–80 % efficiency in the snowplough action. The current sheath is axisymmetric, and almost planar at the insulator end of the gun. As it travels down the gun, its shape becomes parabolic but remains axisymmetric. Magnetic field measurements indicate a 'current shedding' effect, i.e. some current is left as a broad diffuse layer behind the main current sheath. A high-speed photographic study just off the end of the co-axial electrodes shows a rapid

radial collapse of current sheath with a speed of 15 cm μs^{-1} leading to the formation of a plasma focus of length 1·5 cm and radius less than 1·7 mm. An analysis of the voltage and current waveforms indicates a radius of 1·3 mm.

The authors thank Y. H. Chen, B. K. Lee and T. S. Ho for co-operation and technical assistance in this project.

REFERENCES

DATTNER, A. & ENINGER, J. 1964 *Phys. Fluids suppl.* 7, S 41.

LEE, S., THONG, S. P. & TAN, B. C. 1971*a* High current discharge module system. *University of Malaya, Plasma Phys. Lab. Rep.* 2/71.

LEE, S., CHEN, Y. H., CHOW, S. P., TAN, B. C., TEH, H. H. & THONG, S. P. 1971*b* High-speed photography of a plasma focus. *Int. J. Electronics.* (To be published.)

MATHER, J. W. 1964 *Phys. Fluids Suppl.* **7**, S 28,

MATHER, J. W. 1965 *Phys. Fluids Suppl.* **8**, S 366.

MATHER, J. W. 1968 *Phys. Fluids*, **11**, 611.

PATOU, A., SIMONNET, A. & WATTEAU, J. P. 1969 *Le Journal de Physique*, **29**, 973.

PEACOCK, N. J., WILCOCK, P. S., SPEED, R. J. & MORGAN, P. D. 1969 *Plasma Physics and controlled Nuclear Fusion Research*, vol. 2, p. 51. Vienna: IAEA.

ROBERTS, K. V. & POTTER, D. E. 1970 *Methods in Computational Physics* (ed. B. Alder, S. Fernbach and M. Rotenburg), vol. 9, p. 339. Academic.

INT. J. ELECTRONICS, 1972, VOL. 33, NO. 1, 85–90

High-speed photography of a plasma focus†

S. LEE, Y. H. CHEN, S. P. CHOW, B. C. TAN, H. H. TEH and S. P. THONG

Physics Department, University of Malaya, Kuala Lumpur, Malaysia

[Received 9 July 1971]

A coaxial plasma gun is operated with an outer glass cylinder in place of the usual copper cylinder. This enables streak and framing photographs to be readily taken of the shock propagation region, the transition to the focus region and the focus itself.

1. Introduction

The coaxial-gun plasma focus is a simple way of generating a plasma with extreme conditions of temperature, density and pressure (Mather and Bottoms 1968). The dynamics of such a device can be divided into two distinct phases. The first is a shock propagation in a region in which a current sheet, propelled by its own $J \times B$ force, moves down the annular region between two coaxial cylinders, preceded by a shock front. The inner cylinder terminates in a flat face. On arrival at this face, the shock wave diffracts inwards, imploding towards the axis, followed by the current sheet. In this focusing phase, a fraction of the original gas in the tube, heated by the shock wave and ' snow-ploughed ' into the region between the shock front and current sheet, is now further compressed by the inertial forces of the fast-moving plasma and by the magnetic forces of the current sheet. The result is a filament of extremely hot and dense plasma, existing momentarily (0·1 μs).

In such a device, Mather and Bottoms (1968) have estimated the diameter of the filament as 0·1 mm and the particle density as 10^{25} to 10^{26} particles/m^3. With a current of 500 kA, the azimuthal magnetic pressure pinching this column was of the order of 10^{10} N/m^2 or 10^5 atm. Assuming there was a moment of static equilibrium at minimum focus, the plasma temperature was estimated as 2 kev. In most of the work published to date an outer conducting cylinder has been used. This has the disadvantage of not allowing ready optical access to the shock propagation region.

In a recent paper, Butler *et al.* (1969) have eliminated the outer cylindrical electrode and replaced it by an unobstructed current return at the back. Such an arrangement permits of optical access to the pre-focus region. However, the current flow in the shock propagation region is now no longer similar to that of a conventional coaxial plasma gun. In our present experiment we retain the outer cylinder but use Pyrex instead of copper. Brennan (1969) has observed that the gross behaviour and current configuration of a coaxial shock tube is independent of whether the outer electrode is conducting or not; assuming this, we should thus be able to achieve the current configuration of the all-metallic focus devices and yet have the advantage of optical access for

† Communicated by Professor S. P. Thong.

studying the sequence of events leading from the first phase of shock propagation to the second phase of plasma focus. For comparison we also operated another focus device with a conventional outer copper electrode. Focusing was observed for both devices.

2. Apparatus

The present coaxial device is shown in fig. 1. The centre electrode is of adjustable length and is normally used between 5 cm and 25 cm. The focusing face of the centre electrode is either left hollow or closed with a sheet of ' elkonite ', a copper–tungsten alloy.

Fig. 1

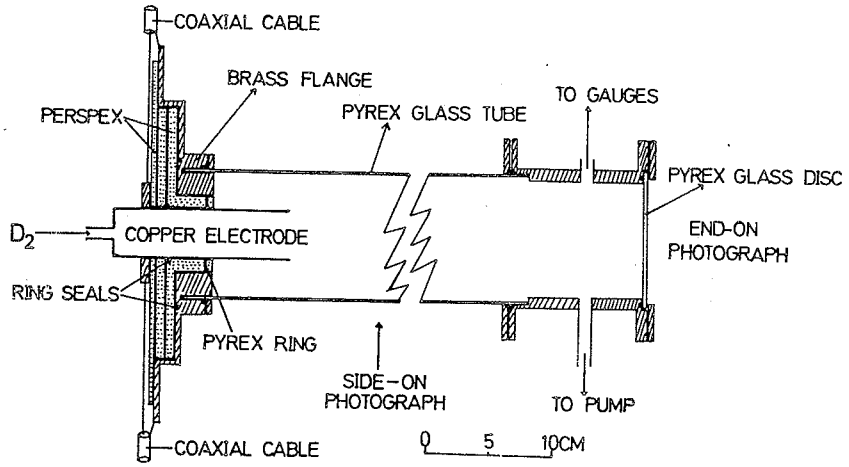

Experimental arrangement.

The energy storage system consists of modules, each of 25 condensers, each condenser rated at 40 kv, 0·6 μF. Each module is switched by a 7703 ignitron. Each condenser is connected via a two-element spark gap of adjustable gap length to a collector plate connected to the anode of the ignitron. For operation below 20 kv the spark gaps are closed and the ignitron operates as a simple switch. Above 20 kv the ignitron cannot be operated as a simple switch since its maximum voltage holding rating is 20 kv. In these cases the anode collector plate is held at $V_A \leqslant 20$ kv whilst the condensers are charged to the operating voltage V_0. The excess voltage $V_0 - V_A$ is held by the gaps which have been pre-set at a suitable gap length (Lim *et al.* 1969). With two modules at 26·8 kv, a peak current of 505 kA was measured at a ringing frequency of 120 kHz.

3. Results

Figure 2 shows a streak picture giving the distance–time relationship of the luminous fronts propagating down the tube. Besides giving the propagation velocities, this picture also shows the second current sheet moving out from the back-wall at the start of current flow in the second half-cycle. It also indicates

Fig. 2

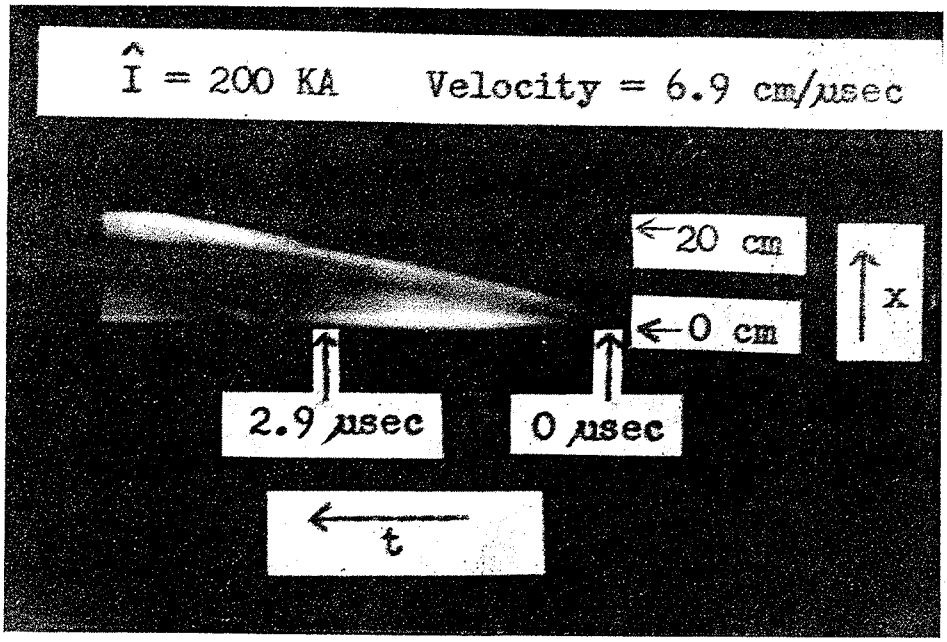

Streak picture from side of Pyrex focus tube. The back-wall is indicated by ' 0 cm ' direction down the tube by x and time by t.

Fig. 3

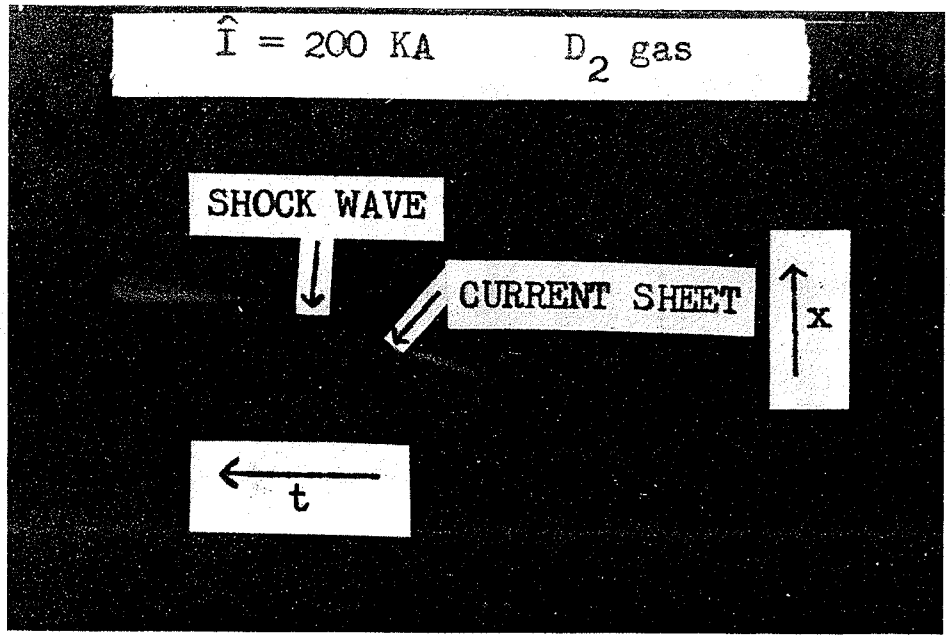

Streak picture showing shock front–current sheet separation. In the shock propagation region, the shock front, indicated here, is faintly visible in the polaroid original. At the focusing face the sudden burst of luminosity indicates the arrival of the shock wave.

Fig. 4

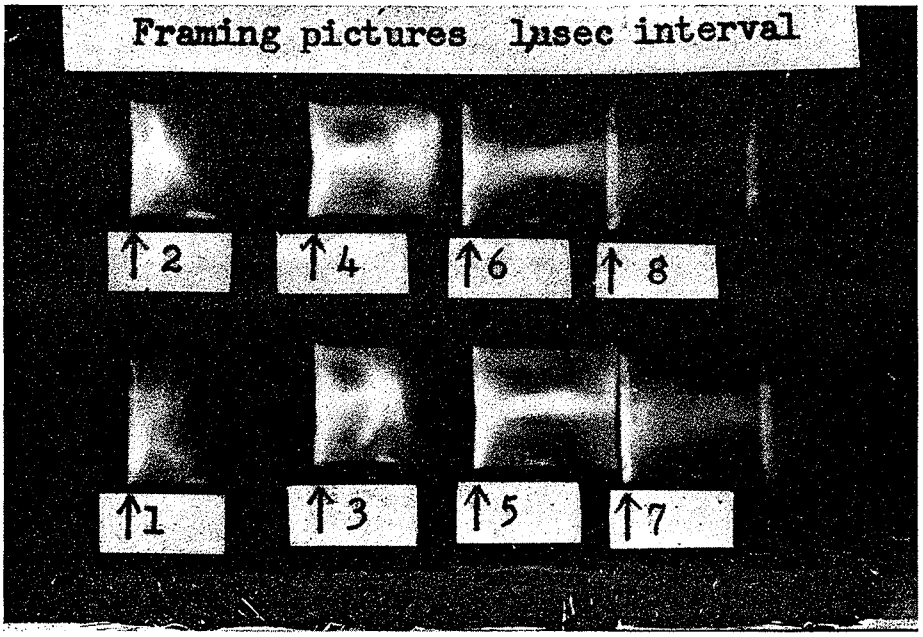

Image converter pictures of gross focusing action, taken from the side. The arrows indicate the position of the right-hand end of the copper electrode (fig. 1).

Fig. 5

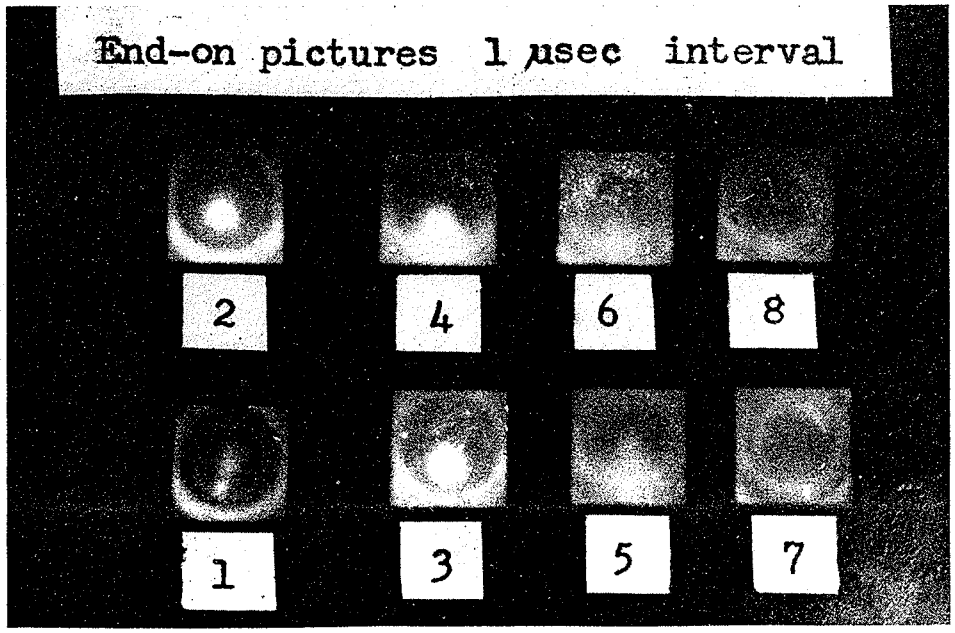

Image converter pictures taken end-on. Minimum focus occurs about the time of frame 2.

'current shedding' during the first half-cycle, i.e. not all the current moves down the tube with the main current sheet; some of it moves with very slow velocity causing the luminous patch that hardly leaves the back-wall at $x = 0$. There is also indication of shock front–current sheet separation in the shock propagation region just preceding the focus.

This is seen more clearly in fig. 3. The less luminous shock front ahead of the more luminous current sheet arrives at the focusing face of the centre electrode first, as indicated by the appearance of luminosity in the face region before the arrival of the current sheet. Focusing of the current sheet itself has been recorded on occasions.

Framing photographs of the focus, both end-on and from the side, have also been taken at a framing rate of 10^6/sec. Figure 4 shows the gross focusing action, followed by expansion, as seen from the side. The sequence is as indicated by the numbers, and in each frame the focusing face is near the left edge of the frame and in line with it.

Fig. 6

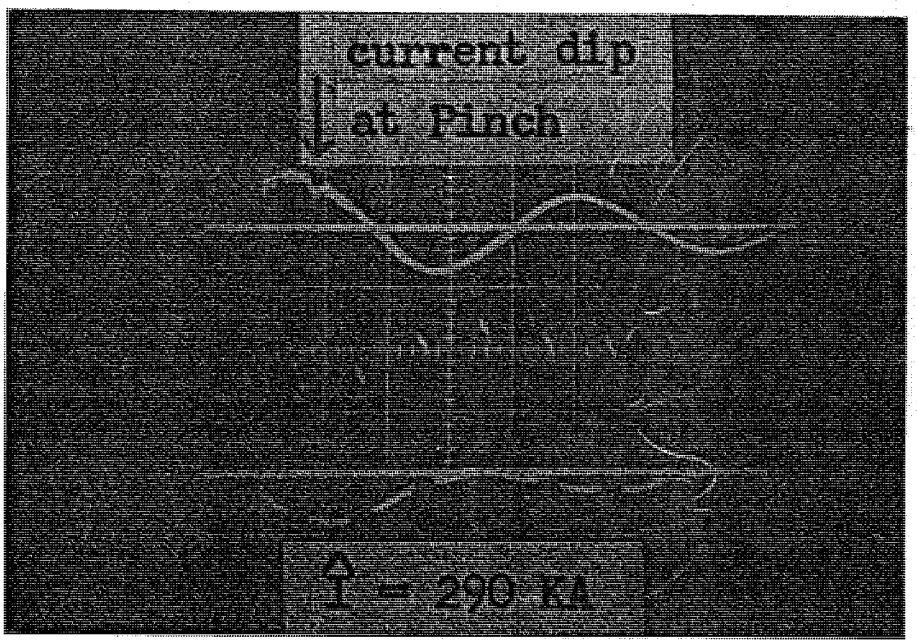

Oscillogram of discharge current, showing current dip at time of focus (top trace). Image converter microsecond timing markers are displayed on bottom trace.

A sequence taken end-on is shown in fig. 5. Maximum focusing occurs at about the time of the second frame.

Figure 6 shows a current trace, monitored with a current transformer, showing a distinct dip occurring at the time of focus, consistent with a sharp rise in tube inductance at this time.

An important observation not yet fully explained is that in certain ranges of operation the current sheet is regular and collapses symmetrically towards the

axis, whereas in other ranges irregularity and asymmetry dominate. A number of parameters which we have varied, namely, operating pressure, peak current, electrode length and even back–wall insulation material appear to affect this situation.

4. Conclusions

The photographic study shows that plasma focusing occurs in an outer glass-bounded coaxial system just as in the more common metal-return device. The glass-bounded device is of advantage for studying the sequence of events leading to focusing, and in particular may prove of value in elucidating further the role of the shock front–current sheet separation.

The close similarity of the phenomena in glass and metal-bounded devices raises the question of whether return currents are not entirely, or mainly, in the plasma itself in both cases.

Acknowledgment

We thank Mr. Lee Boon Kian for technical assistance in this project.

References

Bernstein, M. J., Meskan, D. A., and Van Paasslu, H. L. L., 1969, *Physics Fluids*, **12**, 1904.

Bottoms, P. J., Carpenter, J. P., Mather, J. W., Ware, K. D., and Williams, A. H., 1969, *Plasma Physics and controlled Nuclear Fusion Research* (Vienna : I.A.E.A.), **II**, 67.

Brennan, M. H., 1969, Seventh AINSE Plasma Physics Conf., 'Discharge and Plasma Physics Research at Flinders University' (unpublished).

Butler, T. D., Henins, I., Jahoda, F. C., Marshall, J., and Morse, R. L., 1969, *Physics Fluids*, **12**, 1904.

Lim, C. P., Thong, S. P., and Tan, B. C., 1969, *J. Singapore Natn. Assoc. Sci.*, **1**, 63.

Mather, J. W., and Bottoms, P. J., 1968, *Physics Fluids*, **11**, 611.

Peacock, N. J., Wilcock, P. D., Speer, R. J., and Morgan, P. D., 1969, *Plasma Physics and controlled Nuclear Fusion Research* (Vienna : I.A.E.A.), **II**, 51.

INT. J. ELECTRONICS, 1973, VOL. 35, NO. 3, 341–352

Coaxial plasma gun in mode 1 operation †

Y. H. CHEN and S. LEE
Plasma Laboratory, Physics Department, University of Malaya

[Received 21 March 1972]

Plasma focusing action is observed in two coaxial plasma guns, operating in deuterium in mode 1 operation, one with a non-conducting outer cylinder (gun A) and the other one with a conducting outer cylinder (gun B). For gun A a limiting velocity of 4·5 cm/μsec in the steady propagation region is measured, but despite this low velocity, focusing characteristics in voltage spikes and current dips are observed. This anomalous low velocity is in agreement with a snow-plough model including an ionization retarding force. An estimation of focus radius is made both from framing photograph and voltage spike and current dip, giving a value of 2·0 mm and 1·6 mm respectively for 360 kA input current at 0·3 torr. For gun B at a current of 540 kA and 1·3 torr ambient pressure, a focus radius of 0·7 mm is observed from soft X-ray photographs. The energy of the soft X-ray emission is estimated as between 0·8 and 2·5 keV.

1. Introduction

Two modes of operation in coaxial plasma guns have been reported (Hart 1964), the essential difference in the two modes being the initial breakdown path. In mode 1, the initial breakdown is vertically across the insulating back plate at the breech end. The current sheet is promptly propelled down the tube by the $J_r B_\theta$ force. In mode 2, the first few centimetres of the centre electrode is provided with an insulated flange. The current sheet, on initial breakdown, forms along the insulated flange, expands in an inverse pinch and then is subsequently propelled down the tube by the $J_r B_\theta$ force.

Mather (1965) has claimed that this slow detachment of the current sheet from the back insulator has an important effect on the formation of the focus. Operating in mode 2, he has observed plasma focus of radius less than 1 mm and length of 1 cm.

Results presented in this paper indicate that focus formation is obtainable also in mode 1 operation. A focus radius of 0·7 mm has been observed with a plasma temperature, estimated from soft X-ray measurements, of between 0·8 to 2·5 keV.

The main purpose of this paper however is to compare the performance of two coaxial plasma focus guns, both in mode 1 operation, one with a non-conducting outer cylinder (gun A) and the other with a conducting outer cylinder (gun B). Preliminary results have already been reported for gun A (Lee *et al.* 1972). The dynamics of the current sheet and focus properties of both guns are investigated more deeply in the present experiment. A modified snow-plough model, including an ionization retarding force, is proposed to account for the anomalous low velocities observed in gun A.

† Communicated by the Authors.

2. Apparatus

The schematic drawing of the coaxial plasma gun is shown in fig. 1. The soft X-ray pinhole camera is detachable. The gun is designed with an electrode ratio of 1·7 and with a variable centre electrode length, which is chosen from 10 cm to 20 cm depending on the velocity of the current sheet.

Fig. 1

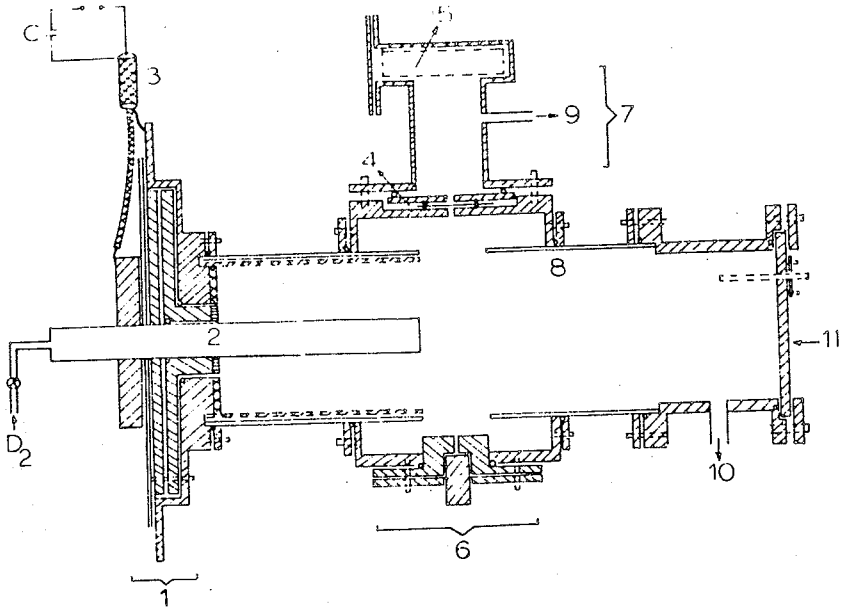

Schematic diagram showing the coaxial plasma gun with soft X-ray pinhole camera. This figure is not drawn to scale. 1 : Breech end, 2 : copper centre electrode, 3 : cable; 4 : beryllium or aluminium foil, 5 : polaroid camera, 6 : terminal for voltage measurement, 7 : soft X-ray camera and flight channel, 8 : pyrex glass cylinder, 9 : to pump, 10 : to pump and vacustat, 11 : brass plate for magnetic probe as shown or glass plate for end-on photography.

Two coaxial focus guns have been built of similar design, except for the outer return cylinder. For gun A, this outer electrode is of pyrex whilst for gun B this cylinder is of copper. Gun A is operated with an open-ended centre electrode and gun B with a close-ended centre electrode.

The soft X-ray camera is built with a pinhole of 1 mm diameter. The main discharge system is separated from the camera flight channel by one mil of beryllium foil. The flight channel is 15 cm in length, giving rise to a magnification of 2·3. The channel can be pumped down to less than 10^{-2} torr. Polaroid 3000 ASA film is used to record the radiation.

The capacitor bank (30 μF) has already been described (Lee *et al.* 1971). The discharge current is measured with a current transformer; voltages are measured with a resistive probe of 10 nsec response time; and magnetic field measurements are made with magnetic probes wound on a 1 mm diameter bobbin.

Average current sheet velocity is measured with a collimated photodiode in gun B. In gun A framing (10^7 frames per second) and streak photography, using an image converter, is used to study the instantaneous velocity and structure of the current sheet in the driving region and the radial collapsing velocity and final pinch radius in the focusing stage.

Fig. 2

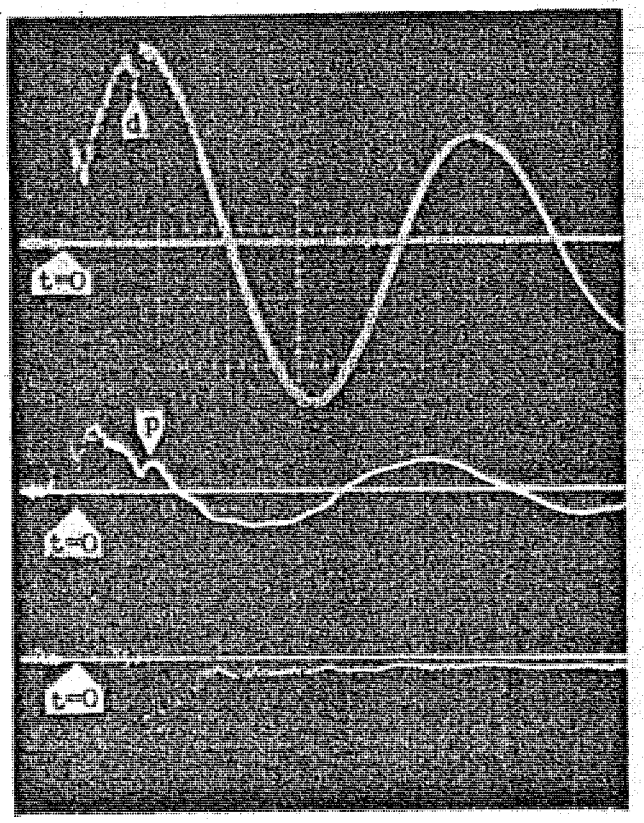

Focusing shot in gun A. 1st trace = current oscillogram (d = current dip); 2nd trace = voltage measured at breech end (p = voltage spike); 3rd trace = signal from photodiode placed at the focusing end of the centre electrode. Condenser bank voltage = 20 kV; ambient pressure = 0·3 torr; time scale = 2 μsec/division. The start of the discharge is indicated by $t = 0$ on the traces.

Typical current, voltage, photodiode signal and framing photographs for a pinching shot are shown in figs. 2 and 3. The current dip and voltage spike are indications of focusing as the current sheet implodes radially inwards at the focusing end of the centre electrode.

Fig. 3

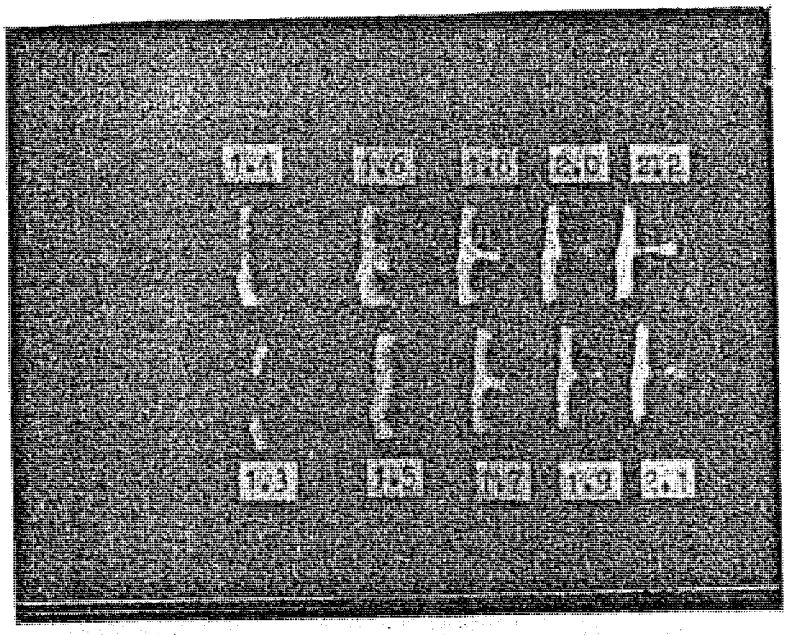

Image-converter framing-photograph in the focusing stage taken transverse to the plasma gun. The centre electrode is on the right side of each frame. Framing interval = 0·1 microsecond ; exposure time = 20 nanoseconds.

3. Dynamics of the current sheet

3.1. *Gun A*

The velocity of the current sheet is usually predictable by the simple snow-plough model. Assuming that the current sheet is a thin disc propelled down the tube by the $J_r B_\theta$ force and collecting all the mass that it encounters, the momentum balance across the current sheet can be written as

$$\frac{d}{dt}\left[m\frac{dz}{dt}\right] = \int_{r=a}^{r=b} \frac{B^2}{2\mu_0}\, dA, \tag{1}$$

where $dA = 2\pi r\, dr$.

Assuming $m = \rho_0 A z$ and $I = I_0 \sin \omega t$, the snow-plough velocity is

$$\frac{dz}{dt} = \frac{U_c}{2}\left(\tfrac{1}{2}t^2 + \frac{\cos 2\omega t}{4\omega^2} - \frac{1}{4\omega^2}\right)^{-1/2}\left(t - \frac{\sin 2\omega t}{2\omega}\right),$$

where

$$U_c^{\,2} = \frac{\mu_0 I_0 \ln\left(\frac{b}{a}\right)}{4\pi^2 \rho_0 (b^2 - a^2)},$$

and a and b are inner and outer radii respectively, ω is the discharge angular frequency, taken to be $6{\cdot}0 \times 10^5$ radians/sec in the computation and ρ_0 is the gas density.

Fig. 4

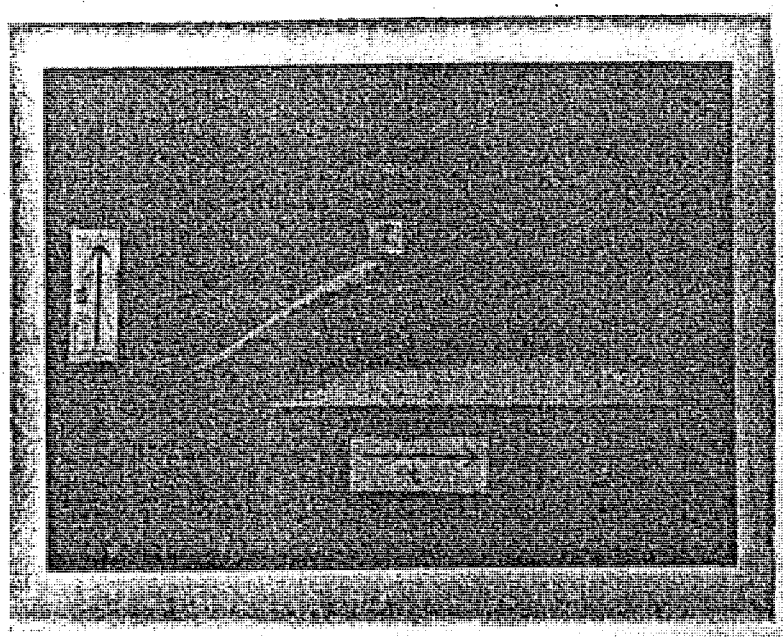

10 μsec duration image converter streak photograph in accelerating region taken with 0·4 mm slit parallel to the centre electrode (z is the distance, t is the time and f is the indication of backward flow of mass).

Fig. 5

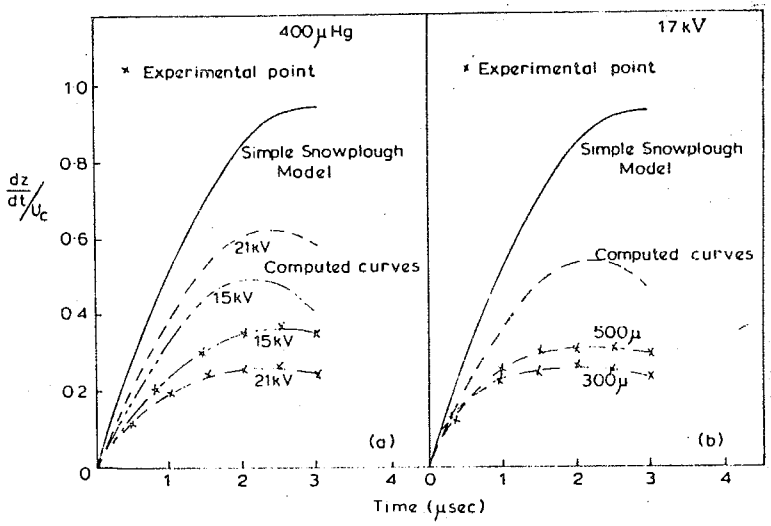

Instantaneous current sheet velocity compared with predicted velocity from simple snow-plough model and modified snow-plough model (a) fixed ambient pressure (i.e. pressure before discharge), (b) fixed condenser bank voltage. The discharge frequency, ω, is taken as $6{\cdot}0 \times 10^5$ rad./sec.

From a streak photograph (e.g. fig. 4), the instantaneous current sheet velocity at each time can be computed. Figure 5 is a series of instantaneous current sheet velocity profiles at different experimental conditions. Experimentally the current sheet reaches the maximum velocity about 1·0 μsec earlier than predicted. The maximum velocity is found to be less than half that predicted from the simple snow-plough model.

There appears to be some dominating mechanisms to slow down the sheet besides the rate of increase in mass as assumed in the simple snow-plough model. It has been demonstrated that only conduction current flows from one electrode to the other (Thom 1964). The electrons carrying the conduction current can be emitted if the cathode return is struck by positive ions from the anode†. In this experiment the outer cylinder is an insulator and no free electrons are available for conduction. The current sheet must create its path by ionizing the gas particles on the surface of the pyrex glass.

If this effect is an important one, then the absence of a conduction return, requiring the current sheet to do work in creating the return path, leads to a retarding force.

It is reasonable to assume the retardation force, f_D, to be

$$f_D = kH, \tag{3}$$

where k is the breakdown electric field intensity. We have then, from eqn. (1),

$$\frac{d}{dt}\left[m\frac{dz}{dt}\right] = \int_a^b \frac{B^2}{2\mu_0}\,dA - kH. \tag{4}$$

Assuming the electric field intensity is constant along the glass surface, and after normalization, we have

$$\frac{d^2y}{dx^2} = \left[\sin^2\theta x - Qx|\sin\theta x| - \left(\frac{dy}{dx}\right)^2\right]\frac{1}{y}, \tag{5}$$

where

$$y = \frac{z}{z_m}, \quad x = \frac{t}{t_1}, \qquad t_1 = \frac{z_m}{U_c},$$

$$\theta = \omega t_1, \quad Q = \frac{V_b I_0}{\pi\rho_0(b^2-a^2)U_c^3}, \quad k = \frac{V_b}{z_m}.$$

In this definition of k, a uniform electric field along the breakdown path is assumed. The absolute value of $(\sin\theta x)$ is used because the frictional force always opposes the motion. Equation (5) was solved numerically with $V_b = 500$ V and $z_m = 10$ cm and the result is displayed in fig. 5 (computed curves).

The result shows that this loss in energy leads to a very significant retardation force. The peak velocity is calculated to be reduced by 40% at 17 kV, 50% at 15 kV and 30% at 21 kV operations compared to the simple snow-plough model calculation.

† The required ionization may also be produced by precursor ultra-violet radiation from the shock front. In this case the energy loss from the shock front must couple back to the current sheet, resulting also in the retarding force f_D. We thank Professor K. G. Emeleus for suggesting this photoionization mechanism to us.

Extensive magnetic mapping of the acceleration region enabled a number of conclusions to be made regarding the current sheet (Chen 1972):

(*a*) the shape of the current sheet is fairly planar and vertical to the axis of acceleration, this shape remaining roughly constant at various operating voltages and pressures;

(*b*) the current sheet, just before radial collapse, has a front region typically 1·5 cm thick of high current density followed immediately by a region of more diffuse current (about a tenth the current density of the front region);

(*c*) the current-shedding effect (Lee *et al.* 1972) is evident; for example, 30% of the total current never leaves the back wall. This current-shedding effect is more serious at higher operating voltages and lower ambient pressures.

Fig. 6

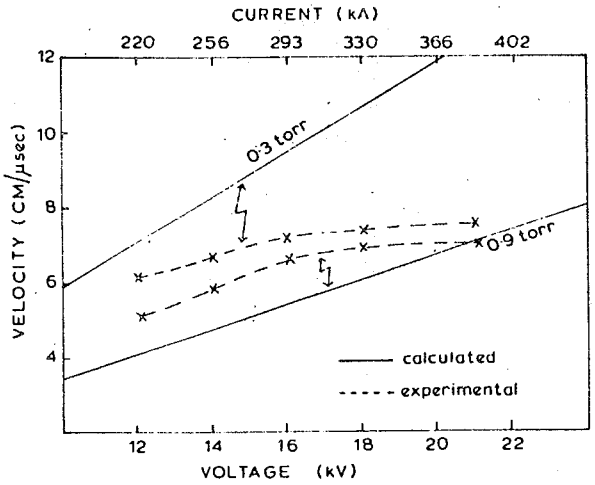

Average velocity of current sheet versus peak current.

3.2. *Gun B*

The average velocities obtained from photodiode signals are compared with predicted velocities by the snow-plough model in fig. 6. Overall, the velocity measured is higher than that with a non-conducting outer cylinder. This indicates that a conducting outer cylinder is necessary to produce a high current sheet velocity.

The shape of the current sheet is similar to that obtained in gun A. Likewise, current shedding is significant at high voltage and low ambient pressure.

The plasma resistance can be computed from the voltage measured at the focusing end of the electrodes, and the main discharge current. For a 16 kV discharge at 1 mm Hg pressure, the plasma resistance decreases from 1·4 milliohm at $t = 0{\cdot}25$ μsec to a constant value of 60 μohm at $t = 2$ μsec (fig. 7). At this time, the measured current sheet velocity is 6 cm/μsec. Calculations based on a current sheet-shock wave system show that, at this current sheet speed, the shocked plasma is fully ionized.

Fig. 7

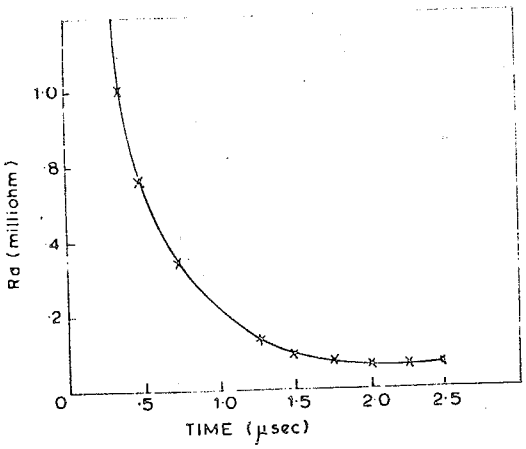

Plasma sheet resistance, computed from voltage measured at the focusing end of the electrodes, and main discharge current. Condenser bank voltage = 16 kV, ambient pressure = 1 torr.

Fig. 8

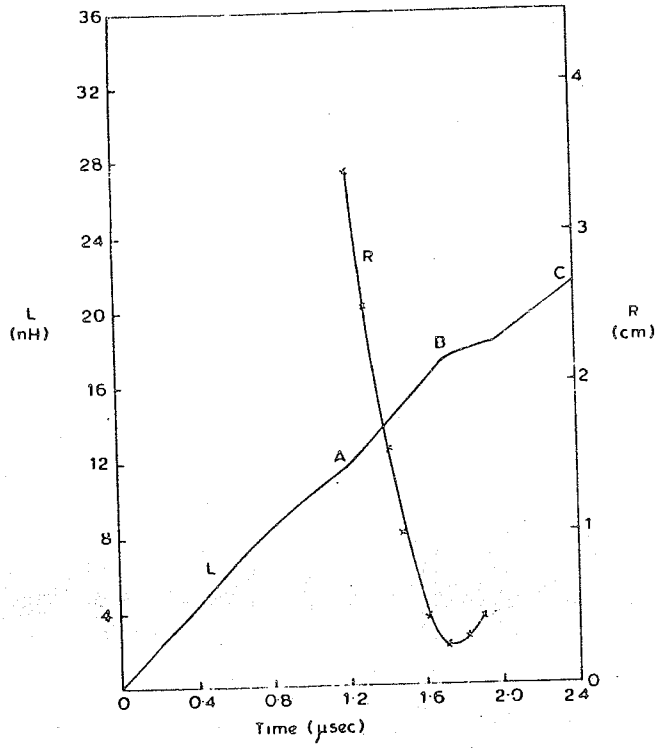

The inductance, L, of the system computed from voltage and current oscillograms. The radius, R, of the plasma column estimated from 10^7/sec framing photograph. Condenser bank voltage = 20 kV ; ambient pressure = 0·3 torr.

In this particular shot the current sheet thickness estimated from magnetic probe traces is 1·5 cm. Using this thickness and the resistance of 60 μohm, an electron temperature of 40 eV at the moment just prior to collapse is obtained from Spitzer's (1967) relationship.

4. Focus study

4.1. *Gun A*

In the case of gun A focusing always occurs at pressures higher than 0·3 torr. Focusing is indicated by the voltage spike and current dip corresponding to the arrival of the current sheet shown by the photodiode signal (fig. 2). Voltage spikes of 2–3 kV and current dips of 80 kA are observed. These values obtained are comparatively lower than reported (Mather 1968). This implies that the radial collapsing and compression are rather slow in the case of gun A.

Figure 8 is a plot of inductance and plasma radius against time, computed from figs. 2 and 3. The inductance is obtained from the voltage and current oscillograms using the equation

$$L(t) = \frac{\int_0^t V(t)\,dt}{I(t)}.$$

The inductance increases almost linearly during the driving period from 0 to A. As the current sheet arrives at the end of the centre electrode, it is likely that part of its mass diffracts around and implodes inwards with a high radial velocity. Hence the inductance increases more rapidly from A to B. As the plasma column expands, the inductance decreases, resulting in a slower rise of inductance (from B to C).

From the radius–time curve (fig. 8), obtained from the framing photographs of fig. 3, an estimate of minimum radius of 2·0 mm is made. An estimate of 1·6 mm is also obtained from the inductance jump (AB of fig. 8) during focusing. This value is higher than reported (Mather 1966), probably because of the loss of radial momentum at the compressing stage. This is indicated in fig. 4, which shows that, during the compressing stage, backward flow of mass into the hollow centre electrode, of velocity as high as 25 cm/μsec, is observed. This represents a loss in initial momentum and is likely to slow down the radial collapse, causing a slower compression, thus giving a larger final radius.

4.2. *Gun B*

In the case of gun B the loss in initial momentum into the hollow centre electrode is more significant, due to the higher radial collapsing velocity (15 cm/μsec). In order to prevent this large loss in initial momentum, the hollow centre electrode is sealed off with a copper disc. Pinching is observed with sharper voltage spikes (fig. 10). Soft X-rays are emitted at a bank voltage of 29·6 kV. For this discharge the collapse is found to be a multiple one, as shown in the voltage and current oscillogram. The half period of the main discharge is lengthened from 4·7 μsec to 6 μsec (fig. 9 *b*). This suggests that the inductance increase due to the focus formation sustains itself long enough to slow down the main discharge, probably due to the long confinement of the plasma focus.

Fig. 9

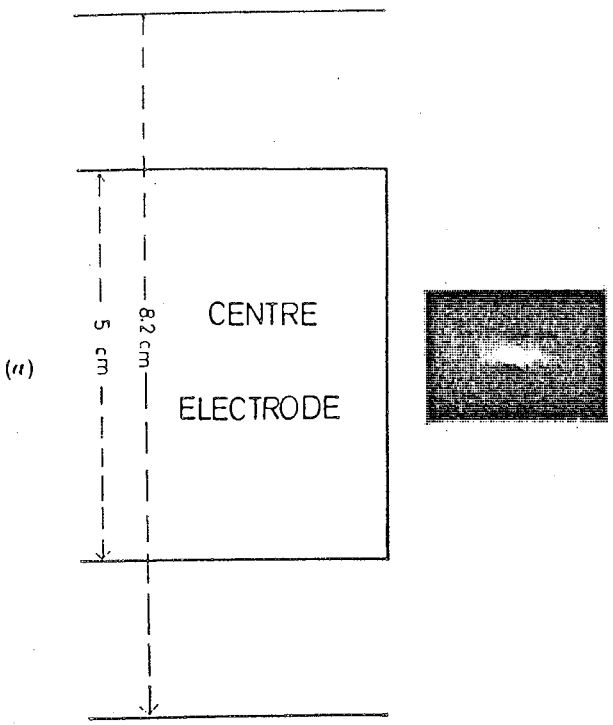

(*a*) Soft X-ray photograph in transverse view. The surface of the centre electrode is beyond the left side of the photograph as shown to scale. Voltage, 29·6 kV. Pressure 1·3 torr. Condenser bank energy 13 kJ. (*b*) The voltage (upper) and current (lower) oscillograms.

The minimum focus estimated from the soft X-ray pinhole-camera photograph (fig. 9 *a*) is 0·7 mm in radius and 3 mm in length, located at 1·7 cm from the surface of the end of the centre electrode. A 1 mil beryllium foil was used to cover the pinhole when this soft X-ray photograph was taken. When a 1 mil aluminium foil was used, under the same conditions, no soft X-ray image was obtained on the polaroid (3000 ASA) film, although the current and voltage waveform indicate severe focusing. From soft X-ray absorption data, the X-ray emitted was estimated to have a wavelength of more than 5 Å, corresponding to an energy of less than 2·5 keV. Assuming the radiation is Bremsstrahlung, the electron temperature of the focus is estimated as between 0·8 keV to 2·5 keV.

Fig. 10

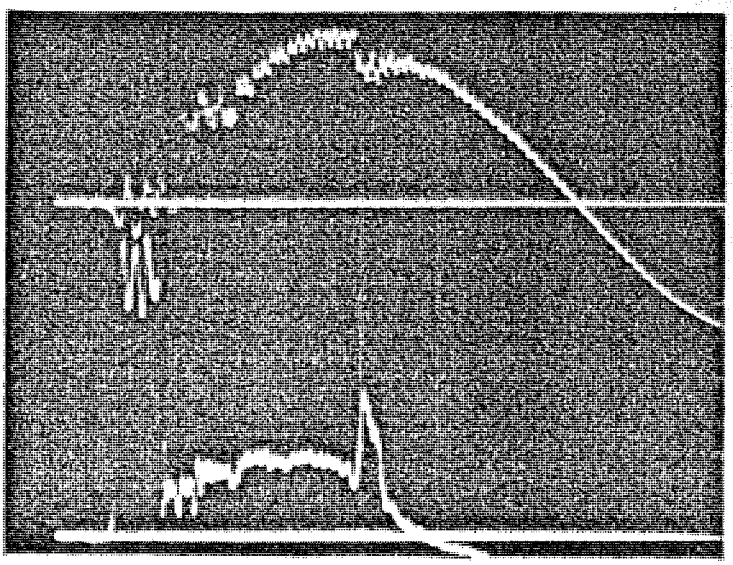

Typical current (upper) dip and voltage (lower) spike of a focusing shot in gun B.

From streak photographs, the average radial velocity measured at different distances from the surface of the end of the centre electrode decreases as the distance increases from the surface. This shows that the radial compression is non-cylindrical in nature. For a non-focusing shot, the average radial velocity decreases from 15 cm/μsec at 0·7 cm to 5 cm/μsec at 2·1 cm from the surface of the end of the centre electrode. Average radial velocities as high as 25 cm/μsec are observed for focusing shots.

5. Discussion and conclusion

The maximum axial velocity of the pre-focus current sheet is lower in gun A compared with gun B. This is in agreement with a snow-plough model including an ionization retardation force term.

A current-shedding effect is observed in both guns and appears to be independent of whether the outer cylinder is conducting or not.

The shape of the current sheet is independent of the nature of the outer cylinder. It is planar and vertical in the whole driving region for both cases. The current sheet is 1·5 cm in thickness and is followed by a blob of dense plasma.

In both guns, focusing is obtained. A focus radius of 0·7 mm and soft X-ray emission of energy between 0·8 to 2·5 keV are observed for gun B. The radial compression is a non-cylindrical one, depending greatly on the initial radial momentum, and on the loss of this momentum in the case of an open-ended centre electrode.

Acknowledgments

We thank Professor S. P Thong for his support of this project. We also thank Mr. S. P. Chow, Mr. B. K. Lee and Mr. T. S. Ho for their assistance in the experiment.

References

Chen, Y. H., 1972, M.Sc. Thesis, University of Malaya.

Hart, P. J., 1964, *J. appl. Phys.*, **35**, 3425.

Lee, S., Thong, S. P., and Tan, B. C., 1971, Plasma Physics Laboratory Report 2/71, University of Malaya.

Lee, S., Chen, Y. H., Chow, S. P., Tan, B. C., Teh, H. H., and Thong, S. P., 1972, *Int. J. Electron.*, **33**, 85.

Mather, J. W., 1965, *Physics Fluids*, **8**, 366; 1966, *Plasma Physics and Controlled Nuclear Fusion Research*, Vol. II (Vienna: International Atomic Energy Agency), p. 389; 1968, *Physics Fluids*, **11**, 611.

Spitzer, 1967, *Physics of Fully Ionized Gases* (J. Wiley), Chap. 5.4, p. 139.

Thom, K., 1964, *Physics Fluids*, Suppl., **7**, S67.

Malaysian J. Sci. 2(B) (1973); 157–169

A simplified method of switching a 2 mega-ampere capacitor bank using a voltage division technique

S. P. THONG[1,2] AND S. LEE[1,3]

Abstract

A 4-module system is described with each module incorporating twenty-five 40 kV, 0.6 μF capacitors. A voltage division technique is used which simplifies a number of technical problems commonly encountered in the assembly of high voltage, fast capacitor banks. On each capacitor is mounted a 2-element adjustable spark-gap across which is held about half the capacitor voltage V_0. The other half of V_0 is held across a group of triggered switches. When the triggered switches are closed, the full value of V_0 is applied across the spark-gaps which then break down.

The advantages of the system include (1) the full capacitor voltage is isolated to the capacitor terminal during charging, (2) reduction of switch-inductance from the paralleling of the triggered switches, and (3) allows the use of 20 kV ignitrons to switch a 40 kV capacitor bank

The peak current, at 40 kV, from the four modules connected in parallel, was measured at 1.91 MA with a periodic time of 7.6 μs and a quarter cycle power of 26.4×10^9 W. The system has a jitter of ± 50 ns.

INTRODUCTION

For capacitor banks used in high current discharges good control and design are necessary, especially if such banks are to be used for research in plasma physics, metal and material forming, laser pumping and high velocity physics (Frungel, 1965). For many plasma devices, a fast current rise-time and precise synchronisation with measuring equipment are additional requirements.

With a high voltage bank of capacitors, the problem of corona is acute during the period of charging of the capacitor bank. Corona radiation can cause failure of the surrounding insulation so that corona discharges must be kept down. Experience under tropical conditions (in an air-conditioned laboratory where the temperature is 22°C and the humidity is 60%) shows that for periods of half a minute or so, the voltage can be held at 25 kV with a tolerable level of corona if all terminations have radii of curvature in excess of 1.5 mm. At 40 kV, the minimum radius of curvature is 3 mm. Thus, sections used at 40 kV have to be engineered from $\frac{1}{4}$ inch plates while sections used at 25 kV require only $\frac{1}{8}$ inch plate. It is, therefore, advantageous to confine the high voltage to the live terminal of the capacitor with the use of a spark-gap at each capacitor terminal.

This principle has been utilized in a number of high voltage banks. Invariably the spark-gap mounted on each capacitor is a triggered spark-gap acting as a switch, so that added to the advantage of voltage isolation is the advantage of reduced switch inductance arising from the parallel connection of a large number of switches (Fitch & Mc-

[1] Physics Department, Universiti Malaya, Kuala Lumpur, Malaysia.
[2] Present Address: Tengku Abdul Rahman College, Kuala Lumpur.
[3] Correspondence should be directed to Dr S. Lee.

Cormick, 1959). However, in a bank assembled from a large number of individual capacitors, the number of spark-gaps mounted in this way exceeds by far the number required to reduce switch inductance to a negligible proportion (Fitch *et al.*, 1959). This excess number of switched spark-gaps represents an undesirable feature because there are technical reasons which favour the reduction of the number of switched spark-gaps. Firstly, these gaps have to be operated near the static breakdown voltage (typically 80 to 90%), so that the larger the number of gaps the greater will be the probability of a premature breakdown in one of them. Secondly, the trigger voltage required is often larger than the bank voltage and has to be applied simultaneously to all the gaps. The larger the number of triggered gaps the greater is the technical problem of providing the trigger pulses.

Some capacitor banks have been operated with a reduced number of triggered switches. Mather (1970) and Carpenter, Williams, Mather, Bottom & Ware (1970) have used a low-inductance graded vacuum-switch for switching modules at 50 kV and 20 kJ. Gross & Miller (1970) have used a low inductance (10 to 20 nH) dielectric gas switch to switch a number of capacitors connected by parallel plates. Barnes, Gruber & James (1967) have operated a pressurized field distortion spark-gap to switch 40 kV, 10 kJ at a peak current of 450 kA. In such systems, however, the capacitor voltage is no longer isolated at the capacitor terminals but extends all the way to the high voltage collector plate of the switches.

All three advantages of voltage isolation, reduced switch inductance and simpler switching requirement can be incorporated in a system in which a 2-element spark-gap is mounted on each capacitor. This spark-gap is arranged to hold about half the capacitor voltage V_0 whilst the other half of V_0 is taken up across a group of triggered switches. When this group of switches are triggered, the voltage across the 2-element spark-gap rises to V_0. If the gaps are set at a static breakdown voltage $V_s = 0.7\ V_0$, the holding voltage is only 71% of V_s whilst the over-voltage on triggering is 43%. This ensures stable holding behaviour and simultaneous breakdown. Further, there is an added advantage in that the triggered switch assembly is required to hold and switch only half the bank voltage. The number and type of triggered switches required can be compromised between minimizing inductance and jitter, and maximizing technical economy.

The present work utilizes this principle of voltage division and uses two 7703 ignitrons as triggered switches for each 12.5 kJ module of 25 capacitors. Other workers (Butler, Henins, Jahoda, Marshall & Morse, 1969; Mather, 1965) have used the 7703 ignitron to switch fast capacitor banks for plasma acceleration experiments, but they have been limited by the ignitron voltage rating to 20 kV capacitors. By using voltage division, the 7703 ignitron is made to switch a 40 kV capacitor bank. The peak current capability per ignitron is tested to be in excess of 300 kA (for pulsed discharges of 132 kHz, 85% reversal, 0.6 coulomb original charge, not more than 1 discharge per minute). The reasons for using the 7703 ignitrons are that the 7703 is readily available commercially, is robust and continuously reliable, will switch 100 V to 25 kV without any adjustment, requires hardly any maintenance and only a very modest trigger input. The switching jitter for a bank of eight ignitrons is ± 50 ns which does not compare with jitters of ± 15 ns to ± 30 ns, typical of capacitor banks (Carpenter *et al.*, 1970; Barnes, *et al.*, 1967) using well designed spark-gaps. However, the ± 50 ns jitter is sufficiently low for most of the plasma devices being operated and planned in this laboratory. For more stringent jitter requirements triggered spark-gaps can be used in place of the ignitrons.

OPERATIONAL ARRANGEMENT

The capacitor bank comprises of 100 pieces of 'Wego' 0.6 μF, 40 kV high frequency discharge capacitors. The internal inductance is rated at 210 nH. Each capacitor has coaxial termination feeding a coaxial transmission cable 8 to 12 ft long (SC322, 23 nH per ft), *via* a two-element spark-gap (adjustable 0 to 10 mm) mounted directly on the high voltage terminal of the capacitor (fig. 1). Twenty five capacitors are connected in this manner into the high voltage collector plate (40 cm × 40 cm) of one module. This connects on to the anodes of two 7703 ignitrons *via* two extension plates. A coaxial clamp on the body of the ignitron serves as the cathode lead. This coaxial clamp is connected to a short wide plate which acts as the high voltage output-plate of the switch (fig. 2). The earth collector-plate is common to all the modules, and a short wide earth extension-plate runs parallel to the high voltage output-plate. Both the earth collector-plate and the earth extension-plate are kept as close as possible to the high voltage

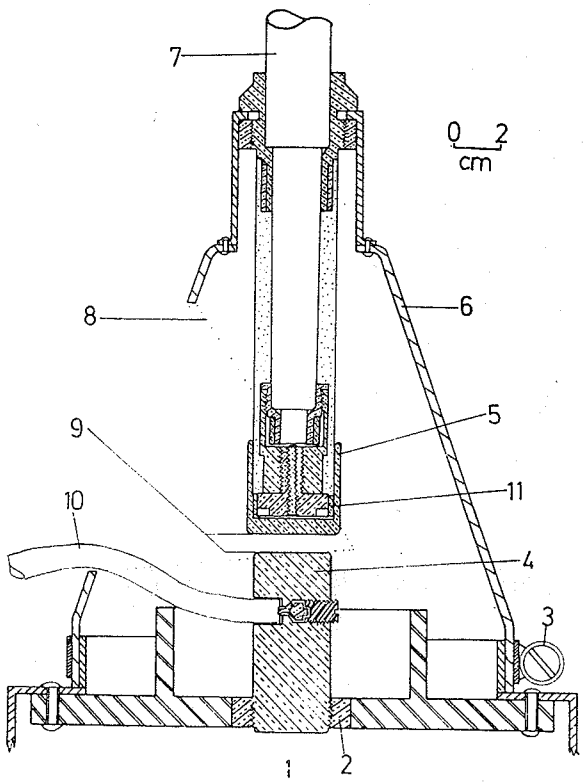

FIGURE 1. Two-element adjustable spark-gap for voltage division.

Key:
1 = 'Wego' capacitor rated at 0.6 μF, 40 kV
2 = live terminal of capacitor
3 = earth-return clamp
4 = fixed electrode
5 = 0 to 10 mm adjustable electrode
6 = earth return enclosure of capacitor
7 = coaxial cable leading to HV collector and earth-return, copper braids not shown
8 = cutaway to allow access to two-element spark-gap
9 = 'Elkonite' face for electrodes
10 = charging lines from 40-kV distributor
11 = bronze spring for electrical sliding contact

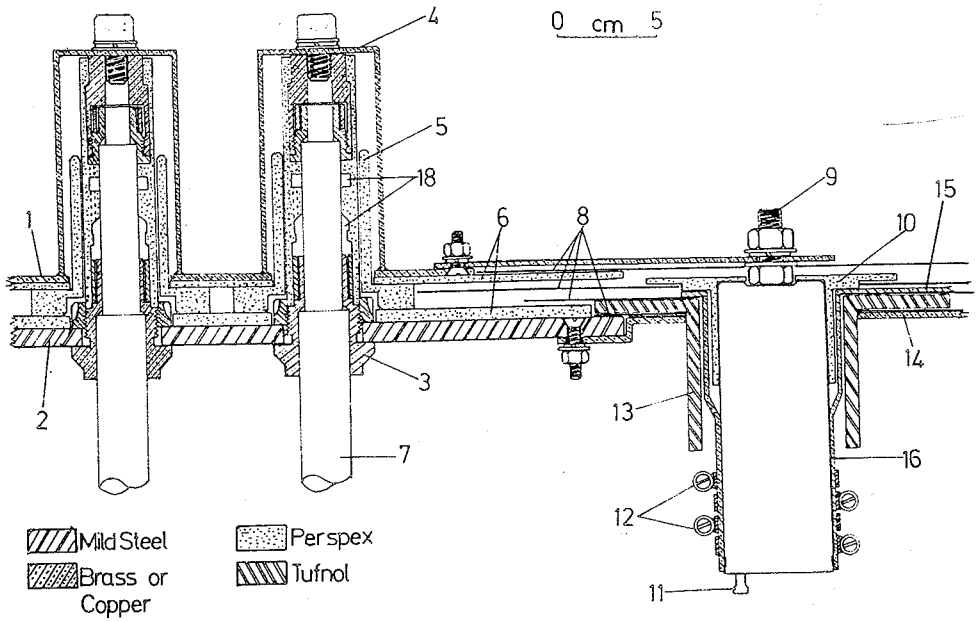

FIGURE 2. High voltage collector-plate and extension-plate showing details of the connections of cables and one ignitron.

Key:
1 = HV collector-plate
2 = earth-return plate
3 = earth-clamp for coaxial cable
4 = HV connection for coaxial cable
5 = perspex hat-insulator
6 = perspex insulating sheets
7 = coaxial cable, copper braids not shown
8 = mylar insulating sheets
9 = ignitron anode
10 = perspex anode-insulating cap
11 = igniter terminal
12 = ignitron cathode-clamps
13 = tufnol cathode-insulator
14 = to earth-return of load
15 = to live-terminal of load
16 = ignitron cathode return
18 = oil spaces

current-path, insulation being supplied by mylar sheets, perspex sheets and perspex caps. The design is to keep down circuit inductance.

The four modules are arranged as shown in figure 3, with ignitrons 1A and 1B switching module 1. The output of each ignitron is connected to the load by coaxial cables (Uniradio 67) of length varying from 3 ft to 8 ft depending on the distance of the ignitron from the load. The number of cables per ignitron ranges from 6 to 12 and is varied to keep the output inductance per ignitron approximately constant at 40 nH. A total of 72 cables are connected to the load; the effective inductance of these cables, all in parallel, is estimated at 5 nH.

The 7703 ignitron used to switch the module is rated at 100 kA peak current, but has been tested in this module arrangement, between 150 kA to 320 kA for more than 1000 discharges without damage or serious deterioration. A number of procedures were found to be necessary when operating these ignitrons beyond its current rating. When first used, an ignitron was subjected to increasing pulsed currents in steps of approxi-

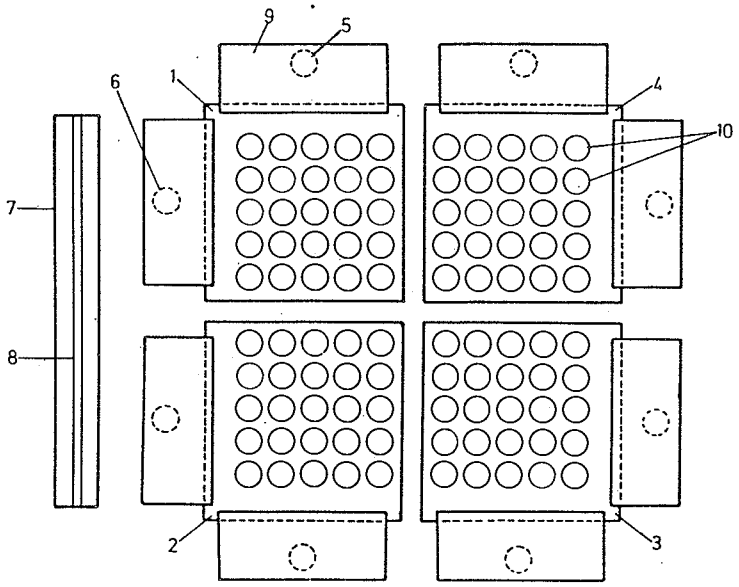

FIGURE 3. Schematic top-view of four modules showing positions of modules, ignitron and load.
Key: 1 = module 1
2 = module 2
3 = module 3
4 = module 4
5 = ignitron 1A
6 = ignitron 1B
7 = 1-metre wide load
8 = groove for current coil
9 = output-plate
10 = HV coaxial connections to HV top-plate

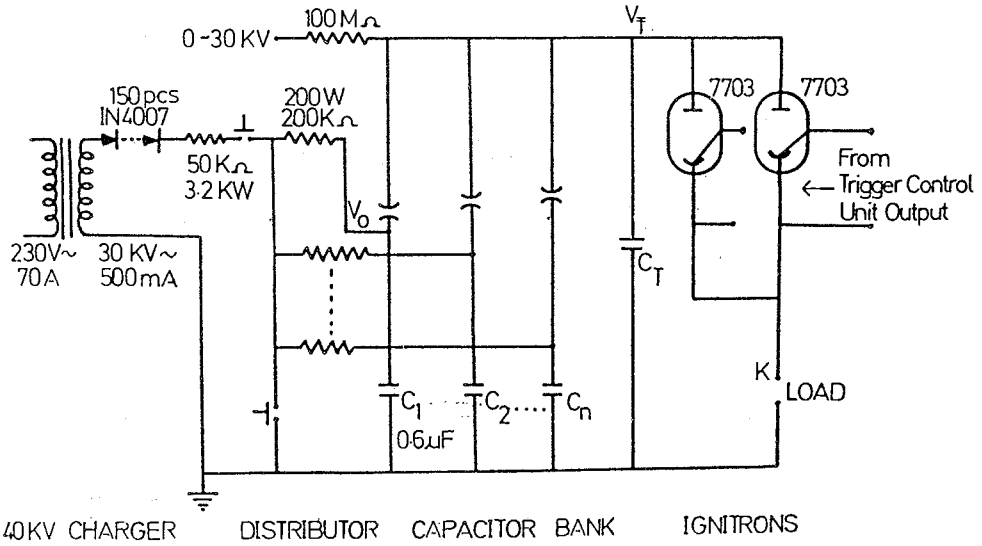

FIGURE 4. Circuit diagram for a module of 25 capacitors, showing charging circuit, distributor, capacitor bank, voltage division spark-gaps, ignitrons and load.

mately 50 kA up to 300 kA. Occasionally, after a discharge at high currents, an ignitron becomes unable to hold voltage probably because of mercury sputtered on to the complex anode seal. By shorting one of the spark-gaps (fig. 4), a.d.c. current of up to 300 mA is then allowed to flow through the ignitron until it holds voltage up to approximately 15 kV; this usually takes less than 10 seconds. Further conditioning up to 28 kV is then carried out with a.d.c. current of 100 μA from the V_T charger (fig. 4). This final process takes from 1 to 5 minutes; at the end of this the ignitron is able to hold a d.c. voltage of 28 kV indefinitely with no noticeable leakage current.

The maximum voltage capacity of the switching system is increased to 40 kV by the use of auxilliary spark-gaps as illustrated in figure 4. The components C_1, C_2 . . . C_n are the 25 capacitors in the module, each with an adjustable 2-element spark-gap mounted directly above it. Each spark-gap isolates its capacitor from the top plate. The trigger capacitance $C_T \simeq 10^{-8}$ F is made up of the combined capacitance of the transmission cables linking the spark-gaps to the top-plate and the stray capacitance of the top plate to earth. For operation at or below 20 kV, the spark-gaps are closed so that the ignitron acts as a simple switch. For operation above 20 kV, the gaps are pre-set to a gap length such that the static breakdown voltage of the gaps is V_s. The trigger capacitor, C_T, is charged to V_T, and the main capacitor C_1 . . . C_n are charged to the desired operating voltage V_o. The following three conditions are fulfilled (Lim, Thong & Tan, 1969):

$$V_T < 20 \text{ kV},$$
$$V_o - V_T < V_s, \text{ and}$$
$$V_o > 1.25\ V_s.$$

The sequence of operation is as follows. When the two 7703 ignitrons are triggered, C_T discharges through the ignitrons with a characteristic time governed by $(C_T L)^{\frac{1}{2}}$, where L is the inductance of the C_T-ignitrons-load circuit. This time is less than 30 ns. For example, if V_T = 15 kV, then the anode voltage-fall rate is 10 kV in an estimated time of 20 ns; this is the isolation time between gaps, provided by the 8 to 12 ft of transmission cables. As V_T falls, the voltage across the spark-gaps increases from $(V_o - V_T)$ towards the full value of V_o. If the first spark-gap to fire breaks down at a value V_{s1} (say), the other spark-gaps are overvolted above V_{s1} by a further 10 kV during the isolation time. This ensures prompt firing of all the spark-gaps within 10 ns of each other.

The ignitron is triggered by the trigger control circuit illustrated in figure 5. Between the sync pulse leading edge and the start of current flow in the ignitron, there is a delay of (1.65 ± 0.05) μs.

For parallel triggering of two or more modules, the control circuit is the same except that the Klytron output stage is modified as shown in figure 6. The circuit for each module is shown in figure 4. The point K of each module is connected to identical points of the other modules. This arrangement affords maximum inter-module isolation.

Moreover, using this cathode-strapped arrangement, the firing of one module can be delayed with respect to another module. Two separate trigger control units are required in this case, the two units being linked by a delay unit. On command, the first unit triggers the ignitrons of module 1. The sync pulse preceding this triggering is then used to trigger a delay unit. After a pre-set delay, module 2 is triggered by its control unit. Such an arrangement is useful in certain applications.

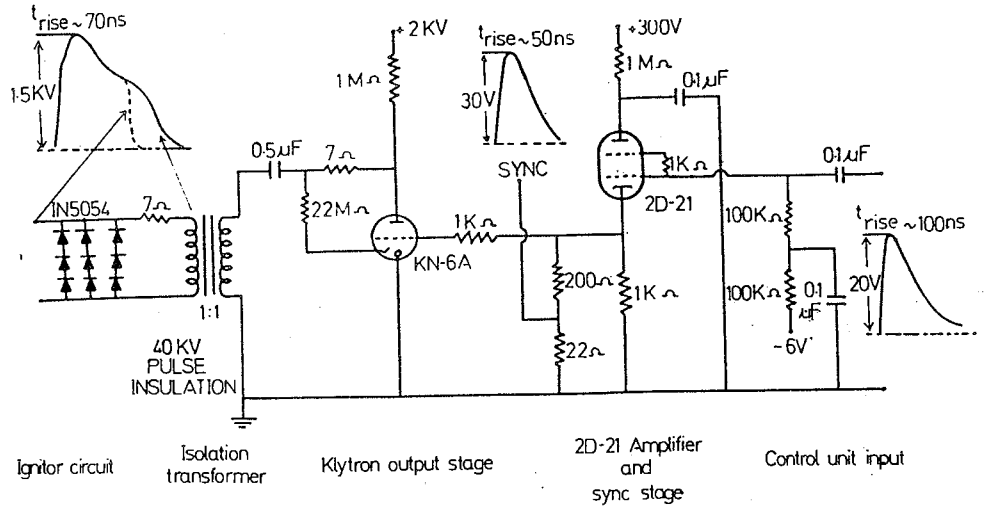

FIGURE 5. Circuit diagram of the ignitron trigger-unit for providing single trigger pulse. This unit is triggered by an input pulse of amplitude 20 V (from the right in above diagram) and releases a 1.5 kV pulse via an isolating transformer (40 kV pulse-isolation) from the left.

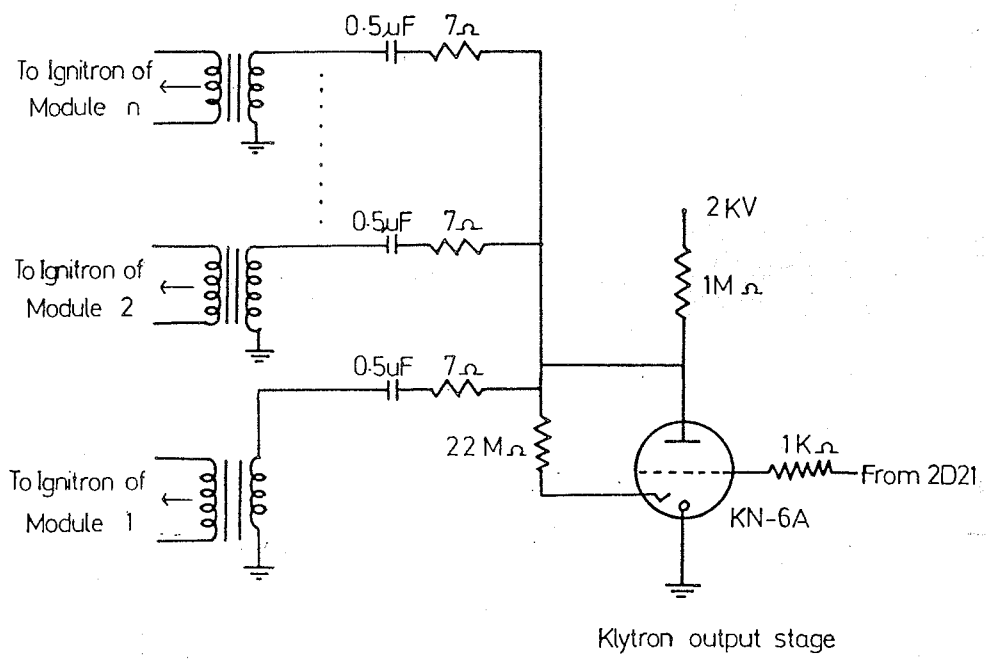

FIGURE 6. Modification to single trigger unit to allow for simultaneous triggering of a number of ignitrons. This arrangement supplies each ignitor with an independent energy source, so that there is minimum interference among the triggering pulses.

MEASUREMENT OF DISCHARGE PARAMETERS

Theory. For a damped oscillatory discharge (L-C-R), the value of the first peak current is,

$$I_1 = \frac{I_o}{(1-p^2)^{\frac{1}{2}}} \sin[\omega t_1(1-p^2)^{\frac{1}{2}}] \exp\left(-\frac{R}{2L} t_1\right) \tag{1}$$

where I_o is the undamped value of the peak current,
t_1 is the time of occurence of the first peak current,
$p = R/2(L/C)^{\frac{1}{2}}$ is a damping factor (Montfoort, 1968), and
ω is the undamped angular frequency.

The time for the first half of the damped cycle,

$$t_{12} = \frac{\pi(LC)^{\frac{1}{2}}}{(1-p^2)^{\frac{1}{2}}} \tag{2}$$

The reversal ratio, f, is given by,

$$f = \frac{I_2}{I_1} = \frac{-\sin[\omega t_2(1-p^2)^{\frac{1}{2}}]}{\sin[\omega t_1(1-p^2)^{\frac{1}{2}}]} \exp\left[-\frac{R}{2L}(t_2-t_1)\right] \tag{3}$$

where t_2 is the time of the second current peak.

From equations (1), (2) and (3), the values of I_1, L and R can be computed once C, t_1, t_{12}, t_2 and f are measured. The computation is cumbersome and for low damping an approximate method is preferred.

Provided the damping is slight *i.e.* $p \ll 1$,

$$I_1 = \frac{\pi}{2}\bar{I} = \frac{\pi}{2}\frac{CV_o(1+f)}{\frac{1}{2}T} \tag{4}$$

where $\bar{I}$ is the average current over the first half cycle. Since f and T, the average periodic time, can be measured, I_1 can be computed. The quantities L and R are then calculated from the approximate equations:

$$T = 2\pi(LC)^{\frac{1}{2}} \tag{5}$$

$$\frac{RT}{4L} = \log\left(\frac{1}{f}\right) \tag{6}$$

Experimental check. The capacity of the bank was measured with a bridge and found to be

$$C = 62.17\ \mu F$$

The following values of T and f were obtained from measurements made over a number of discharges:

$$T = 7.6 \pm 0.1\ \mu s$$
$$f = 0.84 \pm 0.1$$

Parameters of the bank were then computed from equations (4), (5) and (6). These are presented in column 2 of table 1.

For comparison with the more exact equations (1) to (3), additional measurements were made of t_1, t_{12} and t_2:

$$t_1 = 1.85\ \mu s$$
$$t_{12} = 3.80\ \mu s$$
$$t_2 = 5.65\ \mu s$$

Parameters of the bank were then computed using equations (1) to (3). The results are presented in column 3 of table 1. Comparison of columns 2 and 3 shows that the difference between the two methods is within experimental error.

TABLE 1

Comparison of bank parameters computed by the approximate equations with those computed by the exact equations

Bank Parameter	Approximate Method	Exact Equations
L	23.5 nH	23.5 nH
R	2.16 mΩ	2.14 mΩ
Z_0	19.5 mΩ	19.5 mΩ
p	0.056	0.055
I	0.919 I_0	0.918 I_0

$Z_0 = (L/C)^{\frac{1}{2}}$, $I_0 = V_0/Z_0$.

Comparison with Montfoort's Method. In Montfoort's Method (1968), which is applicable for a wide range of values of p, I_1 and t_1 are known; from their values p is calculated by interpolation from his Table 1. The values of L and R are then computed. Using his Table 1 and the value of p = 0.056 computed from equations (4), (5) and (6) it is found that:

$$I_1 = 0.919\ I_0.$$

This agrees with table 1 and confirms the adequacy of the approximate method.

PERFORMANCE OF THE CAPACITOR BANK

The capacitor bank was discharged into a low inductance short made out of a sheet of copper, 1 metre wide, 3″ long and $\frac{1}{8}$″ thick. This sheet has a 1″ × 1″ groove across its full width to accomodate an insulated Rogowski current coil. This coil was operated as a current transformer (Leonard, 1965) with 5000 turns and with a terminating resistance of 0.2Ω. Its nominal sensitivity is thus 1 volt per 25 kA. The coil frequency response was estimated to be adequate in the range of 300 Hz to 1 MHz.

The capacitor bank was charged over a range of voltage values from 1 kV to 40 kV and discharged. In each case the current coil waveform (*e.g.* fig. 7) was displayed on a Tektronix 556 oscilloscope and photographed. Measurements were then made of T (T averaged over 2 cycles) and f (f averaged over 5 peaks); and I_1, L and R were then computed according to equations (4), (5) and (6). The results are presented in figure 8.

DISCUSSION

Parameters of the capacitor bank. The results show that between 5 and 40 kV a number of parameters can be assigned to the bank:

$$T = (7.62 \pm 0.03)\ \mu s$$
$$f = (0.840 \pm 0.007)$$
$$L = (23.7 \pm 0.2)\ nH$$
$$R = (2.17 \pm 0.09)\ m\Omega$$

Peak current per kV: $I_1/V_0 = (47.2 \pm 0.3)$ kA/kV.

Maximum rate of change of current per kV: $I/V_0 = (4.23 \pm 0.03) \times 10^{10}$ (kA/sec)/kV.

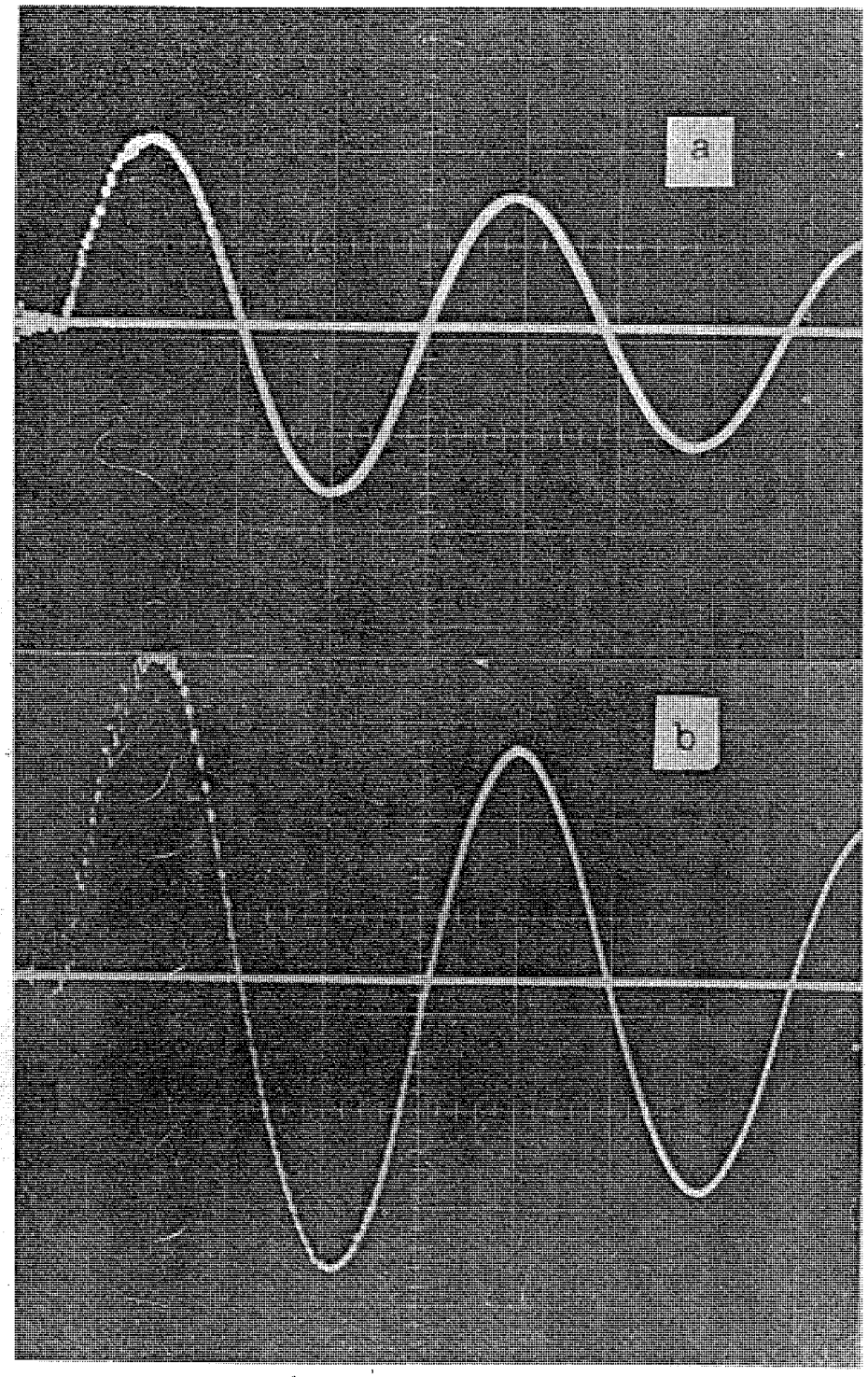

FIGURE 7. Oscillograms of current coil output during a capacitor bank discharge.
(a) spark-gap setting = 0, V_0 = 20.0 kV time scale = 2 μs/cm, current (vertical) scale = 475 kA/cm, I = 940 kA, T = 7.6 μs, f = 0.84.
(b) spark-gap setting = 7 mm, V_0 = 30 kV, time scale = 2 μs/cm, current scale = 435 kA/cm, I = 1.43 MA, T = 7.6 μs, f = 0.84.

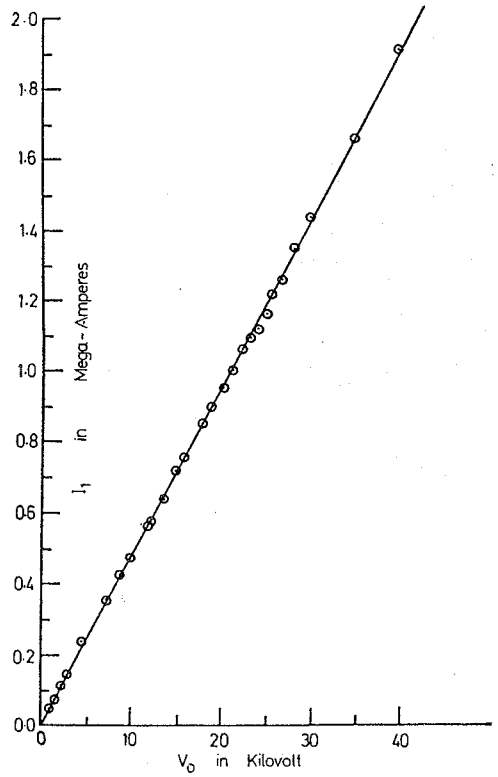

FIGURE 8. Measured peak current as a function of capacitor bank voltage.

It is noticed that the bank resistance, R, is much more variable than the other parameters. Further, for V_0 below approximately 5 kV, the resistance increases towards 5 mΩ. This is a clear indication that the resistance contributed by the ignitrons is beginning to dominate the circuit resistance for currents lower than 20 kA per ignitron.

The average power for the first quarter cycle, defined elsewhere (Gross, 1970) as a 'Figure of Merit', is for this bank = 26.4×10^9 W at 40 kV.

Estimated contributions to bank inductance. The following are the estimated design inductances of the components of the capacitor bank:

1. Capacitors (4 modules in parallel, each module with 25 capacitors in parallel)	— 2.25 nH
2. Transmission coaxial cables and spark-gaps (100 in parallel)	— 2.50 nH
3. Collector and extension plates	— 7.0 nH
4. Ignitrons (8 in parallel)	— 5.0 nH
5. Output coaxial cables (72 in parallel)	— 5.0 nH
6. Shorting plate	— 1.1 nH
Total	22.85 nH

The inductances of items 1 and 4 are computed from the data supplied by the manufacturers. The inductances of the other items are estimated from the geometrical dimen-

sions assuming simple current paths. The value of the total design inductance agrees with the measured inductance to within 4%.

Calibration of the current coil. The waveform of the current coil output enables the peak discharge current to be computed using equations (4) to (6). From these computed values the calibration factor for the coil at different currents are obtained. It is seen that the value of the calibration factor K_s is only approximately a constant over the whole range of currents from 200 kA to 1.9 MA. Over this range the value of K_s decreased by 10% from 22.4 ± 0.4 to 20.3 ± 0.3 kA/volt. The calibration curve of K_s is important because when the capacitor bank is used to operate a plasma device the circuit inductance may be variable (Mather, 1965; Lee, Chen, Chow, Tan, Teh & Thong, 1972; Chow, Lee & Tan, 1972). Neither the exact equations (1) to (3) nor the approximate equations (4) to (6) are applicable to compute the magnitudes of the current during the time when the circuit inductance undergoes a rapid change. When on load, such a calibration curve can be depended upon to measure the current amplitudes.

Synchronisation and interference. It is important that the firing of individual capacitors within a module is closely synchronized. Synchronisation of the discharge of the modules is also important. Extensive tests on the synchronisation of individual capacitors within a module of 10 capacitors have already been reported (Lim *et al.*, 1969). Results indicate synchronisation to be better than ±30 ns.

Extensive tests in the present series on all four modules indicate a total jitter of ±50 ns in the time from the sync pulse to the start of the discharge current. The synchronisation of the modules, based on simultaneous measurements of the currents of individual modules give a value somewhat less than this. The control of the individual modules is best illustrated by the delayed mode of operation for two modules. Discharges were made in this delayed mode with a range of pre-set phase difference up to $\phi = 360°$. Reproducible control of ϕ to better than $\pm2°$ (corresponding to ±50 ns) is readily achieved.

A disadvantage of this system, compared with a system switched purely by ignitrons, as far as diagnostics are concerned is that whenever the spark gaps are not closed (*i.e.* for operation above 20 kV), all electrical measurements exhibit enhanced interference pickup of $\simeq$ 8 MHz (fig. 7*b*). This is attributed to transmission cable-spark gap reflections and the observed noise frequency is in agreement with that expected based on two-way transit times of the transmission cables.

CONCLUSION

A two mega-ampere capacitor bank working at 40 kV is switched by a system of voltage division with considerable simplification in engineering design and of high voltage problems. This principle of voltage division can be extended to working voltages of 100 kV and more by increasing the number of static spark-gaps in series. Holding voltages of a major part of the circuit and the switching voltage itself can be kept at 20 kV. Moreover, it is expected that there is an added advantage of better sychronisation from voltage steepening as the gaps break down in sequence.

Acknowledgement. The capacitors and high voltage transformers used in this fast current bank are part of equipment presented to the Department of Physics by the United Kingdom Government under Colombo Aid Plans. We are grateful to Mr Chen You Hor, Mr Lee Boon Kian, Mr Chow Sai Pew, Mr Ho Tet Soon and Mr Tan Tian Hoo for their assistance in this project, and to Mr Chiang Soo Har for assistance with the technical drawings.

REFERENCES

BARNES, P.M., GRUBER, J.E. & James, J.E. (1967). The parallel operation of low-inductance high-current spark gaps without transit time isolation, *J. Sci. Instrum.*, **44**; 599.
BUTLER, T.D., HENINS, I., JAHODA, F.C., MARSHALL, J. & MORSE, R.L. (1969). Coaxial snowplow discharge. *Phys. Fluids*, **12**; 1904.
CARPENTER, J.P., WILLIAMS, A.H., MATHER, J.W., BOTTOM, P.J. & WARE, K.D. (1970). 50-kV switch and capacitor module development for plasma focus research. *Bull. Am. Phys. Soc.*, **15**; 1462.
CHOW, S.P., LEE, S. & TAN, B.C. (1972). Current sheath studies in a coaxial plasma focus gun. *J. Plasma Physics*, **8**; 21–32.
FITCH, R.A. & MCCORMICK, N.R. (1959). Low inductance switching using parallel spark gaps. *Journal IEE*, **106**; 117.
FRUNGEL, F.B.A. (1965). *High speed pulse technology*, Vol. 1 & 2, Academic Press.
GROSS, R.A. & MILLER, B. (1970). Plasma heating by strong shock waves. In: *Methods of experimental physics*, Vol. 9, Pt. A; 190.
LEE, S., CHEN, Y.H., CHOW, S.P., TAN, B.C., TEH, H.H. & THONG, S.P. (1972). High speed photography of a plasma focus. *Intern. Jour. Electronics*, **33**; 85.
LEONARD, S.L. (1965). Basic macroscopic measurements. In: *Plasma diagnostic technique* edited by Richard H. Huddlestone and Leonard Stanley L., Academic Press.
LIM, C.P., THONG, S.P. & TAN, B.C. (1969). A simple method of fast switching for condenser banks used in high current discharge experiments. *Jour. Singapore National Academy of Science*, **1**; 63.
MATHER, J.W. (1965). Formation of a high-density deuterium plasma focus. *Phys. Fluids*, **8**; 366.
MATHER, J.W. (1970). Dense plasma focus. In: *Methods of experimental physics*, Vol. 9 Pt. B; 192.
MONTFOORT, J.E. (1968). Discharge-circuit formula for the evaluation of capacitor-bank discharges. *Electronic Engineering*, **40**; 194.

)plying research techniques a developing country

Lee Sing

here any relevance in training a student from a developing country high level plasma research? If uestion were put to Dr Lee Sing Universiti Malaya he would r with a firm 'yes'. Dr Lee Sing NU in December 1969 and has n charge of research and develop- of the Plasma Physics atory in the Department of cs, Universiti Malaya, since 1970. leads a team of 4 staff and 5 ch students whose results have included reaching a peak plasma neutron emission rate exceeding 10^{16} in October 1973, thought to be the first in Asia outside the USSR. Dr Lee Sing is also Lecturer-in-charge of the Applied Physics Laboratory which develops experiments in pulsed physics, ultrasonics, photometry and laser optics for third and honours years students. He has recently been awarded an Alexander von Humbolt Research Fellowship for 1975.

Sing with his wife Susan, a school teacher, and their children Suzie and Shannon.

In 1960 when the Physics Department at the University of Malaya was in its infancy Professor Thong Saw Pak proposed an ambitious plasma physics project: to assemble a million-ampere capacitor bank and to use this high current to heat a gas, hydrogen, to a temperature of one million degrees K. Ten years later the project was still bogged down in technical difficulties primarily because of the lack of technical expertise in designing the capacitor bank for high current discharge.

The lack of success of this project gave rise to much criticism and the project was often quoted as an example of what could not be done in physics in a developing country like Malaysia. The 'no-research' physicists and the 'talk-about-research' physicists had a field-day harping on the amount of money and time wasted.

Then in 1970 the tide began to turn for plasma physics research in the country. The capacitor discharge system was redesigned to adopt part of the basic switching and control techniques earlier developed for the electromagnetic shock tube in the School of General Studies, Australian National University. With this adaptation married to the earlier work, the system was gradually assembled and tested until in March 1972, a measured maximum current of 1.9 million amperes was attained, nearly twice the original planned value; and one of the highest currents in the world for this class of capacitor bank.

Concurrently with the electrical testing, a plasma chamber was designed to accelerate and focus the plasma (high temperature ionised gas) into a tiny blob of extreme temperature and pressure, a miniature sun in effect; and in November 1971 Y.H. Chen, then an MSc student, obtained indication of a plasma temperature of 10 million degrees K by using a photographic technique to record the soft x-ray radiated by the transient plasma. This high plasma temperature was confirmed when neutrons from the focus were detected

and on 20 October 1973 we measured the neutron energy to be 2.4 Mev, using a time-of-flight method with millimicrosecond resolution. This proved that our plasma focus was undergoing nuclear fusion, the same process responsible for the energy release in the hydrogen bomb. Operating with 15 kilojoule, which is one-third of the maximum energy of our capacitor bank, the deuterium focus produced a measured neutron flux exceeding 10^9 neutrons per discharge, which placed it among the more efficient of the plasma focusing devices currently operating anywhere in the world.

In my opinion technical successes such as these, i.e. 2-million amperes and a nuclear plasma, have a primary importance in the context of science and technology in a developing country in that they prove wrong the demoralising belief of many people, particularly physicists here, that small isolated research teams in a developing country cannot have the overall expertise to cope with the advanced technology required in the design and development of a facility such as our plasma-nuclear machine. This belief has been commonly fostered in many developing countries, certainly in Malaysia, *not* because physicists in these countries are not competent in their own fields of specialisation. It is rather that these physicists do not have the overall technical backing so necessary for experimental research in physics. This is an extremely important point! A PhD physics graduate returning home from a developed country, where he formed a component in a research network, finds no such network in his home country. To do experimental research he must know, besides his physics, the relative merits of different components and instruments, and how to improvise where necessary; he must know the design and setting up of his experimental system, and the most economical and practical way of setting up his research, e.g. from the purchase of the glass tube for the vacuum vessel to the wiring of the diode chain for the high-voltage charger to the assembly and calibration of the neutron detector from discarded components. Let the doctoral student from a developing country beware of pushing buttons at overseas research institutions!

Now that the plasma physics group is academically productive, the questioning has gone full circle to what must have been one of the first questions asked. Why plasma physics? This is the question that torments my postgraduate students just as it persisted in my mind years ago when I was at the ANU with Dr R.J. Sandeman. A vision of thermonuclear plasmas providing mankind with a plentiful and long-term energy source is not enough. There must be another and more immediate reason. And I believe there is. It is that we do what we can whilst not obstructing the right of others to do what they can in projects more beneficial (?) to the national development. And in Kuala Lumpur we can do plasma physics; after the years of hard work developing the technical systems and the technical support.

It is my belief that the study of physics, as in any other field of human endeavour, should be as many faceted as possible to cater for the varied academic and philosophical appetites of students and academics alike. The Government may prefer, for good reasons, that more students take up the study of the physics of the soil or of rubber, but this preference must not be at the expense of the top students who invariably find it more intellectually challenging to study high energy physics or nuclear physics. Others want to study solid state physics or plasma physics. Actually there are enough qualified people in the five universities in this country to engage in research in all these major areas and in the Universiti Malaya alone, facilities are available not just for plasma physics research but equally for solid state and nuclear physics research. If any serious attempt is made to do research in soil physics no doubt facilities would also be forthcoming. It is not a good reason therefore that plasma physics research should not continue to be supported just because 'more beneficial' research is not being conducted. Likewise it is not a good reason that traditionally the development of plasma physics research in a country comes only after the development of 'more basic' areas of research like nuclear physics and solid state physics. This argument is the more invalid since plasma physicists here became productive relatively early not because of any misguided policy of preference but because of attention paid to technical design and support.

This departure from the traditional sequence of research development does not appear to diminish the quality of our products. The postgraduate students from our plasma laboratory are readily employed by universities and colleges as well as by government bodies and by industry. The research brings life and excitement to the undergraduate teaching on plasma physics and related topics; and our research papers, both theoretical and experimental, contribute to the academic standing of the University.

What the course of plasma physics research in Kuala Lumpur will be in the next five years is difficult to predict. Not only do we have to set suitable academic targets and maintain our research momentum but, and this is perhaps the more difficult, we shall have to continually explain our raison d'etre.

But whether we move on to greater things or are perforce brought to a standstill we have succeeded in proving, not least to ourselves, that we can, on our own, establish a technically advanced and complex research project. And the seed of this success was in part sown in Canberra; in the scent of pine needle and sod in Haig Park, in the spectacular spring blossoms in Manuka, in the graceful swoop of sea-gulls over the cold waters of Lake Burley Griffin; and in the Department of Physics, SGS, at the Australian National University.

DEPENDENCE OF FOCUS INTENSITY ON MASS AND FIELD DISTRIBUTION

S. Lee*, T.H. Tan.
Physics Department, Universiti Malaya, K.L.,Malaysia.
*Presently: Institut für Plasmaphysik, KFA, Jülich, BRD.

Abstract: Using piezoelectric probes we estimate that at the end of the axial run-down region 4-7% of the ambient mass encountered arrive in time to participate in the focusing action. Focusing intensity appears to depend more on the magnetic field distribution than on the mass distribution.

In theoretical computations of focus trajectories it is necessary to include in the radial equation of motion a quantity (m_o) representing the amount of mass that is swept from the axial run down region into the radial focusing region. In the present work measurements are made at the end of the axial run-down region which enable an upper limit to be placed on this m_o. The measurements also throw light on an important associated problem; namely the dependence of focusing intensity on the mass and magnetic field distributions. A knowledge of this dependence could be useful in the design of a fusion machine based on the focus principle.

We use a calibrated PZT piezoelectric probe (1) and a magnetic field coil for these measurements. The calibration pressure signals were carefully studied so that the probe response time and inherent noise harmonics were known. In the actual measurements the pressure signals were processed to eliminate these noise harmonics.

The focus device in which these measurements were made (2,3) was operated with deuterium at o.2 torr with 8 kJ. For these operating conditions it was noticed that the focusing intensity was not reproducible as judged from voltage and current oscillograms. Indeed for some shots, the characteristic focusing voltage spike and current dip were absent.

A comparison is made of the pressure (P) and magnetic field (B) oscillograms for focusing (F) and non-focusing (NF) shots. In Fig. 1 the B oscillograms have been transformed into B as distance coordinates. A distinct difference (very reproducible) can be observed between the B distributions of a F and a NF shot. The F shot has a high current density in the first 1 to 2 cm of the current-sheet with B rising typically to o.8 T in the first 1 1/2 cm. The NF shot has a much lower current density with B rising to only o.4 T over 7 cm. For the P pulses, a somewhat typical distribution (for example Fig.2) for the F shot shows a sharp narrow pulse in the first part of the P signal. For the NF shot, this frontal pulse is not so sharp or distinct.

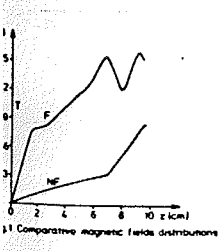

Fig.1 Comparative magnetic fields distributions

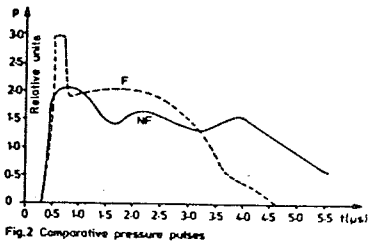

Fig.2 Comparative pressure pulses

In order to quantify the measurements, an empirical model is used in which the frontal part of the P pulse is taken to be a shock in which there is no post shock magnetic field. This is to conform with experimental observations , and has the correct effect of lowering the post shock kinetic pressure (when compared to a gas shock model) for each given shock speed. By empirically taking the ratio of specific heats to be $x = 2$ the pressure measured at the probe face could be related to the free-stream Newtonian pressure (4). The density ratio Γ is then computed from the measured pressure.

The P pulse is divided into 2 regions for study namely (i) the first o.o5 μs and (ii) the first o.3 μs. The mass arriving in the first o.o5 μs is here called the "initial" mass. The mass arriving after this o.o5 μs could not participate in the focus since the focus action occurs in o.o5 μs. The time of o.3 μs corresponds to the e^{-1} diffusion time of the probe. Beyond this time the diffusion of the B field behind the probe face would make the estimate of Γ and hence of mass an underestimate.

The results show that the "initial mass" is 4-7% of the ambient mass with F shots having a slightly greater initial mass than NF shots. Due to the continual axial motion of the imploding plasma, it is expected that "m_o" is only a small fraction of this initial mass. This is in agreement with a recent radial trajectory computation (5). Also F shots have a slightly greater quantity of mass (3o % of ambient mass) in the first o.3 μs than NF shots.

The most important factor in deciding the intensity of a focus appears to be the magnetic field distribution associated with the current sheet; although it is also observed that the structure of the current sheet has some points of correlation with the structure of the pressure pulse.

1. Lee S., Ph. D. Thesis A.N.U. (1969)
2. Lee S., Chen Y.H., Mal. J. Sci. 3 (1975)
3. Chen Y.H., Lee S., Int. J.Elec. 35 (1973) 341.
4. Lee S., Sandeman R.J., J. App. Phys. 43 (1972) 3980.
5. Lee S., Chen Y.H., XII ICPIG Eindhoven (1975) submitted.

Seventh European Conference on Controlled Fusion and Plasma Physics, Lausanne (Vol. 1) 1975

Malaysian J. Sci. 3(B) (1975): 159–163

Measurements of neutrons from a focused plasma

S. LEE AND Y.H. CHEN[1]

Abstract

Using two calibrated neutron detectors, simultaneous measurements were made of the flux and energy of neutrons from a focussed plasma. The typical flux for a 12.5 kJ, 20 kV discharge was found to be 10^8 neutrons. The neutrons emitted in the backward direction were found to have an energy of 2.2 ± 0.1 MeV, which indicated that the reacting deuterons may have been accelerated in the forward direction with a probably energy of 250 ± 100 keV. The neutrons began to be emitted 40 ns after the peak compression of the focus.

INTRODUCTION

The production of a highly compressed and high temperature plasma by means of a plasma focus has been reported by a number of authors e.g. Filippov, Filippova & Vinogradov (1962), Mathers & Bottoms (1968) and Lee, Chen, Chow, Tan, Teh & Thong (1972). Neutrons are emitted from these focused plasmas and measurements of neutrons yield, distribution and energy have been reported e.g. by Bernstein, Meskan & Paassen (1969), Patou, Simonnet & Watteau (1969) and Conrads, Cloth, Demmeler & Hecker (1972). In those measurements, the neutron yields were usually measured by activation methods, the

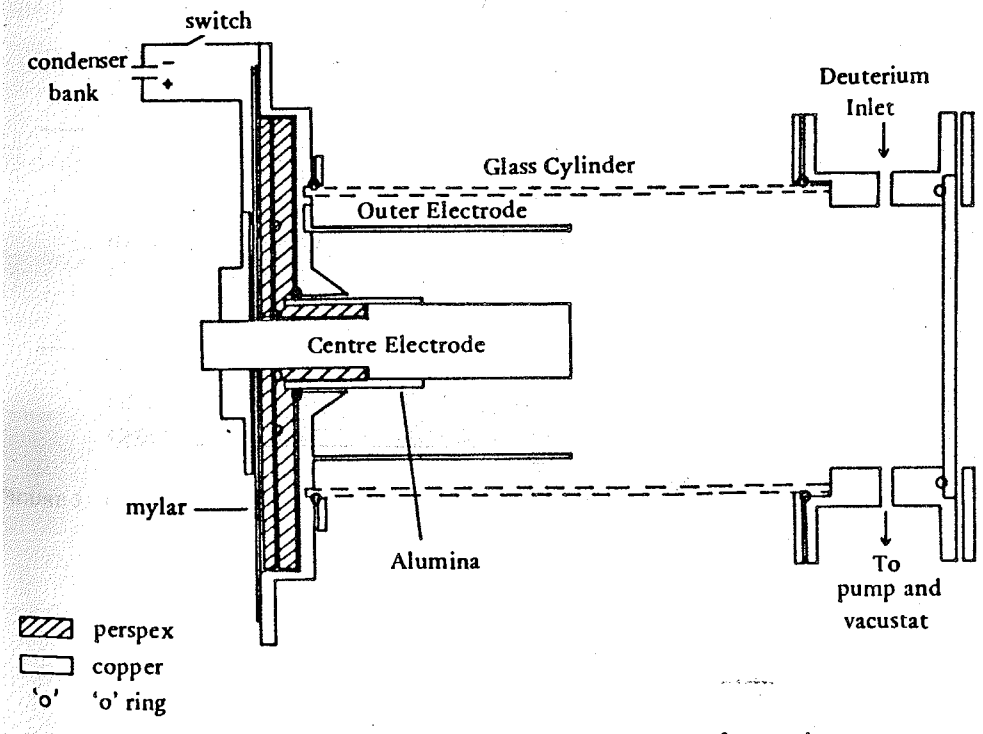

FIGURE 1. Schematic diagram of the plasma focus tube.

[1]Department of Physics, University of Malaya, Kuala Lumpur, Malaysia, 11.2.1974.

spatial distribution by nuclear emulsion and the energy spectra by nuclear emulsion or time-of-flight method.

In the present experiments, we report on measurements made by a time-of-flight method using two calibrated detectors which enabled estimates to be made, at the same time, of neutron yield and neutron energy. The time history of neutron emission was also recorded.

EXPERIMENTAL ARRANGEMENT

The plasma focus chamber for this experiment (fig. 1) was modified from those described by Chow, Lee & Tan (1972) and Chen & Lee (1973). The capacitor bank and control electronics have been described by Thong & Lee (1973). For the present experiments, the capacitor bank was operated at 20kV with a stored energy of 12.5 kJ, a peak current 700 kA and a rise time of 2.5 μs.

The neutron detector comprised of a NE102 disc placed in front of an EMI 9594 photomultiplier. The assembly was shielded by a brass cylinder and lead sheets as shown in figure 2. The rise-time and fall-time of the photomultiplier were checked with a nanosecond spark-gap light source and found to be less than 1ns each.

The detector sensitivity was calibrated at liquid air temperature against a standard polonium-berylium neutron source. For example, the first detector (Mark I) has a sensitivity, when operated at 2.2 kV, of 1 nA per $(5.3\pm1.3) \times 10^2$ neutron per second when these neutrons were emitted from an isotropic point at a distance of 0.1 m. Operating into a load resistance of 50Ω, the calibration constant was (1.0±0.3) V-s per $10^{12} \times x^2$ neutrons emitted by an isotropic point source placed at x m from the front face of the detector.

During a discharge the photomultiplier output voltage was displayed on an oscilloscope, and from the oscillogram, the area of the neutron pulse was measured and used to determine the neutron flux from the plasma, assuming an isotropic point source.

To measure neutron energy, the two detectors were placed a distance of 10.19 m apart in line with the axis of the focus tube. The near detector was displaced slightly below the axis so as not to obstruct the far detector. It was found that this helped to reduce the flux of scattered neutrons arriving at the far detector. The transit time of the neutrons was measured by displaying the outputs of the two detectors on the beams of a Tektronix 556 oscilloscope. The two traces, on a time sweep of 200 ns cm^{-1} were aligned at the centre, with the aid of a time mark, to an accuracy of 4 ns and the two traces were matched in linearity and calibration factor to an accuracy of 1%. The start of the two traces was delayed, relative to the start of the discharge current by, typically, 2.5 μs.

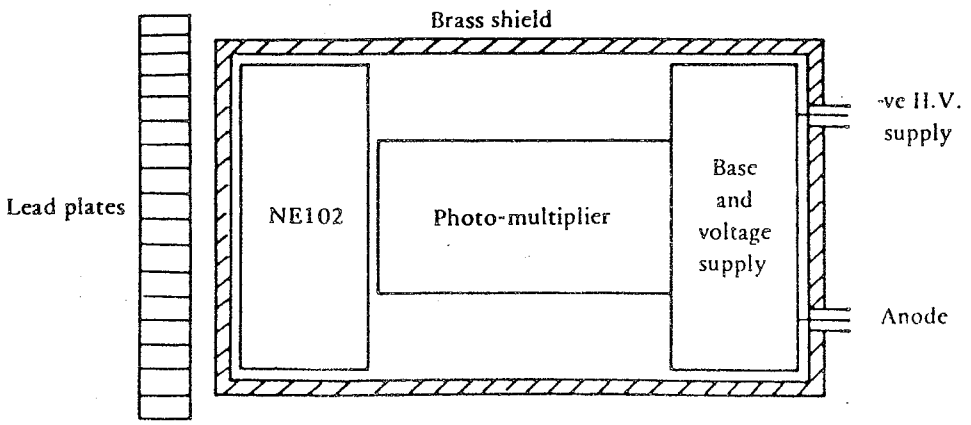

FIGURE 2. Schematic diagram of the neutron detector.

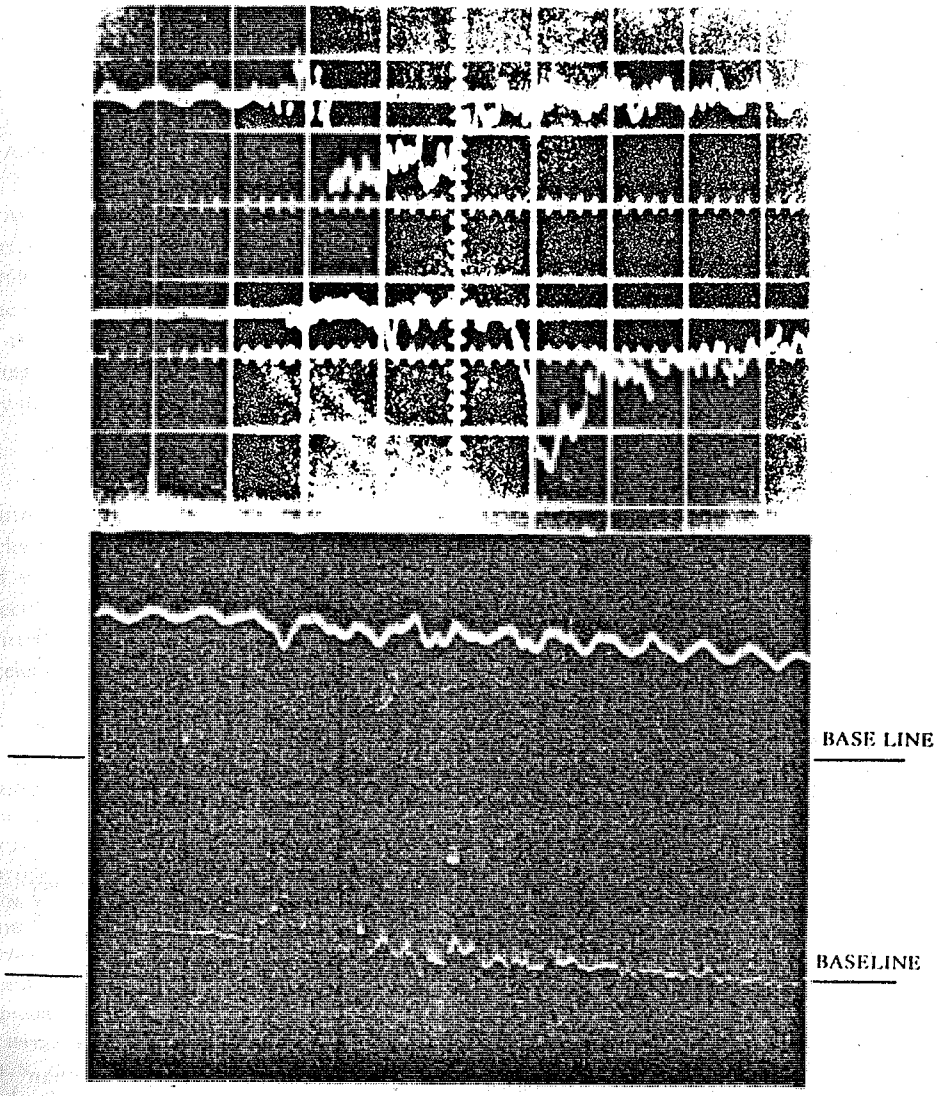

FIGURE 3. Composite of two oscillograms. All four traces 200 ns per cm.
Trace 1: (top trace) : output of front neutron detector; vertical diflection: 5 V per cm.
Trace 2: output of rear neutron detector; vertical deflection: 5 V per cm. Rear detector 10.19m behind front detector.
Trace 3: output of current coil; current sensitivity; 340 kA per cm.
Trace 4: output of voltage probe. voltage sensitivity: 5 kV per cm.

RESULTS AND DISCUSSION

Figure 3 (top two traces) shows a typical time-of-flight oscillogram, together with the voltage and current traces. The photomultiplier of the near detector, operated at 2kV, was saturated as evidenced by the flat-top shape of its signal and the relative amplitude in comparison with the output of the far detector, operated at 2.5 kV.

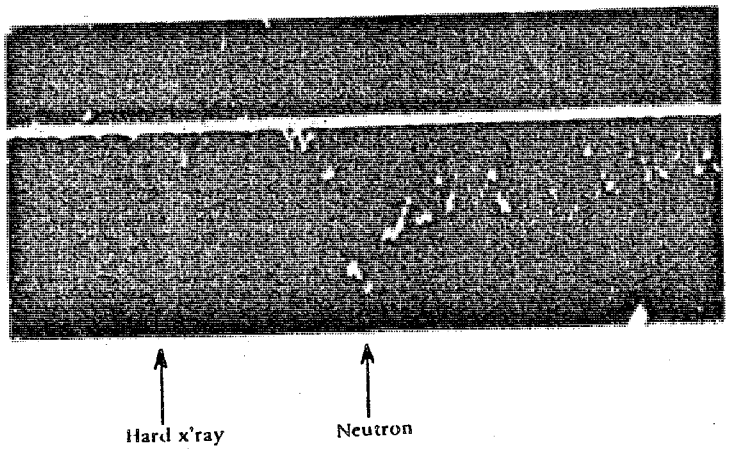

FIGURE 4. Oscillogram of the output of a single neutron detector responding to x-ray and neutron pulses.
horizontal deflection: 200 ns per cm.
vertical deflection: 5 V per cm.

The time difference between the front of the two neutron pulses was measured as 485 ns after accounting for the difference in cable transit times. Over a flight-path of 10.19 m, this gave a flight-time of 47.5 ns per m, a velocity of 2.1×10^7 m s^{-1} and a neutron energy of 2.3 MeV. This indicates that the neutrons are from the $D + D \rightarrow He^3 + n$ reaction which produces a neutron with an energy of 2.45 MeV in C-M coordinates. This provides a justification for our method of measuring flight-time based on a pulse-front to pulse-front measurement. The justification lies in the fact that the plasma, as a whole, had a temperature of about 1 keV, and even considering Bernstein's (1972) crossed field acceleration mechanism, the 'fusioning' deuterons are unlikely to have an energy distribution in excess of 100 keV. This sets a maximum energy spread of neutrons at 4% or a maximum velocity spread of 2%. Thus over 10 m, the transit times of the neutrons are not expected to vary within a range of 1 ns. Comparing this to a transit time of 500 ns and a pulse length of 200 ns, the pulse-front to pulse-front transit time can be regarded as a mean transit time.

The result of four measurements in the backward direction of the focus gives a mean flight time of 48.7 ns per m with a range of variation of 2.8 ns. The best estimate for neutron energy was 2.2 ± 0.1 MeV. The variation of 30 ns in total flight times is larger than the measurement error and it is probable that the estimated error of ± 0.1 MeV may reflect a shot-to-shot variation in neutron energy. The difference between the measured mean neutron energy and the C-M D-D neutron energy indicates that the 'fusioning' deuterons may be moving in the forward direction of the focus with a probable energy of 250 ± 100 keV.

Another method, using one single detector, was also used to measure the neutron flight-time. In these measurements, scattered hard x-ray and neutrons were both detected (*e.g.* fig. 4); and assuming that the start of the x-ray pulse and the neutron pulse occur at the same point in time, the flight time of the neutrons from the focus can be measured, adding the x-ray flight time to the time difference between the x-ray and the neutron pulses. Five measurements gave a mean of 47.6 ns per m with a range of variation of 55 ns in total transit times. The increased variation in total transit times is again significant and probably indicates that the neutron and x-ray pulses do not start at the same time, and that this time difference has a variation of around 25 ns.

Area measurement of the neutron pulse gave the total flux emitted. The typical flux (*e.g.* fig. 3, trace 2) is 10^8 neutrons with a peak flux rate in excess of 10^{14} neutrons s^{-1}.

As can be seen from figure 3, the start of the neutron pulse at the focus occurred 180 ns after the start of the voltage spike or 60 ns after the peak of the voltage spike. Mathers (1968) has shown that the voltage spike measured at the breech end (as in our case) has a time delay of 20 ns relative to the voltage spike measured near the focus. Even accounting for this delay, it appears that the neutrons began to be generated 40 ns after the peak of the voltage spike, which corresponds to the maximum compression. Further study of this delay may provide information regarding the plasma heating mechanism.

CONCLUSION

Neutrons emitted from a plasma focus were found to have an energy of 2.2 ± 0.1 MeV in the backward direction of the focus. This is less than the C-M D-D neutron energy of 2.45 MeV and indicates that the 'fusioning' deuterons may have been accelerated in the forward direction with a probable energy of 250 ±100 keV. The observation that the neutrons are emitted 40 ns after the peak compression of the focus may be in agreement with an acceleration model.

REFERENCES

BERNSTEIN, M.J., MESKAN, D.A. & VAN PASSEN, M.L.L. (1969). Space, time and energy distributions of neutrons and x-rays from a foucsed plasma discharge. *Phys. Fluids*, 12; 2193–202.

BERNSTEIN, M.J., & COMISER, G.G. (1972). Neutron energy and flux distributions from a crossed-field accceleration model of plasma focus and Z-pinched discharges. *Phys. Fluids*, 15; 700–7.

CHEN, Y.H. & LEE, S. (1973). Coaxial plasma focus in mode I operation. *Int. J. Electronics*, 35; 341–52.

CHOW, S.P., LEE, S. & TAN, B.C. (1972). Current sheath studies in a coaxial plasma focus gun. *J. Plasma Phys.*, 8; 21–32.

CONDRADS, H., CLOTH, P., DEMMELER, M. & HECKER, R. (1972). Velocity distribution of the ions producing neutrons in a plasma focus. *Phys. Fluids*, 15; 209–11.

FILIPPOV, N.V., FILIPPOVA T.I. & VINOGRADOV V.P. (1962). *Nucl. Fusion Suppl.* 2; 577.

LEE, S., CHEN, Y.H., CHOW, S.P., TAN, B.C., TEH, H.H. & THONG, S.P. (1972). High speed photography of a plasma focus. *Int. J. Electronics*, 33; 85–90.

MATHERS, J.W. & BOTTOMS, P.J. (1968). Characteristics of the dense plasma focus discharge. *Phys. Fluids* 11; 611–8.

PATOU, C., SIMONNET, A. & WATTEAU, J.P. (1969). *Phys. Letters* 294; 1.

THONG, S.P. & LEE, S. (1973). A simple method of switching a 2 megampere capacitor bank. *Malaysian J. Sci.*, 2; 151–169.

THE PLASMA FOCUS - A RADIAL TRAJECTORY COMPUTATION

S. Lee*, Y.H. Chen
Physics Department, Universiti Malaya, K.L., Malaysia. *Presently: Institut für Plasmaphysik, KFA, Jülich, BRD.

Abstract: A radial collapse model with 3 phases is considered, namely, a forward shock phase, then a reflected shock phase and finally a phase of adiabatic compression. The equation of motion is written, including an appropriate retarding pressure term. The resultant current sheet trajectories are compared with an experimental trajectory obtained from inductance calculations. This comparison shows agreement down to r=6 mm, beyond which there is evidence of current sheet diffusion.

INTRODUCTION

The dynamics of the focus can be divided into three regions, firstly an axial run-down region, secondly a region of expansion during which the flow changes direction from axial to predominantly radial, and a third, the focus region in which there is evidence that a 1-D radial model can be expected to yield some reasonable results, although, because of axial jetting, a 2-D model or the P.I.C. model is necessary for an accurate simulation.

A 1-D radial model has been used for the linear pinch (1) and for the focus (2), but in this latter work a retarding pressure term has not been included. In this paper we have written a retarding pressure term by assuming that the final stages of heating is through adiabatic compression and by incorporating the role of shock heating (3) in the early stages of the collapse. We also include a non-zero initial mass and a finite initial radial velocity as parameters. The radial collapse is divided into 3 phases, W,X and Y, as shown in Fig. 1. In phase W, a shock (S) propagates ahead of the current sheet (CS). The heated deuterium plasma between the S front and the CS is assumed to exert an uniform pressure on its boundary. Due to the finite thickness, d, of the shock plasma there is a retarding force which is computed from the strong shock equations. In phase X, the S front has reached the axis of the tube. A reflected S develops and the plasma heated by reflected S is taken as stationary in the laboratory coordinates. The reflected S reaches the CS at the position r_c. Beyond this point the focus is in phase Y and the reflected S pressure is felt by the CS. In this phase the heating mechanism is adiabatic.

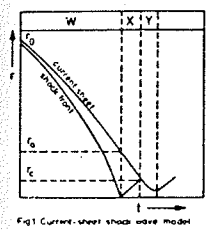

Fig1 Current sheet shock wave model

THE EQUATIONS

In phase W, $r_s \ll r_0$, the equation of motion for unit length of the plasma column is:

$$\frac{d}{dt}\left[m_0+\pi\rho_0\,(r_0^2-r_s^2)\right]\frac{dr}{dt} = -\frac{\mu_0 I^2}{4\pi r} + \frac{\beta}{3}\pi r\rho_0\left(\frac{dr}{dt}\right)^2\sigma$$

where m_0=initial mass per unit length, I=focus current, taken as constant, ρ_0=ambient gas density, r=position of the CS, r_s=position of the S front. At any instant,

$$r_s = r - \tfrac{1}{3}\frac{dr}{dt}\Delta t - d\,, \quad \sigma = (d+\tfrac{1}{3}\frac{dr}{dt}\Delta t)/r$$

where d=initial shock plasma thickness due to m_0 and Δt=time step for integration.

In phase X, $r_c < r < r_a$, the equation of motion becomes :

$$\frac{d}{dt}\left[m_0+\pi\rho_0 r^2-10\pi\rho_0 r_r^2\right]\frac{dr}{dt} = -\frac{\mu_0 I^2}{4\pi r} + \frac{\beta}{3}\pi r\rho_0\left(\frac{dr}{dt}\right)^2$$

where r_r, the position of the reflected S is computed from the instantaneous CS velocity.

In phase Y the equation of motion is:

$$\frac{d}{dt}\left[m_0+\pi\rho_0 r_0^2\right]\frac{dr}{dt} = -\frac{\mu_0 I^2}{4\pi r} + \frac{\beta}{3}\pi r\rho_0 V_c^2\left(\frac{r_c}{r}\right)^{40/9}$$

where v_c is the CS velocity at r_c.

Equations 1 to 3 are normalized and integrated, using the Runge-Kutta scheme.

RESULTS

The trajectories are computed for a focus with conditions as given in Lee and Chen (4,5). With I=500 kA in 1 torr deuterium, the CS trajectories for different initial radial velocities are shown in Fig. 2. A comparison is also made with Patou's results (2). An experimental trajectory is then obtained by computing the focus inductance L(t) from the oscillograms of the focus current and breech voltage (5). Assuming a coaxial cylindrical geometry for the plasma focus current paths, the focusing CS radius r(t) is given by:

$$r(t) = r_0\,\exp\left[-\frac{4\pi L(t)}{\mu_0 \ell}\right]$$

where ℓ is the length of the focus column, estimated from high speed framing photographs to be 1 cm. The experimental trajectory so obtained is shown in Fig. 3.

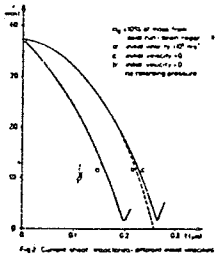
Fig2 Current sheet trajectories: different initial velocities

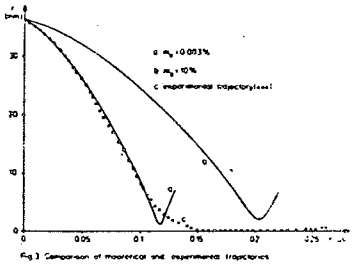
Fig3 Comparison of theoretical and experimental trajectories

To match this trajectory closely it was necessary to reduce m_0 to a near-zero value. Using this value of m_0 the trajectories agree down to r=6 mm. Beyond this point it is not possible to obtain agreement between the experimental and theoretical trajectories. The experimental trajectory does not show the two prominent features of the theoretical trajectory, namely, an increasing CS velocity followed by a sudden CS rebound occurring within 20 ns; with a minimum radius of about 1 mm. Instead the experimental trajectory shows a CS which whilst slowing down continuously, converges until a radius of 0.07 mm; taking 100 ns for this process.

This discrepancy is suggestive of a transition of the current distribution from a boundary current concentration (such as is assumed in both our theoretical model and our experimental current voltage computation) to an axial concentration (6). At r= 1mm, the Hall parameter of the plasma column is already 200, so that the transverse resistivity (7) is increased by a factor greater than 10^5 above the zero-B resistivity. This leads to an anomalous resistive voltage which at r=1 mm already contributes appreciably to the total plasma voltage.

These results indicate that down to r=6 mm a current sheet model with shock wave heating offers a sufficiently accurate description of the focusing trajectory. At smaller radii this boundary current model is no longer adequate. The computation also shows that the initial mass is very small, but that the initial radial velocity plays an important role in determining especially the early stages of the trajectory.

REFERENCES

1. Leontovich M.A., Osovets S.M., Nucl.En.II, 4 (1957) 209.
2. Patou P.C. et al, J.De Phys. (1968) 375.
3. Toepfer A.J. et al, Phys. Fluids 14 (1971) 52.
4. Lee S., Chen Y.H., Mal.J.Sci. 3 (1975).
5. Chen Y.H., Lee S., Int.J. Elec. 35 (1973), 341.
6. Bernstein M.J., Mai F., Phys.Rev.Lett. 25 (1970) 641.
7. Cambel A.B., Plasma Phys. and Magnetofluidmechanics.

Proceedings of the Twelfth International Conference on Phenomena in Ionized Gases, Eindhoven (Part 1) 1975

Malaysian J. Sci. 3(B) (1975); 165–176

Profiles of a transverse ionizing shock wave

S. LEE[1]

Abstract

Profiles for the pressure and magnetic field in an electromagnetic shock tube were measured for shock wave propagation into a zero bias field and into a transverse bias field of $B_1 = 0.25T$. The experimental conditions were such that the magnitudes of the magnetic viscosity ν_m, the kinematic viscosity ν and the thermal conductivity χ fulfilled the conditions $\nu_m \gg \chi$, $\nu \to 0$. The profiles show that during the time when the driver current was prominent it may not be appropriate to consider the properties of the shock wave as independent from the driver current sheet. When the driver current had decayed to small values, in each case of $B_1 = 0$ and $B_1 = 0.25T$, it was found that a gasdynamic shock of high Mach number (> 40) propagated. In the case of propagation into $B_1 = 0.25T$ the observation of this *transverse ionizing gasdynamic* shock with our experimental conditions confirms Kulikovskii's (1960) classification.

INTRODUCTION

Kulikovskii & Lyubimov (1960) have shown that for an ionizing shock wave propagating into a transverse magnetic field, the structure of the shock depends on the relative magnitudes of the dissipative coefficients ν_m, ν and χ, respectively the magnetic viscosity, the kinematic viscosity and the thermal conductivity, as well as on the relative magnitudes of T_1, the pre-shock temperature and T^*, a characteristic temperature at which the gas becomes conducting. Three types of structure are discussed by these authors:

1. If $\nu_m \gg \nu$, $\chi = 0$; or $\nu_m \gg \chi$, $\nu = 0$; then the shock is purely gasdynamic, with no change of magnetic field B through it. The properties of the shock are completely determined by the pure gas shock-jump equations. We shall refer to this class of shocks as transverse ionizing gasdynamic shocks.

2. If $\nu_m \ll \nu$, $\chi = 0$; or $\nu_m \ll \chi$, $\nu = 0$; everywhere that the electrical conductivity $\sigma \neq 0$; then the shock structure has a front portion that is an incomplete pure gas shock through which B is unchanged. This pure gas region extends from the shock front backwards to the point where the gas temperature reaches the value T^*, at which point the gas becomes magneto-gasdynamic. This class of shock has been treated in some detail by Chu (1964), who shows that the shock solutions depend not just on the shock-jump equations, but also on a structure equation and a choice of T^*. We shall refer to this class of shocks as transverse intermediate shocks.

3. If T_1 is close to T^*, then the gas becomes immediately magneto-gasdynamic. For this magneto-gasdynamic shock, it is easily shown that the mass density ratio across the shock, Γ, is equal to the magnetic field ratio β; and this relationship together with the shock-pump equations, completely determine the state of the post-shock gas. It may be conjectured that even if T_1 is far less than T^*, a shock can still be immediately magneto-gasdynamic provided it is sufficiently strong, so that the gas temperature rises to T^* almost immediately behind

[1] Physics Dept., University of Malaya, Kuala Lumpur, Malaysia, 11.2.1974.

the shock front. We shall refer to this class of shocks as transverse hydromagnetic shocks.

The situation in an electromagnetic shock tube is more complicated than the simple cases discussed above, since in addition to the shock wave, there is the current-sheet system which very often cannot be separated from the shock wave. Gross & Leonard (1969) have pointed out that in such a situation, the driver current layer may not be sufficiently separated from the shock front for the shock front to be treated as an independent system.

To obtain the basis for the understanding of transverse ionizing shock waves in an electromagnetic shock tube, the profiles of pressure and magnetic field along the shock tube were measured at different times during the shock wave propagation. These measurements were made in the regime $\nu_m \gg \chi, \nu \to 0$; *i.e.* the regime of the transverse ionizing gasdynamic shock. The results show that, after the driver current layer has decayed away, a gasdynamic shock continued to propagate down the shock tube.

EXPERIMENTAL ARRANGEMENTS

The experiment was conducted with a planar electromagnetic shock tube as described by Lee (1969) and shown in figure 1. The circuits for the capacitor banks providing the drive current and the bias magnetic held are shown in Fig. 2. The bias bank provided a magnetic field which, after a risetime of 250 μs remained constant for 50 μs to within 2% of its peak value which was variable from 0 to 0.6T. The function of the delay unit 1 was to delay the firing of the main bank until the bias field had approached its constant value. Operated at 5kV, the main discharge current reached a value of 80kA at $t = 6\mu s$ and remained approximately constant at this value until $t = 24\ \mu s$ before swinging negative at $t = 34\mu s$.

A mobile probe having a piezoelectric disc for measuring flow pressure, and a coil for measuring transverse magnetic field (fig. 3) was inserted along the shock tube (fig. 1). The coaxial construction of the probe provided good electromagnetic and electrostatic shielding from the plasma; whilst the 0.003" mylar at the front face of the probe provided electrostatic shielding for the piezoelectric disc, at the same time transmitting the plasma total pressure to the front face of the disc. The outputs of the probe were connected to 80 MHz oscilloscopes for display. Tests with the probe mounted in a mechanical shock tube showed that it had a sensitivity of 0.5 ± 0.05 V per (10^5 N/m^2); and a rise time better than 0.3 μs. The magnetic coil had a sensitivity of 27.0 T/V when operated with an RC of 500 μs.

Using the combination probe, a systematic survey along the centre line of the shock tube was made at 3-cm intervals. At each position, the time variation of probe pressure P and magnetic induction B during a discharge, were recorded together with a streak photograph.

RESULTS

Figures 4-6 show some typical results. Each figure is a composite of the P and B traces together with the streak record S of the luminosity along the centre line of the shock tube. In each figure, the time axes of the P, B and S records are accurately aligned and have the same time scale. The horizontal black lines on the streak photographs are position indicators with the help of which the position of the probe is determined and indicated on the streak photograph. The three streak photographs of figures 4-6 each has a bright streak running along the luminous front. This is clearly seen in figure 6, and also clearly distinguishable in the original polaroid photographs of figures 4 and 5. By careful time comparison among the P and B traces and the S photograph, the positions of the pressure and magnetic fronts relative to the probe position are indicated on the S photograph.

The B signal of figure 4 starts from zero, whereas those of figures 5 and 6 start from

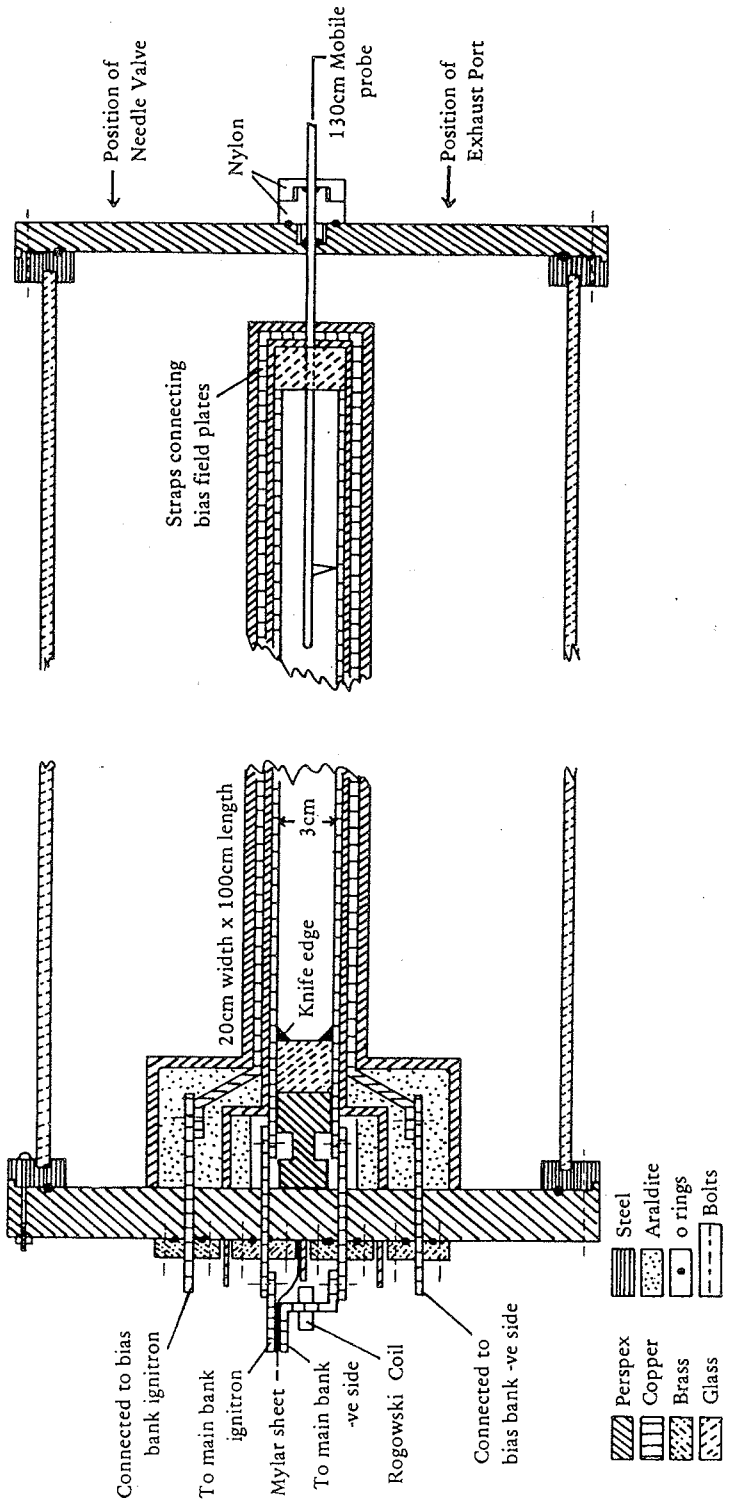

FIGURE 1. Planar electromagnetic shock tube.

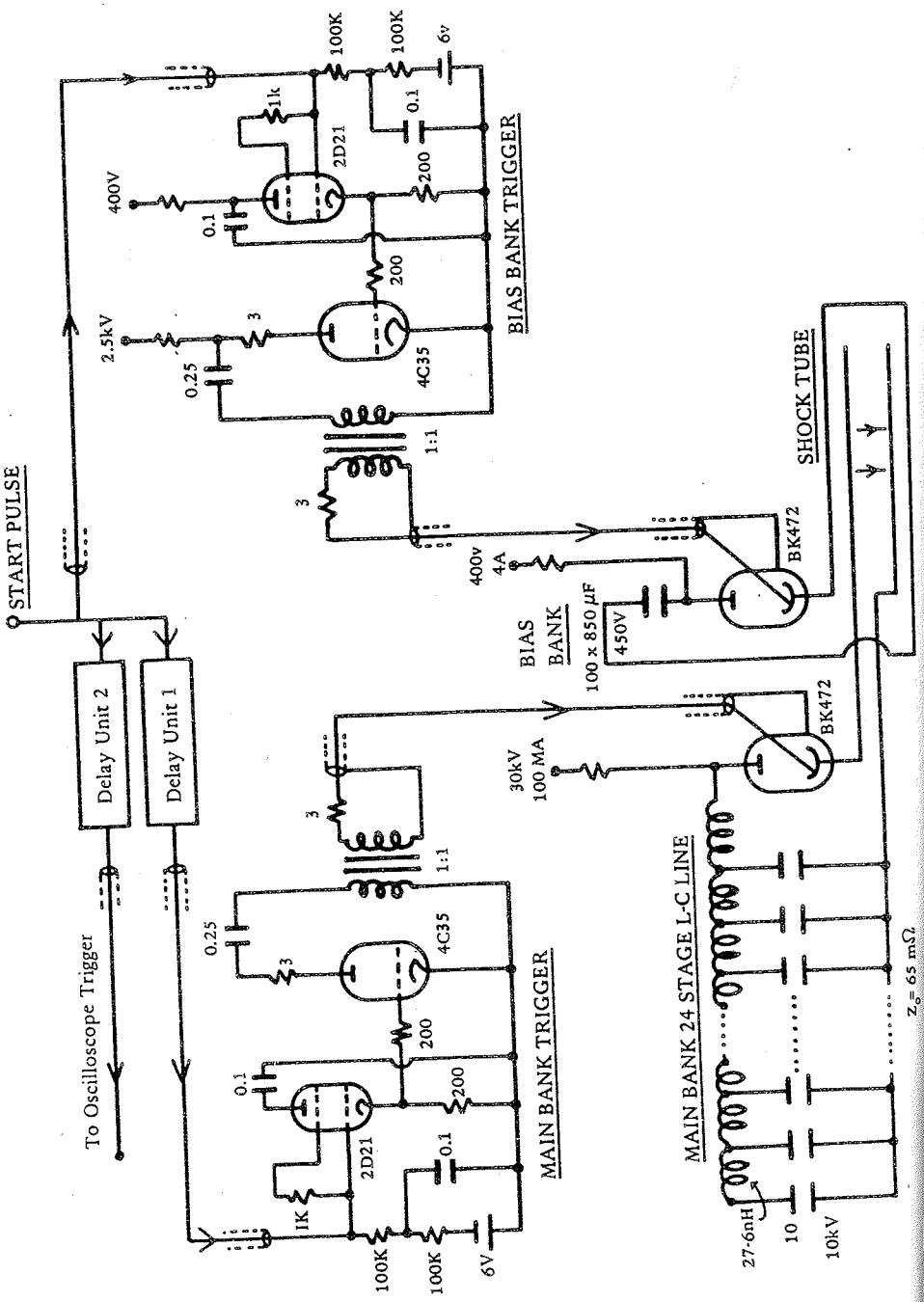
START PULSE
Delay Unit 2
Delay Unit 1
To Oscilloscope Trigger
BIAS BANK TRIGGER
MAIN BANK TRIGGER
BIAS BANK
100 x 850 μF
450V
400v
4A
BK472
SHOCK TUBE
MAIN BANK 24 STAGE L-C LINE
30kV
100 MA
27·6nH
10
10kV
Z_0 = 65 mΩ
2D21
4C35
100K
6V
400V
2.5kV
0.1
0.25
200
1K
1k
3
1:1

non-zero values in the oscillograms. This is because the discharge of figure 4 has a zero bias field, whilst the other two have a bias field of $B_1 = 0.25T$.

The discharge for figures 5 and 6 have the same operating conditions, but the probe was placed at different positions, x = 31 cm for figure 5 and x = 80 cm for figure 6. The pressure pulse arrived at x = 31 cm at t = 14 μs, with the driver current at its peak value. Under these conditions, it is seen (fig. 5) that the pressure front carried current, and was not gasdynamic. At t = 37 μs, however, when the pressure pulse arrived at x = 80 cm, the discharge current had gone negative and it is seen that the pressure front was gasdynamic (fig. 6), with no change in magnetic field through it.

A series of measurements was made with the probe placed at distances varying from 2 cm to 80 cm. The operating point was kept constant through the whole series, these being: drive field $B_D = 0.5T$ (corresponding to a capacitor voltage of 5kV), bias field $B_1 = 0.25T$, ambient pressure 0.1 torr argon. The time variations of B and P at different positions of x were considered together, and converted to spatial profiles of B and P along the shock tube at different instants of time. The profiles thus obtained were subject to two smoothing factors:

(a) shot-to-shot scatter, of about 3% which required averaging over 3 to 5 measurements for every point on the profile:

(b) spatial resolution, of 3-cm since the data was recorded at 3-cm intervals. However, if a feature was steady (i.e. consistently observed in the time profiles taken at three consecutive positions, but was lost because of the 3-cm resolution, then it was included in the spatial profile by direct reconstruction, averaging over the three consecutive positions.

For comparison, the distributions for discharges propagating into $B_1 = 0$ were also measured. These are presented first.

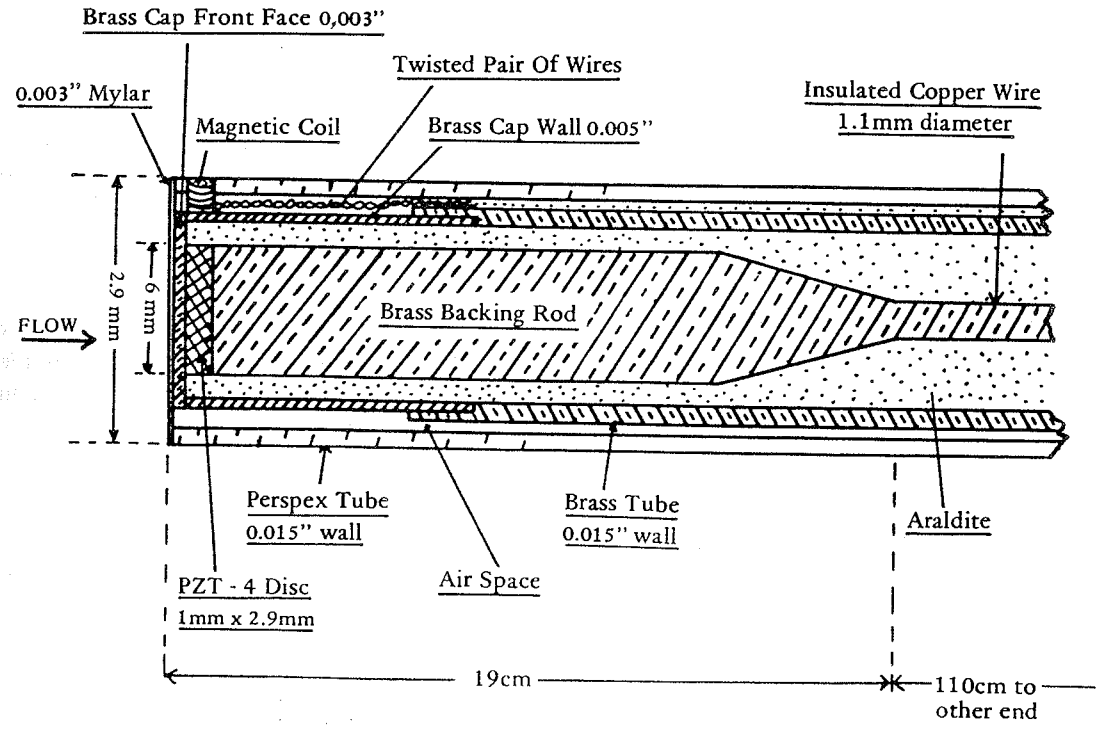

FIGURE 4. Combination probe for measuring plasma total pressure and magnetic field.

PROFILES FOR 0.1 TORR ARGON, $B_D = 0.5T$, $B_1 = 0$

The magnetic field and pressure distributions for this operating point are shown on figure 7. The luminosity profiles, from sychronished streak photographs, are included for comparison. The darker the shading, the brighter was the appearance on the streak photograph. The completely black bands represent intensely bright and sharply defined streaks that were usually associated with argon current sheets and shock fronts. The level of the drive magnetic field due to the capacitor current (as measured by a Rogowski coil) is indicated by an arrow on the right hand side of the diagrams.

From the magnetic field profiles, it is observed that the current propagation down the tube occurred in three distinct regions. Firstly, a diffuse region carrying up to 20 per cent of the total current extended some 5 cm ahead of the pressure front. This was followed by a high density region of 1½ to 2 cm carrying 50 per cent. of the total current. The remainder of the current was spread over a distance of 5 cm (typically) behind the intense sheet.

By $t = 13.2\ \mu s$, the pressure pulse had built up to a fairly constant structure with a front region 2 cm wide, within which resided the peak pressure of 6×10^5 N m^{-2}; and a trailing region of 5 cm width. The gross structure of the front region remained reasonably constant throughout the constant velocity region up to $t = 26.2\ \mu s$. The front of the pressure pulse carried the main current sheet, whilst the rear region carried the remainder of the current. As the drive current began to decrease after $t = 23\ \mu s$, the relative position of the pressure front and current sheet front began to undergo a dramatic change. The front of the main current sheet became less steep and began to draw back from the pressure front. At the same time, the diffuse current sheet ahead of the pressure front decreased. By $t = 28.2\ \mu s$, the main current sheet was 4 cm thick and had pulled back to such an extent that the current in the first 2 cm of the pressure pulse was only 3 kA compared to the 40 kA that was flowing in this region at the time of constant drive. The maximum magnetic pressure in this region was now less than 1 per cent. of that at the time of constant drive, whilst the pressure pulse and velocity were attenuated by 10 per cent. over a distance of 8 cm.

After $t = 30.2\ \mu s$, as the capacitor current rapidly dropped to zero and then swung negative, the decaying current sheet pursuing the pressure pulse became decoupled from the capacitor current and formed a close loop. The formation of this loop had been discussed by Lee (1967) when using a 6 cm x 6 cm x 1 m planar tube. In that tube the other end of this loop was a current sheet that was formed a few cm from the starting end of the shock tube. This became distinguishable on the streak photographs about 2.5 μs before current reversal and moved towards the starting end. The region behind the decaying pressure pulse was therefore a closed and expanding loop of decreasing magnetic flux, until the current reversal. A second current sheet then moved into the tube, pushing the closed loop of remnant flux ahead of it.

PROFILES FOR 0.1 TORR AR, $B_D = 0.5T$, $B_1 = 0.25T$

These are shown in figure 8. In the constant velocity period, the magnetic field profiles show four distinct regions. The magnetic field just ahead of the pressure front was equal to the bias value, but increased to a slightly higher value over a distance of about 3 cm ahead of the pressure front. Behind the pressure front, the magnetic field rose by 0.3T, corresponding to a current of 46 kA, over the first 1½ cm. This was followed by a region of negligible current. Behind this latter region, the rest of the current, about 30 kA, flowed. Of this, 23 kA flowed in the first 6 cm, with the other 7 kA distributed all the way back to the knife edges.

Corresponding to the three distinct regions of front-current, no current, and rearward

expansion current, the pressure pulse exhibited distinct structure. The front-current was carried in a pressure pulse of about the same length whilst the zero current region resided in a more or less flat top region of pressure. The rearward expansion current region coincided with the trailing end of the pressure pulse, which, after $t = 14.2\ \mu s$, also exhibited a trailing hump of small amplitude extending some 12 cm behind the main pressure structure, which itself was about 10 cm long.

As the capacitor current began to drop, the front portion of the pressure pulse (about 1 cm) became gasdynamic, i.e. the magnetic field remained unchanged through it. The velocity

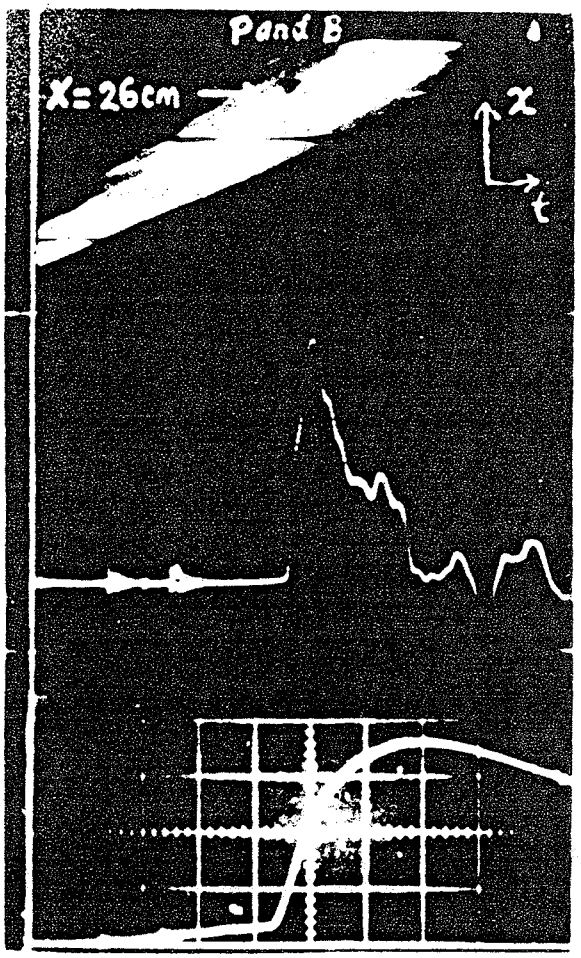

FIGURE 4. Comparison of S, P and B signals;
0.1 torr argon, $B_1 = 0$, x = 26 cm.
All horizontal axes: 2.0 μs per cm. The reference cm. scale in bottom picture is applicable for all three photographs.
Top: streak (S) photograph, black markers are 10 cm apart.
Middle: pressure (P) probe output, vertical sensitivity:
1.3×10^5 N m^{-2} per cm.
Bottom: magnetic (B) probe output, vertical sensitivity:
0.14T per cm.

decreased to 1.9 cm/μs at t = 28.2 μs, from the earlier constant value of 2.6 cm/μs. As
capacitor current approached zero, the speed dropped further to 1.5 cm/μs at t = 32.2 μs.
this time, the first 6 cm of the pressure pulse was gasdynamic; with a small B rise over
next 4 cm, followed by a slight decrease (just measurable) and then an increase of field o
10 cm. At later times (e.g. at t = 36.2μs), the magnetic field was 0.35T ahead of the press
front, indicating field compression ahead of the shock from the ambient bias value of 0.2
This field remained practically unchanged through 3 to 4 cm of the pressure pulse, t
dropped to about 0.25T, over some 18 cm, before rising to about 0.29T in a further 5 cm.

DISCUSSION

From the pressure and magnetic profiles of figure 7, it is seen that for $B_1 = 0$ there was
separation of the current sheet from the pressure front until t = 28.2 μs when the d
current had fallen to 40 kA, half of the peak value. At t = 30.2μs, the pressure pulse
quite distinctly separated from the current sheet. Consider this pressure pulse a
gasdynamic shock, with a velocity of 1.8 cm/μs and a shock Mach number of 56.
shock-jump equations together with the relevant Saha equations form a closed system
equations which are solved to give a post-shock temperature of 31,000°K, with the ar
existing mainly as second-ionized Ar^{++}. The effective specific heat ratio of the post-sh
argon was 1.14 corresponding to a theoretical density ratio of $\Gamma = 15$.

The probe pressure P_{TM} can be used to measure the value of Γ. Lee & Sandeman (19
have shown that a bow shock has to be considered in this measurement, giving in
instance the following equation:

$$P_{TM} = 0.93\, \rho_1 q_1^{\,2} (\Gamma - 1)$$

At t= 30.2 μs, with $\rho_1 = 2.3 \times 10^{-4}$ kg m^{-3}, $q_1 = 1.8 \times 10^4$ m s^{-1}; the measured value
$P_{TM} = 7.5 \times 10^5$ N m^{-2} gives Γ=12. This measured value agrees to within experimental er
with the theoretical value of 15, indicating that the pressure pulse was indeed a gasdyna
shock.

For the profiles with B_1=0.25T, during the time of constant drive current, the th
distinct regions of front-current, zero-current and rearward expansion current may
postulated to be a magnetogasdynamic shock followed by a driver current sheet. If
front-current region were indeed a shock-jump effect, and not an effect due to
interaction with the driver current, then it may be expected that, with the decay of
driver current, the 'shock-jump current' would still persist as the shock pulse continue
propagate through the transverse bias field.

However, with the decay of the driver current, it is seen (fig. 8, t=36.2μs) that
pressure pulse, whilst still propatating through the transverse field at a Mach number of
had become gasdynamic. This indicates that the front-current during the constant d
period may have to be considered as an interaction effect between the shock wave and
current sheet.

To use the measured value of P_{TM} to calculate Γ, a reasonable model to take for
situation (*e.g.* fig. 8,,t=36.2μs) is to assume the primary shock to be gasdynamic but the
shock formed on the probe to be hydromagnetic. With this model, the value of Γ obta
from the measured value of P_{TM} is 10. This indicates that the transition from a sh
wave-current sheet system (as in t=28.2μs) to a gasdynamic shock system was not
completed up to t=36.2μs. However, the observed features of the pressure and magn

profiles of t = 28.2 μs to t = 36.2 μs do show that the state of this shock wave was fast approaching gasdynamic at the time t = 36.2 μs.

For our experimental conditions, the ratio of ν/ν_m can be estimated (following spitzer, 1962) to be 10^{-7} and the ratio χ/ν_m to be 10^{-2}. Therefore the observation of a transverse ionizing gasdynamic shock in our experiment is in agreement with Kulikovskii's theoretical model as discussed above.

CONCLUSION

In these experiments one of the three types of transverse ionizing shocks as classified by Kulikovskii was observed; namely the transverse ionizing gasdynamic shock for $\nu_m \gg \chi$, $\nu \to 0$ It would be interesting to repeat these experiments for the conditions $\nu_m \ll \chi$, $\nu \to 0$; to see if the transverse intermediate shock may be observed. These conditions (i.e. $\nu_m \ll \nu \to 0$) may be achieved for a high velocity hydrogen shock propagating into a small bias field. The present study has also shown that the observation for this type of shock should be made when the driver current has decayed.

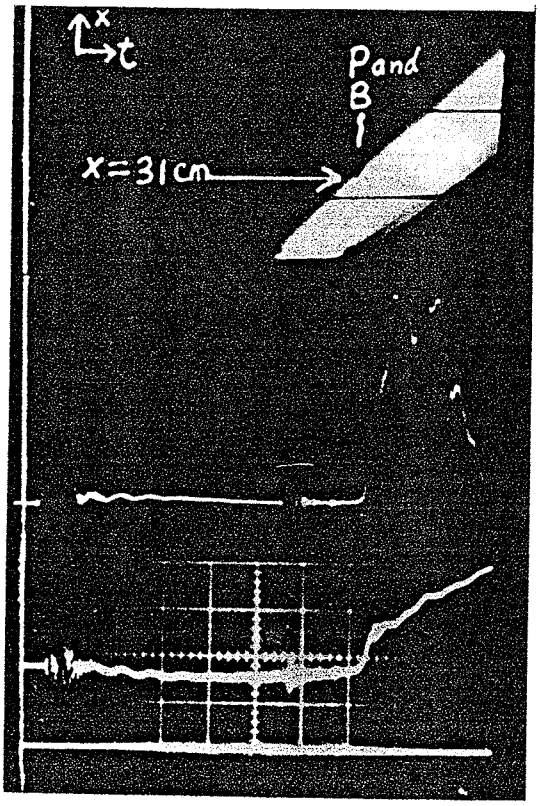

FIGURE 5. Comparison of S,P and B signals;
0.1 torr argon, B_1 = 0.25T, x = 31 cm.
All horizontal axes: 2.0 μs per cm.
Top: streak (S) photograph
Middle: pressure (P) probe output
Bottom: magnetic (B) probe output.

REFERENCES

CHU, C.K. (1964). Dynamics of ionizing shock waves: Shocks in transverse magnetic fields, Phys, *Fluids*, 7; 1349–57.

CROSS, R.A. & LEONARD, B.P. (1969). Private communication.

KULIKVSKII, A.G. & LYUBIMOV, G.A. (1960). Gas-ionizing magnetohydrodynamic shock waves. *Soviet Phys.– Doklady* (English translation) 4; 1185–8.

KULIKOVSKII, A.G. & LYUBIMOV, G.A. (1960). The simplest problems concerning gas-ionizing shock waves in an electromagnetic field. *Soviet Phys. – Doklady* (English translation), 4; 1195–8.

LEE, S. (1969). *Transverse ionizing shock waves.* Australian National University, Ph.D. thesis.

LEE, S. (1967). Matching of an electromagnetic shock tube with a transmission line condenser bank, *Sixth Australian Plasma Physics conference AINSE,* Lucas Heights, paper 27.

LEE, S. & SANDEMAN, R.J. (1972). Bow-shock effects on probe measurements, *J. Appl. Phys.* 43; 3980–3.

SPITZER, L., JR. (1962). *Physics of fully ionized gases.* Interscience, New York.

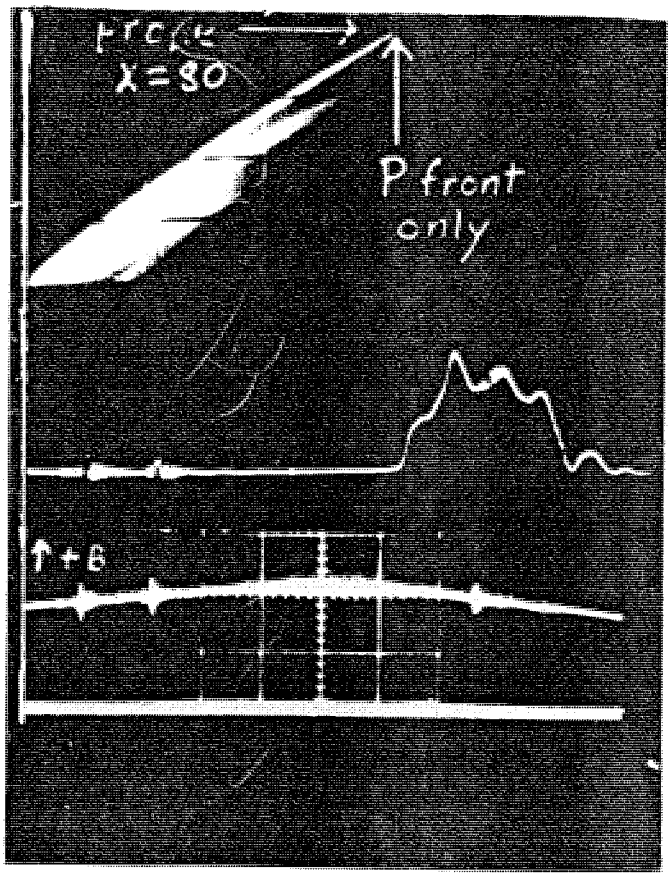

FIGURE 6. Comparison of S,P and B signals;
0.1 torr argon, B_1 = 0.25T, x = 80 cm.
All horixontal axes: 2.0 μs per cm.
Top: streak (S) photograph
Middle: pressure (P) probe output
Bottom: magnetic (B) probe output.

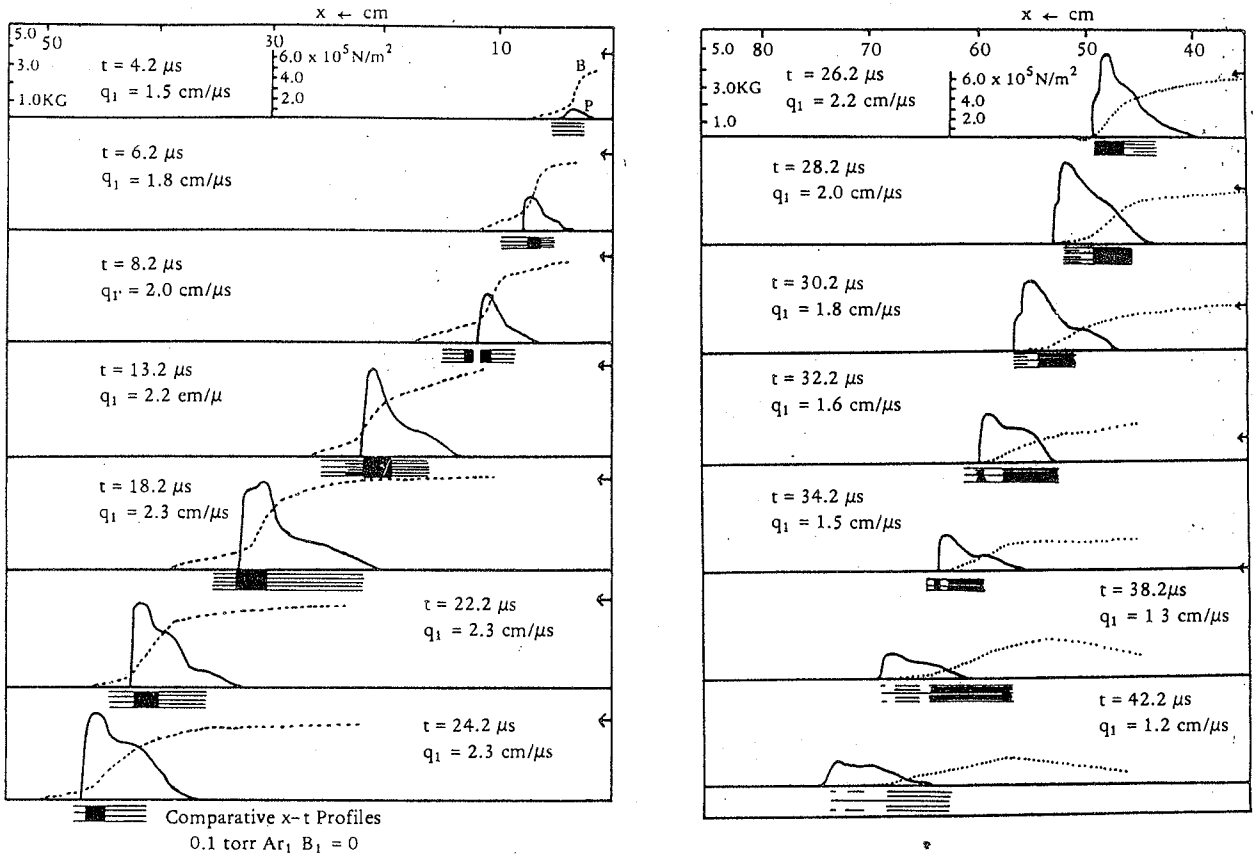

FIGURE 7. Spatial profiles of pressure, magnetic field and luminosity at various time t; 0.1 torr argon, B_1 = 0.25T.
The dotted line represents the magnetic field profile.
The solid line represents the pressure profile.
The shading below the two lines ineach frame represents the luminosity profile.

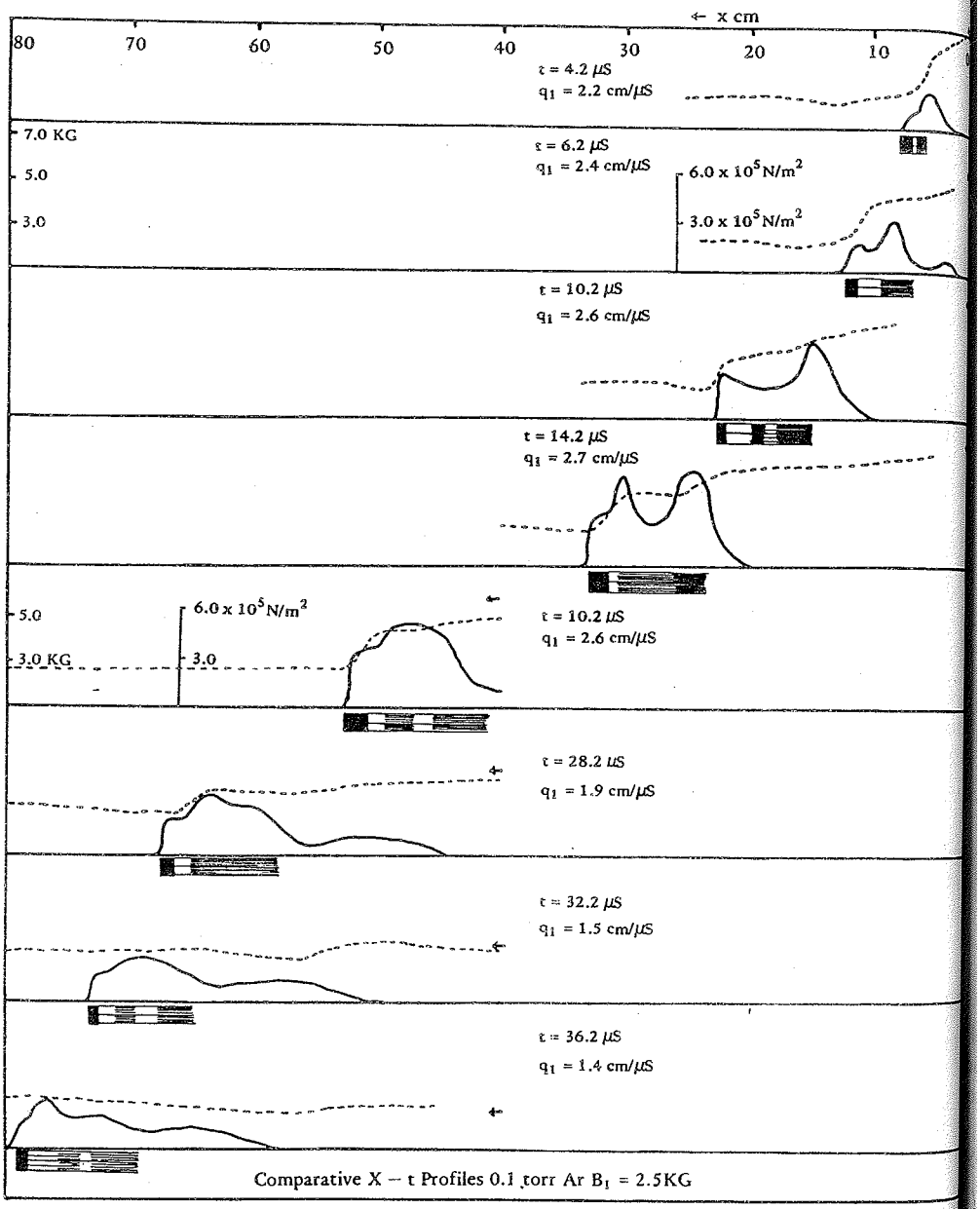

FIGURE 8. Spatial profiles of pressure, magnetic field and luminosity at various time t; 0.1 torr argon, B_1 = 0.25T.

MEASUREMENT OF NEUTRONS AND X-RAYS FROM A VACUUM SPARK

S. LEE[1] and H. CONRADS
Institut für Plasmaphysik der Kernforschungsanlage, Jülich, West Germany
Association EURATOM-KFA

Received 21 February 1976

The Jülich DPF I machine was modified to operate as a vacuum spark. It was established that with an operating pressure varying from 10^{-4} to 10^{-5} torr a voltage within the range of 14–17 kV was necessary to ensure a dense plasma phase as indicated by soft X-ray pinhole photography and current measurements. Operating with a LiD-filled channel in the anode, occasional bursts of neutrons were detected with a time-of-flight scintillator system. The yield, however, was erratic and below 10^7 per discharge.

It has been reported [1] that in a vacuum spark a concentrated thermal plasma of $T_e \sim 8$ keV, $N_e \sim 10^{21}$ cm^{-3} and $T_i \sim 20$ keV is produced, consisting of highly ionized anode material [2] and occupying a volume of 10^{-8} cm^{-3} [3].

A generally accepted principle of operation of the vacuum spark is this [4,5]: a capacitor $c \sim 20\,\mu$F, is connected directly to an anode and a cathode placed about 1 cm apart in a vacuum, from 10^{-4} to 10^{-5} torr, sufficient for a capacitor voltage of 10–20 keV to be held across the electrode system. To start the discharge, a sliding spark is initiated across an insulating surface between the cathode and an auxiliary trigger electrode. Plasma produced in this surface discharge is expelled towards the anode, and on striking it, causes anode material to be thrown out into the interelectrode space producing a plasma which then carries the main discharge current.

The purpose of the present work is to introduce into the anode a central located channel filled with LiD, and to study the characteristics of the resulting plasma, in particular the neutron production. Supposing that with this new electrode a plasma is produced with parameters similar to the normal vacuum spark except that it now consists of Li and D ions. Further supposing that the lifetime of the plasma is 50 ns and that its velocity distribution can be considered as thermal, then the number of neutrons expected to be generated would be in the region of 10^6. However, the presence of large transient electric fields and associated beams, and the possibility of instabilities [6] have to considered in any realistic estimate of neutron production.

The Jülich DPF I facility ($C = 22\,\mu$F, $U_{max} = 60$ kV, $f = 330$ Hz) [7,8] was modified to operate as a vacuum spark, fig. 1. The arrangement is similar to that of Elton and Lie [4]. We have an anode cathode gap of 8 mm and an operating pressure between 10^{-4} to 10^{-5} torr. To monitor the spark characteristics a soft X-ray pinhole camera with a range of sensitivity of 1–2.5 Å was used together with a current coil operated as a current transformer.

To detect neutrons two aligned scintillator-photomultiplier-detectors were used for a "side on" observation of the plasma. A near photomultiplier, 56 AVP, with a 6 cm thick NE 102 scintillator of 2.5 cm diameter was shielded in a lead cylinder of 6 cm wall thickness and placed at a distance of 0.5 m from the spark. A far photomultiplier, XP 1040, was used in conjunction with a NE 102 scintillator of 60 cm diameter and 6 cm thickness [7,8]. A lead wall of up to 6 cm thickness was placed between the spark and this detector. This far detector was positioned at a distance of 3.5 m from the spark. The two photomultipliers were connected by matched cables to a double beam oscilloscope with the two beams carefully aligned and synchronised. The transit interval of neutrons as well as sufficiently penetrating X-rays between these two scintillators could be measured with an overall time precision of 10 ns.

In this device operated at 16 kV, the current waveform for the first half cycle was much extended in time, compared with the second half cycle. Strong dips in the

[1] Present address: Physics Department, Universiti Malaya, Kuala Lumpur, Malaysia.

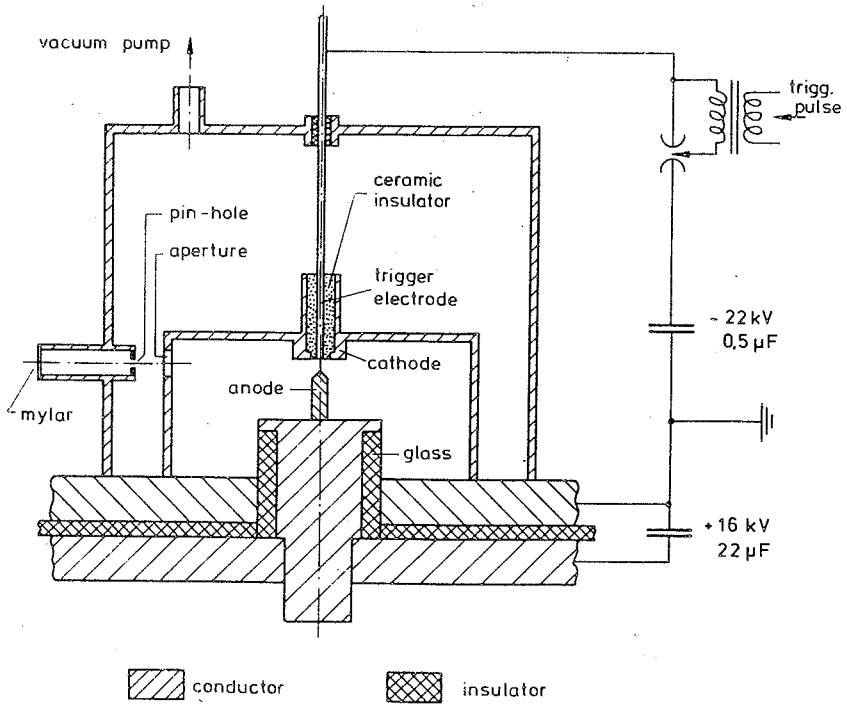

Fig. 1. Schematic of experimental set up.

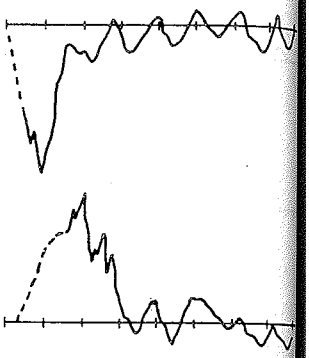

Fig. 2. Time of flight oscillogram of a discharge with neutron prod tion. Time scale: 100 ns/cm. Top trace: output of near (0.5 m) pho tomultiplier. Bottom trace: outp of far (3.5 m) photomultiplier.

current waveform were observed in about 30% of discharges. These current dips correspond approximately in time to the production of hard X-rays, which occasionally penetrated 10 mm of lead. Less penetrating X-rays were also observed earlier in the discharge. But for the present work it appears from correlation with soft X-ray photographs that the dense plasma phase is associated with these strong current dips since for those discharges in which these strong current dips appear the corresponding soft X-ray photographs show the formation of small regions of dense plasmas in the interelectrode space, fig. 3. A faint "glow" of the anode surface is observed due to the electron bombardment.

Above 17 kV, the current waveform becomes much more sinusoidal, the maximum current amplitude rising to 330 kA as compared to the maximum amplitude of 210 kA for the prolonged current waveform of 16 kV. There are no current dips nor hard X-rays bursts and corresponding soft X-ray photographs show only a faint glow around the anode surface. Likewise below 14 kV no hard X-ray and no soft X-ray plasma images were detected.

LiD has been chosen as part of the anode in orde to produce neutrons. This solid low Z material does not cool the plasma too much [7–9]. Since particle energies above 1 MeV have been observed in such plasma sources [4] it is not unconceivable to consid the $^{7}Li(D,n)^{8}Be$ Be-reaction having a cross-section of more than a factor of 6 larger than that of the (D, D)-reaction in the range above 1 MeV.

When the anode was replaced by one with a cent channel of LiD the hard X-ray bursts which corresp to the most severe of the current dips were observed penetrate 60 mm of lead. The soft X-ray photograp also show images of greater optical density particul from some shots, fig. 4, when LiD is ejected from t central channel of the anode into the interelectrode space. Corresponding to these particularly intense s the time-of-flight detection system yielded evidenc neutrons, fig. 2. In this discharge the far detector (recorded a pulse which is displaced in time from th of the near detector by 120–150 ns, this displacem corresponding to the transit time for 2–3 MeV neu Because of the multiple current dips and the corres multiple X-ray pulses, the possibility of multiple n

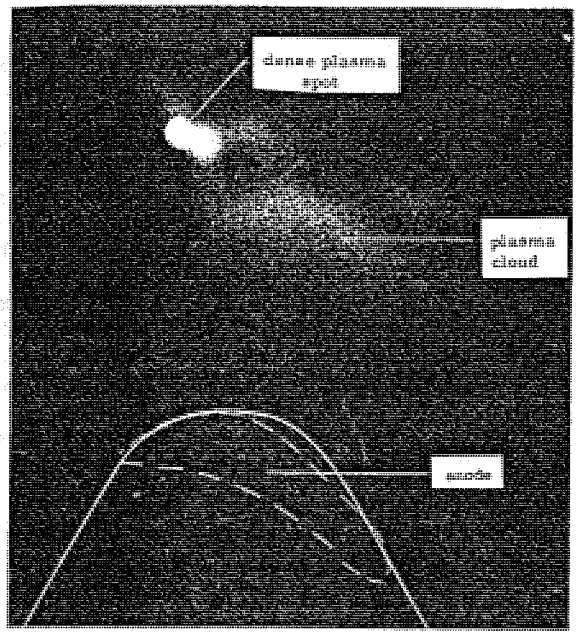

Fig. 3. Soft X-ray pinhole photograph taken with a photographic sensitivity of 1–2.5 Å. The circular distinct bright spot has a diameter corresponding to the pinhole size of 0.4 mm.

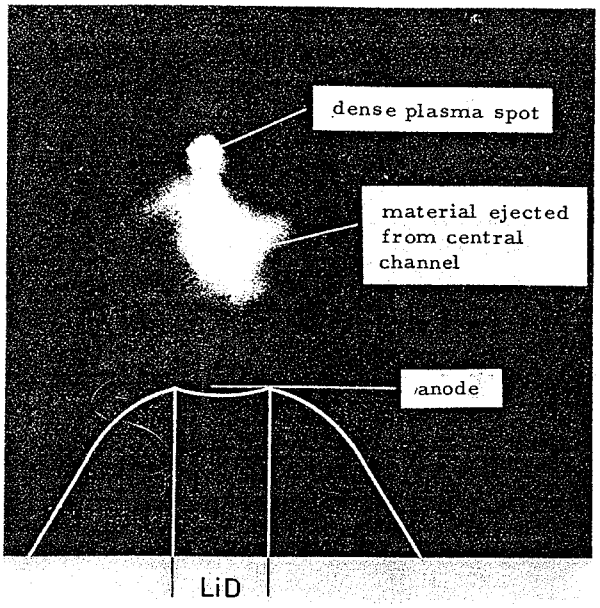

Fig. 4. Soft X-ray pinhole photograph taken with a photographic sensitivity of 1–2.5 Å. The anode, in this case, has a central channel filled with LiD. The circular spot at the top of the intense image has a diameter corresponding to the pinhole size of 0.4 mm.

pulses must be borne in mind, so that with a separation of 3 m it is not possible to make conclusive measurements of neutron flux or energies. However, the time-of-flight oscillograph, fig. 2, indicates the release of $(0.5–1)\times10^7$ neutrons of 2–3 MeV energy. Because of the small number of neutrons produced, an attempt to increase resolution by detectors placed at 10 m and 80 m did not succeed beyond confirming that small quantities ($<10^7$) of neutrons were produced in the most severe of shots.

With the present set-up, the dense plasma phase of the vacuum spark was observed for a narrow range of voltages around 16 kV. This means a limit to the input energy of 3 kJ. Moreover, since in focus-type devices it has been established that neutron production scales as I^4 [9], one would hope that one could increase the current flow in the vacuum spark for the purpose of generating more neutrons. Towards realising this, it is important to establish the factors limiting the voltage and current.

There is evidence from the current trace that above 17 kV the discharge has gone over to a surface discharge mode, i.e. the current flows between the inner anode cylinder and the outer cathode return via the glass insulator. This effectively short circuits the vacuum spark. If this were the case, the observed threshold for the operating voltage could be increased by redesigning the electrode mounting with the aim of reducing the probability of a short-circuiting discharge.

Another factor to note is that the neutron production occurs in those shots in which material, presumably LiD from the central channel of the anode is observed to be ejected into the interelectrode space. To ensure that the device is more reproducible in this aspect of its operation, an anode design is required in which only a small "deuterided" area of the anode surface is exposed to the discharge. This exposed area can, for example, be coated with a conducting layer of deuterided material such as a solution of deuterium in lithium [10]. An alternative method might be to use a laser to trigger the discharge as was demonstrated by Lie [1]. By focusing the high power laser radiation onto the channel of the anode one may ensure that the plasma that initially fills the interelectrode space consists of a large proportion of Li and D ions.

One of us (S. Lee) acknowledges the assistance of an Alexander von Humboldt fellowship within the framework of which this work was completed.

References

[1] T.N. Lee, Proc. 2nd Topical Conf. on Pulsed High-Beta Plasmas, ed. W. Lotz (Max-Planck-Institut für Plasmaphysik, Garching, 1972) Paper G-7, p. 253.
[2] B.S. Fraenkel, I.L. Schwob, Phys. Letters 40A (1972) 83.
[3] L. Cohen, U. Feldman, M. Schwartz, J.H. Underwood, J. Op. Soc. Am. 58 (1968) 843.
[4] R.C. Elton, T.N. Lie, Space Sc. Rev. 13 (1972) 747.
[5] R. Beier, Untersuchung eines Plasmas sehr hoher Dich und Temperatur in einer Niederinduktiven Vakuum-Funken-Entladung, Diplomarbeit, Ruhr-Universität-Bochum, 1975.
[6] T.N. Lie, R.C. Elton, Bull. Am. Astron. Soc. 4 (1972) 386.
[7] P. Cloth, Neutronen-physikalische Messungen an einem dichten Plasma-Fokus, Dissertation TH Aachen, 1974.
[8] H. Conrads, P. Cloth, M. Demmeler, R. Hecker, Phys. Fluids 15 (1972) 209.
[9] P. Cloth, H. Conrads, H.R. Ihle, C. Gourlan, Ch. Maisonnier, B.V. Robouch, The perspectives of a Dense Plasma Focus as a high intensity Neutron Source, Int. Conf. on Radiation Test Facilities for the CTR Surface and Materials Program, Argonne, 1975.
[10] H.R. Ihle, KFA Jülich, private communication.

14-4

Procs. Sem. Plasma Focus Work in K.L. (K.L. Nov. 1974)
Edited 1976

THE FOCUS AND CTR

S. Lee

The Problem

The problem of CTR (Controlled Thermonuclear Reaction) is the problem of the production in the laboratory of a thermalized plasma, so hot and dense that its energy liberation via the nuclear fusion reaction equals to the sum total of the energy expended in heating the plasma. The first machine to achieve this equality would be a 'break-even' machine upon which would be based the design of an energy producing fusion reactor. From cross section considerations, the reaction employed in the first break-even machine would almost certainly be the

D-T reaction ($D^2 + T^3 \longrightarrow He^4 + n$) with the D-D reaction ($D_1^2 + D_1^2 \longrightarrow He^3 + n$)
3.5 MeV 14.1 MeV 0.81MeV 2.45MeV

a much more remote possibility. From the point of supply, using the D-D reaction there is enough deuterium in sea water to supply the foreseeable energy needs of the world for 10^9 years. Using the D-T reaction, tritium has to be bred from Lithium ($n + Li_3^6 \longrightarrow T_1^3 + He_2^4$) and there is enough Lithium for this purpose to supply the energy need of the world for 10^6 years.

The Criteria

The three fundamental criteria of a break-even plasma have long been established and not been altered by two decades of intensive research effort. These criteria relate to the properties I mentioned earlier namely, thermalization, temperature T and density n together with the time of containment τ of the hot plasma.

Thermalization

The first break-even fusion machine is almost certainly going to be a thermal one; i.e. it will use a plasma with a Maxwellian velocity distribution. Although in principle it is possible to have a net gain of energy by accelerating two beams of deuterons (or a beam of deuterons at another beam of Tritons) at each other, calculation show that the technical requirements are less stringent if the particles are energized as a plasma and held together long enough for a sufficient proportion of the particles to undergo in fusion reaction through random collisions. Since the cross section for fusion increases rapidly with particle energy, one contributory factor in favour of a plasma reactor is the fact that in a thermal plasma of average energy E, most of the particles contributing to the fusion reaction have an energy of several E. Thus, thermalization multiplies the fusion cross-section. This, together with the longer reaction time of a contained thermal plasma, as compared to ion beams, make thermalization a fundamental practical requirement for a fusion reactor.

Ideal Ignition Temperature

At low temperatures, say 1 Kev (11 million ^{o}K), Bremstrahlung radiation power P_B far exceeds the fusion power production P_F. Fortunately whereas P_B increases as $T_e^{\frac{1}{2}}$, P_F increases much more rapidly with Temp; e.g. between 1 - 10 Kev, the fusion power output of a D-D plasma increases by a factor of 4000 whereas the Bremstrahlung power increases only by a factor of 3.1.

Thus at a sufficiently high temperature the P_F curve will intersect the P_B curve. The point at which the fusion power (considering that portion carried by the charged particle only) begins to exceed the electronic Bremstrahlung power is called the Ideal Ignition Temperature; and represents the lowest temperature for which a self-sustaining reactor can hope to be operated. For the D-D plasma the I.I.T. is 36 Kev (400 million ^{o}K) and for the D-T plasma it is 4 Kev (44 million ^{o}K).

The $n\tau$ Criterion

At this kind of temperatures, say 10 Kev, if a D-T plasma has a number density corresponding to atmospheric air i.e. 5.4×10^{19} cm^{-3} the power production would be a staggering 3×10^{15} W m^{-3} (i.e. 1 m^3 = 3 million power stations of 1000 MW capacity) and the kinetic pressure an equally staggering 170,000 atm. The only conceivable laboratory devise to operate at such extremes of pressure and power density would be a very tiny and very transient blob of plasma such as exist in the plasma focus or a laser initiated imploding super dense plasma. For a quasi steady plasma, i.e. one that lasts for a time of the order of a sec. a realistic working pressure may be 100 atm. corresponding at 10 Kev to a density of 3×10^{16} cm^{-3} or about $\frac{1}{2000}$ of normal atm. density.

Whether we work at high or low densities, a certain period of time is required for a given sample of heated plasma to completely undergo fusion. A shorter time τ is required so that a sufficient fraction of the nuclei undergoes fusion to provide the break-even condition. Lawson considered a pulsed cycle in which the input energy equals the thermal energy 3 NKT plus the Bremstrahlung energy; and the output energy equals $\frac{1}{3}$ of the sum of the fusion energy released plus the Bremsstrahlung energy plus the thermal energy. That is, Lawson considered that $\frac{1}{3}$ of the Bremsstrahlung radiation and the plasma thermal energy is recoverable together with $\frac{1}{3}$ of the fusion energy. For such a cycle, the break-even condition is:

$$n\tau = 10^{16} \text{ particle-sec } cm^{-3} \text{ for a D-D plasma}$$
$$n\tau = 10^{14} \text{ particle-sec } cm^{-3} \text{ for a D-T plasma.}$$

i.e. for a D-T plasma; if $n = 10^{14}$ cm^{-3} break-even = 1 s
for $n = 10^{20}$ cm^{-3} break-even = 10^{-6} s.

A reactor

Before we discuss the current CTR programs aimed at producing a break-even plasma; let us jump 10 - 20 years ahead and assume that such a plasma can be created at will. Then a schematic of a reactor may be as shown in Fig 1.

The plasma heated from a fuel charge of 40 mg of D + 30 mg of T to 100 million ^{o}K is contained for 1 sec at a particle density of 10^{15} cm^{-3}, thus satisfying the $n\tau$ criterion. Containment is effected by means of a magnetic field which holds the plasma in a stable configuration and a way from the vessel wall. To give an idea of shape and size, Fig 1 may be considered to be a cross section of a torus. The plasma shown in Fig 1 may have a diameter of 1 metre whilst the major diameter of the torus may be 5 metre.

The reactor may operate with a 1-sec burn, followed by a 1-sec shut-down (in order to flush away impurities) and then a 1-sec burn and so on.

The 4000 MJ energy produced in the 1-sec burn consists of:

(a) Kinetic energy of charged particles. This stays in plasma.

(b) K.E. of neutrons which contains the major part of all the energy produced.

(c) energy of e.m. radiation.

The vessel wall must withstand the bombardment of neutrons. The effect of e.m. radiation is even more severe and the wall has to be cooled.

The blanket could consists of a mixture of Berylium and Lithium. Its function are:

(a) to absorb the energy of the e.m. radiation and neutrons; excess energy has to be tapped by gas cooling. The energy thus removed has to be enough to pay for the capital cost and running cost. The power level involved at the blanket would be close to 100 MW/sq. m.

(b) production of Tritons; breeding ratio 1.1 aimed for.

CTR program

To come back to the present, the main emphasis now is on solving the problem of the break-even plasma rather than reactor technology. Of the many programs, the one which is most highly organised is the Tokamak program.

The start of this program can perhaps be traced back to 1952 when the Russian physicist Artsimovich observed a burst of neutrons from a high current discharge in a column of deuterium gas between two electrodes (Fig 2). It was very quickly demonstrated that this linear pinch was severely limited by end losses and instabilities. The instabilities could be reduced by an axial bias magnetic field B_z. To eliminate the problem of end losses two configurations have been attempted. One of these is the magnetic mirror. The other is the toroidal pinch (Fig 3). However, whilst the toroidal pinch has no end losses, the axial stabilization field is now not constant over the minor cross-section. This magnetic gradient lead to plasma drift towards the outer wall, resulting in the rapid destruction of the plasma.

In the U.S. the Princeton Group twisted the toroid into a figure-of-8 introducing a 'rotational transform' which prevented the plasma drift from intersecting the wall of the twisted torus called the Stellarator. Results were however disappointing as the plasma confinement time turns out to scale as B_z/T_e i.e. as temperature was raised, the lifetime of the plasma decreased. This was contrary to the $B^2 T^{\frac{1}{2}} r$ dependence expected from classical diffusion theory.

At the same time the Americans were twisting the torus, the Russians stuck to the simple toroidal geometry observing that an effective rotational transform already existed from the superimposition on the stabilization field B_z of the azimuthal field B_θ. In order for the rotational transform to be effective in confining the plasma, there

is a limit to the heating current I_z (the Kruskal limit) which can be expressed approximately as:

$$k\, I_z < 2$$

$$k \simeq \frac{R}{r} \times \frac{1}{r} \times \frac{1}{B_z}$$

$\frac{r}{R}$ = aspect ratio

r = plasma radius

R = radius of torus

B_z = axial stabilization field

The existing Tokamak cannot have heating currents I_z above 100-200 kA because of this limit. Even so the results are promising especially as regards the confinement time τ which is scaling correctly as $B_z^2\, T^{\frac{1}{2}}$. Scaled-up Tokamaks in which the aspect ratio, the plasma radius and the stabilizing fields are all increased, reducing k by a factor $\frac{1}{60}$, are being planned in Europe the U.S. the U.S.S.R. and Japan. This scaling up will allow the current to be raised to 8 MA increasing the value of T_i, and $n\tau$. If the simple scaling laws already developed continue to be obeyed, a break-even plasma can be achieved. One major problem envisaged is that as temperature increases, the heating effect of the I_z will decrease. Some other heating mechanism may have to be employed.

The following table summarizes the essential factors for scaling a Tokamak towards a break-even machine. The cost of such a machine is expected to exceed 500 million Ringgits.

Plasma Parameter	Model C Stellarator	Princeton Tokamak	Projected Tokamak
T_i (Kev)	-	0.5	10
T_e (Kev)	0.06	1.5	10
n_i (cm^{-3})	2×10^{13}	3×10^{13}	6×10^{14}
τ (m sec)	0.4	10-20	1000
$n\tau$ ($s\text{-}cm^{-3}$)	8×10^{9}	$3\text{-}6 \times 10^{11}$	6×10^{14}
B_z (KG)	35	50	90
2r (cm)	12.5	25	300
$\frac{r}{R}$	$\frac{1}{20}$	$\frac{1}{8}$	$\frac{1}{3}$
I_z (MA)		0.13	8
power density ($MW\ m^{-3}$)			20
Total power (MW)			4000

Plasma Focus

At the present moment, the plasma focus has the best $n\tau$ figure of all laboratory machines. For example even a simple machine such as ours operating at 10 kJ has a focused deuterium density of 10^{19} fuel ions cm^{-3} for a time of 10^{-7} s. The $n\tau$ value of 10^{12} is considerably better than the existing Tokamaks. The focus temperatures too are good, being greater than 1 Kev for both the electron temperature (x-ray measurement) and the ion temperature (neutron measurement).

Thermalization

During focusing an intense burst of neutrons is emitted from the plasma e.g. 10^{9} n (from a 15 kJ D-D focus) in a short time of 10^{-7} s. Measurement on the neutron energy distribution have tended to indicate that the neutrons are from a non-thermal source, particularly from the Mather type focus; although even in these measurements, it could not be ruled out that perhaps 5-10% of the neutrons are from a thermal plasma.

Recently, however, Maisonnier, of the Laboratori Gas Ionizzati in Rome has made a detailed comparative study of plasma focus devices and has found evidence that in the Filippov focus device, the second burst of neutrons which accounts for more than 90% of the neutrons emitted is mostly of thermonuclear origin and comes from a large volume (10 cm^3) of relatively low density plasma (3×10^{17} cm^{-3}) which has been turbulently heated to a temperature of 5-10 Kev. The neutron measurements indicate that the heating is due to interaction, via two stream instabilities, of mm diameter high intensity electron beams (MA at $\simeq$ 100 Kev) with a large diameter (cm) plasma column in expansion. Maisonnier's comparison indicate that this mechanism is likely to act also in the Mather type focus. The Mather focus however is complicated by rapid axial variation

of plasma densities and Maisonnier is not convinced of the present conclusion that most of the neutrons from the Mather type focus is non-thermonuclear in origin.

The origin of the electron beams can be traced to the rapid diffusion of magnetic field lines during the final focusing phase due to the Bernstein anomalous resistivity. This rapid rate of change of flux lead to large electric fields which act to accelerate the electrons, forming the MA electron beams.

For the Filippov type focus Maisonnier has shown that up to 20% of the capacitor bank energy can be transferred to the plasma via these electron beams and that the neutron production vary essentially as the square of the capacitor energy W_o divided by the square of the radius r of the hot plasma. In fig 4 I have compiled data from published literature which shows that in the Mather type focus the number of neutrons also varies as W_o^2. This could indicate that the Mather device share the same basic heating mechanism as the Filippov type and that the plasma radius is essentially constant at various energies.

According to this extrapolation Maisonnier's 1 MJ D-D focus should produce 2×10^{13} neutrons carrying 6J of kinetic energy, and if he converts to a D-T focus, his 1 MJ focus should produce 3 KJ of fusion energy. Since the fusion energy $\sim$ (bank energy)^2, the break-even point for a fusion machine based on the focus principle could be around 300 MJ. At an input energy of 1500 MJ, fusion energy would be 7500 MJ. Firing once per second, such a machine would generate 6000 MJ.

This sort of energy figures would be comparable with the Tokamak reactors being designed at the moment. However, compared to the Tokamak devices, plasma focus devices are in a much earlier stage of development.

For example very little is known about the mass that is swept into the focus, so that for the purpose of modelling an initial mass fraction has to be assumed. The early dynamics of the focus is now sufficiently well known so that even a simple snow plow model can yield results consistent with experimental measurements of trajectory and average densities. Detailed calculations such as the P.I.C. model has yielded detailed 2-D distributions of density, temperature and field lines. However, in the light of Maisonnier's recent model it appears as though once again the more intuitive method has to be used to understand first the mechanism, before these mechanism can be suitably approximated as terms in the equations of motion.

Much remains to be done both theoretically and experimentally in order to develop the plasma focus machine to its full potential in this exciting race towards Controlled Thermonuclear Reaction.

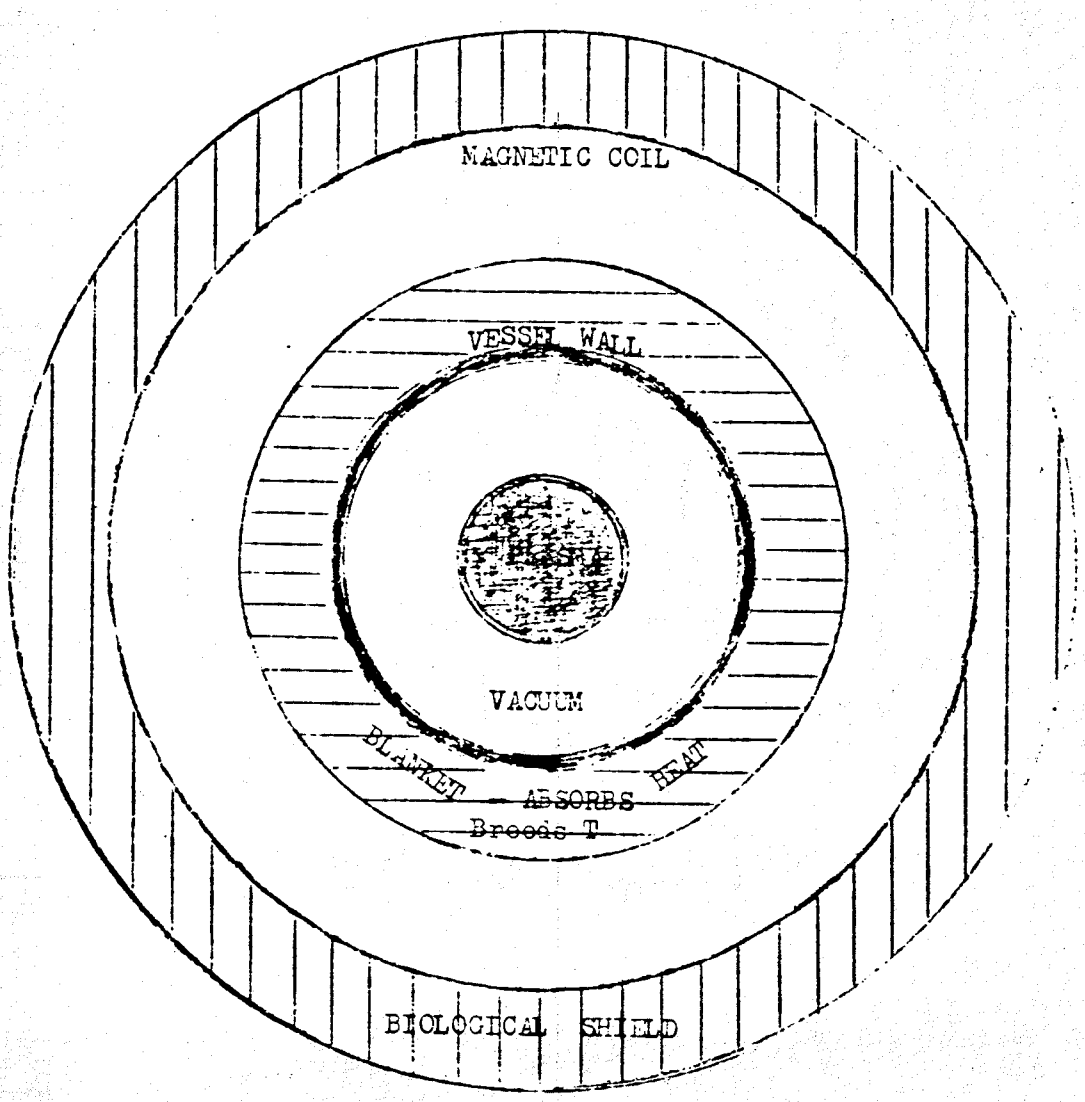

Fig. 1. Schematic of a Reactor.

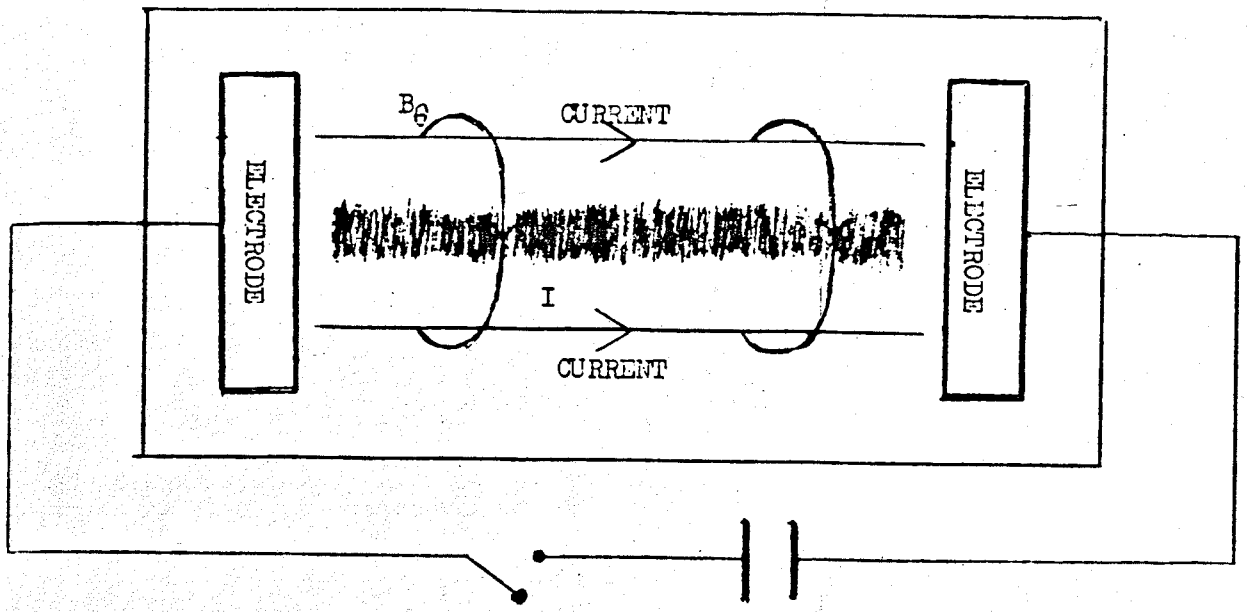

Fig. 2. Schematic of Linear Pinch.

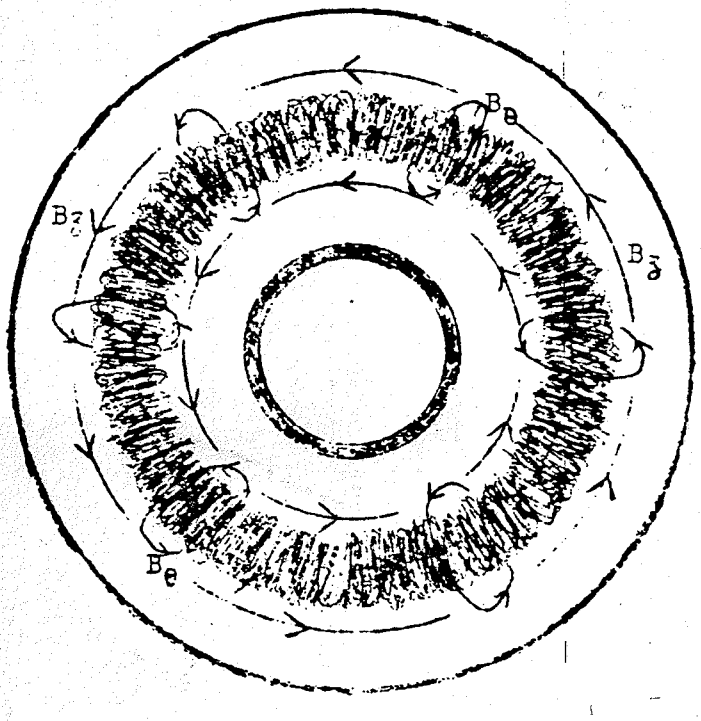

I_z = heating current, induced by means of a transformer.
B_θ = azimuthal field due to I_z .
B_z = stabilization field, produced by a solenoid wrapped around the torus.

Fig. 3. Schematic of Toroidal Pinch.

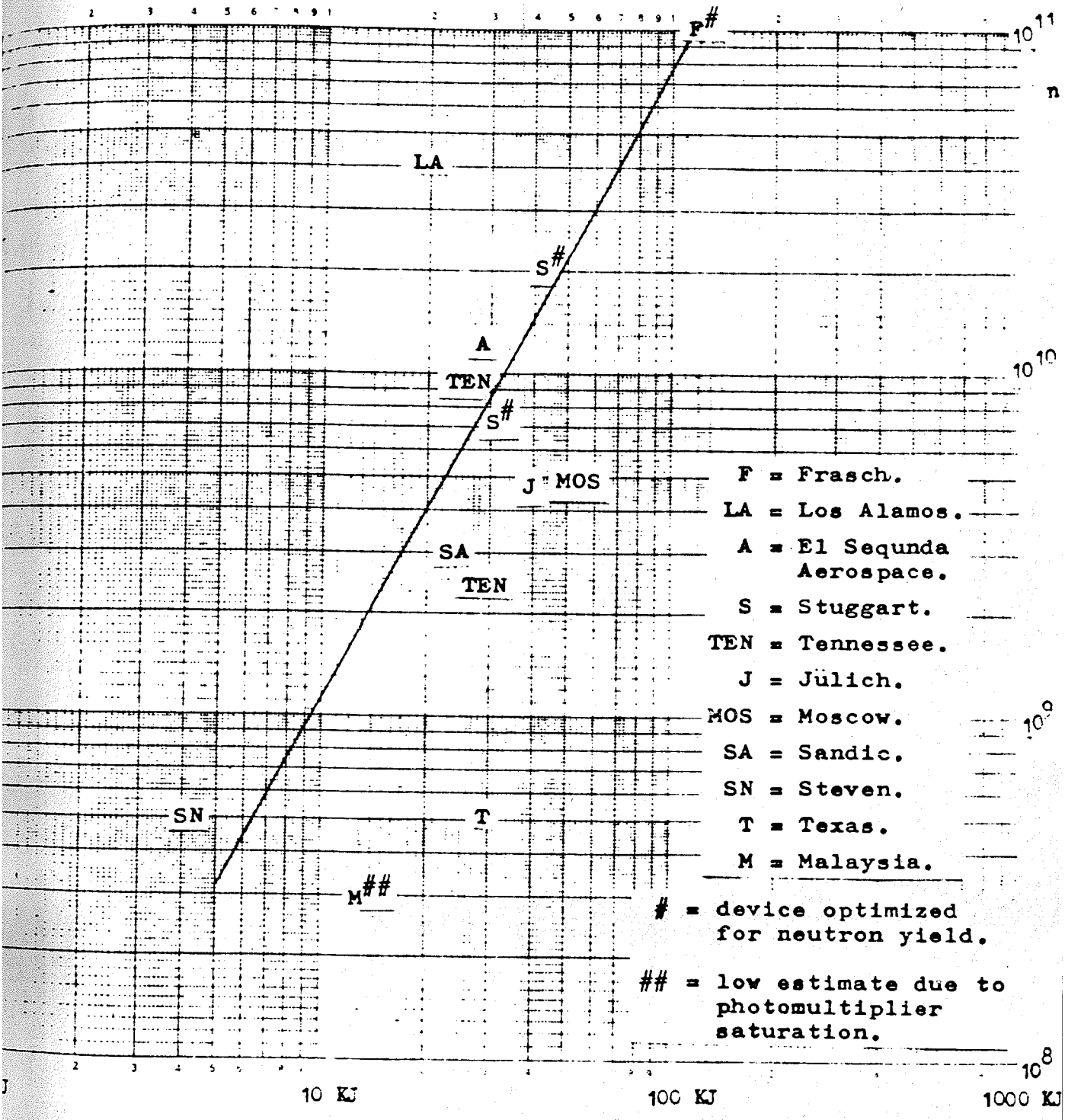

Fig. 4. Neutron productron as a function of energy.

Procs. Sem. Plasma Focus Work in K.L. (K.L. Nov. 1974)
Edited 1976

FOCUS WORK IN K.L. - A REVIEW

S. Lee

Introduction

The focus facility is shown schemetically in Fig 1.

(1) Central to this facility is the capacitor bank (1,2) switched by ignitrons and connected to the focus tube by a combination of parallel plates and coaxial cables. A specially designed control system triggers the capacitor bank and at the same time sychronizes the measurement systems (16).

(2) In the focus tube, part of the capacitor energy is transferred to the deuterium gas, forming and heating the plasma to high temperatures.

(3) A high speed camera records the motion of the luminous plasma in both streak and framing modes (3).

(4) The current coil and the voltage divider respectively measure the current flowing through the focus tube and the voltage across the input terminals of the tube. From these plasma inductance is deduced and such effects as increase of inductance in the presence of plasma rotation has been observed (4).

(5) The magnetic coils record the spatial and temporal changes in the magnetic fields in the focus tube from which the current distribution and current sheet velocity are deduced (5).

(6) The pressure probes measure the total pressure of the plasma from which the distribution and motion of the plasma has been deduced (6).

(7) Soft x-ray photographs are taken by means of vacuum pinhole cameras which record soft x-ray emissions from the plasma (7). Time resolved measurements using soft x-ray diodes are also in progress.

(8) For the neutron measurements, two fast response scintillator-photomultipliers are spaced 10 m apart to measure the speed and hence the energy of the plasma-emitted neutrons. The detectors have been calibrated against a Po - Be source so that total flux from the plasma can also be estimated. The energy measurements have proven conclusively that the plasma neutrons originate from nuclear fusion reactions (8).

(9) Together with the experimental work, theoretical work is also pursued mainly on trajectory calculations (9) and the effect of the plasma rotation (10) and ionization (11) on the focus trajectory.

The Capacitor Bank

The capacitor bank is assembled from 100 pieces of 'Wego' low inductance capacitors. The performance figures are 40 kV, 50 kJ, 22 nH with a measured short circuit current of 1.9 MA rising in 1.9 μs (2). The expected peak current of 1.4 MA into the focus tube has not been reached yet because the present focus tube is not able to withstand the full current; possibly because of the high current density at the back insulation flange. A bigger tube is at present undergoing construction. Fig 2 shows an oscillogram of the short circuit current measured with a toroidal current coil wrapped around the path of the discharge current.

Focus tube

The focus tube is of the Mather type as shown in Fig 3. The current sheet first forms at the insulating back flange and is then accelerated down the coaxial region. At the end of this region the tube geometry constrains the plasma to undergo an expansion during which the flow direction changes from axial to predominantly radial. We have determined (6) that when the current sheet structure is of a suitable type the electromagnetic energy is strongly coupled into the plasma resulting in intense plasma heating with the production of fusion neutrons. The main problem with this tube is that the focusing is not sufficiently reproducible. This irreproducibility could be related to irregular breakdown at the insulator flange which could also account for the frequent damage sustained by this flange. This problem is under study.

Magnetic Field Measurements

The magnetic probe consists of a coil 1 mm diameter x 30 turns inserted into a glass tube. A typical signal as the plasma sweeps over the probe is shown in Fig 4. From such oscillograms, the current sheet velocity, the magnetic field and the variation of field with time can be computed. Transformation of this temporal variation to a spatial distribution can be effected giving the structure of the current sheet. Fig 5 shows current sheet velocity obtained from magnetic probe measurements and Fig 6 shows a typical magnetic field structure.

Focus Trajectory Computed from voltage and current oscillograms

Fig 7 shows oscillograms of voltage and current signals with the characteristic voltage spike and current dip associated with the transfer of energy from the magnetic field to the plasma. Neutrons and soft x-rays are only observed when these voltage spikes and

current dips are observed. We calculate several quantities of interest from the voltage spike and current dips e.g. the integral of the product of these two signals give us the energy transferred into the focus tube. Another important quantity is the focus inductance which, by using a simple model for the current distribution (Fig 8), can be written as:

$$L(t) = \frac{\ell}{4\pi} \ln \frac{b}{r} u_z (t - t_s) \quad \ldots\ldots\ldots\ldots\ldots\ldots \quad (1)$$

where t_s = time of start of focus and u_z is the axial velocity of the current sheet.

But the inductance $L(t) = \frac{\int_0^t V\, dt}{I(t)} - \frac{\int_0^{t_s} V\, dt}{I(t_s)}$ - (2)

The focus inductance L(t) can be computed from the voltage and current oscillograms using Eq. 2. Then from Eq. 1, the focus radius at time t is:

$$r(t) = b \exp \left[\frac{-4\pi L(t)}{\mu_o u_z (t - t_s)} \right]$$

In this manner the current sheet trajectory is computed and compared with (i) photographic and (ii) theoretical 1-D radial snow-plow trajectory. In general, photographic measurement agree with inductance measurements of trajectory down to $r \simeq 1$ mm. Down to this radius there is also agreement with snowplow computation (9). However, in many of the discharges, the inductance measurements show that the radius goes below 1 mm and approaches values of 0.07 mm and less which is physically impossible based on a snow-plow model of a thin current sheet compressing a plasma.

It is quite easy to show that even at around r = 5 mm, the magnitude of the azimuthal (B_θ) field (1 MG) is already sufficiently large to significantly reduced the conductivity along the electric field lines. This leads to rapid diffusion of the B_θ field towards the axis of the tube which can account for the anomalously large value of inductance measured. It is possible that this mechanism is related to the production of electron beams as observed by Maissonier (12).

High Speed Photography

Fig 9 shows a framing photographic sequence of the collapsing plasma. The framing rate is 10^7 per second while the exposure time of each frame is 20 ns. Fig 10 shows a streak photograph showing the collapsing trajectory.

Pressure Measurement - the dependence of focus intensity on mass distribution and current sheet structure

It was suspected that the relative structure of the current sheet and the shock front was important in determining the intensity of focus which was observed to be irreproducible. This question could be of considerable importance in the design of a fusion machine based on the focus principle. To look into this the mass distribution was measured with a pressure probe. Together with the magnetic field distribution the mass distribution was examined for any correlation with focusing intensity.

The results immediately show (Fig 11) that whenever a focus occurs, the current sheet shows a frontal region of high current density in which the magnetic field rises to 1T in a distance of 1 cm. Non-focusing shots are characterised (6) by a

low frontal current density e.g. 0.5 T over 7 cm. There is also correlation with the mass distribution although this correlation is less reproducible and more difficult to quantify. The example in Fig 12 shows that the focusing shot has a sharp narrow frontal pressure peak. In the non-focusing shot this frontal peak is not so sharp and less distinct.

A model based on a bow shock transition followed by an isentropic compression towards the front face of the pressure probe (13) enables us to measure the amount of mass to arrive at the end of the axial run-down region in time to participate in the focus. This mass we call the 'initial mass' and is the upper limit of m_o, the quantity corresponding to the amount of mass from the axial region that is swept into the radial compression. We define the 'initial mass' as that amount of mass arriving within the first 0.05 μs of the start of focus, as any mass coming after this time would be too late to participate in the focus action. The 'initial mass' was found to be 4 - 7% of the axial ambient mass, and was only slightly more for the focusing shot when compared to the non-focusing shot. The measurements also indicate that in the first 0.3 μs from the start of focus, 30% of the ambient mass has arrived at the probe.

The Stuttgart Group (14) has established a criterion for optimum neutron production which shows that the larger the current the bigger is the value of ρL (ρ = ambient density, L = annular gap) at which optimum neutron production occurs. It is also known that the larger the current, the greater is the value of ρL that is required for a separation of the shock front from the current sheet. Our results show that when the current sheet has a high density frontal region concurrent with the pressure front (i.e. no separation) focusing is intense. These results combined could mean that for a given value of ρL the most intense focusing occurs for the largest current at which there is still no effective separation.

Soft x-ray Measurements

Using aluminium and berylium foils of different thicknesses and observing the maximum mass density which permits the penetration of the plasma-emitted soft x-ray enables an estimate to be made of the wavelength. The conclusion (7) is that an electron temperature of 1 KeV has been observed and that a typical focus soft x-ray radius is 1 mm (Fig 13). Multiple structures have also been observed.

Neutron Measurements

The detector consists of an NE 102 plastic scintillator used in conjunction with a PM9546 photomultiplier and a 556 oscilloscope giving a rise time of 10 ns. The two beams of the oscilloscope were carefully adjusted and centre-sychronised to an accuracy of 2 ns. Fig 14 shows the output of 2 detectors placed 10.2 m apart. After CRO linearity and cable corrections the result measured for several shots is 2.2 ± 0.1 MeV. As these scintillators were placed in the backward direction of the focus, the difference from 2.45 MeV (the C-M neutron energy of the D-D reaction) could mean that the reacting deuterons are moving forward in the laboratory coordinates (8). The maximum total flux in these measurements exceed 2×10^8 neutrons for 1 discharge. Further measurements of flux and energy are in progress.

Effect of rotation on the focus

Preliminary experiments have been carried out on this (4). The main results are that with an axial bias field plasma rotation is observed in the axial drive region and that the focus inductance is enhanced.

When the rotating plasma is focused due to the conservation of angular momentum we can expect the rotational velocity to increase inversely as the radius. Some interesting results should be observed when we apply a sufficiently large bias field so that the rotational energy stored in the plasma is comparable with the other energy terms during the focusing.

Computation

We have developed a 1-D radial model for computation involving some interesting physics including a retarding pressure term. The main features are (i) all the mass encountered by the current sheet is swept up (ii) a shock wave is assumed to move ahead of the current sheet in accordance with the strong shock equations (iii) this shock wave heating is followed by a reflected shock phase and finally a phase of adiabatic compression. The result show that this model agrees with experimental measurements down to r = 1 mm and that such agreement is achieved by using a small value of m_o equivalent to 0.0003% of the ambient axial mass and initial radial velocity of about 10 cm/us. For r < 1 mm this model appears to break down since the currents in the plasma diffuses inwards due to the enhanced resistive effects.

This model is being used to examine the effects of multiple ionization on focus dynamics (11). Argon is considered for this computation as experimentally we have observed that an argon focus is more intense than one in deuterium. The main problem here is that we expect multiple ionization up to A_r XVII so that 16 saha equations have to be used.

The effects of rotation on focus dynamics are also being examined (10) by considering the centrifugal force term and including the fact that the shock wave is now a transverse magnetic shock (15).

Work on the basic model is also continuing. It is expected that for $r < 1$ mm, a diffusive term would have to be included as this phase of compression appears to be of immense importance in that it precedes the turbulent heating phase (12) during which most of the neutrons are produced.

In conclusion, it may be seen that the last four years have been rather fruitful ones for the plasma focus group here in Kuala Lumpur. Some of our lines of research for the future may be glimpsed in the following papers of this seminar.

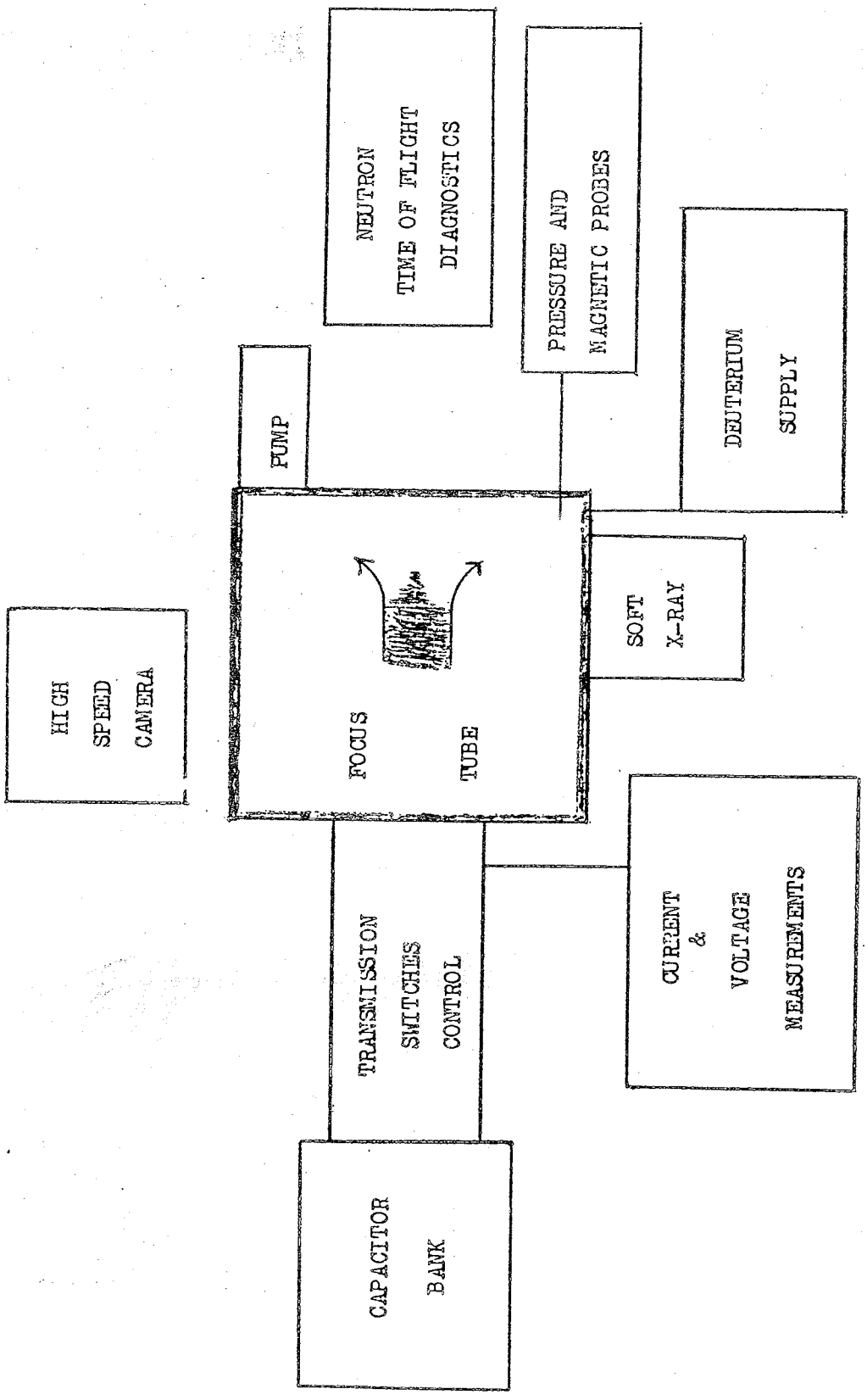

Fig. 1 Experimental set-up of focus facility.

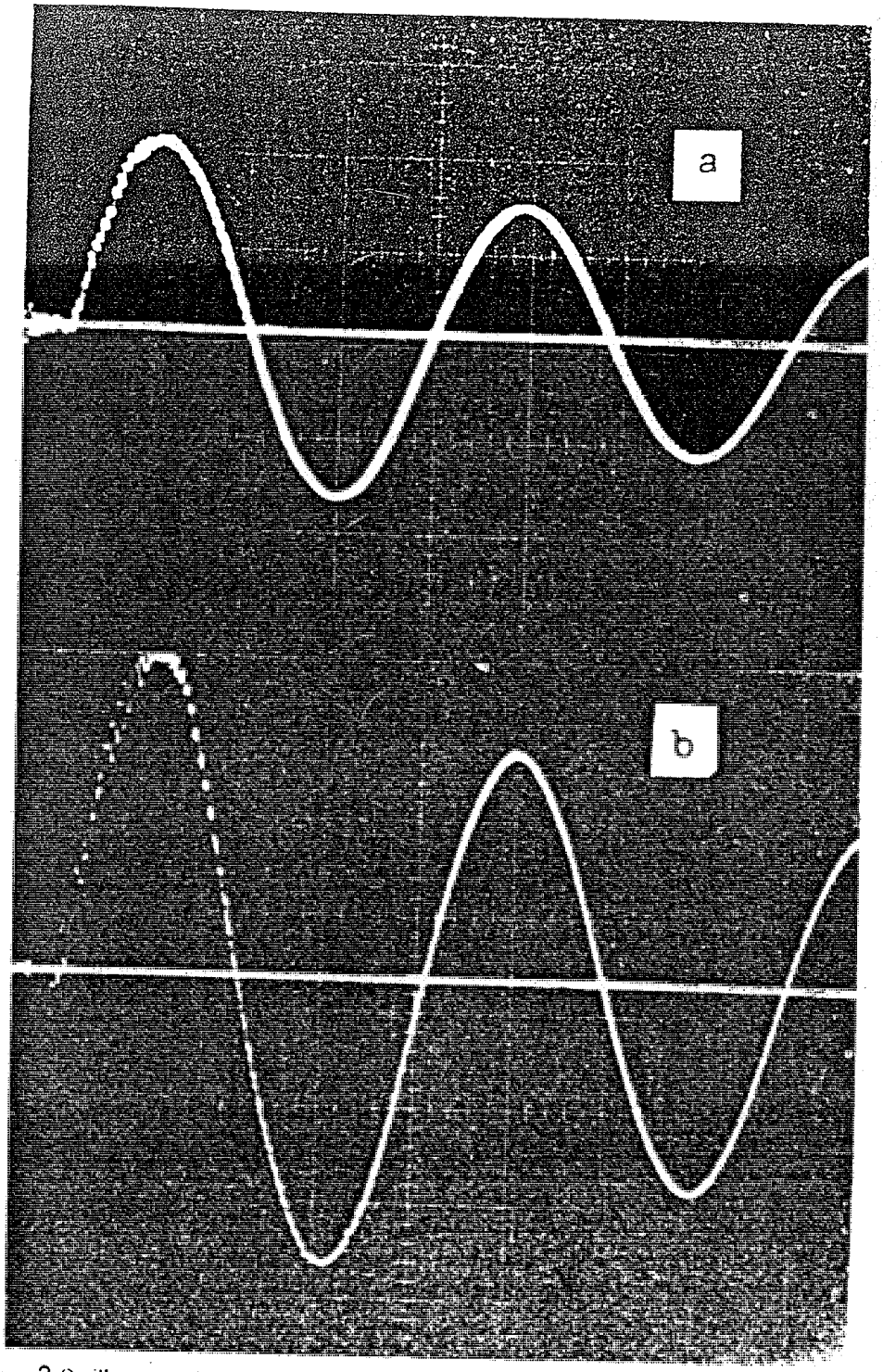

FIGURE 2. Oscillograms of current coil output during a capacitor spark discharge.
(a) spark-gap setting 0, V_c = 20.0 kV, time scale = 2 μs cm, current vertical scale = 475 kA cm, I = 940 kA, T = 7.6 μs, f = 0.84.
(b) spark-gap setting 7 mm, V_c = 30 kV, time scale = 2 μs cm, current scale = 435 kA cm, I = 1.43 MA, T = 7.6 μs, f = 0.84.

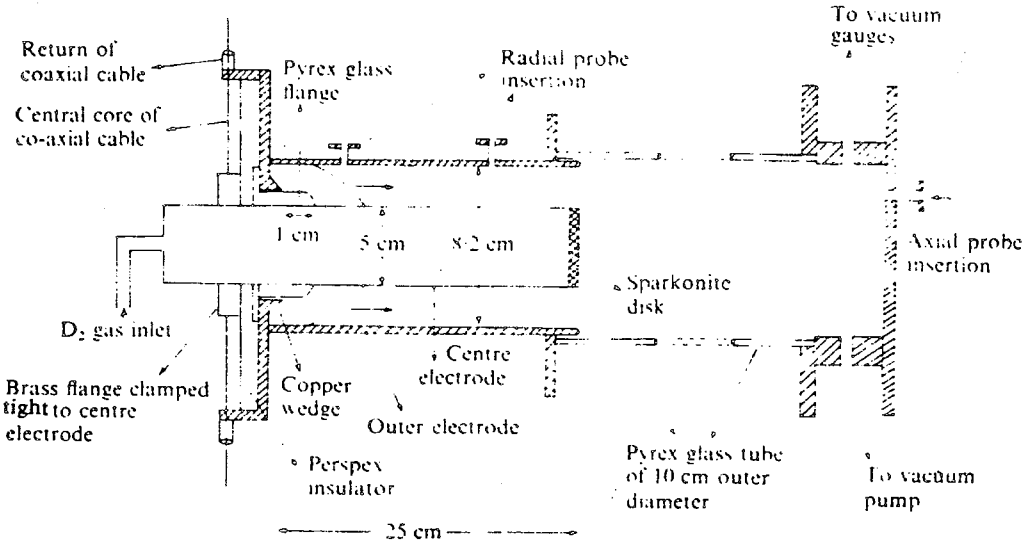

Figure 3: Schematic diagram of plasma focus device.

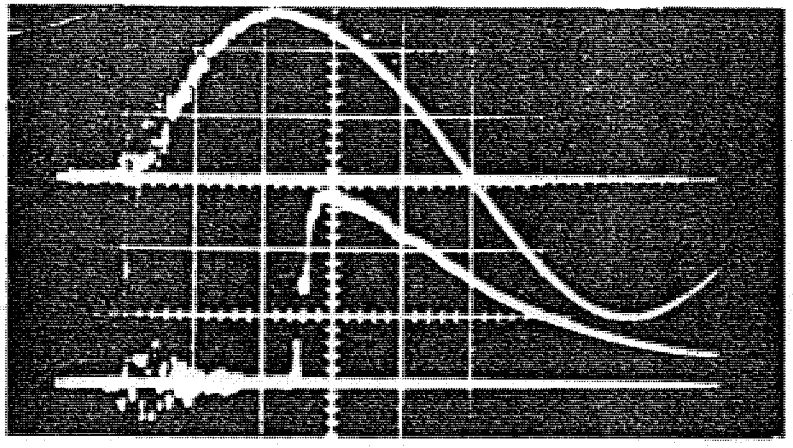

Figure 4: Oscillogram of a magnetic field signal, bottom trace.

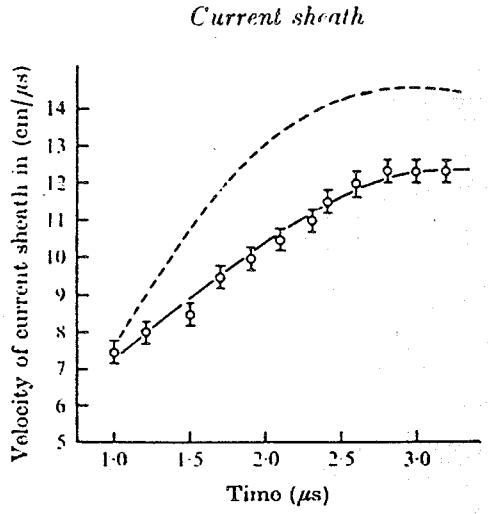

Figure 5: Velocity of current sheath as a function of time, deduced from magnetic probe measurements. ---- , a theoretical prediction based on snowplough model.

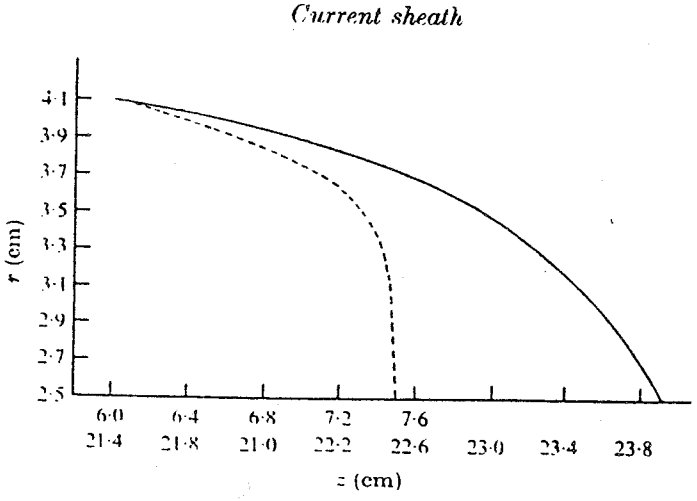

Figure 6: The current sheath profiles at (a) t = 1.12 μs (z varies from 21 cm to 23.8), (b) t = 2.66 μs (z varies from 6 cm to 7.5).

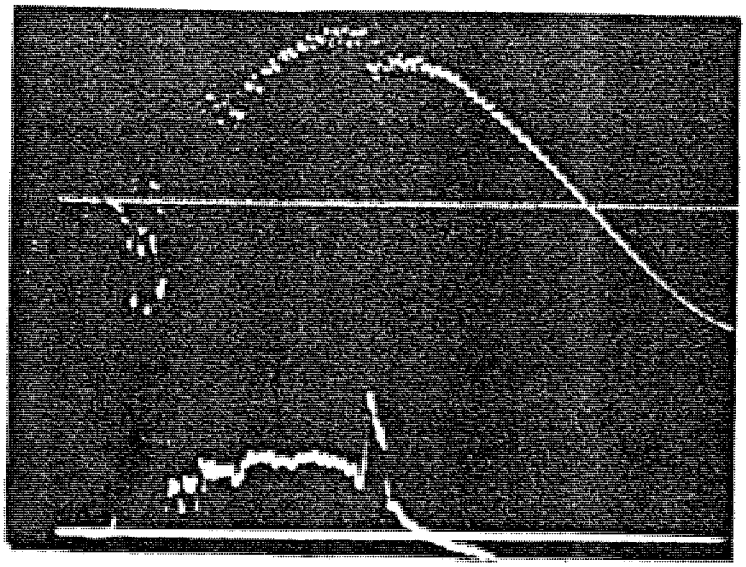

Figure 7: Typical current (upper) dip and voltage (lower) spike of a focusing shot.

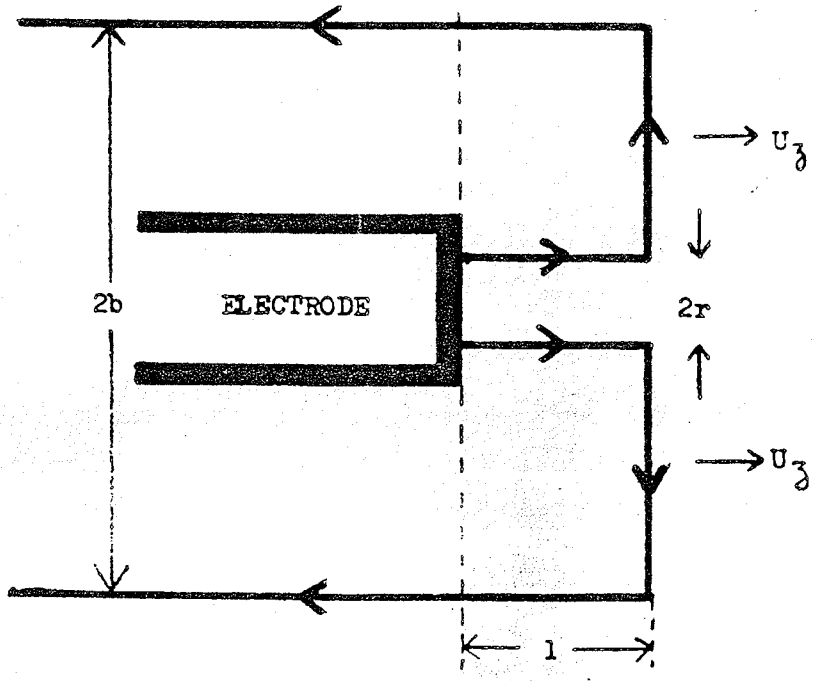

Figure 8: Focus radius from voltage and current curves.

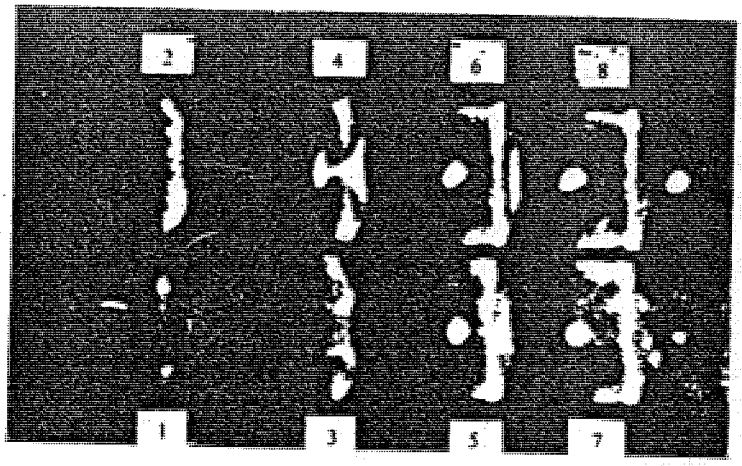

Figure 9: Image-converter photographs taken transverse to the discharge tube off the end of the electrodes, interval between frames is 0.1 us; exposure time 20 ns. Frame 1 shows the arrival of the current sheath.

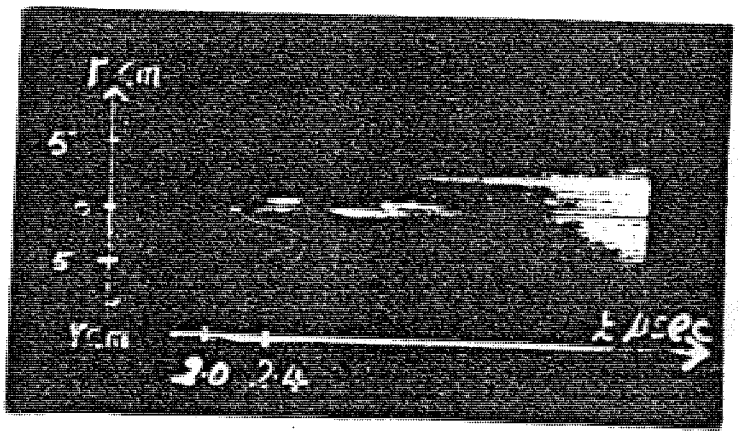

Figure 10: Streak photograph showing radial collapse viewed at Z = 23 cm.

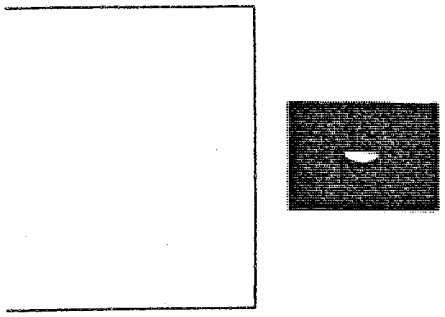

Figure 13: Soft x-ray photograph of the focused plasma. The photographic image was formed by the soft x-rays emitted from the super-hot plasma; the visible radiation being screened off by a sheet of berylium foil covering the pin-hole of the camera. The position of the focused plasma relative to the centre electrode is shown by the line drawing on the left.

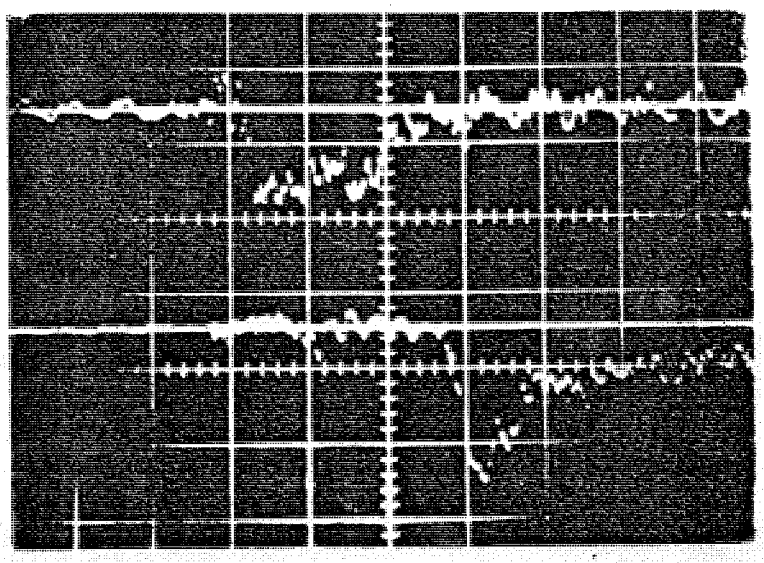

Figure 14: Time-of-flight oscillogram used for the measurement of neutron velocity. The horizontal axis is the time axis with a time sweep speed of 0.2 microsecond per large division. The top trace is the output signal of the near neutron detector and the bottom trace is the output signal of the far neutron detector. The separation between the two detectors is measured directly from the oscillogram and the velocity computed from the known flight length. The detectors had been calibrated so that the number of neutrons arriving at each detector is calculated from the area of the signal.

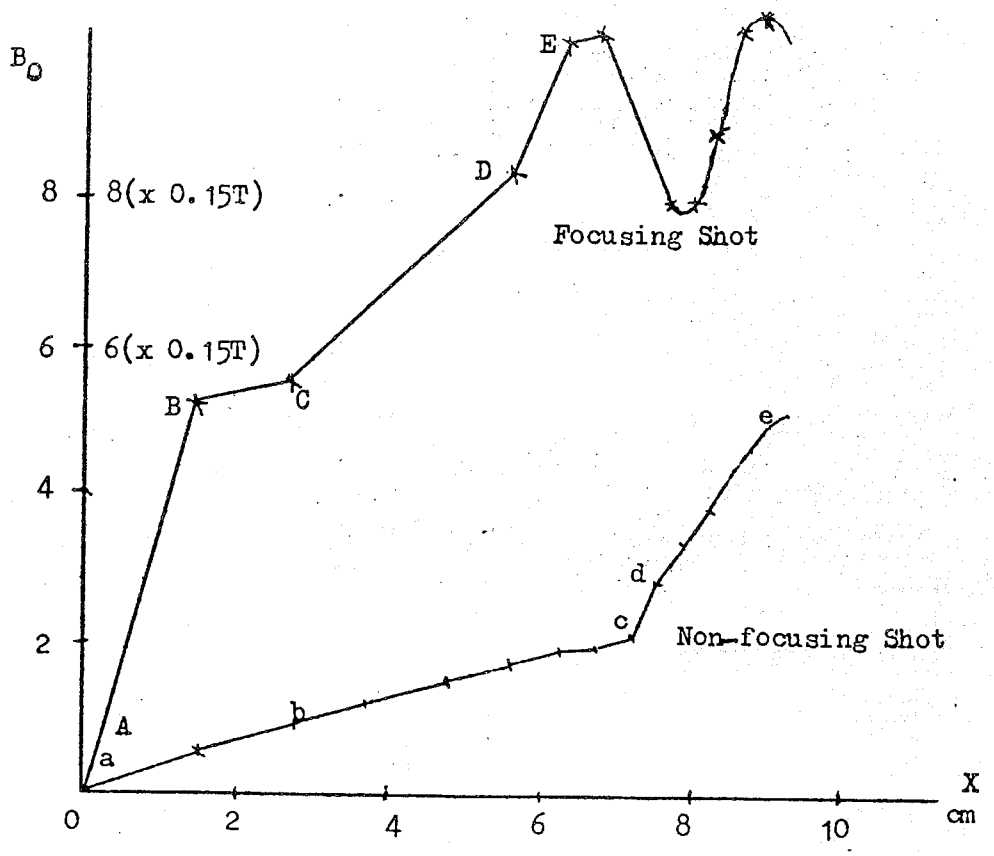

Figure 11. Comparative Profile of Magnetic Field.

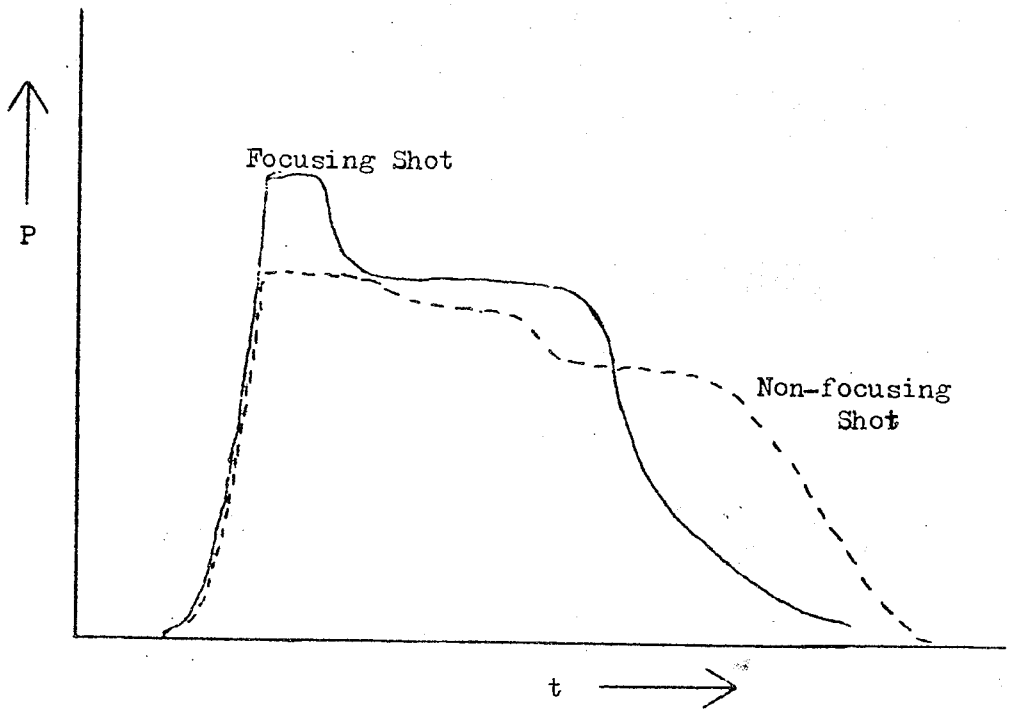

Figure 12. Comparision of pressure pulses for Focusing and Non-focusing shots.

References

1. Lee S., Chen Y.H., Chow S.P., Tan B.C., Teh H.H., Thong S.P.; Proc. Symp. Phys., Nan. U. Singapore (1971) 182.

2. Thong S.P., Lee S., Mal. J. Sci. 2 (1973) 157.

3. Lee S., Chen Y.H., Chow S.P., Tan B.C., Teh H.H., Thong S.P.; Int. J. Electronics 33 (1972) 85.

4. (a) Chew A.C., Lee S., Tan B.C. "Focus in an Axial Magnetic Field" Seminar on "Focus Work in K.L." Kuala Lumpur (1974). To be published.
   (b) Chew A.C., M.Sc. Thesis Universiti Malaya (1974).

5. (a) Chow S.P., Lee S., Tan B.C. J. Plasma Phys. 8, (1972) 21.
   (b) Chow S.P., M.Sc. Thesis Universiti Malaya (1972).

6. (a) Lee S., Tan T.H., "Focus Intensity - Dependence on Mass and Field Distributions" Procs. of seventh European Conference on Controlled Fusion and Plasma Physics, Lausanne (1975); Paper 65.

7. (a) Chen Y.H., Lee S., Int. J. Electronics 35, (1973) 341.
   (b) Chen Y.H., M.Sc. Thesis Universiti Malaya (1972).

8. Lee S., Chen Y.H., Mal. J. Sci. 3B (1975) 159-163.

9. Lee S., Chen Y.H., Procs. Twelfth Int. Conf. Phen. in Ionized Gases (1975) Paper 353.

10. Leong K.H., "Model for Plasma Focus with Axial Magnetic Field" Seminar on "Focus Work in K.L." Kuala Lumpur (1974).

11. Yong Y.C., "Ionization Effects in an Argon focus" Seminar on "Focus Work in K.L." Kuala Lumpur (1974).

12. Maisonier Ch. et al: Fifth Conference on Plasma Physics and Controlled Nuclear Fusion Research p. E6-2 (1974).

13. Lee S., Sandeman R.J., J. App. Phys. 43, 3980.

14. World Survey of Major Facilities in Controlled Fusion Research, IAEA (1973) pg. 109.

15. Lee S., "Transverse Ionizing Shock Wave" Mal. J. Sc. 3B (1975) 165-176.

16. Lee S., Thong S.P., Tan B.C., "High Current Discharge Module System" Plasma Phys. Lab. Rep. 2/71 (1971).

Procs. Sem. Plasma Focus Work in K.L. (K.L. Nov. 1974)

Edited 1976

PLASMA FOCUS IN AN AXIAL MAGNETIC FIELD

A.C. Chew, S. Lee & B.C. Tan

Abstract

Some effects of an external dc axial magnetic field on the plasma formed using a plasma focus gun are studied. On comparison with similar conditions without a magnetic field it was found that in the presence of a magnetic field:

(i) a faster initial breakdown of the deuterium gas (e.g. from 1.3 μs (without field) to 0.6 μs (with field) occurs,

(ii) the inductance increases at a higher rate (e.g. from 9.2 nH/μs to 12.4 nH/μs),

(iii) the plasma possesses induced rotational motion,

(iv) more energy (e.g. from 0.38 kJ to 0.50 kJ) is pumped into the plasma focus during the time of focus,

(v) the applied magnetic field is compressed at the time of focusing of the plasma,

and (vi) neutron emission is delayed by about 150 ns.

Introduction

The high energy plasma focus discharge produced in a hydro-magnetic coaxial plasma accelerator can broadly be divided into three stages, namely, the initial breakdown at the launching end, followed by the acceleration and propagation of the Current

Sheath in the annular region between the electrodes due to the self ($J_r \times B_\theta$) force, and finally the rapid collapse of the current sheath at the open end of the centre electrode. The final heating and compression of the plasma is accomplished by the partial conversion of the stored magnetic energy to plasma energy.

The present work attempts to observe and explain the effects of an externally applied dc axial magnetic field on the plasma in a coaxial plasma focus device, and to compare the differences between operation with and without an axial dc magnetic field.

Theory

When the initial breakdown takes place at the launching end of the plasma focus gun, the current starts flowing. A magnetic field then develops behind the current sheath. The coupling between the current and the magnetic field produces a $J_r \times B_\theta$ force which pushes the current sheath outward. The current sheath sweeps up all the gas particles it encounters and these particles move at the same speed as the current sheath. In the presence of an axial dc magnetic field, B_z, the accelerating plasma has an additional degree of motion (Spitzer 1962), that is, the azimuthal motion due to the coupling between J_r and B_z. The rate of change of momentum can be equated to the force exerted by the magnetic field to obtain

$$\rho q_1 \pi (b^2 - a^2) \underset{\sim}{V} = \int\int\int \underset{\sim}{J} \times \underset{\sim}{B}\, r\, dr\, d\theta\, dz \quad \ldots\ldots\ldots\ldots\ldots\ldots (1)$$

where $\underset{\sim}{V}$ is the plasma velocity, given by $\underset{\sim}{V} = V_r \underset{\sim}{r} + V_\theta \underset{\sim}{\theta} + V_z \underset{\sim}{z}$.

q_1 the flow velocity in shock co-ordinate (Lee 1969).

ρ the deuterium gas density, b the inner radius of the outer electrode

and (a) the outer radius of the inner electrode.

Writing Ampere's Law in cylindrical co-ordinates,

$$\underset{\sim}{J} = \frac{1}{\mu} \nabla \times \underset{\sim}{B} = \frac{1}{\mu r}\left[- \frac{\partial (rB_\theta)}{\partial z} \underset{\sim}{r} + \frac{\partial}{\partial r}(rB_\theta) \underset{\sim}{z} \right. \quad \ldots\ldots\ldots\ldots (2)$$

by assuming that B_z = constant and Br = 0
Hence,

$$\underset{\sim}{J} \times \underset{\sim}{B} = - \frac{B_\theta}{\mu r} \frac{\partial}{\partial r}(rB_\theta) \, t + \frac{1}{\mu r} B \frac{\partial (rB_\theta)}{\partial z} \underset{\sim}{\theta} - \frac{1}{\mu r} B_\theta \frac{\partial}{\partial z}(rB_\theta) \underset{\sim}{z} \ldots (3)$$

on substitution of equation (3) into equation (1), the following equations are obtained. In the z direction:

$$\rho q_1 \pi (b^2 - a^2) V_z = \frac{\mu I^2}{4\pi} \ell u \frac{b}{a} ,$$

Using $B_\theta = \frac{u I}{2 r}$, where I is the discharge current ..... (4)

In the θ direction:

$$\rho q_1 \pi (b^2 - a^2) V_\theta = - B_z I (b - a) \ldots\ldots\ldots\ldots\ldots\ldots (5)$$

In the $\underset{\sim}{r}$ direction:

$$\rho q_1 \pi (b^2 - a^2) V_r = 0 \quad \ldots\ldots\ldots\ldots\ldots\ldots\ldots\ldots (6)$$

Thus,

$$\left(\frac{V_\theta}{V_z}\right) = \frac{B_z (b - a)}{\frac{\mu I}{4\pi} \ell u \frac{b}{a}} \quad \ldots\ldots\ldots\ldots\ldots\ldots\ldots\ldots (7)$$

and V_θ can be calculated if values of V_z, B_z and I are known.

The value of B_z has no effect on the motion of the current sheath in the forward direction. This null effect is shown in equation (4).

During the radial collapsing stage, the axisymmetric current 'piston' sweeps up the dc axial magnetic field in front of the electrode end. The magnitude of the compressed magnetic field may be 10^3 times that before the compression as was found by Mather (1962). Since the total magnetic flux remains unchanged,

$$Bz_1 \, \pi r_1^2 = Bz_2 \, \pi r_2^2 \qquad \ldots\ldots\ldots\ldots\ldots\ldots\ldots\ldots\ldots\ldots \quad (12)$$

where subscripts 1 and 2 refer to quantities before and after the collapse. The increased axial magnetic field trapped by the current sheath provides some cushioning effect or magnetic insulation. Rosenbluth (1956) and Taylor (1957) showed that a B_z field minimized the m = 0 instabilities and prolonged the time of confinement of a plasma pinch column. On the other hand, Glasstone and Lovberg (1960) found from the pressure balance equation, that the final radius of a pinch column was larger than in the case when no axial dc magnetic field was applied.

Assuming the current is axially symmetric and flows radially from one electrode to the other as a thin plane disk which contains all the mass that it has swept up in moving outward from the launching end, the magnetic field behind the disk is given by

$$B = \frac{\mu I}{2\pi r} \qquad \ldots\ldots\ldots\ldots\ldots\ldots\ldots\ldots\ldots\ldots \quad (13)$$

and there is no magnetic field in front of the disk. For such a coaxial electrode symmetry, the constant inductance per unit length is

$$L_1 = \frac{\mu_o}{2\pi} \ell u \frac{b}{a} \qquad (H/m) \qquad \ldots\ldots\ldots\ldots\ldots\ldots\ldots\ldots\ldots\ldots \quad (14)$$

The dynamic behaviour of the plasma current sheath can be determined by using the measured time dependent values of the voltage V(t) across the electrodes and the tube current I(t).

The discharge tube inductance is given by

$$L_D(t) = \frac{\int_0^t V(t)\,dt}{I(t)} \qquad \ldots\ldots\ldots\ldots\ldots\ldots\ldots\ldots (15)$$

and $L_D(t)$ can thus be measured from the V(t) and I(t) oscillogram of the discharge. A comparison can be made with the theoretical value of

$$L_D = L_1 z \qquad \ldots\ldots\ldots\ldots\ldots\ldots\ldots\ldots (16)$$

where z is the distance that the current sheath has travelled.

Experimental set up

The main capacitor bank has four modules connected in parallel; each module consisting of twenty-five 40 kV, 0.6 μF capacitors. At 40 kV a peak current of 1.91 MA and periodic time of 7.6 μs has been measured (Thong and Lee 1973), when the system is discharged into a shorting plate.

The bias capacitor bank to provide the external axial magnetic field consists of forty-nine 400 V 1,900 μF electrolytic capacitors connected in parallel. The bank discharges into a single turn loop wound around the focus tube near the region of focus. At 400 V, it delivers a peak current of 100 kA, and induces a peak magnetic field of 0.27 T along the axis of the focus tube. The rise time of this magnetic field is 150 μs.

The electrodes of the coaxial plasma gun are made from copper. The inner electrode has an outer diameter of 5 cm while the perforated outer electrode has an inner diameter of 10 cm.

Throughout the investigation, deuterium is used as the operating gas. The operating static ambient pressure ranges from 0.2 torr to 0.6 torr.

Experimental results and analysis

Part A. Operation without an external dc axial magnetic field

Fig 1 shows a typical oscilloscope trace of the voltage across the discharge tube and the current flowing into it. The collapse of the plasma at the open end of the electrodes accompanied by a rapid compression of the plasma by its self azimuthal magnetic field, are manifested by an abrupt rise in voltage and fall in current. The voltage and current singularities are consistant indications of the plasma focus action.

The value of the tube inductance L_D was found by using equation (15). $L_D(t)$ was plotted against t (Fig 2). It was observed that the inductance increased gradually at a rate of 9.2 nH/μs from the time t = 0 (time of discharge breakdown) to t = 2.38 μs. However, between 2.38 μs and 2.80 μs, corresponding to the voltage and current singularities the inductance increased at a much greater rate of 36 nH/μs.

From equation (14) and (16), the rate of change of inductance is given by

$$\frac{dL}{dt} = \frac{\mu_o}{2\pi} \ln \frac{b}{a} \frac{dz}{dt} \qquad \text{..... (17)}$$

From (17), $\frac{dz}{dt}$, the velocity of the current sheath in the forward direction was found to be 6 cm/μs in the acceleration region.

From Fig (1) values of V(t) and I(t) were obtained and the product V(t) I(t) which is the total power input to the discharge tube was plotted against t as shown in Fig 3. From this figure, it could be seen that the power input to the discharge tube rose from zero to about 2,800 MW in 1.75 us and it increased further to 3,500 MW at the time of focus.

The unshaded area under the curve represents the energy pumped into the discharge tube if there was no focus action of the current sheath. The shaded area of 0.38 kJ represents the additional energy pumped into the tube during the formation of the dense plasma focus. The energy input $\int VI\,dt$ vs t was also plotted in Fig 3.

The production of neutrons during the radial collapsing phase of the focus was observed from the output of a scintillator-photomultiplier neutron-detection system. It was observed that the start of the neutron signal was about 50 ns after the start of the voltage spike. The rate of emission of neutrons was found to be of the order of 10^{12} neutrons s^{-1} and the neutron yield was found to be 10^5 to 10^6 neutrons per discharge. The half-maximum width of the neutron pulse was 0.3 us. From time of flight measurements, Lee and Chen (1974) found that the neutrons have an average energy of 2.2 ± 0.1 MeV when measured in the backward direction (-z). They concluded that the neutrons produced were from D-D reactions.

Part B. Operation with an external dc axial magnetic field, B_z.

Under identical operating conditions, that is, with the same gas density and capacitor voltage, it was found that the introduction of an axial dc magnetic field caused the discharge at the insulated end of the electrode to break down more promptly than in the case without an axial magnetic field. Fig 4a show that in the case when B_z was absent, the electrodes held the capacitor bank voltage for 1.3 μs before breakdown. However when B_z = 0.13 T, the discharge broke down almost instantaneously when the voltage across the electrodes reached the capacitor bank voltage after a rise time of 0.6 μs Fig 4b. This phenomenon of prompt breakdown was always observed even though the applied B_z may be as small as 0.02 T.

When the plasma collapsed off the end of the centre electrode, the magnetic field field was compressed, as predicted in equation (13). Fig 5 shows the B_z signal as a function of time.

The applied external magnetic field was 0.02 T. The magnetic probe was placed along the axis of the discharge tube (r = 0) and at 4 cm away from the end of the centre electrode. The compressed magnetic field had a peak value of 1.05 T. This indicated that B_z increased by a factor of 53 times. It follows that the rotational velocity of the plasma during the radial collapse increased by a factor of $(53)^{\frac{1}{2}}$.

The rotational velocity of the current sheath caused by the interaction of the radial current and the axial field acted as another energy sink. The rotation of the plasma caused an increase in the rate of change of magnetic flux. Thus the inductance of the system increased and more energy was stored inductively. With external dc axial magnetic field of 0.02 T, signals of voltage and current similar to that of Fig 1 were obtained. Using a similar analysis to that discussed in part A, it was found that the power input rose from zero at the start to about 3,200 MW after 1.5 μs and it increased further to 4,500 MW at 2.6 μs during the focusing action. The extra energy input pumped into the system during the focusing action was found to be 0.5 kJ. This energy came from the conversion of the magnetic energy stored inductively into plasma energy.

The tube inductance increased linearly at the rate of 12.4 nH/μs and reached 38 nH/μs at 2.38 μs when focus began. The higher value of rate of change of inductance when an axial magnetic field was applied did not mean that the current sheath moved at a higher velocity as would be expected from equation (17). The experimentally measured values of time of arrival of the current sheath at the end of the electrodes, corresponding to the start of the voltage and current singularities, were the same for both operations with and without axial magnetic field. This shows that the forward velocity was unaffected by B_z, and is in agreement with equation (4). The higher value of rate of change of inductance was due to the rotational motion induced B_z, as discussed earlier.

During the radial collapsing stage, part of the plasma energy was used to compress the trapped axial dc magnetic field. This led to a slower implosion velocity. It was found that the start of neutron emission was 200 ns after the start of voltage spike compared to 50 ns in the case where $B_z = 0$. Thus the application of an external dc axial magnetic field delayed neutron emission by 150 ns. The half-maximum width of the neutron pulse was 0.75 μs compared to that of 0.3 μs in part A where $B_z = 0$.

Over a number of shots, no good correlation was obtained between the yield of neutrons and the value of the external dc axial magnetic field including the case where no field was present.

Conclusions

It can be concluded that an external axial magnetic field has a number of effects on the coaxial plasma focus. It causes a prompt initial breakdown of the gas at the launching end of the focus tube. Though the external axial magnetic field has no effect on the forward axial velocity, it induces a rotational motion of the current sheath and this in turn causes an increase in the rate of change of inductance of the system. It is found from measurements that the axial magnetic field is compressed at the time of collapse. More energy is pumped into the system and neutrons are emitted during the focusing action. The presence of the magnetic field causes the neutron emission to be delayed by about 150 ns and to have a large half-maximum width of 0.75 μs. The correlation between the neutron yield and the value of axial magnetic field is uncertain in this investigation using a discharge energy of 6 kJ.

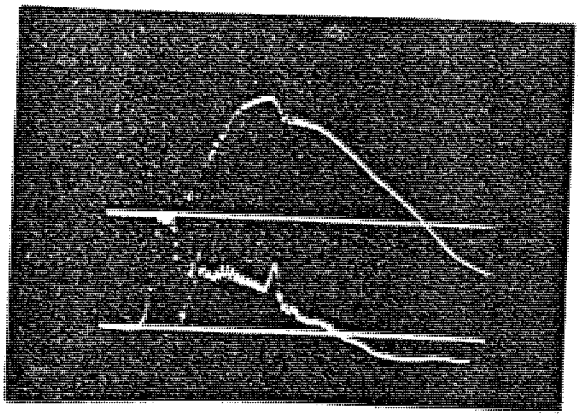

Figure 1: Current and voltage traces.
V_o = 15 kV, P = 0.4 mm Hg. of D_2.
Top: 1 μs/div. 140 kA/div.
Bottom: 1 μs/div. 5 kV/div.

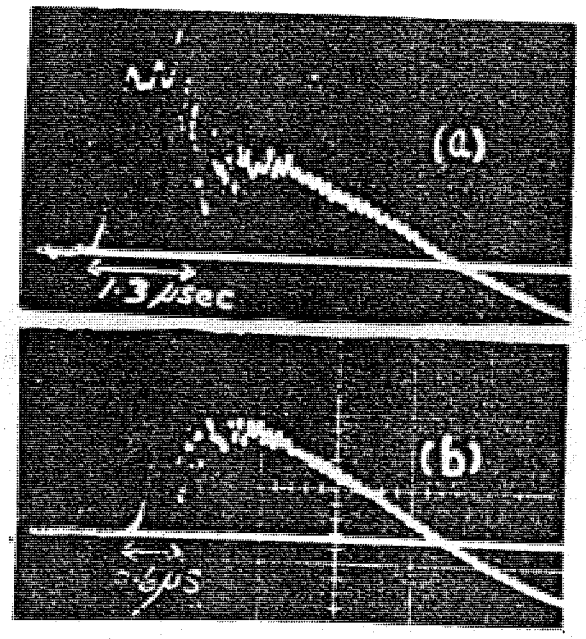

Figure 4: Effects of B_z on initial breakdown.

(a) & (b): V_o = 12 kV.
P = 0.3 mm Hg. of D_2.;

horizontal: 1 μs/div.,
vertical : 5 kV/div.

(a) B_z = 0,

(b) B_z = 1,320 G.

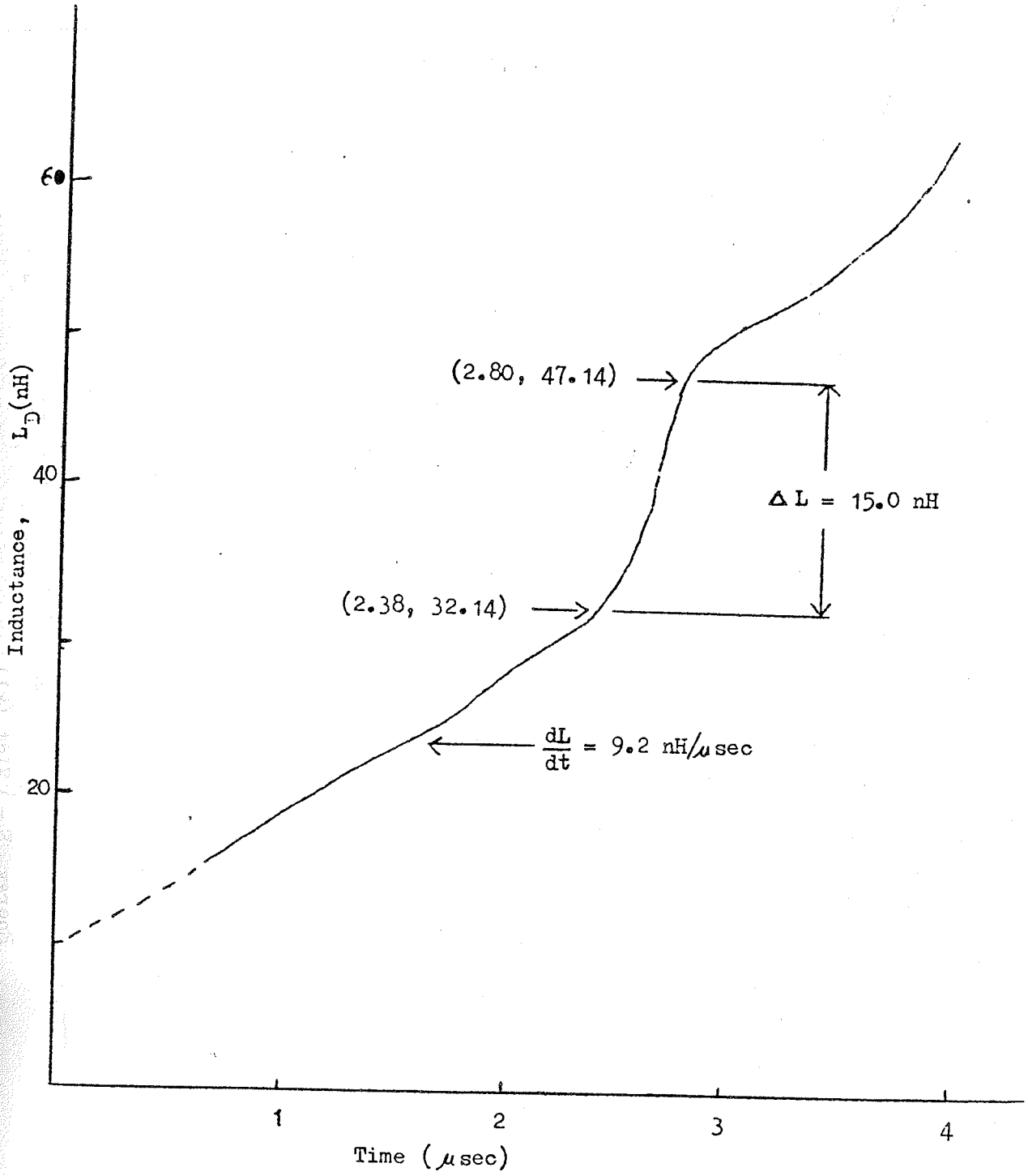

Figure 2. Variation of inductance as a function of time.

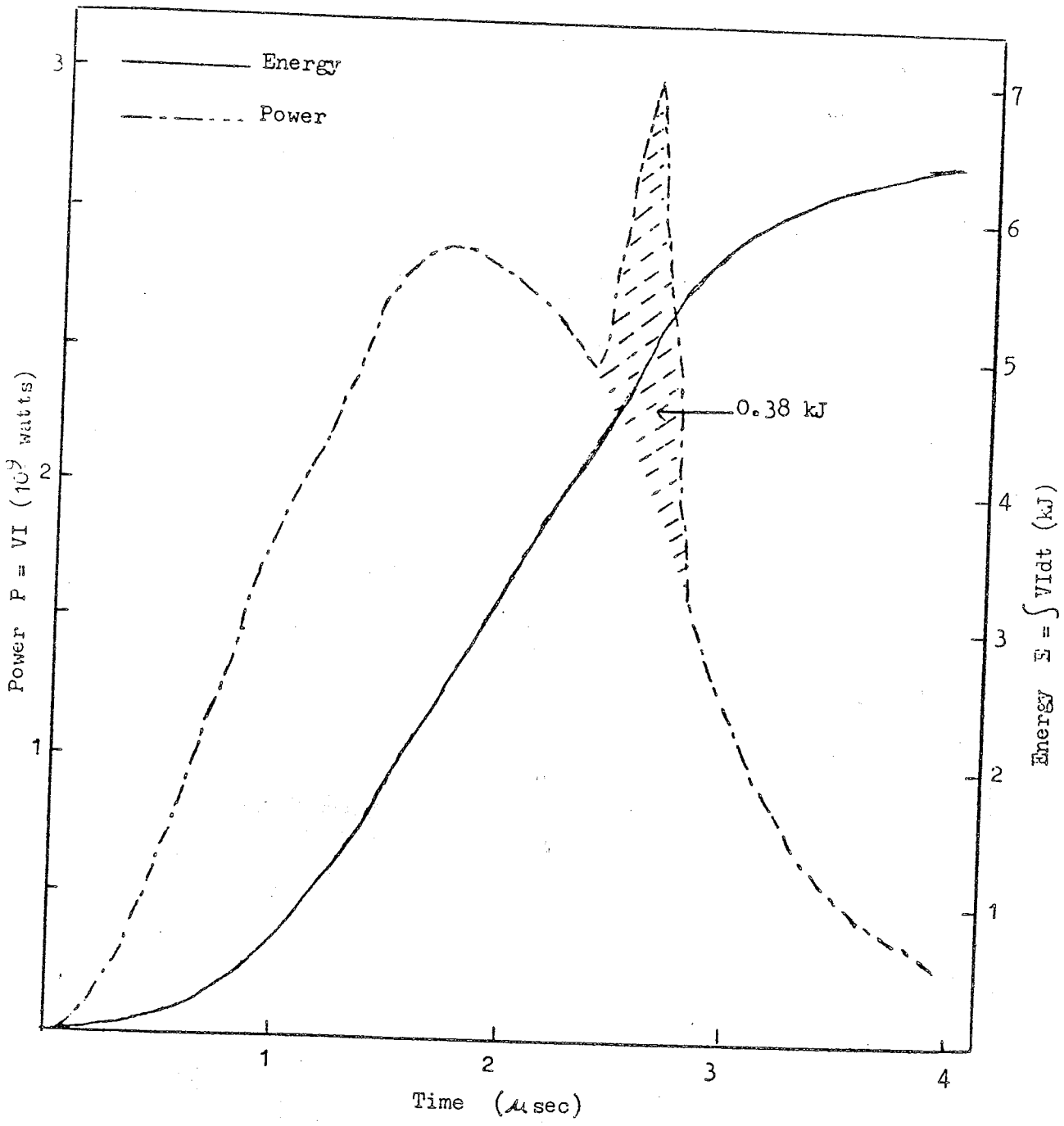

Figure 3. Power & Energy vs Time.

References

1. Chen Y.H. and Lee S. (1973) Int. J. Electronics Vol. 35 No. 3, 341-352.

2. Glasstone S. and Lovberg R.H. (1960) Controlled thermonuclear reaction. p.238 D. van Nostrand Company Inc.

3. Lee S. (1969) Ph. D. Thesis. Australian National University.

4. Lee S. and Chen Y.H. Malaysian J. Sci. Vol. 3B (1975), 159-163.

5. Mather J.W. (1969) Method of Experimental physics Vol. 9 Part B Chapter 15. Academic press N.Y.

6. Rosenbluth M. (1956) USAEC Report. LA - 2030.

7. Spitzer L. Jr. (1962) Physics of Fully Ionized Gases (Interscience, N.Y.).

8. Taylor F.J. (1957) Proc. Phys. Soc. (London) B70, 31, 1049.

9. Thong S.P. and Lee S. (1973) Malaysian J. Sc. 2(B) 157.

PLASMA FUSION RESEARCH AT THE UNIVERSITY OF MALAYA

S. LEE
Jabatan Fizik, Universiti Malaya

The existing 50 kJ plasma focus is briefly discussed and a summary of some important results are given. Current local trends are outlined. A 35 kJ 'laser initiated fusion spark' facility is at present being installed here. The proposed experiment, generating a Lithium-Deuterium plasma with $N_e \sim 10^{21}$/cc and $T_i \sim 10^8$ °K, is briefly described. With the two facilities operational, the plasma physics group will define for itself an area of research within the existing international program for controlled fusion energy research.

PLASMA FOCUS FACILITY

The plasma focus facility in the plasma laboratory is powered by a 50 kJ capacitor bank[1] with a short-circuit current of 1.91×10^6 A and a quarter-cycle power of 2.64×10^{10} W. This capacitor bank is switched into the plasma focus tube shown schematically in Fig. 1. On switching, the current sheet first forms at the insulating flange and is then accelerated down the coaxial region sweeping along and heating up all the gas particles encountered. At the end of this region, the tube geometry constrains the plasma to undergo an expansion during which the flow direction changes from axial to predominantly radial.

Important results

We have determined that when the current sheet structure is of a suitable type[2,11] the magnetic energy associated with the large electric current is strongly coupled into the plasma resulting in intense plasma heating. During this compression phase the plasma is hot and dense enough to generate copious quantities of Bremsstrahlung so that a soft x-ray image of the focused plasma may readily be obtained[3] as shown in Fig. 2. From a series of such soft x-ray photographs using x-ray absorbers made from different thicknesses of berylium and aluminium foils the temperature of our plasma was determined to be between 0.8 to 2.5 keV. When deuterium is used as the test gas a burst of 10^8 to 10^9 neutrons is typically observed with a discharge energy of 12 kJ. Fig. 3 shows the neutron yield of our focus compared to focus devices of other laboratories. A 1973 time-of-flight measurement[4] indicated that the average neutron energy from our focus is 2.2 ± 0.1 MeV in the backward direction (see Fig. 4). These neutrons are certainly from the D–D fusion reaction, although the measurements show that the centre-of-mass of the reaction is not stationary in the laboratory frame of reference.

After this initial research phase[5] much of the effort of our Group for the last two years have been to:

1. make simultaneous measurements with neutron detectors and current and voltage oscillograms to interpret plasma dynamics and focus mechanism;
2. perform computer simulation to calculate plasma trajectory and configuration and to compare these with experimentally observed plasma trajectory[5,6];
3. study the effect on the focus of multiple ionization, up to Argon XVIII[7] and of plasma rotation[8];
4. consider the improvement of focusing reproducibility, as judged from neutron yield, by formulating appropriate operational regimes; to consider machine optimization and energy scaling laws[9];

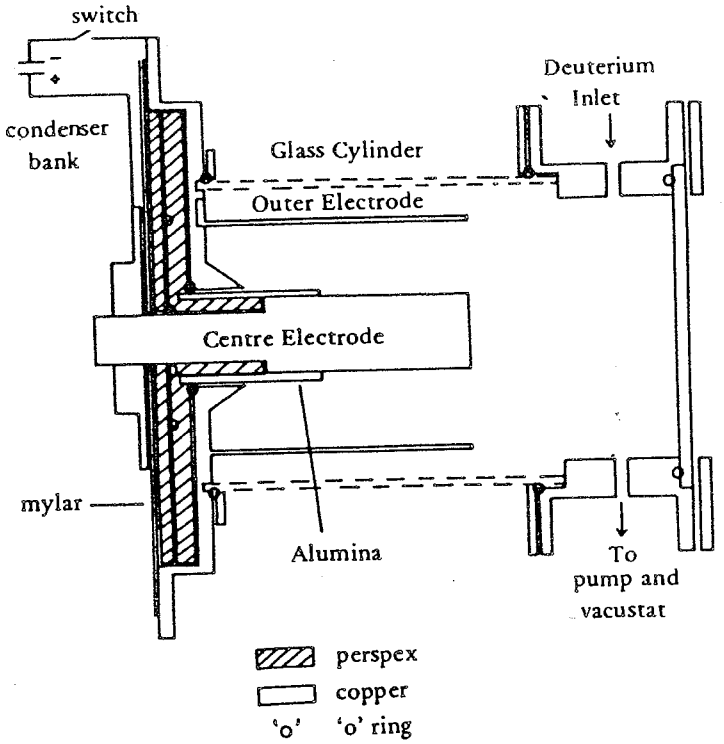

Fig. 1. Schematic diagram of the plasma focus tube.

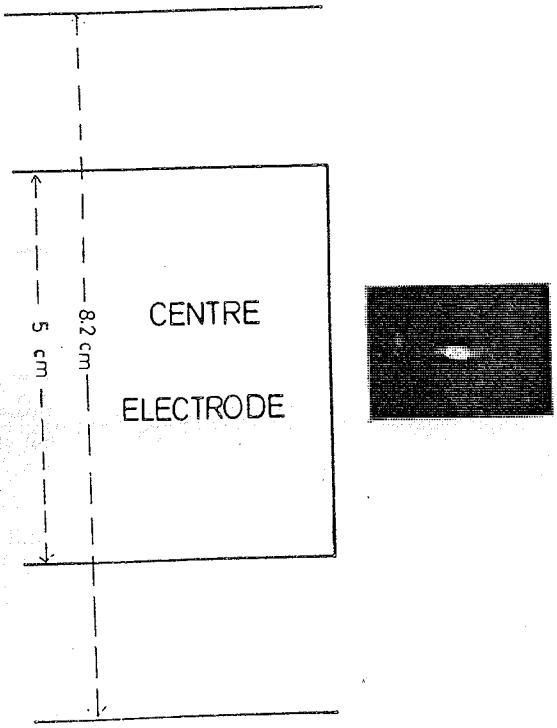

Fig. 2. Soft x-ray photograph in transverse view. The surface of the centre electrode is beyond the left side of the photograph as shown to scale. Voltage, 29.6 kV. Pressure: 1.3 torr. Condenser bank energy 13 kJ.

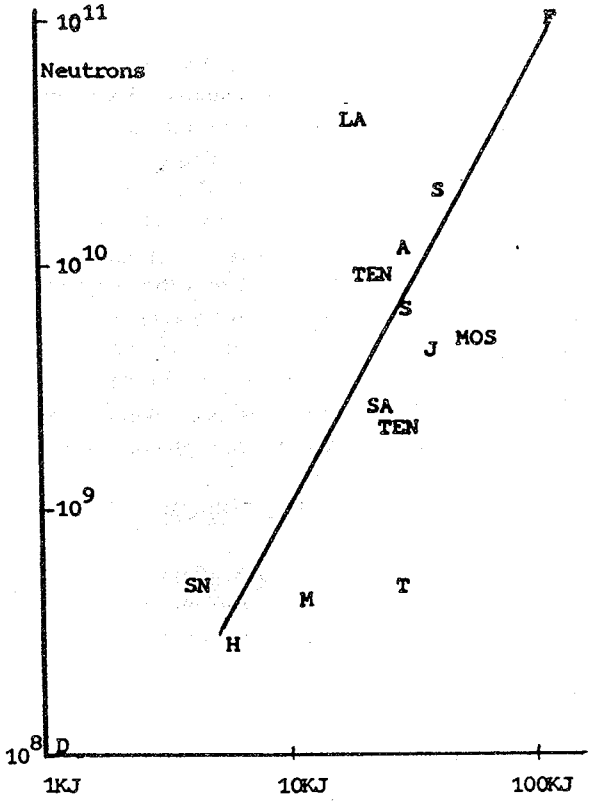

F=Frascati; LA=Los Alamos; S=Stuggart;
A=El Sequnda Aerospace; TEN=Tennessee;
MOS=Moscow; J=Julich; SA=Sandia;
SN=Steven; T=Texas; M=Malaysia;
H=Hoboken; D=Darmstadt.

Fig. 3. Neutron production as a function of energy.

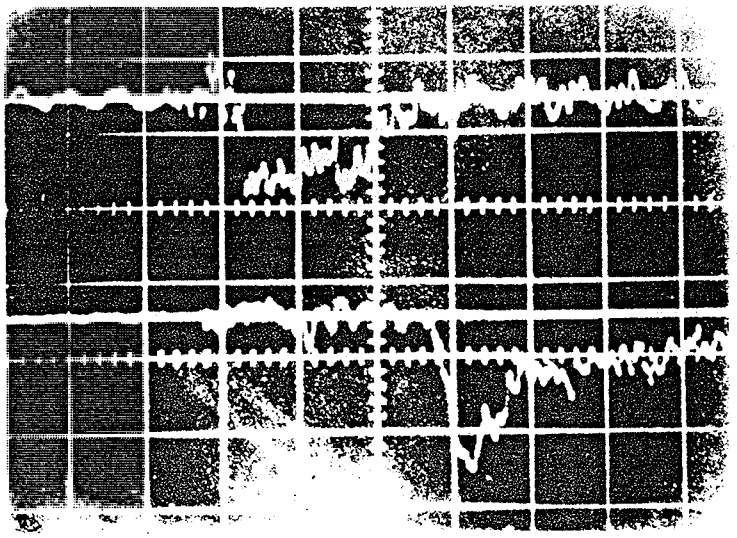

Fig. 4. Time-of-flight oscillogram obtained in the measurement of neutron energy. Top trace records output from near detector. Bottom trace records output from far detector placed 10.2 m behind near detector. Horizontal scale 200 ns per cm.

Fig. 5 shows typical current and voltage oscillograms used to calculate the imploding trajectory of the plasma current-sheet and Fig. 6 shows a comparison of this experimentally deduced trajectory with a trajectory computed using a radially imploding current-sheet (CS) shock-wave (SW) model. The agreement between theoretical and experimental trajectories indicate that the CS–SW model that we use is adequate down to approximately r = 6 mm. Beyond that point the disagreement shows that the infinite conductivity assumption implicit in the CS–SW model breaks down. This is not surprising when we look at the physics of the compression. Although the plasma temperature is rising rapidly and with it the electrical conductivity, the magnetic field is also rising. We note that the Hall parameter which is proportional to $T^{3/2}$ and the magnetic field and inversely proportional to the number density, rapidly rises in this situation. For example at r = 1 mm the electron Hall parameter is already 500 so that the relevant conductivity for our current flow has been reduced, because of the Hall effect, by a factor of 500^2. This means the breakdown of our infinite conductivity convective model. The magnetic field instead of convecting with the plasma now diffuses through it and the current flow becomes on-axis as indicated by the experimental trajectory. We are currently looking at techniques for including this effect into our calculations.

THE INTERNATIONAL FUSION PROGRAM

Let us now digress a little to do a general survey of plasma physics and fusion research. In the past few years the developed nations have been pursuing with increasing vigour research programmes to tap new energy sources. In the area of fusion research, the last three years have brought renewed optimism primarily because of two developments. Firstly the value of nt, the product of particle density and energy confinement time,[10] has been experimentally pushed up to 10^{12} particle-sec cm^{-3} in the French TFR machine. Moreover there are good indications that enough is now known to scale machine parameters to reach the 10^{14} required by the Lawson Criterion. The second development is the advent of laser fusion experiments, and the tremendous excitment these experiments are currently generating. Stimulated largely by these two factors in a world scenario depressed by the vision of depleted energy resources, the European Economic Community, Japan, the USA and the USSR are now spearheading an International Program to build a fusion reactor. This program is depicted in Fig. 7.

It is seen that in this international program the emphasis is on the Tokamak program, which at this stage appears a likely contender to be the world's first prototype fusion reactor. Among the other plasma devices, equally intensive, though less expensive and extensive research work is also being planned and carried out. For example there is an agreement on plasma focus work among West Germany (Juelich), Italy (Frascati) and England (Culham) with the cooperation of several other countries and laboratories in the EEC and EURATOM.

LASER-INITIATED FUSION SPARK FACILITY

Our laboratory has been fortunate to develop in 1975 a link with the Institute fuer Plasmaphysik of the Nuclear Research Establishment (KFA) Juelich, West Germany and to acquire recently the Juelich DPFI facility which has been donated to our Physics Department as part of a Post-Fellowship program of the Alexander von Humboldt Foundation. This facility is listed in the IAEA 'World Survey of Major Facilities in Controlled Fusion Research'[16] It is a 60 kV, 35 kJ machine originally operated as a fast plasma focus but converted in its last year at the Institute of Reactor Development KFA Juelich, see Fig. 8, as a vacuum spark.

In this device, Fig. 9, a capacitor C ~ 20 uF is connected across an anode and a cathode placed 1 cm apart in a vacuum, from 10^{-4} to 10^{-5} torr, sufficient for a voltage of 10–20 kV to be held across the electrode system. To start the discharge a sliding spark is initiated over an insulating surface between the cathode and an auxiliary trigger electrode. Electrons released in this surface discharge are accelerated towards the anode, and on striking it, causes anode material to be thrown out into the inter-electrode space producing a plasma which then carries the main discharge current. Experimental evidence[13] indicates an extremely

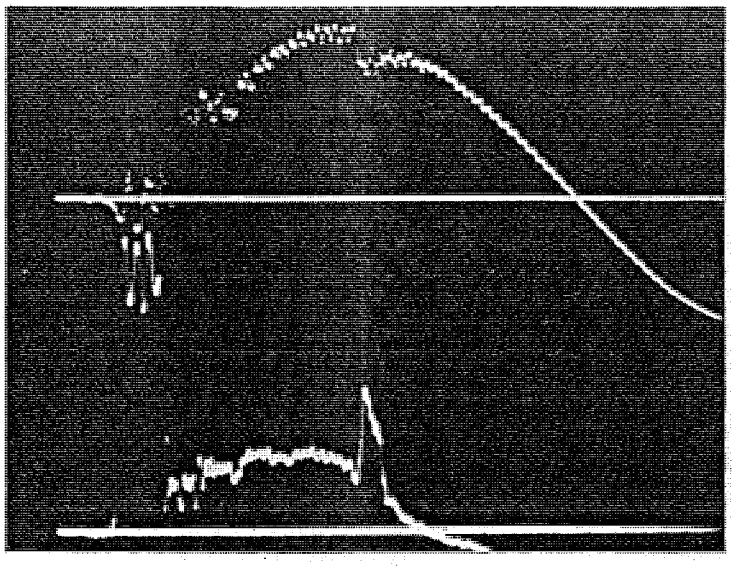

Fig. 5. *Typical current dip and voltage spike of a focusing shot. Top trace: current oscillogram: vertical scale: 200 kA per cm. Bottom trace: voltage oscillogram: vertical scale: 6 kV per cm, horizontal scale: 1 μsec per cm. The characteristic current dip and voltage spike of a good focus are evident at t = 4 μsec.*

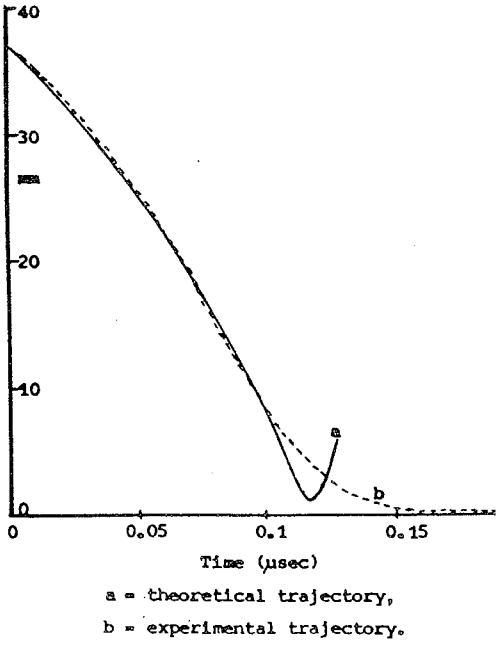

Fig. 6. *Comparison of theoretical and experimental trajectories.*

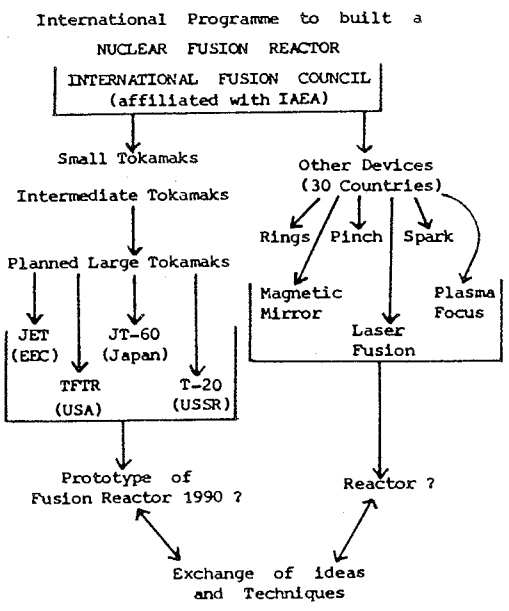

Fig. 7. *International Fusion Research Programme.*

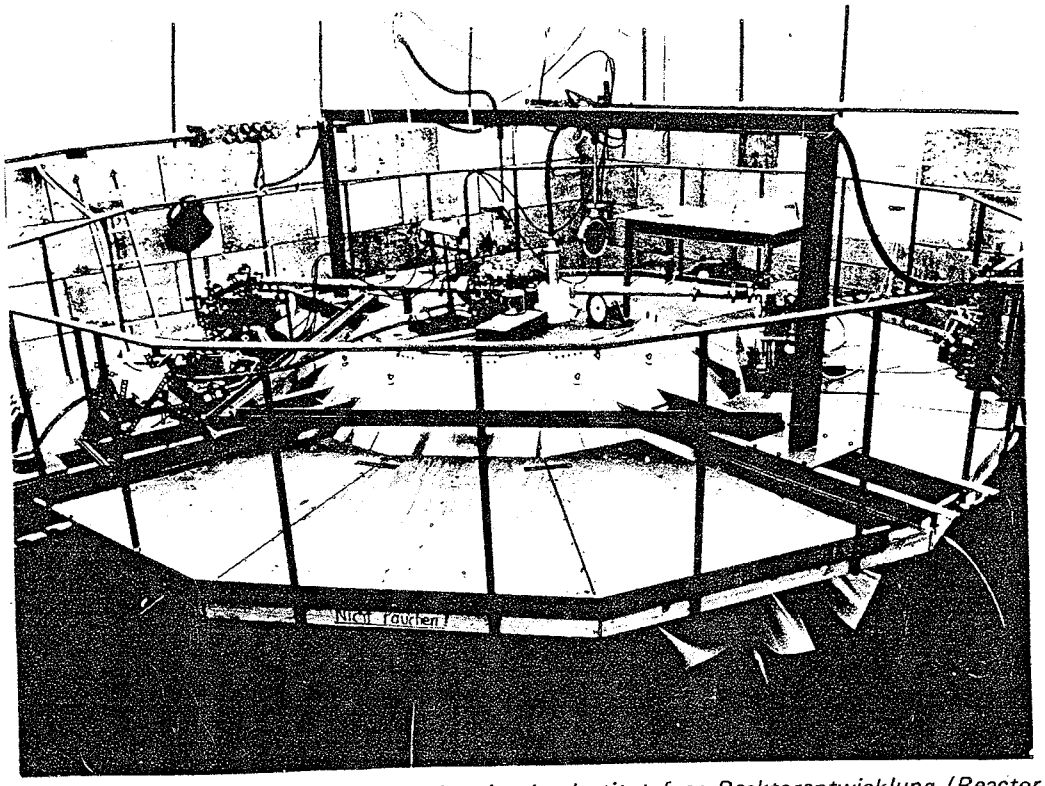

Fig. 8. *DPF I in its former location in the Institut fuer Reaktorentwicklung (Reactor Development), Nuclear Research Establishment, KFA Juelich, West Germany. This machine is now installed in the Plasma Physics Laboratory at the Universiti Malaya.*

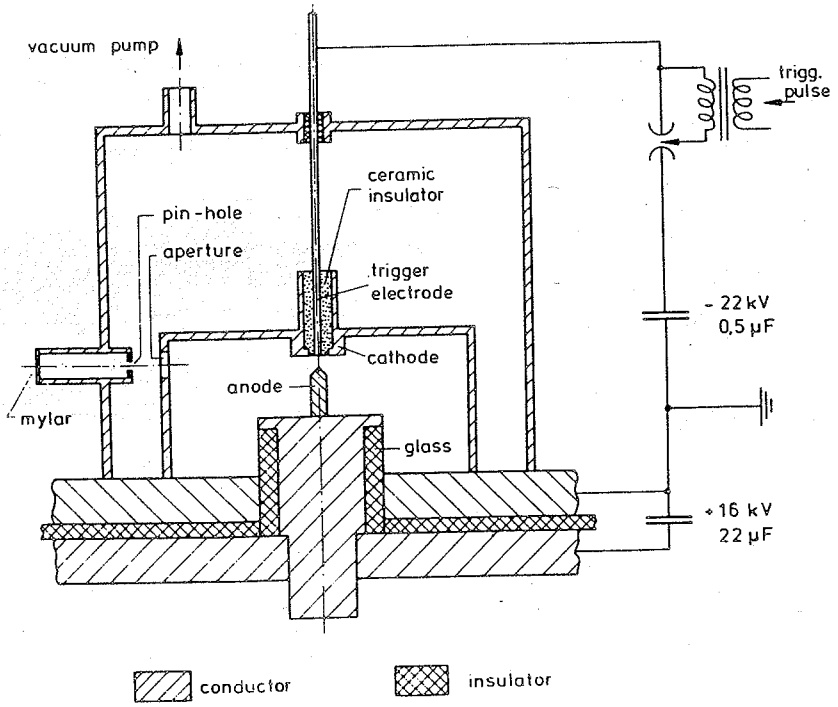

Fig. 9. *Schematic of experimental set up for vacuum spark.*

intense compression phase during which a thermal plasma of $T_e \sim 8$ keV, $T_i \sim 20$ keV and $N_e \sim 10^{21}$ cm^{-3} is produced consisting of highly ionized anode material and occupying a volume of 10^{-8} cm^{-3}. Apart from laser compressed plasma, this device generates the densest and hottest plasmas of all the existing laboratory devices, denser than the focus by 2 orders of magnitude and hotter by an order of magnitude. Fig. 10 shows the intense compression phase as indicated by the large dip in the electric current correlated to a simultaneous hard x-ray pulse. Fig. 11 shows a soft x-ray image of the vacuum spark plasma.

In the winter of 1975, Lee and Conrads[12] inserted Lithium-Deuteride into the anode of the Juelich vacuum spark and, for the first time, a burst of neutrons was observed from such a device. The yield however was low and erratic due primarily to two factors: a. limited energy due to backwall insulator structure and b. the method of triggering. Here in Kuala Lumpur we intend to improve on the insulation structure and use a 100 Megawatt ruby laser to trigger the fusion spark. This laser has also been donated by the Alexander von Humboldt Foundation. The associated problems of laser-target interaction, vacuum spark formation, plasma and laser diagnostics will form the basis of some interesting physics research work.

SUMMARY

The past years especially the last six have been very rewarding ones for the Plasma Physics Group. In the technological area our efforts have enabled us to establish the plasma focus nuclear fusion research facility with comprehensive diagnostics and instrumentation including x-ray and nuclear radiation and piezoelectric instrumentation, methods involving magnetic fields, high voltage and currents, pulse techniques and computational techniques, electronics, high speed photography, MHD methods and shock wave measurements and calculations[14,15]. In the academic area, our research has enabled the successful completion of six M.Sc. theses and the publication of many papers. Two Ph.D. and three M.Sc. theses are currently in preparation.

The establishment in the last two years, within the Plasma Physics Group, of a greater awareness of the international fusion research program has made us lean more in the direction of fusion energy research. However, being a University research group, with all the inherent ideals and limitations of such a group, we require that each research project undertaken in the Plasma Physics Laboratory, besides fulfilling the national need for technology development, should also be of a good academic standard.

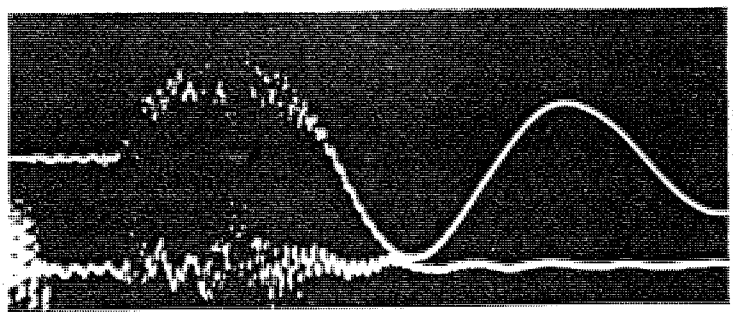

Fig. 10. Oscilloscope traces of current and hard x-rays. Time sweep: 1 μs/cm. Top trace current wave form showing severe current dips beginning 1.4 μs after the start of current. Bottom trace: hard x-ray pulse detected through 1 mm lead. Note multiple pulse characteristics.

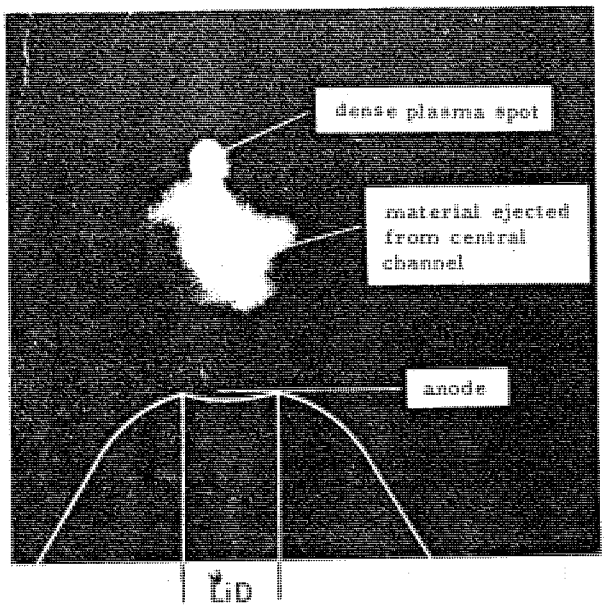

Fig. 11. Soft X-ray pinhole photograph taken with a photographic sensitivity of 1–2.5 Å. The anode, in this case, has a central channel filled with LiD. The circular spot at the top of the intense image has a diameter corresponding to the pinhole size of 0.4 mm.

REFERENCES

1. S.P. THONG, S. LEE, "A Simplified Method of Switching a 2 mega-ampere Capacitor Bank" Mal. J. Science *2(B)*, 157–169 (1973).
2. S. LEE, T.H. TAN, "Dependence of focus intensity on mass and field distribution" Procs. of Seventh European Conf. on Controlled Fusion and Plasma Physics, Lausanne, Switzerland; *I*, Paper 65. (1975).
3. Y.H. CHEN, S. LEE, "Coaxial Plasma focus gun in mode I operation", International J. Electronics *35*, 341–352 (1973).
4. S. LEE, Y.H. CHEN, "Measurement of neutrons from a focussed plasma", Mal. J. Science *3(B)*, 159–163 (1975).
5. Procs. of Seminar on Plasma Focus Work in K.L. – Edited by S. LEE (1976).
6. S. LEE, Y.H. CHEN, "The plasma focus-a radial trajectory computation", Procs. of Twelfth International Conf. on Phenomena in Ionized Gases, Eindhoven, Netherland; *I*, paper 353 (1975)
7. Y.C. YONG, S. Lee, "Multiple Ionization in an argon plasma focus" – Paper in this Symposium.
8. A.C. CHEW, S. LEE, B.C. TAN, "Plasma focus in an axial magnetic field", Ref. 5, 53–65 (1976).
9. C.S. WONG, S.P. MOO, S. LEE, "Neutron detectors for verification of focus energy scaling" – Paper in this Symposium.
10. S. LEE "The focus and CTR", Ref. 5, 1–13 (1976).
11. S.P. CHOW, S. LEE, B.C. TAN, "Current Sheath studies in a coaxial plasma ofcus gun", J. Plasma Phys. *8*, 21–31 (1972).
12. S. LEE, H. CONRADS, "Measurement of neutrons and x-rays from a vacuum spark" Phys. Lett. *57A*, 233–236 (1976).
13. S. LEE, "The Juelich DPF I as a neutron emitting vacuum focus" Association EURATOM–KFA Report; to be published.
14. S. LEE, "Transverse ionizing shock wave", Mal. J. Science *3(B)*, 165–176 (1975).
15. S. LEE, R.J. SANDEMAN "Bow shock effects on prpbe measurements" J. Applied Phys. *43*, 3980–3983, (1972).
16. "World Survey of Major Facilities in Controlled Fusion Research" a Special Supplement of J. Plasma Phys. and Thermonuclear Fusion, IAEA, page 106 (1973).

MULTIPLE IONIZATION IN AN ARGON PLASMA FOCUS

Y.C. YONG
Kajian Kejuruteraan,
Institiut Teknologi MARA

S. LEE
Jabatan Fizik,
Universiti Malaya, Kuala Lumpur

A model based on Local Thermodynamic Equilibrium is justified and adopted for the Argon plasma focus. A set of Saha equations is then coupled with equations of state and Shock-jump equations to relate inoization fractions to Argon shock temperatures. An equation of motion for the current sheet is then derived based on a 1-dimensional radial compression model. The chemical composition of the Argon plasma is allowed to affect the motion through a kinetic pressure term. This equation of motion is numerically integrated and the current sheet trajectory obtained. The ionization fractions are estimated and show that fully ionized Argon (Ar XVIII) can be expected in the Argon focus.

INTRODUCTION

A corona model is usually applied to a plasma of sufficiently low density. In the case of a high density plasma, a model based on Local Thermodynamic Equilibrium (LTE) is employed. Taking into the considerations of the criteria[1] for the applicability of the two models, the LTE model is applied to argon gas in the focus.

With the assumption of LTE model the equilibrium ionization of the gas at different temperature and pressure is defined by a set of Saha equations.[2] The degrees of ionization are obtained by solving the Saha equations.

A 1-dimensional radial compression model[3] is taken as the focussing mechanism for the argon plasma. The radial collapse is divided into stages of shock heating, shock reflection and adiabatic magnetic compression. From the equation of motion, the current sheet trajectory can be computed and the degrees of multiple ionization achieved in the focus can be estimated.

THE APPLICABILITY OF LTE MODEL TO AN ARGON GAS PLASMA

The LTE model assumes that the distribution of population densities of the electrons is determined exclusively by particle collision processes and each process is accompanied by its inverse. The rate at which these transitions take place may be expressed as:

$$n(p)\, A(p, q) = n_e\, n(p)\, X(T, p, q)$$

where $n(p)$ = population density of level designated by quantum number p,
n_e = the total density of free electrons,
$A(p, q)$ = the atomic transition probability,
and $X(T, p, q)$ = the de-excitation coefficient.

A criterion is taken that the collisional rates must be at least ten times the radiative rates. With this consideration a lower limit[1] for the electron density is given by:

$$n_e \geqslant 7 \times 10^{18} \left(\frac{z^7}{p^{17/2}}\right)\left(\frac{kT}{z^2 E_H}\right)^{1/2} \text{ cm}^{-3}$$

with

$$\left(\frac{\Delta E}{z^2 E_H}\right) \approx \frac{2}{p^3}$$

where z = ionization stage,
E_H = ionization energy of Hydrogen Atom,
and ΔE = lowering of ionization energy.

Wilson[4] and Griem[5] pointed out that LTE model should not apply to a plasma of sufficiently low density. This mainly refers to the laboratory shock tube plasma and T-tube plasma. For such low densities[1], a steady-state corona model is proposed. In this model the balance is between the collisional ionization and radiative recombination. A criterion[1] is expressed as:

$$\sum_{s<p}^{g} A(p, s) \geqslant n_e X(T, p, q)$$

There is always some value of p for which the criterion is not satisfied no matter how low the density. This happens because with increasing quantum number the probability of spontaneous decay decreases, whereas that of collisional excitation increases.

To decide between the two models we have claculated a set of LTE limits (see table I) of the electron density at various stage of ionization and temperature for argon plasma at an ambient pressure of 0 1 torr. The electron density of argon plasma at this pressure is of the value 4.5×10^{16} cm^{-3}. This exceeds the LTE limits of the electron density. Thus the applicability of the LTE model to an argon plasma focus is seen to be valid.

DEGREES OF IONIZATION

With the assumption of LTE, the distribution of population densities is defined by Saha equations. A general form of the Saha equation is expressed as:

$$\frac{\alpha_r}{\alpha_{r-1}} \sum_{s=1}^{n} s\alpha_s = 2 M_A \frac{U^r(T)}{U^{r-1}(T)} \left(\frac{2\pi m k}{h^2}\right)^{3/2} \left(\frac{T^{3/2}}{\rho}\right) \exp -\frac{E_\infty^{r-1} - \Delta E_\infty^{r-1}}{kT}$$

where M_A = mass of one atom of the gas,
m = mass of electron,
h = Planck's constant,

Table 1 Electron Density at various temperature (LTE limit)

Temperature $T \times 10^3$ K	Ionization Stage Z	Quantum Number p	Electron Density n_e cm^{-3} (LTE limit)
13	1	5	2.3×10^{12}
25	2	7	1.2×10^{13}
35	3	9	1.9×10^{13}
51	4	9	1.3×10^{14}
65	5	10	2.2×10^{14}
81	6	11	3.3×10^{14}
93	7	11	8.9×10^{14}
133	8	12	1.1×10^{15}
285	9	13	1.7×10^{15}

k = Boltzmann's constant,
ρ = mass density of the gas,
E_{∞}^{r-1} = ionization energy of the gas atom $(r-1)$th stage.
ΔE^{r-1} = lowering of ionization energy
and $U^{r-1}_{\infty}(T)$ = the partition function at $(r-1)$th stage.

To solve for m number of degrees of ionization, a set of m Saha equations are taken. The equations are non-linear and no exact solutions are likely to be possible. Iterative methods are used for finding solutions of the equations.[6] 18 degrees of ionization at an ambient pressure of 0.1 torr are computed. Figure I illustrates the behaviour of ionization of the argon gas at various temperature. The results showed that below 15000 K there is only α_1, 1st degree of ionization. The 2nd degree of ionization α_2 is dominant at about temperature 21000 K. Traces of α_7 and α_8 can be obtained at temperature 95000 K and above. Traces of α_{18} would be at 2.4 million K and a complete ionization up to Ar XVIII needs about 4 million K.

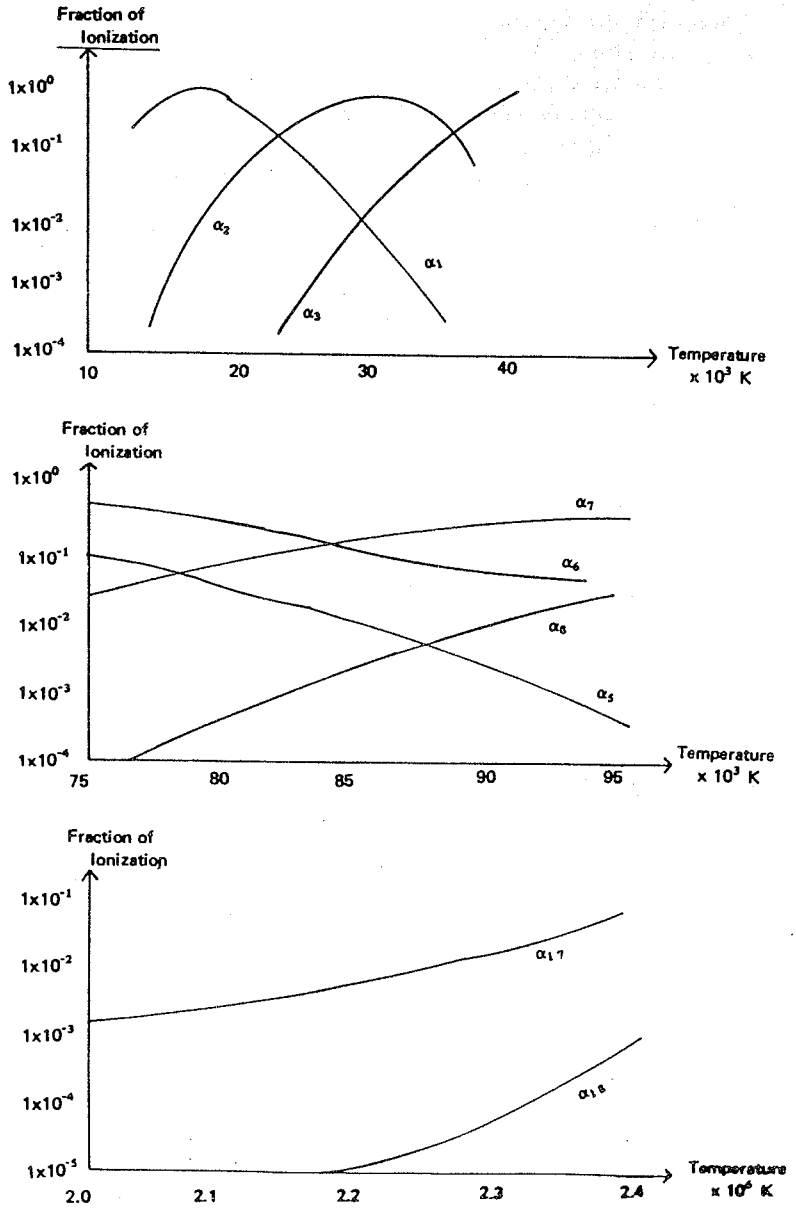

Figure 1 Ionization Curves

COMPRESSION MODEL FOR THE PLASMA FOCUS

A 1-dimensional radial compression model based on a current-sheet-shock wave structure is used. This model equates the rate of the increase of momentum in the imploding plasma layer to the driving magnetic force and a kinetic retarding pressure term. The focussing mechanism is described by an equation of motion as:

$$\frac{d}{dt}\left[m_o + \pi\rho_o (R_o^2 - R^2)\right]\frac{dR}{dt} = -\frac{B^2}{2\mu_o} 2\pi R + 2\pi R \bar{P}$$

where m_o = mass per unit length swept into the focus,
R = current sheet position.
ρ_o = ambient gas density,
B = compressing magnetic field
and $\bar{P}$ = mean kinetic pressure.

The radial collapse is divided into 3 stages: Shock heating, shock reflection and adiabatic magnetic compression. In the shock heating stage, a strong shock is assumed whereby the shock propagates ahead of the current sheet. The kinetic pressure is estimated from the shock theory. In the shock reflection stage, the shock front has reached the axis of the focus tube. The kinetic pressure is assumed to depend on the current sheet velocity in exactly the same manner as it would if the forward shock were still propagating. Adiabatic compression stage begins when the reflected shock meets the current sheet. The equation of motion for the 3 stages are given by:

SHOCK HEATING

$$\frac{d}{dt}\left[m_o + \pi\rho_o (R_o^2 - R_s^2)\right]\frac{dR}{dt} = -\frac{\mu_o I^2}{4\pi R} + \pi\rho_o R(\gamma + 1)\left(\frac{dR}{dt}\right)^2 \sigma$$

where σ = a factor due to the finite thickness of the shock,
R_s = the position of shock front
and γ = the specific heat ratio.

SHOCK REFLECTION

$$\frac{d}{dt}\left[m_o + \pi\rho_o (R^2 - R_r^2)\right]\frac{dR}{dt} = -\frac{\mu_o I^2}{4\pi R} + \pi\rho_o R(\gamma + 1)\left(\frac{dR}{dt}\right)^2$$

where R_r = the position of the reflected shock front.

ADIABATIC COMPRESSION

$$\frac{d}{dt}\left[m_o + \pi\rho_o R_o^2\right]\frac{dR}{dt} = -\frac{\mu_o I^2}{4\pi R} + \pi\rho_o R(\gamma + 1)\left(\frac{dR_c}{dt}\right)^2\left(\frac{R_c}{R}\right)^2$$

where $\frac{dR_c}{dt}$ = the current sheet velocity at the position when the reflected shock front meets the current sheet.

These equations are integrated using Runge-Kutta method. The current sheet trajectory is obtained (see Figure II). From the current sheet velocity, the ionization fractions are estimated. We also estimated that argon plasma of ambient pressure 0.1 torr has achieved a fully ionization of Ar XVIII at the minimum focus.

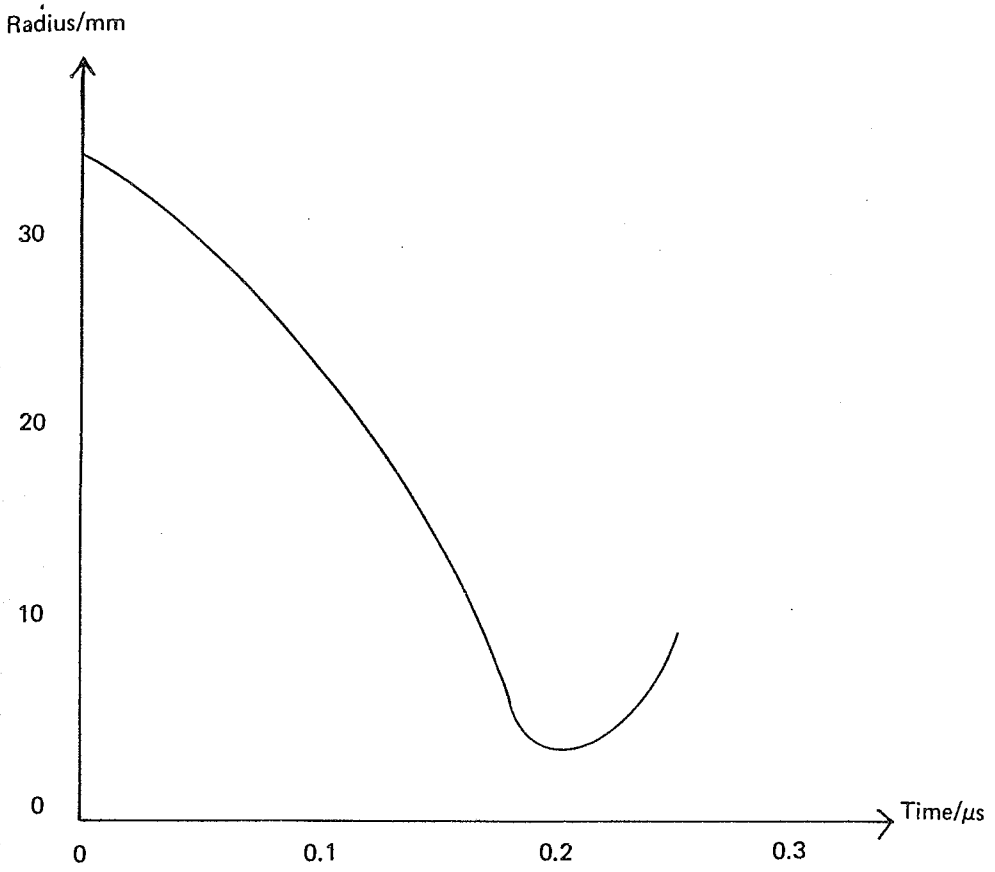

Figure II Current Sheet Trajectory

CONCLUSION

The applicability of the LTE model to an argon plasma focus is shown to be valid. A set of Saha equations then defines the equilibrium ionization at different temperature and pressure. The solution of the Saha equations shows that an argon plasma is completely ionized up to Ar. XVIII at a temperature of 4 million K. Using a radial focussing model the trajectory of the current sheet and the associated plasma parameters are computed. A fully ionized argon plasma is achieved at the focus.

REFERENCES

(1) R.W.P. McWHIRTER, Plasma Diagnostics Techniques.
(2) HANS. R. GRIEM, Plasma Spectroscopy.
(3) S. LEE, Y.H. CHEN, Plasma Focus – A radial trajectory computation. Twelfth International Conference on Phenomena in Ionized Gas, Eindhove 1975.
(4) R. WILSON, Quant. Spectry. Radiative Transfer *2*, 477 (1962).
(5) H.R. GRIEM, Phy. Rev. *131*, 1170 (1963).
(6) S. LEE, 'Transverse Ionizing Shock Waves in Planar Electromagnetic Shock Tube'. PhD Thesis (ANU), 1969.

NEUTRON DETECTORS FOR VERIFICATION OF FOCUS ENERGY SCALING

C.S. WONG, S.P. MOO and S. LEE
Department of Physics, University of Malaya

The study of the focussed plasma has been extended using neutron diagnostic with the objective of providing data for a neutron yield energy scaling law. Results obtained by various laboratories have been reported to fit the scaling law $N = AE^{2.1}$ where N is the neutron yield per pulse, A is a constant and E is the energy of the discharge system. Typical yield of 5×10^8 neutrons per pulse has been obtained in this laboratory for a 12.5 KJ, 20 KV discharge. An indium activation detector, a silver activation detector and a ^{6}Li glass scintillator detector have been tested and calibrated against a Th-Be source for absolute neutron yield measurement. At a distance of 8.0 cm from the source, the sensitivity factor is 1.5×10^4 neutrons per count for the indium activation detector; 1.8×10^4 neutrons per count for the silver activation detector and 3.7×10^2 neutrons per count for the glass scintillator detector. The activation detectors are suitable for measuring yields exceeding 10^6 neutrons per pulse. With these two types of detectors, the whole range of neutron yields expected from the plasma focus will be adequately covered.

I. INTRODUCTION

The plasma focus has been the subject of much experimental and theoretical research since the first reports of Filippov et al[1] and Mather.[2] A schematic diagram of the plasma focus device of the Mather type used by the University of Malaya Plasma Physics Group is shown in Fig. 1. Upon discharging the capacitor bank by closing switch AB, the gas in the chamber

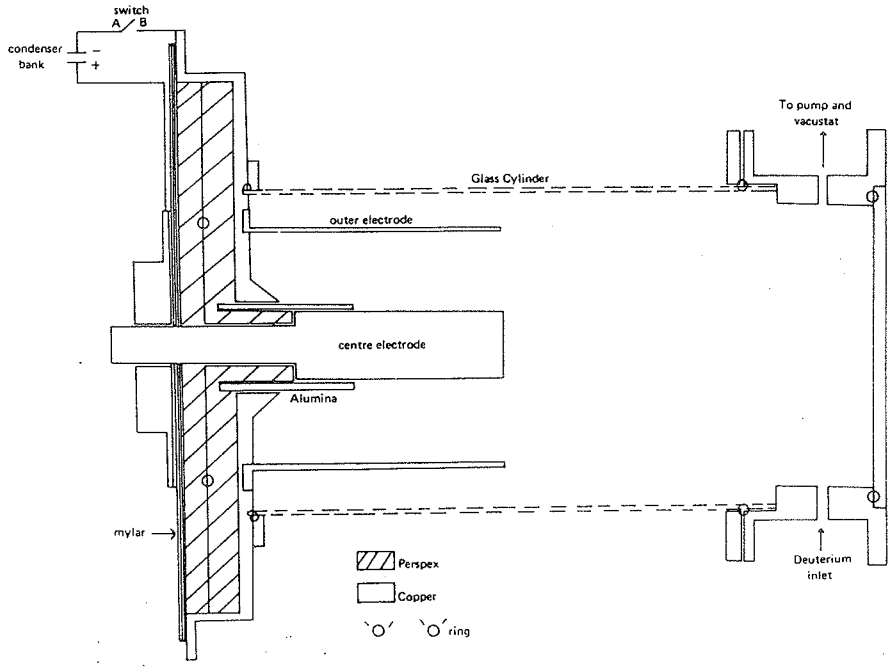

Fig. 1. Schematic diagram of the plasma focus tube

undergoes dielectric breakdown at the insulating back flange. A current sheet is formed and this is accelerated down the coaxial region by $J \times B$ forces. At the end of the central anode, a rapid radial collapse occurs resulting in a hot dense plasma. With deuterium (or deuterium-tritium mixture) as the filling gas, the plasma in sufficiently hot and dense for D–D (or D–T) fusion reactions to occur with consequent production of neutrons. The neutron emission lasts for about 100 ns.

Both neutron yield and neutron energy measurements are necessary for a better understanding of the plasma heating mechanism that take place. This paper deals with neutron detectors for yield measurements. The objective is the verification of the scaling law for neutron production.

II. THE SCALING LAW FOR NEUTRON PRODUCTION

Michel et al[3] have made a compilation of the neutron yield measurements reported by a number of laboratories. The results fit the power law

$$N = A\,E^{2.1}$$

where N is the total neutron yield at stored energy E, and A is a constant (see Fig. 2).

According to Maisonnier,[4] the neutron scaling law should have energy index of 1.5 to 2. Any compilation, such as Fig. 2, shows considerable vertical spread of points. This may be related to the different machine parameters and operating conditions of the various laboratories. The work of the Stuttgat Group[5,6] has shown the complex interplay among the various machine parameters in the optimization of neutron yield. Briefly, for a given capacitor bank operated at fixed voltage, capacity and discharge time, there exists an optimum combination of electrode length and diameter and gas pressure. Factors considered important to this optimization include a back-wall 'lift-off time', the time period available for axial acceleration and radial compression and the formation of short-circuiting current 'spokes' or re-strikes. Our own experience has indicated that proper focus formation depends critically on adjusting operating pressure so that a snow-plow speed of 6–7 cm/μs is obtained in the

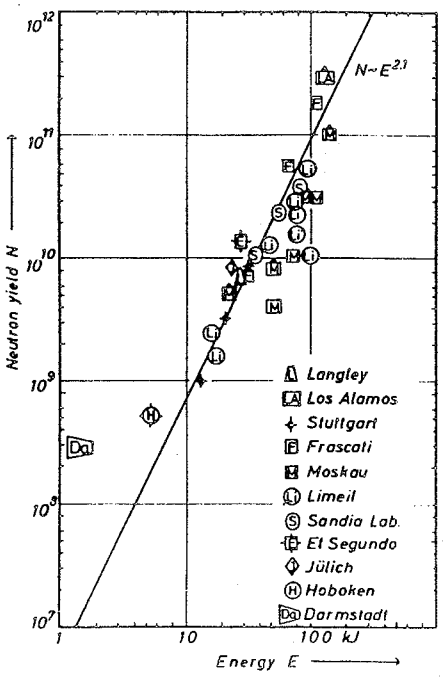

Fig. 2. Neutron yield (N) against energy (E) as reported by Michel et al

axial acceleration region. It is probable that this critical speed is associated with the highest back emf that the annular region can sustain without the formation of short-circuiting restrikes. Considering all these empirically observed factors it is clear that in the past little emphasis has been placed on device optimization and that a proper discussion of energy scaling should take into consideration whether a machine is optimized or not.

III. NEUTRON DETECTORS FOR YIELD MEASUREMENTS

From a 15 kJ D—D focus the typical neutron yield is 10^9 neutrons per burst which corresponds to an intensity of about 10^{16} neutrons s^{-1}. This high intensity rules out many conventional neutron detection techniques. The requirement on the accuracy of yield measurements is, fortunately, not severe since shot-to-shot variation in neutron production is large — a factor of two is not uncommon. An accuracy of about 25% will be sufficient for absolute yield measurements.

Two different types of detectors has been investigated. The first type is based on slow neutron activation of either a Ag foil or an In foil. The second is based on slow neutron counting by a ^{6}Li glass scintillator. Both types of detectors are vast improvements over the earlier one used by Lee and Chen.[7] However, these early time-of-flight measurements also serve to give an estimate of neutron energy, whereas the present detectors are designed to improve on the yield measurement and give no indication of neutron energy.

ACTIVATION DETECTORS

The basic features of a detector based on activation are (1) the slowing down of fast neutrons in a hydrogeneous moderator, (2) the capturing of slow neutrons by a suitable foil, and (3) the detection of β- or γ-radiation from the activated nuclei at the end of the irradiation. Several variations of the activation detector have been reported. For instance, Maisonnier et al[8] employed silver-activated Geiger Counters of the type developed by Lanter and Bannerman[9] while Lee et al[10] used a NaI(Tl) scintillator and counted the 656 keV γ-radiation from activated silver.

The activation detector that has been developed and investigated for the present purpose is similar to the one reported by Young.[11] It is shown schematically in Fig. 3 and consists of

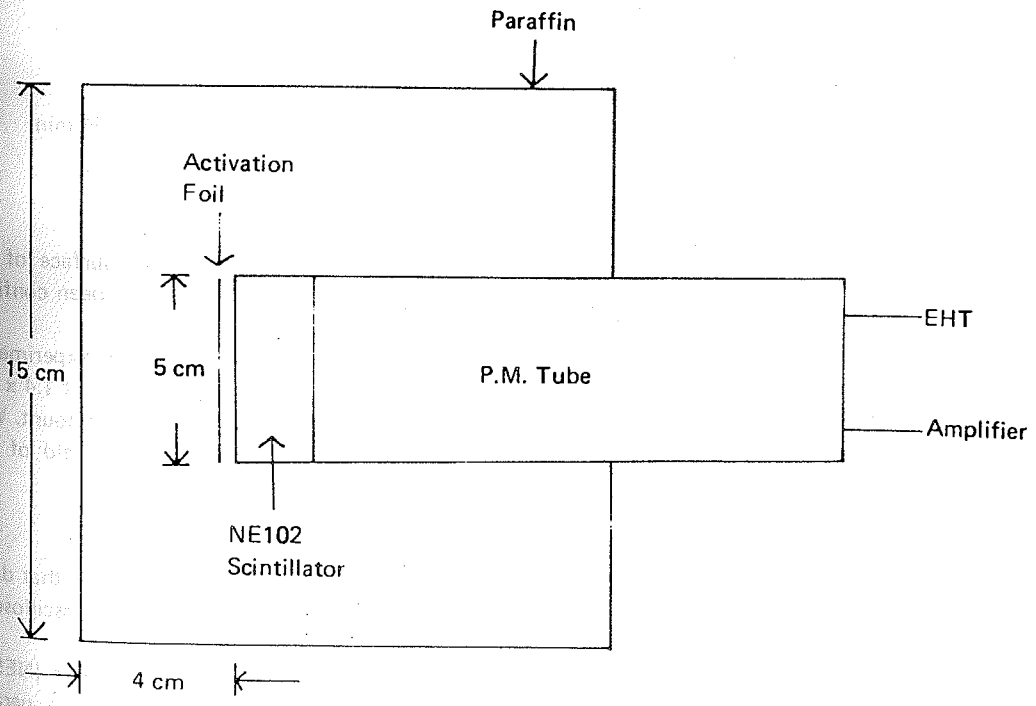

Fig. 3. Schematic diagram of an activation detector

a paraffin moderator enclosing a 5 cm diameter activation foil. In contact with the foil is a 5 cm diameter, 1 cm thick plastic scintillator (NE102) which is optically coupled to a photomultiplier. The plastic scintillator has been chosen for the detection of β-particles. The output of the photomultiplier is amplified and shaped, and all pulses with heights exceeding those produced by electrons of about 50 keV are scaled for a preset time.

The activation foil is either Ag of thickness 0.125 mm or In of thickness 0.215 mm. Table 1 lists some useful data of Ag and In as activation foils.

The principal reactions of interest are

$$^{109}Ag + n \rightarrow {}^{110}Ag \rightarrow {}^{110}Cd + \beta^- \quad (\tau_{1/2} = 24s,\ E_\beta(max) = 2.8\ MeV)$$

$$^{115}In + n \rightarrow {}^{116}In \rightarrow {}^{116}Sn + \beta^- \quad (\tau_{1/2} = 14s,\ E_\beta(max) = 3.29\ MeV)$$

The short half-lives of ^{110}Ag and ^{116}In enable such counters to be used repeatedly at short intervals.

The activation detectors have been calibrated against a ^{228}Th-Be source with a strength of about 2×10^5 neutrons s^{-1}. Activation and counting times are both about $3\tau_{1/2}$. Following Young[11], the sensitivity, F, of the detector is expressed as the number of source neutrons emitted isotropically into 4π solid angle per measured count.

Table 1 – Some useful data of Ag and In

Material	Isotope (abundance in %)	Thermal Activation Cross Section (barns)	Radioactive Isotope (half-live, $\tau_{1/2}$)
Ag	^{107}Ag (51.8)	35	^{108}Ag (2.3 min)
	^{109}Ag (48.2)	3.2	^{110m}Ag (253 d)
		91	^{110}Ag (24 s)
In	^{113}In (4.3)	56	^{114m}In (49 d)
		2	^{114}In (72 s)
	^{115}In (95.7)	157	^{116m}In (54 min)
		42	^{116}In (14 s)

The variation of F with d, the distance of the source from the front surface of the moderator is shown in Fig. 4 for the case of the In counter. Calibration have been confined to values of d less than 14 cm because of the weak source available.

The closest position to the plasma focus a detector can be placed in the present experimental arrangement is 8 cm. At this distance the sensitivity of the Ag counter is $1.8 \times 10^4 \pm 1.4 \times 10^3$ neutrons/count, while that for the In counter is $1.5 \times 10^4 \pm 1.2 \times 10^3$ neutrons/count. With these detectors yield measurements of 10% accuracy can be achieved at a yield of 10^8 neutrons per burst. For yields of 10^6 neutrons per burst, the accuracy is 16%.

^{6}Li GLASS SCINTILLATOR DETECTOR

The ^{6}Li glass scintillator detector is similar to that reported by Young[11] except that direct scaling of the scintillation pulses is employed instead of counting them on the oscilloscope trace. This improves the counting dynamic range by an order of magnitude.

The core of the detector is a 2 mm thick, 5 cm diameter ^{6}Li glass scintillator (NE912) which is very insensitive to γ-radiation. The glass scintillator is enclosed in a paraffin

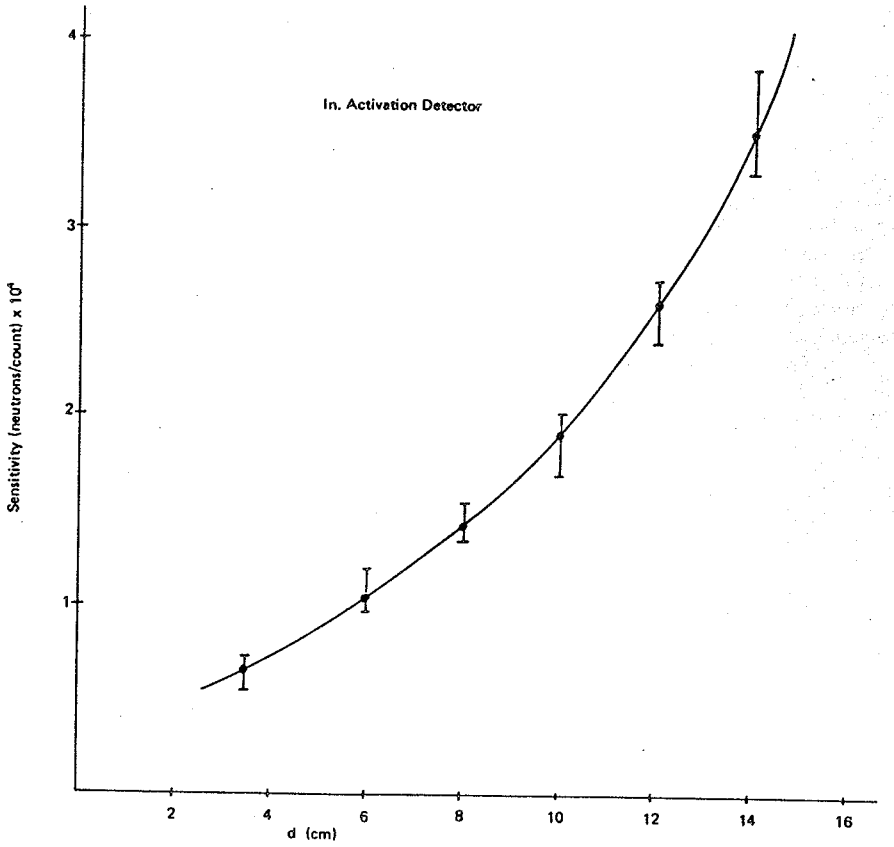

Fig. 4. Variation of the sensitivity of an indium detector with the source to detector distance (d)

moderator which serves two functions: to slow down the fast neutrons and, in the process to disperse them temporally. Thus neutrons from the plasma focus which are emitted for about 100 ns are dispersed in time up to several hundred miscoseconds duration.

The glass scintillator is optically coupled to a photomultiplier, the output of which is fed directly to a scaler. The time response of the entire system is limited mainly by the glass scintillator and is about 10 MHz. Thus assuming a counting period of 200 μs, the measured counts should not exceed 2000 to avoid pulse pile-up.

The glass scintillator has been calibrated against the ^{228}Th-Be source. At d = 8 cm, the sensitivity is 370 ± 20 neutrons/count. Hence accuracies of 20% and 10% can be obtained for yield measurements of 10^4 and 10^5 neutrons per burst respectively. For yields exceeding 10^6 neutrons per burst it is necessary to place the detector further away from the source to avoid pulse pile-up.

IV. DISCUSSION AND CONCLUSION

The ^{6}Li glass scintillator detector is much more sensitive than the activation detectors, and yields as low as 10^4 neutrons per burst can be measured with sufficient accuracy. However, at a given source-to-detector distance, the counting dynamic range is rather small, being limited at the lower end by statistical accuracy and at the upper end by pulse pile-up. The activation detectors are more suitable if a large counting dynamic range is required but yields must be in excess of 10^6 neutrons per burst for the desired statistical accuracy. With these two types of detectors the whole range of neutron yields expected from the plasma focus will be adequately covered.

V. REFERENCES

(1) N.V. FILIPPOV, T.I. FILIPPOVA, V.N. VINOGRADOV, Nucl. Fusion Suppl. Pt. 2, 577 (1962).
(2) J.W. MATHER: Phys. Fluids Suppl. I, 528 (1964).
(3) L. MICHEL, K.H. SCHONBACK, H. FISHER, Appl. Phys. Letters. *24*, 57 (1974).
(4) Ch. MAISONNIER, F. PECORELLA, J.P. RAGER, M. SAMUELLI: "Recent Progress in Research on Plasma Focus" – Preprint.
(5) M. TRUNK; J. Plasma Phys. *17*, 237 (1975).
(6) G. DECKER, R. WIENECKE, "Plasma Focus Devices" Proc. 12th Int. Conference on Phenomena in Ionized Gases, Pt. 2, 155 (1975).
(7) S. LEE, Y.H CHEN: Malaysian J. Sci. 3(B), 159 (1975).
(8) Ch. MAISONNIER et al: Proc. 4th Int. Conference on Plasma Physics and Controlled Nuclear Fusion Research, Madison, 1971, IAEA (Vienna, 1972) Vol. I, p. 523.
(9) R.J. LANTER, D.E. BANNERMAN: Rev. Sci. Instr. *39*, 1588 (1968).
(10) J.H. LEE, L.P. SHOMO, K.H. KIM: Phys. Fluids, *15*, 2433 (1972).
(11) F.C. YOUNG: IEEE Trans. on Nucl. Sci. *NS-22*, 718 (1975).

Procs. Colloq. Laser Developments and Applications (K.L. Feb. 1979)

(Laser Laboratory Internal Report 1/79, Universiti Malaya, Jan. 1979)

"Laser Safety Precautions"

by

B.C. Tan, S.A. Husain, S. Lee, K.O. Lee,
K.S. Low, A.C. Chew, Y.H. Chen & C. Grey Morgan.

Introduction

Lasers are lamps of a very special kind. They can produce very powerful beams of light. This laser light has important properties which distinguish it from the light produced from more familiar conventional lamps like electric light bulbs, fluorescent tubes, arc lamps, etc. For present purposes the main differences of interest are the extraordinary range of brightness and light intensities available (up to as much as 10^{16} $W.cm^{-2}$) and the highly directional parallel properties of the light beam from a laser. Both of these properties contrive to make any laser a potentially dangerous device capable of causing personal injury. These two properties alone make the brightness of lasers exceed that of conventional lamps by several order of magnitude. Consequently even the simplest laser producing only a milliwatt or less of power can cause severe eye damage or even blindness. The huge power densities and the high directionality of laser light beams are due to the fundamental physical mechanisms responsible for the generation of light in lasers. These mechanisms are the spontaneous emission and stimulated emission of energy in the form of light from suitably treated atoms or molecules. In conventional lamps only the former, a random stochastic process, occurs, whereas in a laser the latter, a coherent process, totally dominates. Hence the name LASER which is an acronym for Light Amplification (by) Stimulated Emission (of) Radiation.

Since their invention in 1960 lasers have found application in ever-widening fields. These range in Medicine, for example, from opthalmology (destruction of blood clots in glaucomic conditions, welding of detached retinas), dermatology (treatment of facial port wine stains, and of skin melanomas), surgery (simultaneous incision and cauterisation of highly vascular tissue such as the liver, and treatment of cervical cancer) to mention but a few. In Industry & Technology applications range from cutting and drilling of highly refractory materials (e.g. diamond) and metals, the welding of metals in highly clean vacuum conditions, trimming of resistors and components in microelectronic circuits and myriad other practical application. It is commonplace nowadays for laser geodolites to be used by surveyors.

In science lasers are being used for a remarkably wide range of purposes - pollution detection, isotope separation, productions of new chemical compounds on the one hand to attempts to induce controlled thermonuclear reactions in very high power laser-produced high temperature plasmas. There are many more besides, especially at a fundamental level in atomic and molecular spectroscopy. All these applications serve to emphasise the fact that more and more lasers will be used in future and while at present there are probably more lasers in university physics, chemistry and medical departments throughout the world than in industry, this situation will change and workers in other disciplines and in industry will find themselves using lasers. Thus, as part of their training and experience in university it is important that students observe a strict code of safety procedures so that when they eventually become employees or employers using or concerned with the many types of lasers available they will possess the skills and knowledge necessary to prevent laser accidents. Medical students and practioners should also be aware of laser hazards since they may have to examine and probably treat laser users. What follows are comments on lasers and safety recommendation made by the Laser-Group of the Physics Department of the University of Malaya. They are based on the experience gained by members of the group in many laser laboratories throughout the world.

Relevant Properties of Laser Beams

Operational Modes of Lasers

The output from a laser may be in the infra-red, visible or ultraviolet parts of the electromagnetic spectrum. Strenuous efforts are being directed to widen this range, especially towards shorter wavelengths and it seems likely that the generation of coherent x-rays will be achieved relatively soon. Direct laser action at present covers the range from about 172 nm to 20 μm. Lasers can operate in either continuous or pulsed modes.

(i) Continuous Operation

The laser output beam is switched on for relatively long periods of time - which may be varied at will by the operator. This is sometimes called CW (i.e. continuous wave) operation. A well known example is the helium-neon laser.

(ii) Pulsed Operation

The laser output is on for only a very short period of time giving a pulse of light generally less than about 0.1 μsec duration. We must distinguish between several types of pulsed operation:-

(a) Free running or spiking operation

(b) Q-switched or Q-spoiled or Giant Pulse operation, - single shot

(c) Mode-or phase-locked operation, single shot

(d) Long duration repetitively mode-locked operation

(a) In free running or spiking operation of solid state, e.g. ruby lasers the flashlamp pumping produces a lasing threshold

population inversion so that light amplification can occur. This can only be sustained for a time ~ cavity loss time t_c* ~ usually $\leq$ 0.1 μsec. Thus the output consists of a pulse of this duration followed by a period spent in waiting for the inversion to build up again as pumping continues. When the threshold is exceeded another pulse forms, again in a time ~ t_c. In this way a series of spikes of about 0.1 μsec or less and generally of random height and separated by periods tens of μsecs continues throughout the pumping period, typically for about 10^{-4} - 10^{-3} sec. The peak power emitted during a spike may be ~ 1 MW from a ruby laser.

(b) In Q-switched or Q-spoiled or Giant pulse operation amplification and laser action is delibrately suppressed so that a very large population inversion is achieved and hence there is a large amount of stored energy in the upper laser level. This is done by inserting a suitable absorber in the laser cavity or by misaligning the mirrors momentarily, i.e. spoiling the quality factor Q of the cavity. When sufficient inversion is attained the Q is restored very rapidly and the stored energy released in a giant coherent pulse of duration t_c ~ 100 nanoseconds. The peak power per pulse in this form of operation may be 10 to 100 MW from ruby and neodymium-in-glass lasers.

---

*Footnote The cavity loss time t_c may be defined on the time taken for radiation to leak from the laser cavity so that the energy density is reduced by a factor e in the time t_c. Thus $t_c = 2L/C(1-R_1R_2)$ where L = cavity length, R_1 + R_2 are the mirror reflectivities and C is the velocity of light in the laser medium.

(c) Ordinarily many modes of electromagnetic field can oscillate simultaneously in the laser cavity provided they satisfy the frequency condition $\nu = n\ C/2L$ where n is the set of integers 1,2,3... and L is the cavity length. The number of modes n which may oscillate is governed by the amplification band width of the laser medium $\Delta\nu_{amp}$ and hence the number of oscillating modes M will be about $\frac{2L\,\Delta\nu_{amp}}{C}$

$$\text{i.e.}\quad M \simeq 2L\ \Delta\nu_{amp}/C$$

since the separation between adjacent modes, corresponding to $n = 1$ is $d\,n = C/2L$.

There is no special phase relationship between these various modes. They start up fortuitously and at random. Some may couple constructively while others do so destructively. Thus the laser power output which is the square of the vector sum of the amplitudes of individual modes can fluctuate in a random manner. However, if the phases of the individual modes can be controlled and fixed relative to each other the output becomes a series of pulses of duration $t_p = \frac{2L}{MC} \simeq \Delta\nu_{amp}^{-1}$ separated by intervals $\frac{2L}{C}$ which is of course the cavity transit time. This train of pulses will be sustained as long as pumping continues. Thus one can get a train of mode-locked pulses lasting as long as the flashlamp pumps the ruby or Nd^{3+} above the threshold for lasing action - typically for 1 Msec and obtain hundreds of flashes of a picosecond ($\gtrsim 10^{-12}$ sec) duration.

In the case, of, for example, cw argon ion-pumped dye lasers, a train of picosecond flashes lasting for hours can be obtained. This is an example of case (d) above.

In the case of the solid state laser picosecond flashes the peak power can be as high as gigawatts (10^9 w) or even terrawatts (10^{12} w). It is clear that such enormous powers can cause severe damage to biological tissue.

We should note here that even with ordinary cw operation spontaneous mode or phase-locking may occur so that superimposed on a relatively low (milliwatt to watt) average output, there may be pulses of very high peak power.

Mechanism of damage to biological tissue

Since light is an electromagnetic wave it interacts via the E and B vectors on the charged particles which constitute biological material which is principally of a dielectric character. Their electrons are made to oscillate and polarisation and energy absorption takes place. By means of collisions energy transfer to neighbouring atoms and molecules occurs. This latter process is of course, thermal conduction and irreversible damage can result. In the case of the eye photo-induced chemical changes in the retina can also occur. Only in extreme intensity cases is the laser beam able to ionize atoms and molecules and this feature distinguishes laser radiation from the hazardous ionizing radiations viz x-rays and nuclear $\alpha\beta\gamma$ radiation and protons produced in n, p reactions in tissue. Hence laser radiation is not regarded as ionizing radiation and it seems generally agreed that no somatic or long term genetic damage is caused by laser light. The principal damage mechanism is thus absorption causing local heating and thermal degradation. In the case of pulsed laser light falling on the cornea of the eye the energy is focussed at a small spot (diameter 50-100 μm) on the retina and rapid absorption can in addition to causing the local thermally - induced damage, also cause shock wave generation and propagation through the vitreous humor to cause damage to neighbouring portions of the organ. At high powers both cornea and retina will suffer damage but because of the magnifying effect of the eye lens the main region to sustain damage at low powers is the retina. The temperature rise there depends upon the energy density and duration of exposure. Experiments and statistical data

Lappin et al Arch Opthal 84 721 (1970),
Ham W.T. et al Arch Opthal 84 797, 1970, Wolbarsht M.
Amer. Nat Standard Inst. September 1972

suggest that minimal observable lesions are caused in monkeys by an input power of 8_mJ i.e. exposure for 1 second at 8_mJ incident on the eye causes a lesion detectable by an opthalmologist. Human eye damage appears to occur with 50% probability at 20 mW but at 40 mW the probability is about 100%. A minimum lesion occuring in the paramacular area is undetectable by the accident victim who should experience no loss of vision. It would however be detectable to a skilled trained opthalmologist knowing where the irradiation has taken place. Consequently, it would appear that for powers of 5 mW and less the hazards are minimal. Nevertheless all lasers must be treated with respect. Thus not only must direct viewing along the beam be prohibited but also great care must be taken to avoid reflected light. The Committees of Vice Chancellors and Principals of the Universities of the United Kingdom in the Guidance Notes emphasise that with CW lasers a power density of 1×10^{-5} w mm^{-2} must not be exceeded for short term viewing and only - 1×10^{-7} w mm^{-2} for longer periods. With pulsed lasers the energy unit is 5×10^{-9} J mm^{-2}.

Other hazards associated with lasers

Lasers are complex devices involving electrical, chemical and mechanical components all of which are potential sources of danger. So, in addition to taking precautions against the obvious dangers stemming from the laser radiation itself further precautions are necessary to ensure safety from the following:-

(i) Electrical hazards

High voltages and charged condenser banks are almost invariably used with pulsed lasers. The usual boxing, screening and earthing procedures must be followed. Condensers should be provided with bleed resistors. Interlocks and trips should be provided so that access to high voltage components is impossible when they are switched on.

(ii) Explosions and Fire hazard

Explosions and fires may be caused by flammable solvents used with certain types of lasers, particularly dye lasers. With very powerful pulsed or CW beams materials in the path of the beam can be ignited and a fire result.

(iii) Poisonous Fumes

Sometimes the amplifying medium may be a toxic substance, e.g. hydrogen fluoride, or the solvents used in certain dye lasers may induce toxaemia. Appropriate steps to ensure adequate ventilation must be taken. Ozone may be generated by pumping radiation and should be removed.

(iv) Incoherent Radiation

The flashlamps of optically pumped solid state lasers radiate intense flashes with a strong ultra-violet component. Inadvertent exposure of the eye and face must be avoided.

(v) Ionising radiation

When very powerful lasers are focussed on to solid targets X-ray generation can occur.

Precautions to be taken when using lasers

1. In no circumstances look along a laser beam. Special Goggles should be worn when using high power lasers.

2. For high pwoer pulsed lasers warning lights should be provided to indicate when the condenser bank is charged and the laser ready to fire.

3. For very high power pulsed lasers an interlock on the doors leading to the room containing the laser should be used to prevent admission when the laser is in use.

4. Where possible only one high power laser should be in use in any given room at a time.

5. High power beams should be enclosed in light pipes and the optical paths should be as short as possible.

6. If possible a high level of background illumination should be the produced in laser rooms so that the eye pupil has minimum dilation.

7. Laser room should be painted white or cream matt paint

8. Reflecting surfaces such as glass-fronted cabinets and gloss painted items should be avoided in laser rooms.

9. Hazard notices designating lasers should be placed on doors leading to laser rooms.

10. Adequate ventilation should be provided to remove toxic vapours generated from laser targets and to prevent build up of noxious gases or vapour which may leak from the laser.

11. If a pulsed laser is to be used out of doors, for example in pollution detection or cloud lidar special precautions must be taken to ensure public safety. When the beam is directed in a skyward direction consultation with local civil aviation authorities must be considered in relation to the volume of air traffic.

Procs. Colloq. Laser Developments and Applications (K.L. Feb. 1979)

Laser Research Program at the University of Malaya

B.C.Tan, S.A.Husain, S.Lee, K.O.Lee, K.S.Low, A.C.Chew,
Y.H.Chen, Raja Mustapha and C. Grey Morgan*.

Introduction

A laser Research Group with little background on Laser related fields was formed in late 1976 with the intention of initiating laser related research in the Physics Department. A research grant from the University was finally awarded in early 1978 when Lasers and other spectrometric equipments were ordered. In the mean-time a series of informal seminars on lasers and their applications was conducted by members of the group both in the long vacations of 1978 and also this year. Today's colloquium on Laser Developments and Applications is the culmination of this year's series of informal seminars with the invaluable contributions and guidance of Prof. C. Grey Morgan, who conducted the major part of this year's informal seminars.

In this report, the research facilities acquired by the group and the progress of activities of the group will be presented. The main activities of the group are classified into two categories; in the development of Lasers as a technology and in the applications of Lasers in various areas of research like pollution study, plasma fusion research and other areas of related research. In the following sections, these will be outline separately.

* Currently Visiting Professor at University of Malaya. Permanent address: University College of Swansea, Swansea, South Wales, United Kingdom.

II. Laser Research Facilities

As shown in Table 1, the laser facilities of the group are based on a high power argon ion laser pumping a dye laser system. This choice is based on the high power offered by the argon ion laser and the versatility of the tunable dye laser for spectroscopic applications.

The argon ion laser (a Spectra Physics Model 171-06) has a BeO discharge tube with a high efficiency cooling system. It provides 9 Watts on all lines from 454.5 - 528.7 nm with 3 watts each at 514.5 and 488 nm. It has also significant uv radiation at 351 and 364 nm. This laser provides a powerful source for the optical pumping of dye lasers and can also be operated independently, as for example in the non-resonant fluorescence detection of pollutant gases. By changing the discharge tube and the optics, it can also be upgraded to work as a krypton ion laser which is a powerful pump source in the infra-red.

The dye laser (Spectra Physics Model 375) is of jet-stream design and the dye used is Rhodamine 6G. With the argon ion laser lines of 488 and 514.5 nm as the pumping source, the dye laser output is tunable from 570 - 640 nm. As much as 1.4 watt output radiation can be obtained using the 9 watt argon ion laser. With a wedge tuning and a fine etalon elements, 40 GHz linewidths are obtained. If upgraded to piezoelectric tuning, very fine linewidths of 5MHz can be obtained.

The spectro-photometric detection system is based on a 1-M Czerny-Turner spectrometer and a 100 MHz photon counter system. It will be discussed in greater detail in a following paper[1].

It should finally be mentioned that a high power pulse Ruby laser is available to the group presently installed in the Plasma Laboratory for laser initiated plasma and plasma diagnostic studies.

Equipment	Make	Specifications
1. Argon Ion Laser -continuous	Spectra Physics Model 171	9 W all line (454.5-528.7 nm) 3 W each at 514.5 & 488 nm
2. Dye Laser -Rhodamine 6G	Spectra Physics Model 375	572-640 nm tunable 1.4 W with 9 W input 40 GHz linewidth 8 GHz tuning resolution
3. Scanning interoferometer	Spectra Physics Model 410	scanning range = 550-650 nm FSR = 1200 GHz Bandpass < 24 GHz
4. 1 M Czerny-Turner spectrometer	Spex Model 1704	175 nm - 1.5 μ resolution ~40 GHz
5. Fast dual-trace storage scope	Tetronix 7834	400 MHz
6. Photon Counting system	Ortec-Brookdeal 5C1	100 MHz (10 ns pulse pair resolution) dual channel disc. ampl. digital lock-in with chopper
7. Photomultiplier with Housing	Emi 9558 QB	200-850 nm
8. X-Y/t chart recorder	Watanable WX-4401	100 cm/sec writing speed 0.5 sec/cm to 50 sec/cm sweep
9. Pulsed Ruby laser (Plasma Lab.)	JK System 2000	1.5 J (25 ns) multimode 30 mJ (2 ns) single mode

Table 1 : Laser equipment at University of Malaya

III. Development of Lasers

In order to participate in the development and construction of lasers, the group has undertaken to construct a variety of lasers, both pulsed and CW, radiating from uv to far infrared region. Table 2 summarizes the five lasers under construction by the group. Some of these lasers are at a more advanced stages of development (a uv - N_2 laser lasing already) and will be presented in greater details in some of the following papers. Brief accounts will be given here to each of these projects.

Nitrogen Lasers

A pulsed N_2 laser which lases in uv region at 337.1 nm has been constructed[2]. This laser, with a very short pulse duration of 10 ns and peak power in the range of 100 kW is very useful in various spectroscopic studies of transient phenomenon in plasmas. It is a TEA (transverse discharge) design and require very fast switching circuits.

A different design of this transverse discharge N_2 laser with higher peak power of the order of 700 kW is under construction. This will be a useful pump source of dye cells and the amplification with dye cells to obtain a wide range of high power tunable short pulse radiation.

Details of these lasers will be given in a following paper[2].

Flashlamp pumped dye Laser

Dye lasers are characterised by their tunability over a large spectral range. Under development is a tunable dye laser pumped by a flashlamp. This flash tube and dye cell is collinear in design. With a circulating dye laser medium of Rhodamine 6G, the laser is tunable from 570 - 680 nm. With input energy of 50 J at the flashlamp,

Type of Laser	Wavelength	Energy, Power	Status
1. Pulsed N_2 Laser (10 ns)	337.1 nm	(a) ~100 KW, 1 mJ	lasing
		(b) ~ 700 KW, 7 mJ	under construction
2. Flashlamp pumped dye laser (2 μs)	570–680 nm tunable	~50 KW, 100 mJ	under construction
3. CO_2 laser -continuous	10.6 μ	> 20 W continuous	completed and testing stages
4. Pulsed TEA - CO_2 Laser (100 ns)	10.6 μ	$\lesssim$ 10 MW, 1 J	under construction

Table 2 : Laser Development Program at University of Malaya

the dye laser is expected to produce a 100 mJ output of 2 μs pulse length. Due to its relatively high energy radiation ($\sim$ 50KW) and is relatively inexpensive to construct, it is a useful tunable laser source for the absorption spectroscopic studies of various gases.

CO_2 Lasers

The only continuous wave (CW) laser under construction[3] by the group is a CO_2 laser lasing at 10.6 μ . This laser is near completion and is expected to produce more than 20W of CW power. A second amplifying stage is planned to boost power to the 100 W region to obtain sufficient power for cutting, drilling and other material processing purposes.

TEA - CO_2 Lasers and others

TEA - CO_2 lasers which operate in the pulse mode at 1 J or more output levels are under construction for the study of transient phenomenon in electrical breakdown of gases to form plasmas[4]. It is planned that Hybrid TEA - CO_2 laser with the CW - CO_2 laser will be constructed in a later stage.

Other lasers which are considered by the group are excimer lasers, an extension of the basic transverse design of the N_2 and TEA - CO_2 lasers. These are powerful vacuum uv laser sources. On the other hand, tunable semi-conductor lasers could also be pursued by the group to provide inexpensive laser sources.

IV. Applications of Lasers

Using the laser facilities acquired by the group and the lasers constructed, the group intends to pursue various area of research and in particular in the development of detection techniques of atmospheric pollutants. Other areas of research planned are multiphoton spectroscopy

of gases, laser initiated plasma discharge as well as diagnostic techniques.

Pollution Monitoring

Using the high power argon ion laser, fluorescence detection of atmospheric pollutants like NO_2 and NO could be performed. This is based on the non-resonant absorption and the detection of the fluorescence signals from the pollutant gases. After calibration of the system for known concentration of pollutant gases the system can be used for in-situ measurements of atmospheric pollutants. This experiment has now being initiated and will be reported in more detail in a following paper's[5].

Light Detection and Ranging (LIDAR) techniques based on non-resonant Raman backscattering is also under investigation. This has to be performed with a high power pulse laser. A possible candidate is either the Ruby Laser available in the Department or the N_2 or flashlamp pumped dye lasers under construction by the group. This LIDAR technique offers the advantage of providing information on the range, the concentration as well as the different types of pollutant gases existing in the atmosphere.

Multi-photon Spectroscopy

High resolution spectroscopy could be performed with the development of high power tunable laser sources, together with techniques like the Doppler free method. In the Doppler free method, two beam travelling in opposite direction, effected by a mirror, results in the absorption of two photons. Doppler broadening will be eliminated completely in the addition of these two oppositely travelling photons. This Doppler free method allows spectroscopy to be carried out with very high resolution and permits fine and hyperfine structure, isotope shifts, Zeeman and Stark levels, etc to be obtained accurately.

Using the argon ion pumped dye laser or those developed by the group, selective absorption processes could also be carried out. With fine tuning resolution, selective multi-photon ionisation or dissociation of various gases could be performed[6].

Laser Initiated Plasmas and Diagnostic Techniques

The Plasma Physics group in the Department is currently using a Ruby laser (20 ns, 1.5 J multi-mode) to initiate a vacuum spark to produce high density plasmas initiating fusion reactions[7]. This Ruby laser can also be operated single mode (2 nS, 10 mJ) as a diagnostic tool in holographic studies of density contours of the plasmas produced.

At the same time, TEA - CO_2 lasers which provide very high power are under construction by the group. With energy more than 1 J per pulse, plasmas can be produced when the laser light is focussed to a spot. This can be used for the study of transient events in gas discharge and other related plasma phenomena.

Diagnostic techniques using the short pulse N_2 lasers under construction by the group can also be performed.

V. Outlook and Conclusions

We have outlined the laser facilities available, the development program of laser constructions and the research program using lasers at this Department. Presently, the laser components are arriving and the Laser Laboratory is being renovated. In the layout of this Laser Laboratory, two or three experiments can be set up simultaneously in three adjoining rooms to optimize the usage of these facilities. We take this opportunity to invite anyone interested to use our laser facilities and to plan out collaboration schemes with us. When the needs arise, a User Committee can be formed to accomodate the needs of all users.

References

1. K.O. Lee, proceedings this colloquium.

2. A.C. Chew and B.C. Tan, Mal. Jour. of Sc. 4 (1976) 111, and proceedings, this colloquium.

3. Y.H. Chen, proceedings this colloquium.

4. C. Grey Morgan, Sc. Prof. Oxf. (1978) 65, 31 and proceedings, this colloquium.

5. K.S. Low, proceedings, this colloquium.

6. C. Grey Morgan, proceedings this colloquium.

7. S. Lee, proceedings, this colloquium.